EVALUATION OF MODIS PRODUCTS
OVER FOUR EUROPEAN ECOLOGICAL STUDY SITES

A dissertation submitted to the

FACULTY OF BIOLOGY, CHEMISTRY AND GEOSCIENCES

UNIVERSITY OF BAYREUTH, GERMANY

to obtain the academic degree of

DR. RER. NAT.

presented by

NGUYEN QUOC DINH

M. Sc.

born June 16, 1970

in Namha, Vietnam

Bayreuth, December 2008

EVALUATION OF MODIS PRODUCTS

OVER FOUR EUROPEAN ECOLOGICAL STUDY SITES

By

Nguyen Quoc Dinh

Departments of Micrometeorology

And Plant Ecology

University of Bayreuth

Germany

Supervisors:

Prof. Dr. Thomas Foken

Prof. Dr. John Tenhunen

Vollständiger Abdruck der von der Fakultät für Biologie, Chemie und Geowissenschaften der Universität Bayreuth genehmigten Dissertation zur Erlangung des akademischen Grades eines Doktors der Naturwissenschaften (Dr. rer. nat.).

Promotionsgesuch eingereicht am: 16. Dezember 2008

Wissenschaftliches Kolloquium am: 16. April 2009

Prüfungsausschuss:

Prof. Dr. Thomas Foken (Erstgutachter)

Prof. Dr. John Tenhunen (Zweitgutachter)

Prof. Dr. Michael Hauhs (Vorsitzender)

Prof. Dr. Bernd Huwe

PD. Dr. Werner Borken

Dekan: Prof. Dr. Axel Müller

Die vorliegende Arbeit wurde in der Zeit von Oktober 2001 bis Dezember 2008 an der Universität Bayreuth am Lehrstuhl für Mikrometeorologie und Pflanzenökologie, unter Betreuung von Prof. Dr. Thomas Foken und Prof. Dr. John Tenhunen angefertigt.

To four women of my life:

Mom, Huong, Minh Hanh, and Minh Anh

SUMMARY

Global vegetation is a key component of the climate system due to its key role in geosphere-biosphere-atmosphere interactions. Understanding these processes is of important for predicting future climate and the future state of terrestrial ecosystems. Land surface properties such as the land cover type and leaf area index (LAI) are used as essential inputs in many hydrological, ecological, and climate models. They are key parameters that describe the functioning of vegetation and are required for modeling vegetation productivity, land surface climatology, global carbon budgets and agricultural outputs as influenced by resource management. Successful modeling of these processes to quantitatively and accurately characterize global dynamics requires definition of these parameters periodically and globally with high accuracy. For this purpose the MODIS-based land surface products were designed and are now regularly available worldwide.

Nevertheless, analyses based on MODIS inputs of land cover and LAI must be tested with respect to their reliability, in order that we can trust and use the outputs from simulation models quantifying water and carbon balances at large scale. The purpose of the research reported here is to determine the reliability of the MODIS spectral reflectance, land cover and LAI products for European landscapes which are highly fragmented and not necessarily homogeneous at the 1 km scale characteristic of MODIS products. A stepwise analysis has been carried out for reflectance, land cover and LAI products, comparing results from ground truth data and from high resolution remote sensing images (Landsat) to the coarser scale MODIS information. In this way, the influence of landscape fragmentation on the MODIS products should be clear and advice can be given about how they should be used in land surface modelling efforts.

Four European locations were chosen for study; landscapes dominated by deciduous forest at Hesse, France; by coniferous forest at Tharandt, Germany, and by forest and grassland in mountainous terrain in the Berchtesgaden National Park, Germany and in Stubai Valley, Austria. All of these landscapes, however, have a mixture of land use. In order to compare measurements at intensive study plots with MODIS (1 km resolution), it was necessary to build a bridge via remote sensing data derived with Landsat TM (30 m resolution). It was demonstrated that for all study sites, the registration accuracy of Landsat TM images did not deviate by more than half of one pixel, and that the root mean square of error (RMSE) was less than 0.3 pixel when utilizing at least 40 ground control points and nearest-neighbor

resampling technique. Comparing Landsat images with aerial photography clearly demonstrated that specific study sites on the ground could be identified and that the measured characteristics could be associated with Landsat pixel properties.

The evaluation results showed that the MODIS reflectance product is reasonably accurate (less than 10 % absolute error). Certainly it is appropriate to utilize reflectance data from the two types of satellite images and to use these information in comparative examinations of land cover mapping and leaf area index estimation. The land cover comparison demonstrates that both the scale applied in classifications and the number and type of land use categories that are permitted lead to important shifts in the characterization of land cover when moving from 30 m to 1 km resolution of MODIS. Fragmentation in European landscapes is a fundamental problem encountered in the use of MODIS products. A true representation of the land surface cannot be obtained from the current MODIS land cover classifications at 1 km scale. The use of these descriptors in models describing land surface properties may potentially lead to large errors. Thus, exchange between the land surface and the atmosphere of water and CO_2 as estimated by models using MODIS inputs will have a high level of uncertainty, and the results must be considered with caution. The problems in classification that are encountered lead to further difficulties in land surface characterization, since the retrieval of LAI uses land cover as an input variable. At the peak of vegetation development, MODIS LAI appears to strongly underestimate values of the Landsat based maps. During winter, the comparison is even worse, but is not consistent from grassland to deciduous forest and coniferous forest. The results cast doubt on the usefulness of MODIS LAI products as input to continental scale simulation models for carbon and water balances, at least in Europe where land cover is highly modified and fragmented due to centuries of human use and management. Use of the MODIS products in Europe requires that new techniques be considered to search for compatibility in averaging and aggregating information on land cover and reflectance that is used to estimate LAI for large areas.

Keywords: Remote sensing, vegetation, MODIS, Landsat, LAI, Land cover, reflectance, evaluation

ZUSAMMENFASSUNG

Aufgrund der komplexen Interaktionen zwischen Geosphäre, Biosphäre und Atmosphäre spielt die Vegetation auf der Erde eine der Schlüsselrollen des globalen Klimas. Das Verständnis dieser Interaktionen und Prozesse ist von grundlegender Bedeutung zur Vorhersage zukünftiger Klima- und Vegetationsszenarios. Eigenschaften der Kontinentoberflächen, wie Vegetationsbedeckung und Blattflächenindex (LAI) fließen ein als essentielle Vorgaben für die Berechnung hydrologischer, ökologischer und klimatischer Modelle. Es sind dies Schlüsselparameter zur Erklärung der „Funktion" der Pflanzendecke und sie werden daher benötigt für die Modellierung der Biomasse-Produktion, des Klimas der Landoberflächen, der globalen Kohlenstoff-Bilanz und der Landwirtschafts-Erträge in Abhängigkeit zum anthropogenen Ressourcen-Management. Ihre realistische Modellierung für eine exakte quantitative Charakterisierung globaler Dynamiken verlangt die periodische und globale Definition dieser Prozesse in höchster Genauigkeit. Hierfür wurden MODIS-basierte Land-Oberflächen-Modelle entwickelt, welche inzwischen weltweit verfügbar sind.

Zur Überprüfung der Vorhersagegenauigkeit der MODIS-Modellierungen sind dennoch Tests hinsichtlich Land-Vegetationsbedeckung und LAI erforderlich, um die Simulationen hinsichtlich der Quantifizierung der großmaßstäblichen Wasser- und Kohlenstoff-Bilanz überprüfen zu können. Die vorliegende Arbeit befasst sich mit der Bestimmung der Zuverlässigkeit von MODIS-Produkten, die die spektrale Reflexions-Eigenschaften der Land-Bedeckung, der Landnutzung und des LAIs in typischen europäischen Landschaften räumlich charakterisieren sollen, welche aber hinsichtlich des viel zu großen 1 km-Rasters von MODIS als äußerst fragwürdig zu werten sind. Durchgeführt wurde deshalb eine stufenweise Analyse für die Licht-Reflexion, Landbedeckung und LAI, wobei hoch aufgelöste LANDSAT-TM-Satelliten-Bilder und reale Daten von den jeweiligen Orten mit den gröber aufgelösten MODIS-Informationen verschnitten wurden. Dabei wird der Einfluß der Landschaftsfragmentierung auf die MODIS-Simulation verständlich und es müssen daher in der Zukunft klare Regeln angewandt werden, sie einzusetzen.

Vier europäische Orte wurden für die vorliegende Studie ausgewählt; Landschaften in denen folgende Vegetationsformen dominierten: laubabwerfende Wälder in der Umgebung von Hesse (Frankreich), Nadelholzforste bei Tharandt (Deutschland), Mischwälder sowie alpine Matten im Nationalpark Berchtesgaden (Deutschland) und im Stubai-Tal (Österreich). Alle vier Regionen besitzen darüber hinaus eine stark variierende Landnutzung. Um die detaillierten vor-Ort-Messungen mit MODIS (mit 1 km-Rasterauflösung) vergleichen zu können, war es notwendig, eine Brücke zu schlagen mit Hilfe der LANDSAT TM-Satellitenbilder in 30 m-Rasterauflösung. Es zeigte sich, dass die Bestimmungsgenauigkeit von LANDSAT TM-Bildern für alle 4 Regionen nicht mehr als um einen halben Pixel abwich und dass die Standardabweichung weniger als 0,3 Pixel betrug. Hierzu war es notwendig, mindestens 40 vor-Ort-Punkte mit der Nearest Neighbour-Resampling Methode einzubeziehen.

Die Ergebnisse der Evaluation zeigten, dass die modifizierten MODIS-Reflexdaten-Produkte hinreichend genau sind (weniger als 10 % des absoluten Fehlers). Entsprechend sollten die Reflexions-Daten von zwei verschiedenen Satelliten-Bildern verwendet werden und diese Informationen sollten in Vergleichsuntersuchungen eingesetzt werden zur Feststellung der Landbedeckung und zur Schätzung der Blattflächenindices. Der Vergleich der Landbedeckung zeigte, dass sowohl der Maßstab bei der Klassifizierung als auch die Zahl und der Typ der Landnutzung sich wesentlich verschiebt beim Sprung von der 30 m- zur 1 km-Auflösung. Die kleinräumliche Fragmentierung der europäischen Landschaft bleibt ein zu lösendes Problem bei der Verwendung von MODIS-Produkten. Eine echte Repräsentierung der Landbedeckung kann jedenfalls nicht aus der geläufigen MODIS-Landbedeckungs-Klassifikation im 1 km-Raster gewonnen werden. Die Verwendung solcher Deskriptoren in Modellen zur Landbedeckungs-Klassifikation kann daher zu erheblichen Fehlern führen. Dementsprechend sind MODIS-basierte-Modelle, die sich mit dem Verhalten von Wasser und CO_2 im Austausch zwischen der Landoberflächen und der Atmosphäre befassen, fehlerbehaftet oder zumindest nur mit Einschränkungen zu betrachten. Die sich dabei ergebenden Probleme der Klassifikation führen zu weiteren Schwierigkeiten in der Ansprache der Landnutzung, solange der LAI auf Annahmen der Landnutzungen als Input-Variable basiert. Auf dem Höhepunkt der jährlichen Vegetationsentwicklung erscheinen LAI-

Werte, jeweils ermittelt aus den LANDSAT-Satellitenaufnahmen und der MODIS-Modellierung als stark unterschätzt. Während des Winters treten diese Fehlerraten noch stärker ins Gewicht, sind jedoch nicht übereinstimmend für Grasland zu laubabwerfendem Wald oder Nadelwald. Die Ergebnisse lassen Zweifel aufkommen über die Nützlichkeit von MODIS LAI-Berechnungen als Inputs für Simulationsmodelle auf kontinentalem Maßstab hinsichtlich der Kohlenstoff- und Wasserbilanz. Dies gilt zumindest für das in der anthropogenen Landnutzung stark fragmentierte und heterogene Europa. Die Anwendung von MODIS-Produkten innerhalb Europas verlangt daher die hier vorgestellten neuen Technologien bei der Suche nach vergleichbaren und aggregierbaren Dateninformation zur Landnutzung und ihrer Reflexions-eigenschaften zur Bestimmung des LAI für großräumige Maßstäbe.

ACKNOWLEDGEMENTS

TABLE OF CONTENTS

LIST OF TABLES

LIST OF FIGURES

LIST OF ABBREVIATIONS

a.s.l.	Above sea level
APAR	Absorbed Photosynthetically Active Radiation
ASD	Analytical Spectral Device
AVHRR	Advanced Very High Resolution Radiometer
BRDF	Bidirectional Reflectance Distribution Function
CIR	Color Infrared
DBH	Diameter at Breast Height
DEM	Digital Elevation Model
EOS	Earth Observing System
ETM+	Enhanced Thematic Mapper Plus
FPAR	Fraction of Photosynthetically Active Radiation Absorbed by Vegetation
IFOV	Instantaneous Field of View
IGBP	International Geosphere-Biosphere Program
LAI	Leaf Area Index
LUT	Look-Up Table
MISR	Multi-angle Imaging Spectroradiometer
MODIS	Moderate Resolution Imaging Spectroradiometer
MSS	Multispectral Scanner System
NDVI	Normalized Difference Vegetation Index
NIR	Near-Infrared Region
RMSE	Root Mean Squared Error
RT	Radiative Transfer Model
SD	Standard Deviation
SLA	Specific Leaf Area
SR	Simple Ratio
TM	Thematic Mapper
TOA	Top of Atmosphere Reflectance

CHAPTER 1.   INTRODUCTION

1.1. Background

Recent studies in earth science have revealed the important role of terrestrial ecosystems in sustaining the global environment. Global vegetation, covering three fourths of the earth's land surface, has been identified as one of the key components of the climate system due to its key role in geosphere-biosphere-atmosphere interactions. The biogeochemical processes of vegetation, which involve land-atmosphere exchanges of energy, mass, and momentum, are influenced by and in turn influence the climate system (Bonan, 1996; Sellers et al., 1997). Understanding these processes is of importance for predicting future climate and the future state of terrestrial ecosystems.

It is recognized that the most important properties at the land surface for climate modeling are those that determine biogeochemical and biogeophysical processes (Hall et al., 1995). Land surface properties such as the land cover type, leaf area index (LAI), and fraction of incident photosynthetically active radiation (0.4 - 0.7 μm) absorbed by the vegetation canopy (FPAR), are used as essential inputs in many hydrological, ecological, and climate models (Sellers et al., 1995). They are key parameters that describe the functioning of vegetation and are required for modeling vegetation productivity (Gower et al., 1999), land surface climatology (Sellers et al., 1997), global carbon budgets and agricultural outputs as influenced by resource management (McVicar and Jupp, 1998). Successful modeling of these processes to quantitatively and accurately characterize global dynamics requires definition of these parameters periodically and globally with high accuracy.

Remote sensing is the most effective means of collecting information of global extent on a regular basis. Thus, satellites have a unique capability to monitor and quantify the dynamics of the earth's surface. This information can help improve the accuracy of the quantitative assessments of the above-mentioned processes. Recent studies have revealed the possibility of using remote sensing information to characterize vegetation properties, and much knowledge has been gained about the role of vegetation in environmental and climate change (Sellers et al., 1994; Bonan, 1995; Kimes, 1995; Zhou and Robson, 2001). Using radiative transfer modeling, Kuusk (1985), Verstraete et al. (1996), Myneni (1991a), and Kimes et al. (2002)

greatly improved the possibility of obtaining accurate estimates of biophysical variables from spatial, spectral, and temporal dimensions of remotely-sensed data.

Among the above-mentioned biophysical parameters, which can be derived from remote sensing data, land cover and LAI are recognized as two of the most important. They are used in all models as essential input parameters to estimate canopy photosynthesis and transpiration at global and regional scale. The first attempt to produce global land cover and LAI maps used data from the Advanced Very High Resolution Radiometer (AVHRR), which was the only satellite sensor able to observe the land surface at regional and global scales with high temporal frequency until year 2000. The first global map of LAI was produced from AVHRR data with the use of biome-dependent semi-empirical and radiative-transfer-based relations between LAI and vegetation indices (Myneni and Williams, 1994b).

Since 2000, the launch of the moderate resolution imaging spectroradiometer (MODIS) instruments onboard of Earth Observing System EOS-AM 1 platform (Terra) began a new era in remote sensing of the earth system. As a continuation of AVHRR, MODIS data will provide long term information about the earth surface, providing the chance to quantitatively and more accurately model global vegetation dynamics and to distinguish short-term and long-term trends of global vegetation change. This new sensor (MODIS) has higher spectral and angular sampling of the radiation field reflected by the earth surface. It also has a more accurate signal in terms of radiometric calibration and improved quality of atmospheric and geometric corrections (Knyazikhin et al., 1998a; b). High quality data from MODIS now provide a unique opportunity to improve accuracy when producing maps of land cover and LAI globally. The MODIS land group of the MODIS Science Team has been developing algorithms for operational retrievals of land cover, LAI, FPAR, and several other important parameters from MODIS data (Justice et. al., 1998). The synergistic algorithm for the estimation of global LAI and FPAR from MODIS (Knyazikhin et al., 1998a; b) is based on a three-dimensional formulation of radiative transfer in vegetation canopies and allows full use of information provided by MODIS (7 shortwave spectral bands) and the Multi-angle Imaging SpectroRadiometer, MISR (nine angles and four spectral bands).

1.2. MODIS Land cover Algorithms

The MODIS Land cover Product is produced at spatial resolution of 1 km. This product followed the International Geosphere–Biosphere Program (IGBP) (Loveland et al., 1999) global vegetation classification scheme. This classification defines 17 classes for the globe. The MODIS land cover classification algorithm uses a supervised classification methodology (Schowengerdt, 1997). Supervised classification algorithms are used to classify the highly-dimensional (multispectral and multitemporal) data provided by MODIS. The algorithm is based on supervised classification methodology, which uses a decision tree classification approach and exploits a global database of training sites, is a pixel-based classification process. The algorithm uses reflectance and its derived parameters such as Vegetation Indices (VIs), Bidirectional Reflectance Distribution Function (BRDF), surface temperature, etc., as input data. The spectral, radiometric, and geometric quality of MODIS data provides a significant improvement in the input feature space used for global land cover mapping. A detailed description of model and algorithm is presented in (Friedl, 2002).

1.3. MODIS LAI Algorithms

1.3.1. *Definition of LAI*

LAI is a key variable for the evaluation of evapotranspiration and is used as an input in mesoscale weather forecasts and in general atmospheric circulation models (Dickinson, 1984; Bonan, 1995)). In the literature, LAI is defined in a number of different ways. Throughout this dissertation, the following definition will be used. Leaf area index is defined as the one-sided green leaf area per unit ground area. LAI for conifer needles is defined as the projected needle leaf area per unit ground area in needle canopies (Oker-Blom et al., 1991; Chen and Cihlar, 1996). Quantitative and accurate values of LAI at regional and global scales with sufficient temporal frequency are important for quantifying mass and energy transfers at the atmosphere-biosphere interface and for characterizing and monitoring the biosphere and its functioning. As such, there is considerable interest in developing algorithms for the estimation of LAI/FPAR from satellite measurements of vegetation reflectance (Knyazikhin et al., 1998a; b).

1.3.2. LAI Algorithms

There are two methods that have been used to derive LAI from remote sensing data: empirical approaches and inversion of physical models (Price, 1993; Hall et al., 1995; Asner et al., 1998; Knyazikhin et al., 1998b). Empirical approaches are based on curve fitting in order to correlate various measures of surface reflectance, including vegetation indices, to ground-based measurements of LAI (Peterson et al., 1987; Verma et al., 1993). Many attempts have been made to combine spectral bands linearly or nonlinearly to form vegetation indices, which maximize sensitivity of the indices to LAI, while minimizing the sensitivity to unknown and undesired canopy characteristics (e.g., background reflectance). Among the various vegetation indices, the normalized difference vegetation index (NDVI) and the simple ratio (SR) are most frequently used to derive LAI from remote sensing data (Myneni and Williams, 1994a; Chen and Cihlar, 1996). LAI is nonlinearly proportional to NDVI, while it is linearly related to SR (Myneni et al., 1997b). Numerous studies have described the relation of vegetation indices to LAI of agricultural crops, grass, and deciduous forests (Asrar et al., 1984). There are even several studies relating Landsat Thematic Mapper (TM) and AVHRR data (Chen, 1996) to LAI of conifer stands. The limitations of empirical methods have been well studied. No unique relationship between LAI/FPAR and the vegetation index is generally applicable everywhere because the reflectances of plant canopies also depend on other factors, such as measurement geometry and spatial resolution (Asrar et al., 1992; Price, 1993; Friedl, 1995; Friedl, 1996). These empirical relationships are, therefore, site- and sensor-specific, and are consequently unsuitable for application to large areas or in different seasons (Gutman, 1991; Gobron et al., 1997). In addition, soil background, as well as sun-earth-sensor configuration and atmospheric effects can have a large effect on the variation of vegetation indices (Kaufman, 1989; Yoshioka et al., 2000).

Another approach is to use physically-based models (or canopy reflectance models) to describe the propagation of light in plant canopies, and subsequently to retrieve biophysical parameters. Physical models attempt to define the relationship between leaf, canopy, and biophysical characteristics such as LAI/FPAR and reflected radiation. These models can be subdivided into four classes: (i) radiative transfer models (Myneni, 1991b; Goel and Kuusk, 1992), (ii) geometric models (Li and Strahler, 1986, 1992), and (iii) hybrid models (combinations of (i) and (ii)) (Li et

al., 1995; Chen and Leblanc, 1997; Ni et al., 1999), and (iv) Monte Carlo and complex computer simulation models (North, 1996; Govaerts et al., 1998; Lewis, 1999). Once the model is developed and tested, the understanding inferred from the models can be used to develop algorithms to relate biophysical characteristics to reflectance or its derived indices. The reflectance model can be used directly in inversion modeling, deriving the biophysical parameters (for example, LAI) from given input of reflectance. The common technique used in inversion of the model is the look-up Table (LUT) method, which pre-calculates the reflectances from all possible combinations of different parameters, as well as the geometrical combinations, and stores these values in the Table. The satellite measurements are compared with the entries of the LUT to find the best solution (best resemblance to the measured set). Model inversion, which is thought to have some advantages over the empirical techniques, has been used for the estimation of MODIS LAI, because it relies on fewer assumptions and is based on fundamental physical theories (Privette et al., 1994; Gobron et al., 1997; Knyazikhin et al., 1998a).

1.3.3. The MODIS LAI/FPAR Algorithm

The MODIS LAI/FPAR algorithm is developed for estimation of global LAI and its closely related biophysical parameter FPAR. The algorithm was implemented for operational processing prior to the launch of Earth Observation System (EOS) Terra. A three-dimensional (3-D) formulation of the inverse problem underlies this algorithm in order to improve description of natural variability of vegetation canopies (Knyazikhin et al., 1998a; b). A complicated 3-D radiative transfer problem was split into two independent, simpler sub-problems using the Green's function and adjoint formulation (Knyazikhin et al., 1998a; b). In the model, three processes within a vegetation canopy were formulated in accordance to the law of energy conservation: canopy transmittance, reflectance, and absorptance. In this manner, the model provides the independence of the retrieval algorithm to any particular canopy radiation model. A detailed description of model and algorithm is presented in Knyazikhin et al. (1998a; b).

1.4. Statement of the Research Problems

The MODIS LAI/FPAR product has been operationally produced since the launch of Terra in December 1999. The performance of the algorithm must be

assessed as appropriate data become available, since the MODIS LAI/FPAR products are widely used by the science community interested in global change questions. Because land cover and reflectance data are used as input into the MODIS LAI algorithm, the first steps must include an assessment of the MODIS reflectance and MODIS land cover products. Then, assessment of performance of the MODIS LAI algorithm can be carried out via the use of ground truth data, considering the effects of spatial resolution on LAI retrievals as well as the accuracy of MODIS land cover and reflectance on LAI retrievals.

1.4.1. Assessment of MODIS reflectance product

Accuracies and uncertainties of surface reflectances used in the algorithm strongly influence the quality of retrieved LAI. The radiance measurements at the sensor require corrections for spectral calibration and atmospheric effects, and this introduces uncertainty in surface reflectances. The MODIS LAI estimates depend on the sensitivity of a canopy radiation model to respond correctly to the observed variability in surface reflectances. This research will answer the following questions: (1) How well does MODIS reflectance characterize the land surface, i.e. does MODIS reflectance correspond to Landsat reflectance, which is used as a reference baseline? (2) What is the effect of uncertainties in the geo-referencing process of the MODIS image on the retrievals of surface reflectance?

1.4.2. Assessment of MODIS land cover product

Accuracies of MODIS land cover used in the LAI algorithm also strongly influence the quality of retrieved LAI. The accuracy of the land cover map derived from remote sensing data depends on the spatial resolution of data. Especially, in European landscape, most pixels at 1 km resolution are a mixture of several land cover types. This dissertation attempts to answer the following questions: (1) how accurate is the MODIS land cover description (compared to ground truth maps derived from different sources) and (2) how does data resolution and complexity of landscape influence the accuracy of the MODIS land cover map?

1.4.3. Assessment of MODIS LAI

Few attempts were conducted by the MODIS team to demonstrate the physical functionality and performance of the algorithm for LAI, and the influence of spatial resolution of the data. Existing studies were carried out in North America, Africa,

Australia, and Northern Europe, where landscapes are relatively homogeneous. This study examines the quality of MODIS LAI products at four sites which are representative for Central European landscapes. The questions that need to be addressed include: (1) what is the effect of inaccuracies in surface reflectances on the quality of retrieved LAI? and (2) what is the effect of inaccuracies in the MODIS land cover map on the quality of retrieved LAI?

1.5. Objectives and Organization of This Dissertation

The overall objective of this research is to evaluate the performance of the MODIS LAI algorithm, with special emphasis on the effects of scale and spatial resolution. To achieve this goal, evaluations of MODIS reflectance and land cover must first be addressed. Thus, this thesis is organized as follows (see also Table 1.1):

The State of the Art concerning remote sensing of vegetation properties is summarized in Chapter 2. The four chosen study sites, Hesse deciduous forest, Tharandt coniferous forest, Stubai Valley grassland, and Berchtesgaden National Park forests, and their characteristics, e.g. vegetation homogeneity at the site and especially the existing data required for the analysis, are described in Chapter 3. The sites were chosen because of their representativeness for important Central European land cover, the degree of complexity of the surrounding landscape, and the availability of long-term monitoring data around eddy covariance towers. Chapter 3 also presents methodology used in this study. In Chapters 4 through 6, the details of the research analysis are presented for several sites as shown in Table 1.1 where the details are unduly repetitive, the analysis for certain sites is only provided in comparative summary (cf. Table 1.1).

In Chapter 4, Landsat TM reflectance data were used to upscale reflectance measurements to MODIS resolution at all four sites. The performance of the MODIS reflectance product and uncertainties in surface reflectance were evaluated using available Landsat TM scenes from the four study regions. Chapter 4 examines the following hypotheses:

(1) The MODIS reflectance product characterizes the landscape in the same way as fine resolution Landsat TM does.

(2)   The complexity of European landscape does not affect the performance of MODIS reflectance algorithm.

Table 1.1. Topics in different degree of detail presented in this thesis

Topic	Chapter 4: Reflectance	Chapter 5: Land cover	Chapter 6: LAI
1. Sites analyzed with a stepwise detailed presentation of methods	Hesse, Tharandt	Berchtesgaden, Stubai Valley	Berchtesgaden, Hesse, Tharandt, Stubai Valley
2. Sites described only in a comparative summary across sites	Berchtesgade, Stubai Valley	Hesse, Tharandt	

In Chapter 5, land cover classification at the Berchtesgaden and Stubai Valley sites is described in detail as derived using Landsat TM data. The classification is done with different methods, which allows one to address the advantages and disadvantages of the supervised method used by the MODIS team. The best classification method is then utilized for all four sites using Landsat TM. The land cover maps derived from Landsat TM images were upscaled to MODIS resolution to facilitate an assessment of the quality of the MODIS land cover product. Three aspects are brought into scrutiny: (1) the relation between land cover heterogeneity and spatial resolution, (2) a statistically based method for scaling land cover to MODIS resolution, and (3) the impact of heterogeneity on the accuracy of MODIS land cover retrievals. Chapter 5 examines the alternative hypotheses:

(1)   The MODIS land cover product permits adequate differentiation of European land cover types.

(2)   The fragmentation and roughness of European landscapes confines the robustness of MODIS land cover algorithm and limits its usefulness.

In Chapter 6, ground-based LAI data are used that were collected at the four European study sites from 2000 to 2003 by different methods. The measured data were aggregated to 1km resolution via upscaling strategies. After scaling up the fine resolution LAI to MODIS resolution, a pixel-by-pixel comparison method is introduced, which is easily implemented on a routine basis for validation. The effect

of misclassification of MODIS land cover is also examined. Chapter 6 evaluates the hypotheses:

(1) Despite coarse resolution, MODIS LAI product characterizes well the leaf area index (biomass) of vegetation in European landscapes.

(2) Fragmentation and roughness of the landscape decreases the accuracy of the MODIS LAI algorithm.

Conclusions from the investigations in Chapters 4 through 6 are summarized in Chapter 7.

CHAPTER 2.   STATE OF THE ART: REMOTE SENSING OF VEGETATION

2.1. Introduction to remote sensing

Remote sensing is a very broad field of studies. Some of the important applications of remote sensing technology are with respect to:

- Global change detection and monitoring (global warming, deforestation, flooding, atmospheric ozone depletion, biomass)

- Meteorology (atmosphere dynamics, weather prediction)

- Mapping (topography, land use, leaf area index)

- Forest and agriculture (vegetation condition, yield prediction)

- Environmental assessment and monitoring (hazardous waste, soil erosion)

Remote sensing has been described in many aspects by numerous authors, cf. review by Campbell (1996) and (Lillesand et al., 2004). One of the most cited definitions was provided by Colwell (1997), who identified the central concepts of remote sensing:

"Photogrammetry and remote sensing are the art, science and technology of obtaining reliable information about physical objects and the environment, through a process of recording, measuring and interpreting imagery and digital representations of energy patterns derived from noncontact sensor systems"

This definition serves well as a description of remote sensing as used in this thesis, e.g. by mean of discernment of information about some entity or object properties on the earth's surface, using data acquired from equipment mounted on tower, aircraft, or satellites without physical contact. Remote sensing systems, particularly those deployed on satellites, provide a repetitive and consistent view of the earth that is invaluable to monitoring the earth system and the effect of human activities on the earth.

Thus, remote sensing makes use of electromagnetic radiation reflected or emitted from the earth's surface. The strongest source of electromagnetic radiation is the sun, which emits radiation over the entire electromagnetic spectrum (see Table 2.1). Besides passive remote sensing which uses this natural source of illumination, it is also possible to use an artificial source of electromagnetic radiation;

in this case we speak of active remote sensing. In the context of this study, only passive remote sensing data were used. When the radiation reaches the surface of the earth, part of it will be reflected. Another part will be absorbed and subsequently emitted, mainly in the form of thermal (far infrared) energy. The fraction of the irradiance that is reflected (or absorbed and re-emitted) is dependent on wavelength and differs for each material, as is illustrated in Fig. 2.1. By measuring the amount of electromagnetic radiation that is reflected or emitted and comparing it to the spectral reflectance curves of known materials, information about the earth's land and water surfaces can be derived.
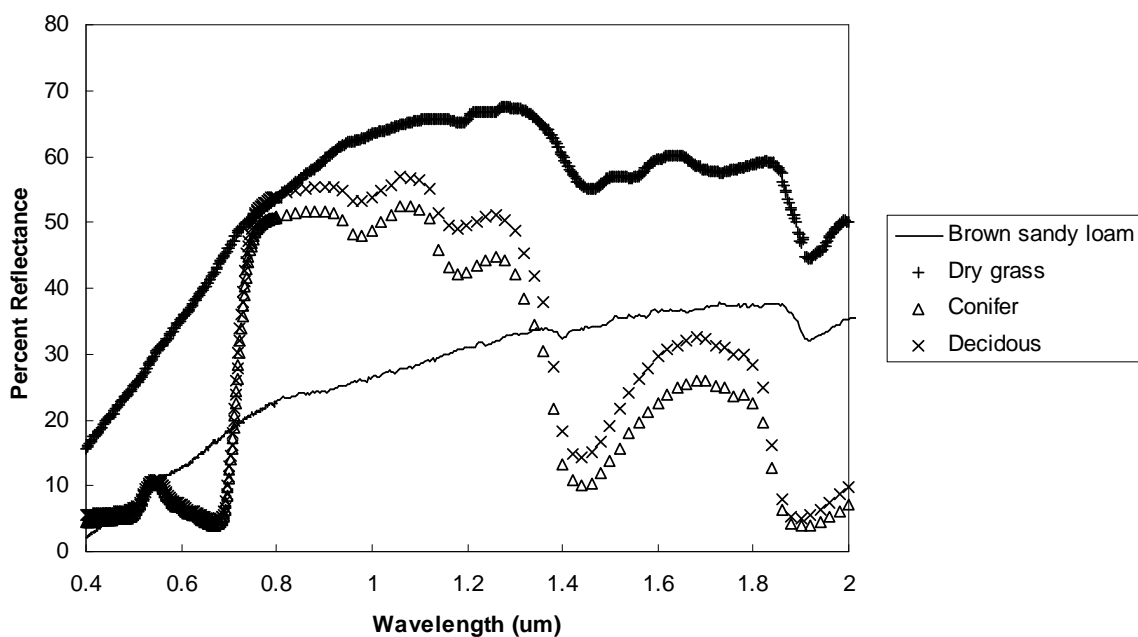
Figure 2.1. Spectral reflectance curves for four different materials (ASTER Spectral Library).

To measure the reflected and emitted radiation, usually an imaging scanner aboard an airplane or satellite is used. The details of sensor construction vary with the wavelength of interest, and the dimension of the optical systems; and detectors are subject to the technical limitations in particular spectral regions. However, all passive remote sensing sensors operate on the same principles of optical radiation transfer, photon detection, and formation of images. Basically, there are three types of passive imaging scanners; e.g., line, whiskbroom, and pushbroom scanners.

The line scanner uses a single detector to scan the entire scene. It uses scan mirror to direct the surface radiation onto an electronic detector, taking a measurement at regular intervals (Floyd, 1987).
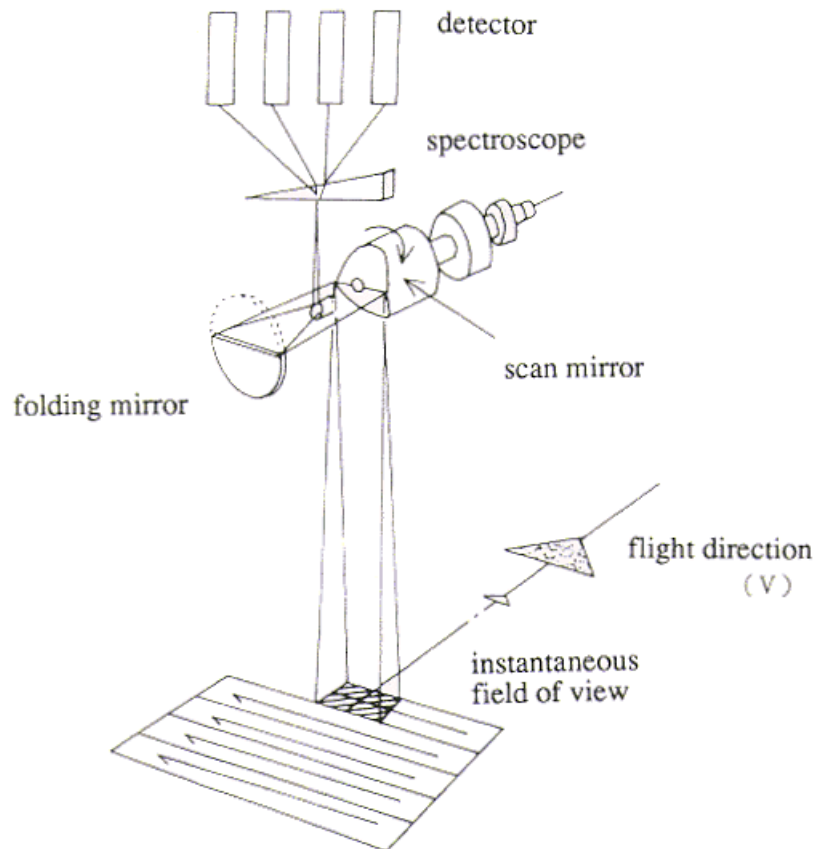
Figure 2.2. A line scanner uses a scan mirror to direct the radiation inside the instantaneous field of view (IFOV) towards a spectrometer.

Fig. 2.2 shows an example of a multispectral line scanner. The incoming energy is dispersed into a spectrum and led to detectors that are sensitive to specific wavelength bands. Rotation of the scan mirror moves the instantaneous field of view (IFOV) cross-track, while the in-track movement is provided by the platform motion. Whiskbroom scanners, such as the Landsat TM, use several detectors, aligned in-track, to achieve parallel scanning. The pushbroom scanner, such as SPOT, uses a linear array of detectors aligned cross-track - usually Charge-Coupled Devices – to take a number of measurements simultaneously over the full width of the scene. Apart from these cross-track readings, scanners also take measurements in the in-track direction, which is defined by the platform's motion (Landsat 7 science data users' handbook,

Line and whiskbroom scanners clearly have many motions occurring during acquisition of the image (mirror rotation, earth rotation, satellite roll) and consequently require some complex post-processing to adjust to accurate geometry. With some effort, this two-dimensional grid of measurements can be transformed into a digital image consisting of picture elements or *pixels*. Every pixel represents an average in each of three dimensions: space, wavelength, and time. Not only do the corresponding ground locations of the measurements have to be corrected due to factors like the earth's curvature and irregular movements of the scan mirror and the platform (geometric corrections), but the measurements themselves must also be corrected for atmospheric and sensor effects (radiometric corrections). The resolution of the resulting image or series of images, which expresses the level of fine detail that can be distinguished, has four aspects. (Floyd, 1987).

Table 2.1. Principal divisions of the electromagnetic spectrum (Campbell, 1996)

Division	Wavelengths
Gamma rays	< 0.03 nm
X-rays	0.03 - 3.0 nm
Ultraviolet	3.00 - 380 nm
Visible	0.38 - 0.72 µm
Blue	0.40 - 0.5 µm
Green	0.50 - 0.6 µm
Red	0.6 0 - 0.7 µm
Infrared	0.72 - 1000 µm
Near infrared	0.72 - 1.30 µm
Mid infrared	1.30 - 3.00 µm
Far infrared	3.00 - 1000 µm
Microwave	0.10 - 30 cm
Radio	≥ 30 cm

Table 2.2. Characteristics of scanners, which are used in this study. The exact specifications may differ for other models carried by different platforms

Scanner	TM[a]	ETM[b]	MODIS[c]
Platform	Landsat-4/5 satellite	Landsat-7 satellite	Terra satellite
Scene coverage	185 x 170 km^2	185 x 170 km^2	2330 x 10 km^2
Image size	6167 x 5667 pixels	6167 x 5667 pixels	
Resolution			
- spatial	30 x 30 m^2 [d]	30 x 30 m^2 [e]	250 x 250m, 500 x 500m
- radiometric	8 bits	8 bits	12 bits
- temporal	16 days	16 days	16 days [f]
- spectral			
	Band 1: 0.45 - 0.52 µm	Band 1: 0.45 - 0.52 µm	Band 1: 0.62 - 0.67 µm
	Band 2: 0.52 - 0.60 µm	Band 2: 0.52 - 0.60 µm	Band 2: 0.84 - 0.87 µm
	Band 3: 0.63 - 0.69 µm	Band 3: 0.63 - 0.69 µm	Band 3: 0.46 - 0.48 µm
	Band 4: 0.76 - 0.90 µm	Band 4: 0.76 - 0.90 µm	Band 4: 0.54 - 0.56 µm
	Band 5: 1.55 - 1.75 µm	Band 5: 1.55 - 1.75 µm	Band 5: 1.23 - 1.25 µm
	Band 6: 10.4 - 12.5 µm	Band 6: 10.4 - 12.5 µm	Band 6: 1.63 - 1.65 µm
	Band 7: 2.08 - 2.35 µm	Band 7: 2.08 - 2.35 µm	Band 7: 2.10 - 2.15 µm
		Panchromatic: 0.52 - 0.90 µm	

a Thematic Mapper.
b Enhanced Thematic Mapper.
c Moderate Resolution Imaging Spectroradiometer.
d Spatial resolution of band 6 is 120 x 120 m^2
e Spatial resolution of band 6 is 60 x 60 m^2, panchromatic band is 15 x 15 m^2
f Quasi repeat time is 2 days

The *spatial resolution* is the ground area that is represented by a single pixel; this area is approximately equal to the geometrical projection of a single detector element at the earth's surface, which is sometimes called the *instantaneous field of view* (IFOV) (Campbell, 1996).

The *radiometric resolution* is defined by the number of brightness levels that can be distinguished by the sensor. Radiometric resolution is dependent on the number of bits into which each measurement is quantified and stored.

The *spectral resolution* denotes the width of the wavelength interval at which the electromagnetic radiation is recorded. If a *multispectral* (e.g. TM) or *hyperspectral scanner* (e.g. AVIRIS) is used, which takes measurements in a few up to several hundreds of spectral bands, the spectral resolution may well not be unique (c.f. TM bands 3 and 4) (Campbell, 1996).

The *temporal resolution*, finally, only applies to time series of images and describes the length the interval between two successive recordings of the same scene. In case the scanner is carried by a satellite, the temporal resolution is determined by the satellite's orbit.

The characteristics of scanners used in this study are listed in Table 2.2.

2.1.1. Landsat data

The modern era of earth remote sensing began with the first Landsat Multispectral Scanner System (MSS) in 1972, which provided for the first time a consistent set of high-resolution earth images. The characteristics of this sensor were multiple spectral bands with reasonably high spatial resolution (80 m), large area (185 by 185 km) and repeating coverage (18 days).

After the first MSS system, we have seen four additional MSS systems, as well as the Landsat Thematic Mapper (TM) and Enhanced Thematic Mapper (ETM) with 30 m spatial resolution and 7 spectral bands (see Table 2.2) (Landsat 7 science data users handbook,

http://ltpwww.gsfc.nasa.gov/IAS/handbook/).

2.1.2. MODIS data

The MODerate Imaging Spectroradiometer (MODIS) system, launched in 1999 onboard the Terra satellite, provides images in numerous spectral bands over a range 0.4 to 14 µm. The sensor significantly improves the quality of information that

can be gathered about the earth's surface and near environment. The sensor is also important for monitoring global dynamics of vegetation, the atmosphere and global warming due to its daily coverage of the earth's surface (MODIS technical specifications, *http://modis.gsfc.nasa.gov/*) (see Table 2.2).

2.2. Remote sensing of vegetation

Approximately 70 % of the Earth's land surface is covered with vegetation. Knowledge about variation in species and community distribution patterns, change in vegetation phenological cycles, and natural modifications in plant physiology and morphology provide invaluable insight into climatic, geological and physiographic characteristics of an area (Jones et al., 1998). By using remote sensing data, vegetation can be distinguished from most other (mainly inorganic) materials by its nature of notable absorption in the red and blue segments of the visible spectrum, its higher green reflectance and, especially, its very strong reflectance in the near-IR. Different types of vegetation show distinctive variability from one another owing to such parameters as leaf shape and size, overall plant shape, leaf water content, and associated background (e.g., soil types and density of vegetative cover within the scene).

2.2.1. Leaf reflectance

The reflectance from a leaf is determined by the leaf structure as well as the biochemical constituents of the leaf. To understand the optical properties of a leaf, studies at a detailed level must be undertaken, see Fig. 2.3.

The cell structure of leaves is highly variable depending upon species and environmental condition during growth. A typical leaf consists of several different layers with diverse optical characteristics. The uppermost layer, the upper epidermis, consists of cells fitted closely together. The other side of the leaf consists of the lower epidermis that has openings in the cell layer called stomata, which allow an exchange of water and carbon dioxide with the atmosphere. A wax layer called the cuticle covers the upper cell layer. Below the upper epidermis is the palisade layer that consists of cells rich in chlorophyll. The chlorophyll along with other pigmentation molecules is situated in organelles called chloroplasts. These organelles are vertically arranged in the palisade layer. Below the palisade layer is the spongy mesophyll tissue. It consists of irregularly shaped cells separated by

connected air spaces. This gives the tissue a very large surface area. Leaf structure is not identical for all plants but this description gives a general idea of the major elements common to most species.

In the visible region of the spectrum the chlorophyll content controls the optical properties of the leaves. The chlorophyll absorbs the sunlight that makes photosynthesis possible. It is most absorptive in the blue and red regions. Here, as much as 70 to 90 % of the incident radiation is removed. In the green region, the absorption is lower, which allows a large portion of the green light to be reflected. That causes healthy green foliage to appear green to the human eye.

In the near infrared spectrum, leaf reflectance is controlled by the structure of the spongy mesophyll tissue. In this region, the healthy green leaf is characterized by high reflectance (40 – 60 %), high transmittance (40 – 60 %) through the leaves onto underlying leaves, and relatively low absorptance (5 – 10 %). Notice that a healthy green leaf reflectance and transmittance spectra throughout the visible and near-infrared spectrum are almost mirror images of one another. The cuticle and epidermis are nearly completely transparent to infrared radiation. Radiation passing through the upper epidermis is strongly scattered by the mesophyll tissue and the cavities at the cell wall to air interface within the leaf (Peterson and Running, 1989). Very little radiation is absorbed and most is scattered upwards (reflected). Downward scattering leads to transmittance. As illustrated in Fig. 2.4, the reflectance in the near-infrared region (NIR) is greater than the reflectance in the visible region. Differences in reflective properties of plant species are more pronounced here than in the visible region (Campbell, 1996).

In the longer infrared wavelengths (beyond 1300 nm), leaf water content appears to control the spectral properties of the leaf. The term equivalent water thickness has been proposed to designate the thickness of a film of water that can account for the absorption spectrum of leaf at 1400 to 2500 nm. However, results from Gao and Goetz (1995) indicate that it is not only water content that is responsible for the optical properties in this spectra but also, to some extent, the content of lignin.

a)
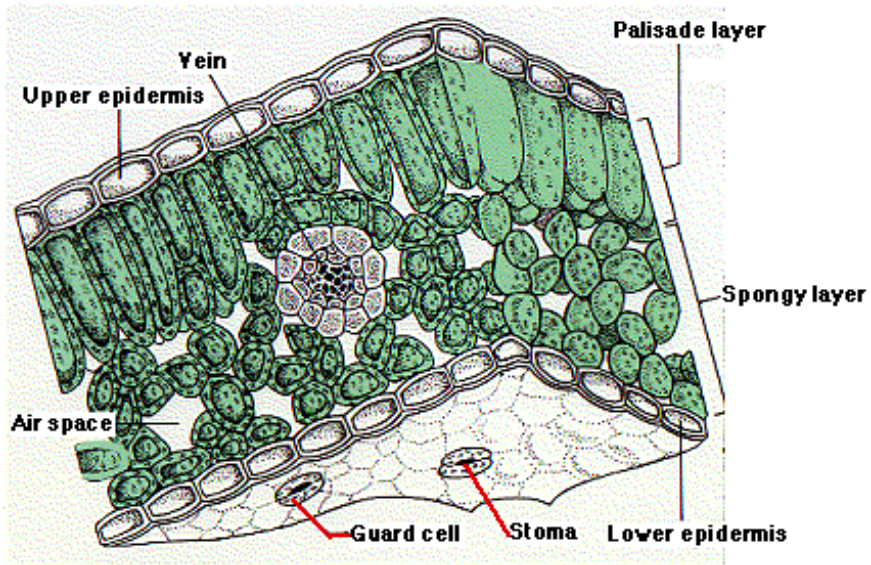
b)
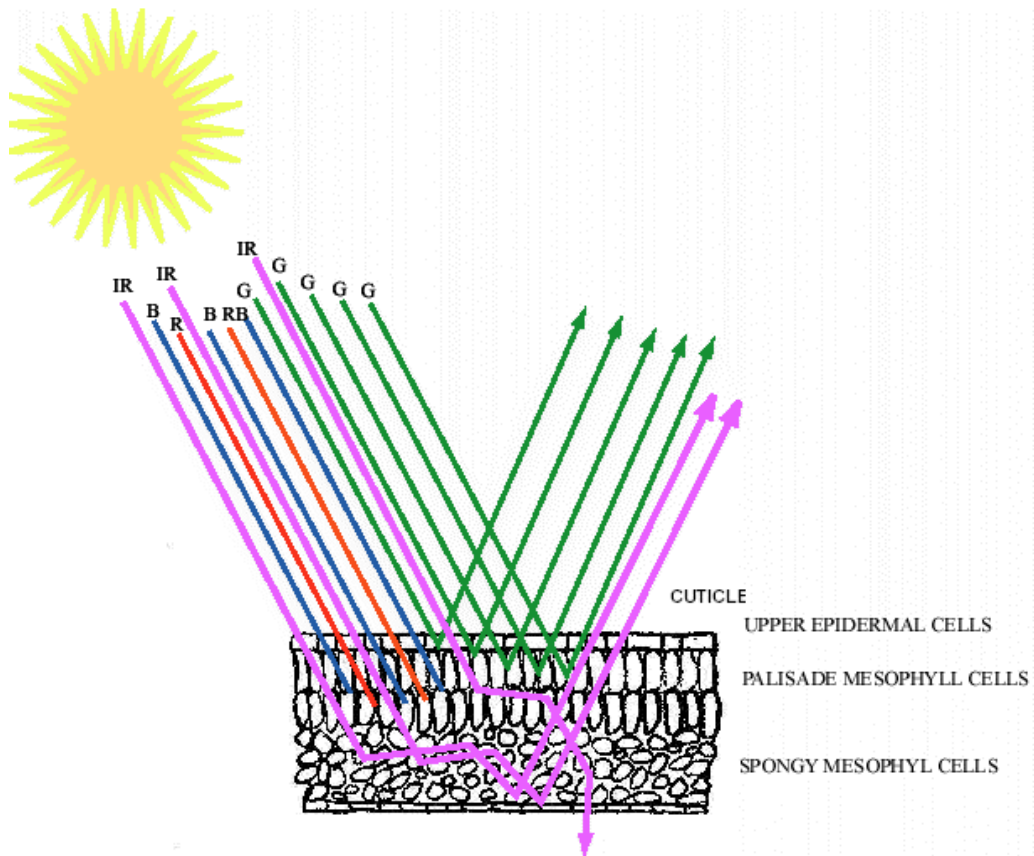
Figure 2.3. (a) Cross section of a typical leaf, and (b) its interaction with sunlight (Kimball, 2005).
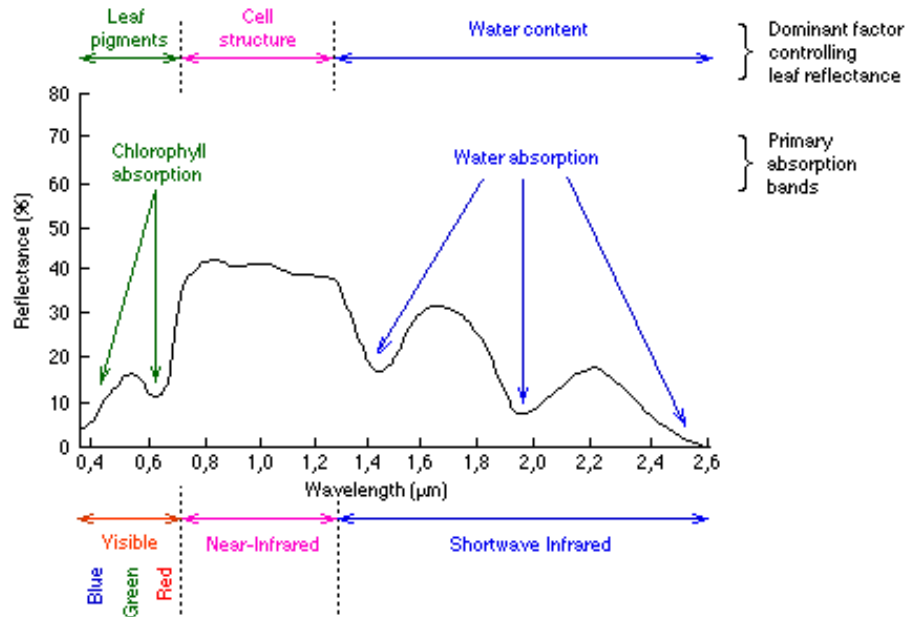
Figure 2.4. Typical spectral response characteristics of green vegetation.
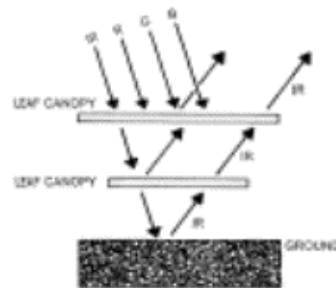
Figure 2.5. Simplified illustration of behaviour of energy interacting with canopy. In the NIR, radiation transmitted through the top layer is available for reflection from lower layers (Campbell, 1996).

2.2.2. Canopy reflectance

In the field, a vegetation canopy is composed of many layers of leaves, branches, stems and understory vegetation. Each of these components is variable and, therefore, the reflectance from a canopy varies considerably from the reflectance of a single leaf. Leaves may vary in size and orientation, which leads to shadowing of various canopy elements, such as leaf, soil and understory vegetation. This decreases reflectance below the values measured from single leaves, see Table 2.3 and Fig. 2.6. However, the relative decrease is much lower in the NIR

region than in the visible region. This is due to the optical properties of leaves in the NIR region.

Table 2.3. Single leaf and canopy reflectance measured in Hesse, 2002

	Percent Reflected	
	Visible	Near infrared
Single leaf	5.5 %	65 %
Canopy	3.0 %	40 - 45 %

**Leaf and canopy reflectance
Hesse 7/2002**
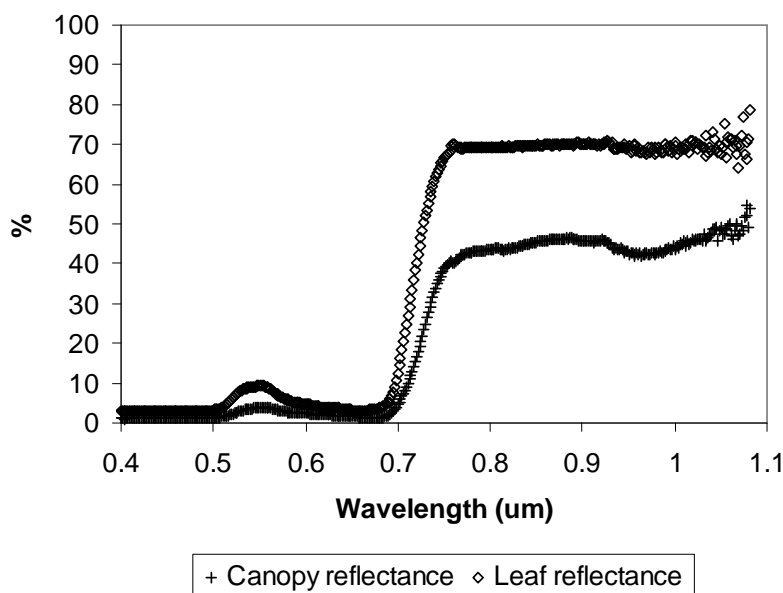
Figure 2.6. Canopy reflectance is lower than single leaf reflectance due to canopy structure.

The part of the radiation that is transmitted in the top layer of leaves is re-scattered on the next layer and transmitted back through the first layer. Therefore, infrared radiation passes back through the upper leaves, resulting in a high reflectance (Campbell, 1996), see Fig. 2.5. This effect is called leaf additive reflectance.

Other factors affecting the reflectance from a surface are the view angle and the illumination angle (Deering, 1989). The effect of reflectance variation due to

changes in these variables is described by the BRDF. The reflectance model takes all of the above variables into account when calculating the reflectance from a forest collection, i.e., it calculates the BRDF in specified view and illumination. The BRDF often yields a peak of reflectance, if the source of illumination (the sun) is directly behind the sensor. This peak in reflectance is called "the hot spot". A typical BRDF is illustrated in Fig. 2.7 where the hot spot is seen with increased reflectance in the right part of the figure. It occurs because only the illuminated parts of an object are viewed by the sensor (Deering, 1989).
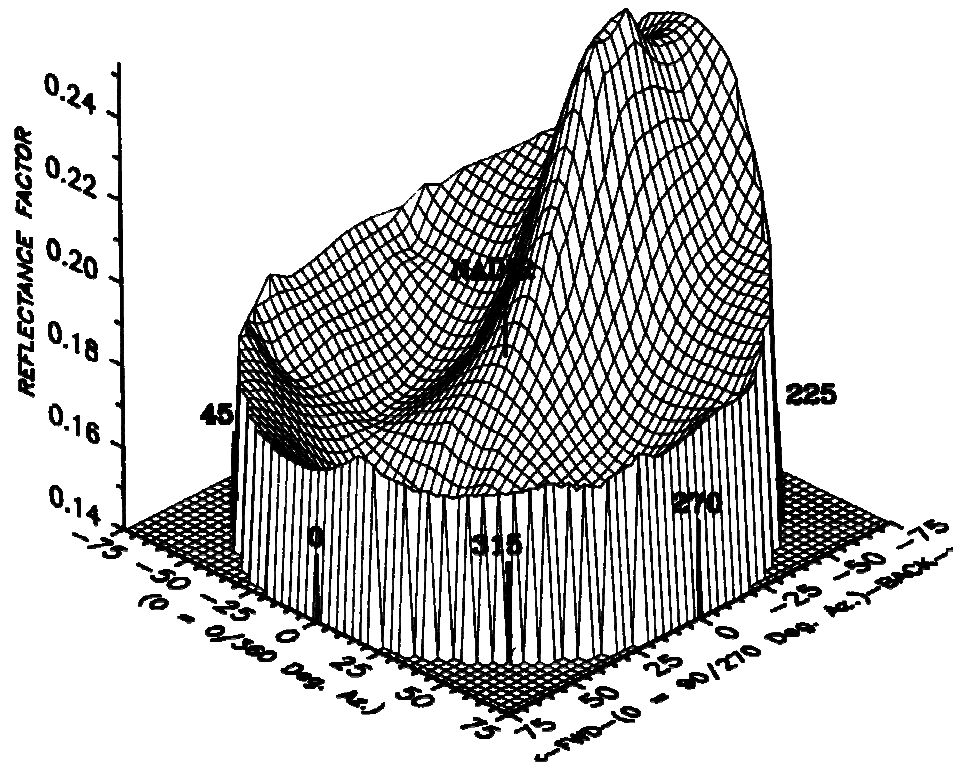
Figure 2.7. Oak-rangeland community bi-directional reflectance surface for 826 nm (Deering, 1989).

2.2.3. Applications of remote sensing of vegetation

The use of remote sensing data for vegetation study can be seen in two ways. The traditional approach is called image-centered. Its primary purpose is in determining spatial relationships among objects and features on the ground. In fact, the goal of image-centered analyses is creation of a map. Previously, aerial photographs were analyzed by photointerpretation. This process requires experience of the analyst, who distinguishes the differences in features of interest (Campbell, 1996).

With remote sensing data now available in digital form, the use of computers and image processing software for information extraction is a standard practice. In the last three decades, image classification to create thematic maps is a common application for remote sensing data in vegetation studies. Various degrees of success in image classification has been achieved with different sources of images at different scales, from species mapping at stand scale to land cover mapping at regional, continental, and global scale (Gopal et al., 1999; Sandmeier and Deering, 1999; Thomlinson et al., 1999; Friedl, 2002; Ballantine et al., 2005; Giri et al., 2005). Traditionally, pixel-based classification is a standard approach towards land cover classification. The method is based on the statistics of spectral similarities of each pixel in the image. Those pixels having similar spectral properties belong to the same class. The most used pixel-based classifiers are: K-means clustering (unsupervised training) and maximum likelihood (supervised training). The pixel-based classification is suitable for medium to coarse resolution remote sensing data.

In practice, however, it proves difficult to classify high-resolution images with a pixel-based method due to the high level of information captured by these images (de Jong et al., 2000; Blaschke and Strobl, 2001; Hofman, 2001; Limp, 2002). Important semantic/spatial information required to interpret the image is not accounted for by the pixel-based classification algorithms. In the past two decades, various segmentation techniques have been developed to incorporate context, texture, and neighborhood information into the image classification procedure (Janssen, 1993). The new software package eCognition (eCognition, 2002) brings together several of these contextual and object-oriented approaches and gives promising results for high-resolution image analysis (Baatz and Schäpe, 2000). This new method used in the current study, first extracts image objects by segmentation. The segments are subsequently classified using combinations of spectral and spatial information (Baatz and Schäpe, 2000).

The second approach applied in remote sensing of vegetation is called data-centered. Here, the information inferred from remote sensing data itself is of interest, rather than the spatial relationship of features on the ground. The most common approach is to make use of the reflectance measurement from remote sensing data for deriving biophysical parameters, either by applying empirical or process-based models. For example, an algorithm based on the physics of radiative transfer in

vegetation canopies was developed and implemented for the retrieval of vegetation green leaf area index (LAI) and fraction of absorbed photosynthetically active radiation (FPAR) from MODIS surface reflectances (Myneni et al., 2002) at global scale, or from Landsat TM reflectances (Eklundh et al., 2001; Fang et al., 2003) at stand scale. In the same manner, chlorophyll content and water content can be estimated from hyperspectral reflectance measurements, Landsat TM reflectances, and MODIS reflectances data using empirical (Hu et al., 2004) and radiative transfer models (Jacquemoud et al., 1995; Zarco-Tejada et al., 2003; le Maire et al., 2004). Phenological cycles of vegetation can be determined by analyzing the temporal variation of NDVI from time series of satellite images (Kang et al., 2003; Zhang et al., 2003). Accurate absolute radiometric calibration and atmospheric correction is generally more important for data-centered analysis than for image-centered analysis. The results and products of data-centered analysis should also be presented in the context of spatial maps in order to fully understand the spatial distribution and behavior of the biophysical parameters.

In recent years, increasing interest in global change and in long-term monitoring of the human effects on environment has led to the use of remote sensing data at global scale (Kang et al., 2003). In this sense, the two approaches, image-centered and data-centered, converge. The requirement for global monitoring leads to the need for integration of information, which is extracted from spectral and temporal dimensions, into a spatial framework that can be used at global scale. It is particularly important in this context to ensure that the data are spatially and radiometrically corrected, is consistent over time, and is calibrated from one sensor to another.

CHAPTER 3.   STUDY SITE CHARACTERISTICS, DATA BASES AND REMOTE SENSING METHODOLOGY

3.1.   Study site characteristics

3.1.1.   Hesse

The state forest at Hesse, France (48º40´30''N, 7º03´59''E) has been extensively researched during the last decade (Baldocchi et al., 1996; Tenhunen et al., 1998; Granier et al., 2000; Valentini et al., 2000) (Fig. 3.1). The site has been included in several European carbon balance research programs, beginning with EuroFlux ('Long-term carbon dioxide and water vapor fluxes of European forests and interactions with the climate system'; (Baldocchi et al., 1996; Tenhunen et al., 1998)) and continuing currently with the CarboEurope-IP (Assessment of the European terrestrial carbon balance; *http://www.carboeurope.org/*).

The area is underlain by sandstone or limestone bedrock. The topography is classified as a plateau (elevation ranging from 260 to 350 m); with mean slope of 5 % (Fig. 3.3). The pH of the topsoil (0 – 30 cm) is 4.9 with a C/N ratio of 12.2 and an apparent density of 0.85 kg dm^{-3}, and it is covered with a mull type humus (Epron et al., 1999). The cool climate leads to a short summer with growing season of 130 – 140 days, and cold winter (-1℃ on average from December and February over a recent 6 year period). Average annual precipitation is ca. 820 mm (Granier et al., 2000).

The forest is composed mainly of naturally established beech (*Fagus sylvatica* L.) trees, which constitute more than 90 percent of the forest vegetation cover at the Hesse site. The other tree species include *Carpinus betulus* L., *Betula pendula* (Roth), *Quercus petraea* (Matt.), *Larix decidua* (Mill.), *Prunus avium* L. and *Fraxinus excelsior* L. The stand is considered to exhibit good productivity in the first class of Shrober's yield Table for beech, which predicts a mean increment of 9 m^3 ha^{-1} year^{-1} at age of 100 year (Granier et al., 2000). The understorey vegetation (mainly *Carpinus betulus*) is undeveloped due to the closed canopy. The stand was approximately 40 years old with a stand density of 3800 stems ha^{-1}, and a basal area of 19.6 m^2 ha^{-1} in 1999. The average tree height and circumference (at 1.3 m) were 12.7 and 227 mm, respectively, in 1996 (Granier et al., 2000).

Surrounding the deciduous forest area are stands with coniferous forest, areas with urban land use, agricultural land and grassland. After harvest, fields are left fallow and appear similar to bare soil and grassland (Fig. 3.2).
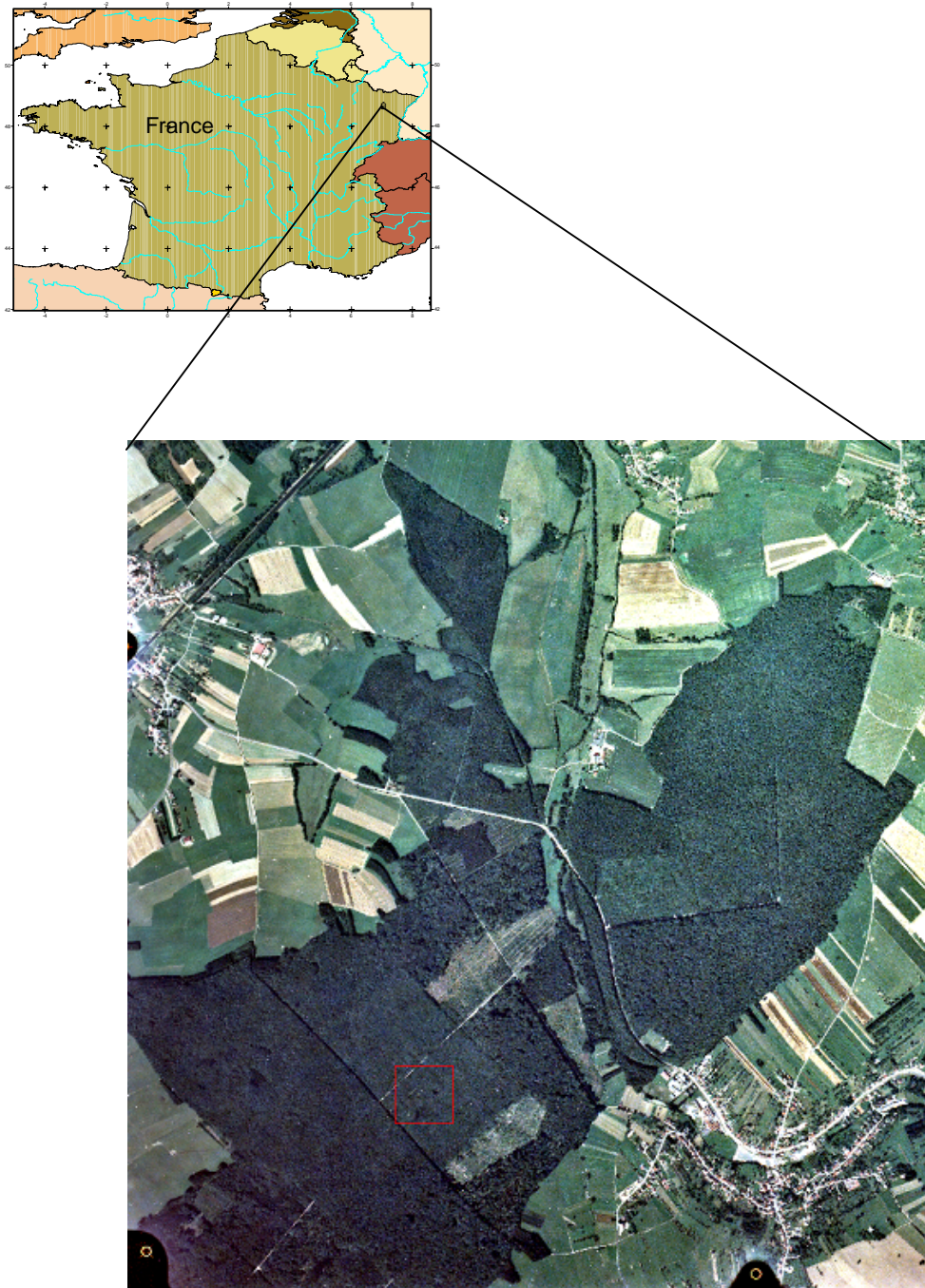
Figure 3.1. Hesse forest site in eastern France as seen from aerial photography, the red square indicates the immediate vicinity of the tower used for eddy covariance measurements.
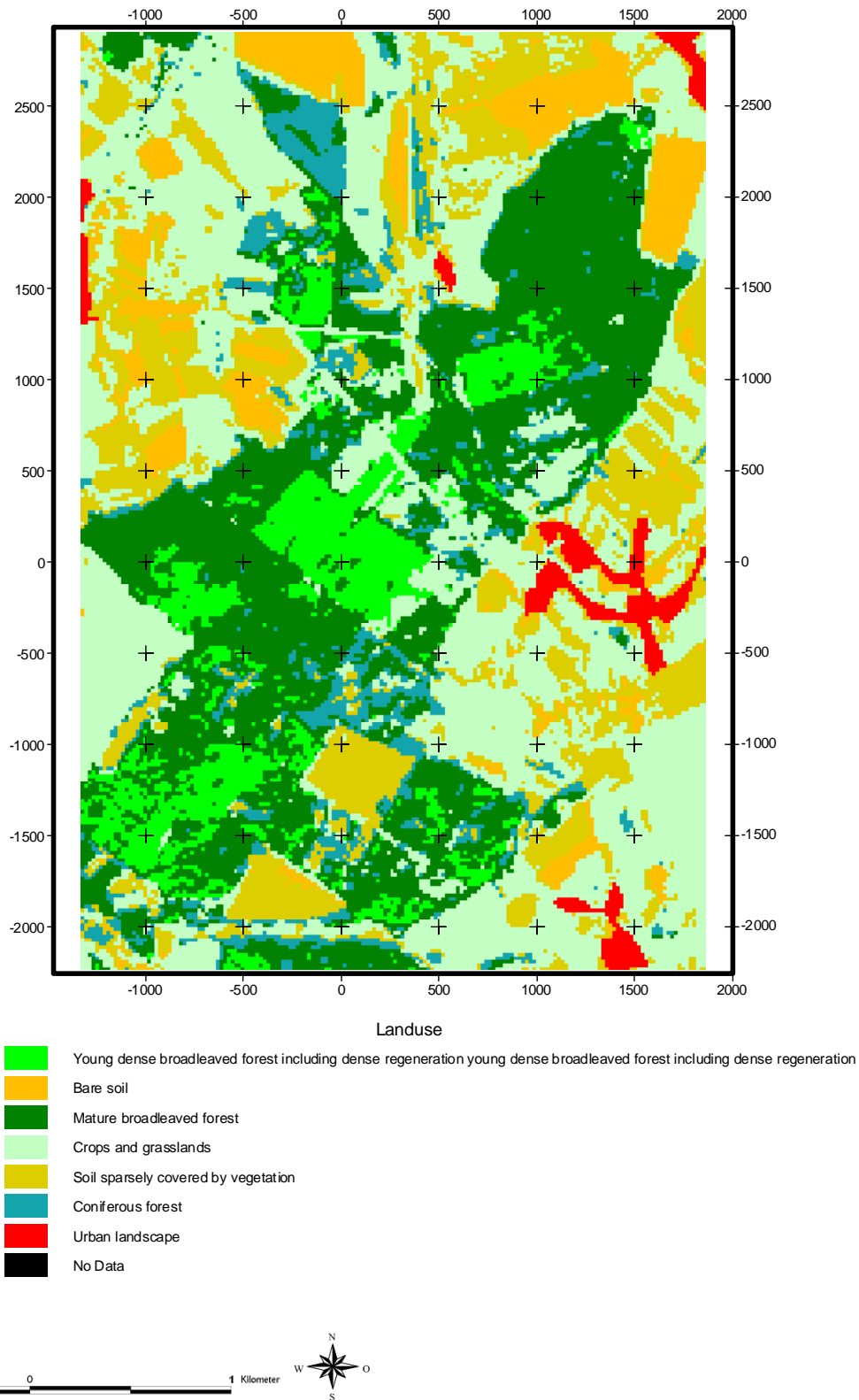
Figure 3.2. Land cover map of Hesse site derived from a SPOT image (date 24 June 2001) and aerial photo. The tower site for eddy covariance measurements is located at (0, 0) corresponding to 48°40 N, 7° 3' E. (Grani er A., personal communication, 2003).
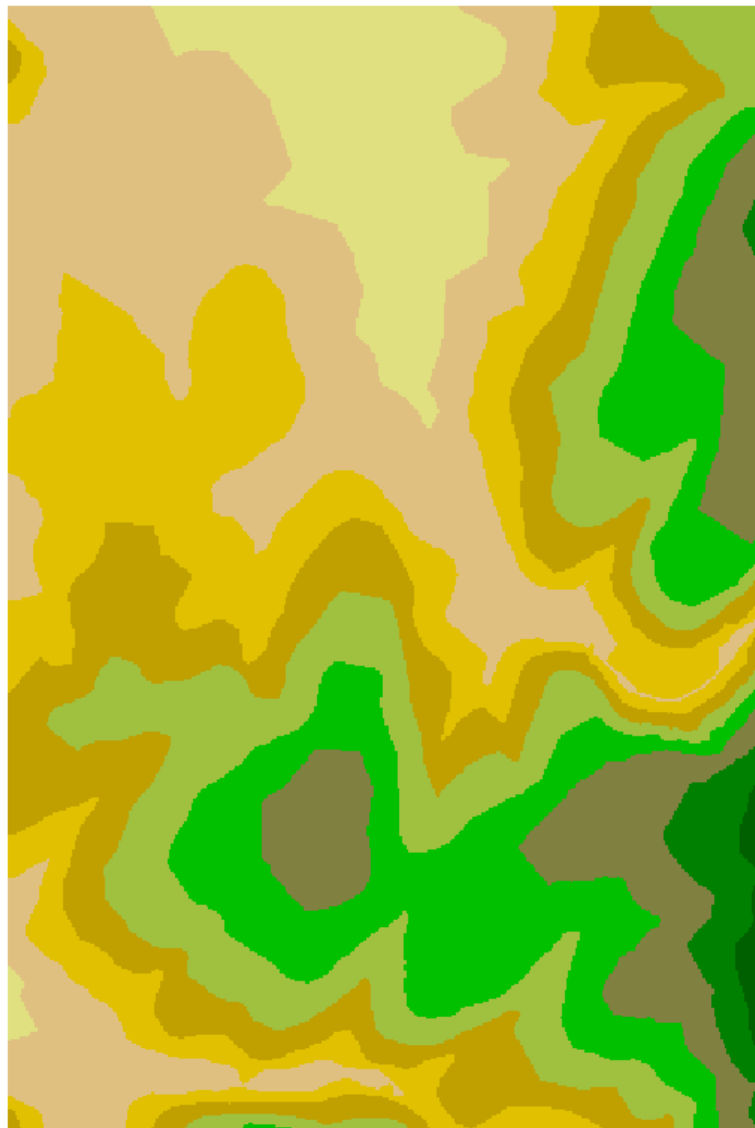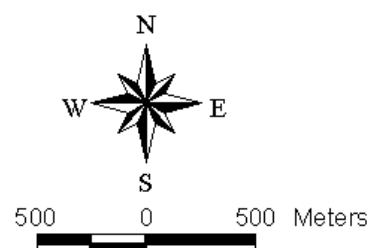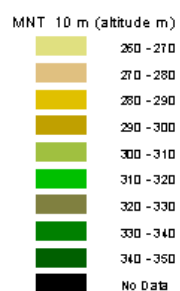
Figure 3.3. Digital elevation model (DEM) of the Hesse forest study site. (Granier, personal communication, 2003). The image corresponds to those in Figs. 3.1 and 3.2.

3.1.2.   Tharandt

The selected research area is located at the long-term Ecological Monitoring Station of the University Dresden (50°58'N 13°38'E, 380 m) (Fig. 3.4), in Tharandt Forest, 20 km SW of Dresden (Germany). The site is characterized by gentle slopes with an elevation of ca. 380 m above sea level (Fig. 3.5). The climate is temperate continental with a mean annual precipitation of 820 mm and a mean annual temperature of +7.6°C. The soils are sandy-loamy br own-earths (rhyolith type) developed on porphyry rocks with a moder humus form with sandy-loamy texture (Dystric Cambisol - FAO). The mean pH of the organic layer varied between 3.6 and 4.3 (Zaitsev et al., 2002).

The indigenous vegetation in this area is mixed forest with multiple stories that consist of spruce, beech, fir, and maple (Bitter et al., 1998). Due to the strong impact of anthropogenic activities, pure even-aged spruce forests now dominate this area, resulting in a decrease in forest diversity, and a deterioration in soil fertility (Nebe and Fiedler, 1985; Bitter et al., 1998). Some parts of the area are covered by spruce forests (*Picea abies* (L.)) mixed with a small fraction of pine and deciduous trees.

At the tower site for eddy covariance measurements of forest gas exchange, the dominant species is Norway spruce (*Picea abies*) which was planted as early as 1887. Other tree species include *Pinus sylvestris*, *Larix decidua, and Betula spp.,* but these only occupy a small area. In the spring of 1995, beech (*Fagus sylvatica*) was planted in some plots. The understorey vegetation is undeveloped due to the dense forest canopy and low soil pH. The stand age was on average 107 years in 1999 with the stand density of 444 stems*ha^{-1} near the tower site. Average tree height and breast height diameter (at 1.3 m) were 27.9 and 328 mm. The plots together with their inventory characteristics surrounding the tower site within a 0.5 km circle are shown in Fig. 3.6 in detail (Wang et al., 2004). More background information on the Tharandt site is also presented in Table 3.1.
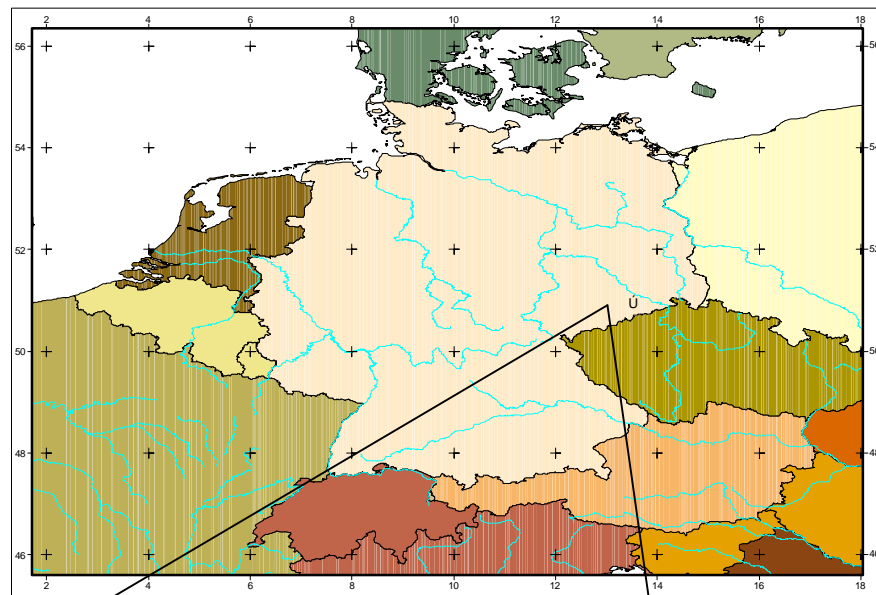
Figure 3.4. Location of Tharandt forest site in Germany
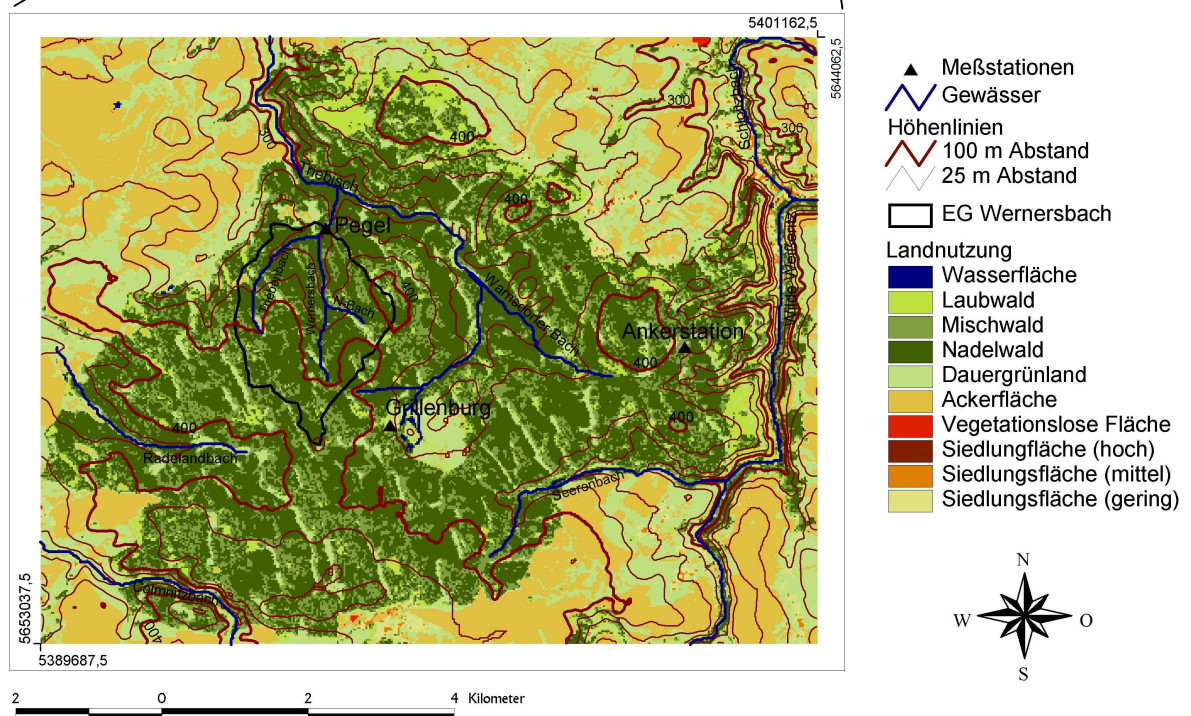
Figure 3.5. Land cover map and elevation contour of Tharandt forest site (Bernhofer C., personal communication, 2003). The grassland meadow at Grillenburg is seen clearly in the middle of the forest. Stripes in the forest vegetation result from clear cutting of the forest according to the harvest method practised, i.e., indicate early stages in forest succession after clear cut.
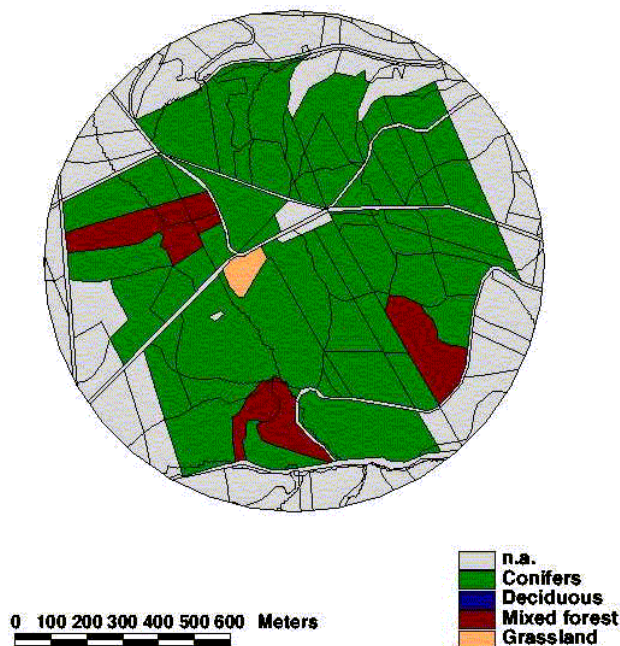
Figure 3.6. Forest stand types located within a 0.5 km circle centered on the tower used for eddy covariance measurements of gas exchange.

Table 3.1. Summary of the main characteristics of the Tharandt forest near the eddy covariance tower site

	Unit	Tharandt site
Location		50°58´N, 13°34´E
Elevation	m	380
Dominant canopy species		*Picea abies*
Stand age	years	110 (in 2000)
Canopy height	m	27.9
Tree density	ha^{-1}	477
Stem diameter	cm	33.8
LAI		8.0
Aboveground biomass	kg m^{-2}	22.7

The meadow experimental site, which is situated within the forest, covers an area of ca. 1.5 ha and is extensively managed with 2 to 3 hay harvests per year. The vegetation is dominated by the native fescue (*Festuca pratensis),* meadow foxtail *(Alopecurus pratensis)* and timothy *(Phleum pratense).* The meadow is clearly distinguishable in aerial photos and remote sensing scenes. Intensive studies of

grassland structure, e.g., time dependent changes in LAI and above and belowground biomass, have been carried out during 2004 through 2006. Meadow gas exchange is documented both with the eddy covariance technique in the context of the CarboEurope-IP project and with large chamber measurements (Mirzaei, 2008).

3.1.3. *Berchtesgaden*

The Berchtesgaden National Park (210 km^2), established in 1978 by decree of the Bavarian government, is located in south-eastern corner of Germany between 12°47'E and 13°05' E and 47°27'N and 47°45 N (Fig. 3.7). In 1990, the Berchtesgaden National Park became a UNESCO Biosphere Reserve based on existing nearly natural alpine ecosystems. The park belongs to the oldest protected areas in the Alps, and it is the only alpine biosphere reserve in Germany.

The park is a part of the Northern Limestone Alps, characterized by thick mesozoic carbonate deposits. The dominant bedrocks in this region are limestone and dolomite. The topography is classified as rough terrain, the elevations range from 603 m, at the lowland lake Königsee, to 2713 m a.s.l. at the summit of the Watzmann Mountain. The occurrence of steep, precipitous, and very precipitous slopes is much higher than found for land surface in other categories. The landscape characterized by high mountains with steep valleys illustrates recent glacial recession.

Soils are composed of many types (according to FAO classification) depending on the bedrock and landscape. Cambisols are the most frequently occurring soil type in the park, while Rendzic soils exist frequently in the areas where dolomite decomposition occurs. Cambic Podzol and Podzol are found over the radiolarian rocks. In some areas because of the influence of groundwater Stagnic Gleysol and Gley are present.

The climate of the region is characterized by both atlantic and continental influences. At high altitudes, typical mountain climate conditions prevail. The mean annual temperatures range, depending on altitude, from +7℃ (Königssee) to -2℃ on the Watzmann summit (2713 m). Annual precipitation varies between 1500 and 2200 mm; the mean annual precipitation in the region is ca. 1880 mm (Konnert, 2001).
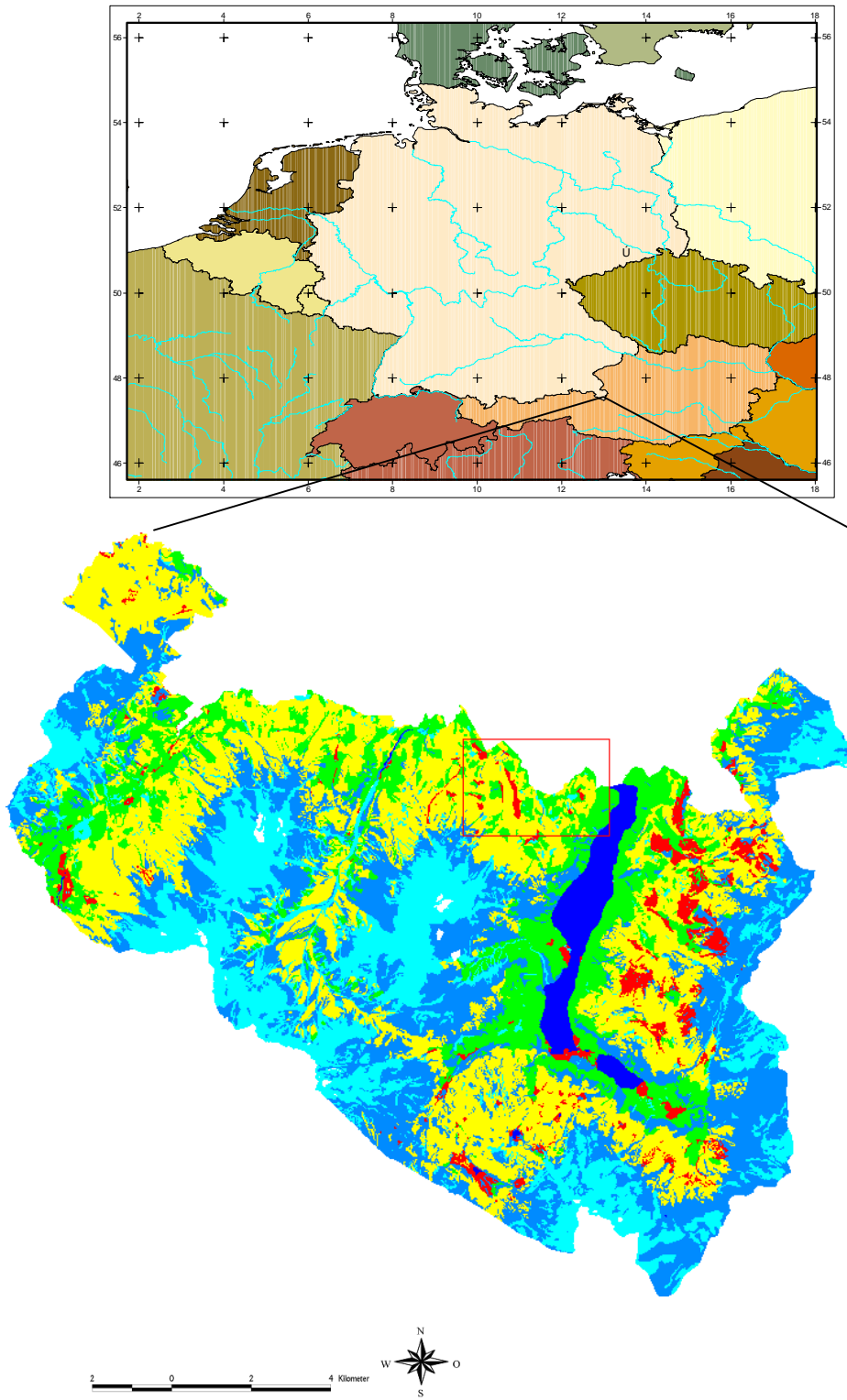
Figure 3.7. Location and land use map of National Park Berchtesgaden. Source of the map is the Berchtesgaden National Park Administration as interpreted from aerial photography during 1997 at a resolution of 1 m.

Vegetation in the National Park Berchtesgaden is strongly influenced by highly variable microclimate due to elevation gradients. This leads to pronounced altitude zonation of the vegetation. The composition of forest species changes naturally with altitude, the proportion of conifers increases going from low to high elevation (Fig. 3.7; Table 3.2).

Table 3.2. The composition of forest species at the Berchtesgaden National Park

Zone	Composition of forest species
Submontane zone (at 700 m a.s.l.)	Deciduous forests are dominant. Beech forests (*Fagus sylvatica*) are well represented. *Acer pseudoplatanus, Fraxinus, Ulmus glabra, Tilia platyphyllos* and *Alnus incana excelsior* are regularly found within the beech forests.
Montane zone 700 m a.s.l. – 1400 m a.s.l.	Comprised of mixed forest – *Fagus sylvatica, Picea abies, Abies alba* and *Acer platanoides*. In many cases coniferous forest prevail, which is due to anthropogenic impact and planting in past centuries. In the northern part of the National Park, deciduous forest and silver fir (*Abies alba)* are missing.
Subalpine zone 1400 m a.s.l. – 2000 m a.s.l.	Spruce-larch forests dominate – *Picea abies* and *Larix decidua*. In some areas of the park, (Funtensee, Steinernes Meer, Blaueistal und Reiteralm) larch-alpine pine forests (*Larix decidua* with *Pinus cembra*) occur.
Alpine zone above 2000 m a.s.l.	Wind-dwarfed bushes and alpine meadows. *Pinus mugo, Alnus viridis* and *Rhododendron ferrugineum* are very common.

The forested area and forests composition in the National Park Berchtesgaden have been also altered due to hundreds of years of human management practices. This anthropogenic impact has had the result, that in many places conifer forest dominate, and in the northern part of the park deciduous forest and silver fir (*Abies alba*) are missing. Recently, programs have been implemented that attempt to restore the forest to a more natural state.

Grassland and meadows are present in the mosaic landscape and have undergone long-term change due to management practices such as grazing and cutting. Grass and meadows communities are *Trisetetum flavescentis*, with the dominant species *Alchemilla vulgaris, Dactylis glomerata, Leontodon hispidus, Plantago lanceolata, Geranium sylvaticum,* etc*.*

In the subalpine zone, a large variety of different herbage plants grow in the pastures, the plant association being classified as Alchemillo–Cynosuretum (Oberdorfer, 1993). The main species were *Alchemilla vulgari*s, *Cynosurus cristatu*s, *Trifolium repen*s, *Phleum alpinu*m, *Poa alpin*a, *Crepis aure*a.

3.1.4. Stubai Valley

The Stubai Valley in Tirol (Austria) covers an area of 120 km^2, with the center situated at approx. 47°07' N, 11°17' E (Fig. 3.8) .

Climate

The Stubai Valley study area is characterized by temperate continental inner alpine climate with frequent precipitation and heavy thunderstorms in the summer (Zeller et al., 2000; 2001). About 50 % of the annual precipitation is snow during the winter months (Cernusca et al., 1999). Average air temperature and annual precipitation range from 6.3℃ and 850 mm to 3.0℃ and 1100 mm at the valley bottom and the treeline, respectively. Snow cover duration is approximately 100 days. The altitude ranges from 900 m at the valley to 3450 m at the top of the surrounding mountains. The study area consists mainly of medium to steep slopes exposed S to E. The bedrock consists of siliceous and calcareous deposits.
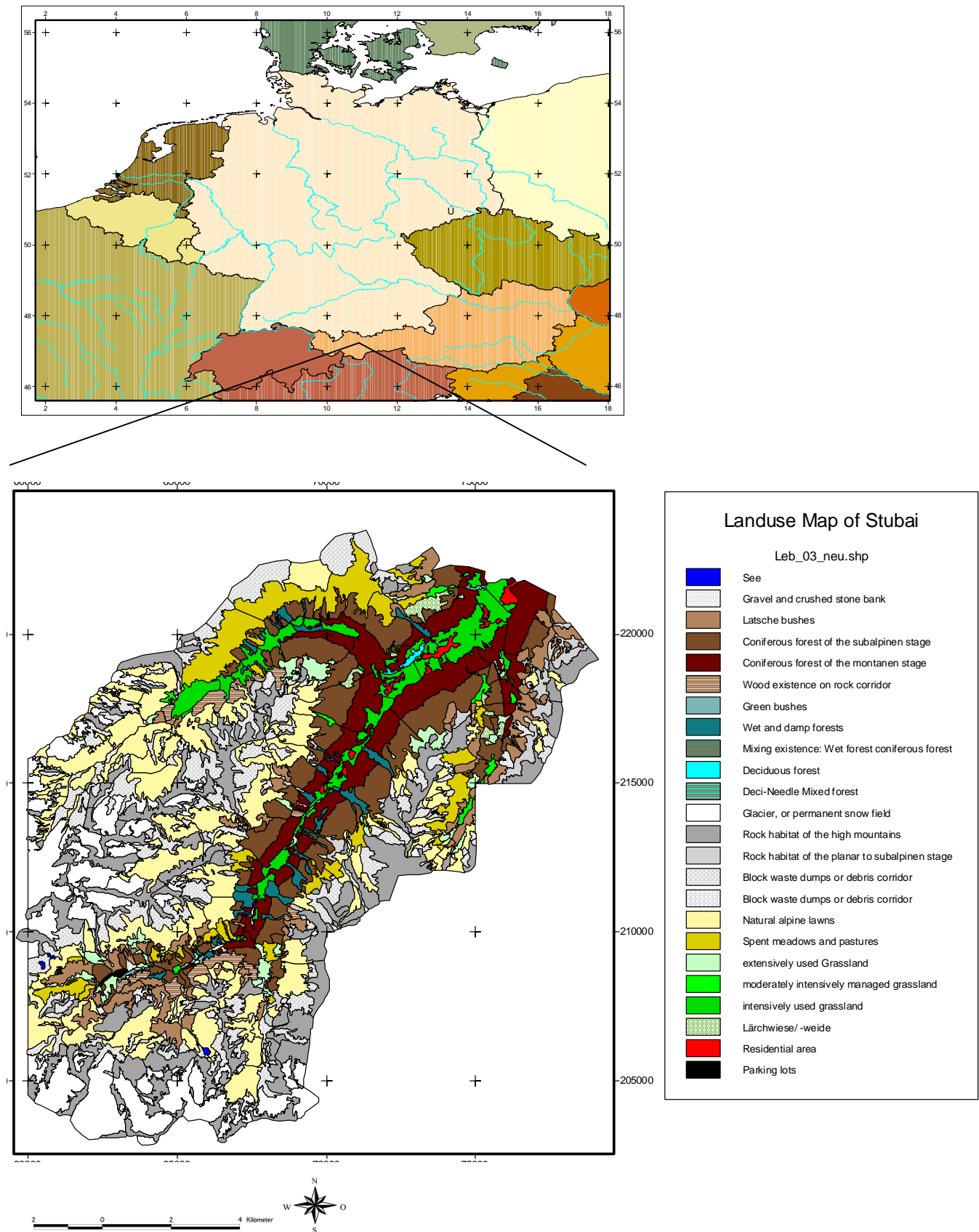
Figure 3.8. Location and land cover map of Stubai Valley (Wohlfahrt, 2004).

The soils on siliceous rock belong to the pedogenesis Lithic Leptosol – Leptosol – Cambisol – Semipodzol – Podzol (Bitterlich et al., 1999); thus, Eutric and Oligotrophic Cambisols are developed on the alpine meadows and pastures, and on mown *Larix decidua* meadows. In the abandoned areas, largely Oligotrophic to heavily Cambic Podzols occurred, depending on the time since abandonment. In addition, on old fallows with a close cover of dwarf shrubs Ferric and Haplic Podzols occur. In turn, on limestone of the Brenner mesozoikum, large areas of Rendzina and smaller areas of Calcaric Cambisol were found.

Vegetation

Vegetation in the Stubai Valley includes alpine grasslands, subalpine coniferous forest, and cultivated areas at the bottom of the valley (ECOMONT project, (Cernusca et al., 1999)) The alpine grassland distribution in the study area is heavily influenced by land use as seen in Table 3.3 (Tasser et al., 1999).

Table 3.3. The composition of grassland communities in Stubai Valley

Zone	Composition of species
Intensively managed hay meadow 1850 m a.s.l.	The characteristic plant community of these hay meadows is *Trisetetum flavescentis*, with the dominant species *Alchemilla vulgaris, Dactylis glomerata, Leontodon hispidus, Plantago lanceolata, Geranium sylvaticum,* etc.
Lightly managed hay meadow	*Sieversio-Nardetum strictae* is the prevailing plant community. Species typical for intensively used hay meadows are also present.
Intensively managed pasture 1900 – 2000 m a.s.l.	*Seslerio-Caricetum* is adjacent to the pasture. Dominant species are *Alchemilla millefolium, Plantago media, Ranunculus montanus, Lotus corniculatus,* etc.
Lightly managed pasture above 2000 m a.s.l.	The proportion of forage plants (*Alchemilla millefolium, Lotus corniculatus, Trifolium pratense,* etc.) has decreased. Dominant plant species such as *Calluna vulgaris, Carex montana, Sesleria varia, etc.* are present.

The dominant trees are spruce (*Picea abies)*, *Larix decidua* at tree line and *Pinus sylvestris.* Mixed and deciduous forests cover a small part of the investigated area. Some broad-leaved trees such as *Sorbus aucuparia, Salix sp.* and *Alnus viridis* also occur locally.

3.2. Methodology

The overall objective of this study is to provide a ground-surface-based evaluation of MODIS reflectance, land cover, and LAI products. There are two steps required with respect to accomplishing these aims, namely:

1) To build an appropriate database, gathering all ancillary data which is necessary to carry out the assessments, and

2) To carry out the ground-based evaluation of the products across several scales (Fig. 3.9).

Figure 3.9. Conceptual model from the Bigfoot project. illustrating the use of field measurements and remote sensing to characterize the vegetation cover and LAI for study sites (*http://www.fsl.orst.edu/larse/bigfoot/*).

Important in this thesis is the development of relationships between ground-surface data, Landsat-TM observations at 30 m resolution, and MODIS remotely sensed data at 1 km resolution, thereby obtaining a ground-surface-based test of publicly available products.

3.2.1. Building an appropriate database

An extensive collection of reflectance, land cover, and LAI were obtained from previous studies at the four study sites as summarized in the following sections.

3.2.1.1. National Park Berchtesgaden

a. Alpine habitat mapping and its derivation - land cover map

The alpine habitat map series were produced using color infrared (CIR) photos within the framework of the Project "Alpine Habitat Diversity–HABITALP–INTERREG IIIB Alpine Space Program" by the administration of the National Park Berchtesgaden. The first version was carried out using images acquired in 1980. The other two versions were updated during 1990 and 1997. Interpretation of these data was carried out using on-screen digitizing methods, which are mostly based on experience of the interpreter to differentiate type of vegetation according to the brightness, texture and surface, shadows, and stereoscopic effect. As a result, a map that is composed of 153 biotope types in the Berchtesgaden National Park was created (Bobeva, 2003).

The alpine habitat map was reclassified as part of this thesis work into a land cover map (Fig. 3.11), which is composed of six land cover types: deciduous forest, coniferous forest, mixed forest, grassland, rocks, and water. The land cover map then is used as reference data for validation of the remote sensing classification.

b. Landsat TM images (for all sites) and its derivations: reflectance and land cover

Field studies provide detailed measurements over relatively small space and time scales. Remote sensing data provide synchronous measurements over very large areas but with reduced potential for local details (Kerr and Ostrovsky, 2003). Combining remote sensing and field measurements can lead to spatially integrated measures of ecosystem structure and function. Landsat TM data was chosen as a remote sensing source in this study due to its well-known characteristics and its regular use for land cover determinations, LAI mapping, as well as good resolution in comparison with ground measurements.

```
┌─────────────────────┐
│  Original Landsat TM │
│   scenes (raw data)  │
└─────────────────────┘
          │
          ▼
┌─────────────────────┐
│    Co-registration   │
└─────────────────────┘
          │
          ▼
┌─────────────────────┐
│   Geo-referencing    │
└─────────────────────┘
          │
          ▼
┌─────────────────────┐
│  Convert to at sensor│
│      reflectance     │
└─────────────────────┘
          │
          ▼
┌─────────────────────┐
│    Convert to at     │
│  surface reflectance │
└─────────────────────┘
          │
          ▼
┌─────────────────────┐
│     Atmospheric      │
│      correction      │
└─────────────────────┘
          │
          ▼
┌─────────────────────┐
│     Topographic      │
│      correction      │
└─────────────────────┘
          │
          ▼
┌─────────────────────┐
│       Landsat        │
│      Reflectance     │
└─────────────────────┘
```
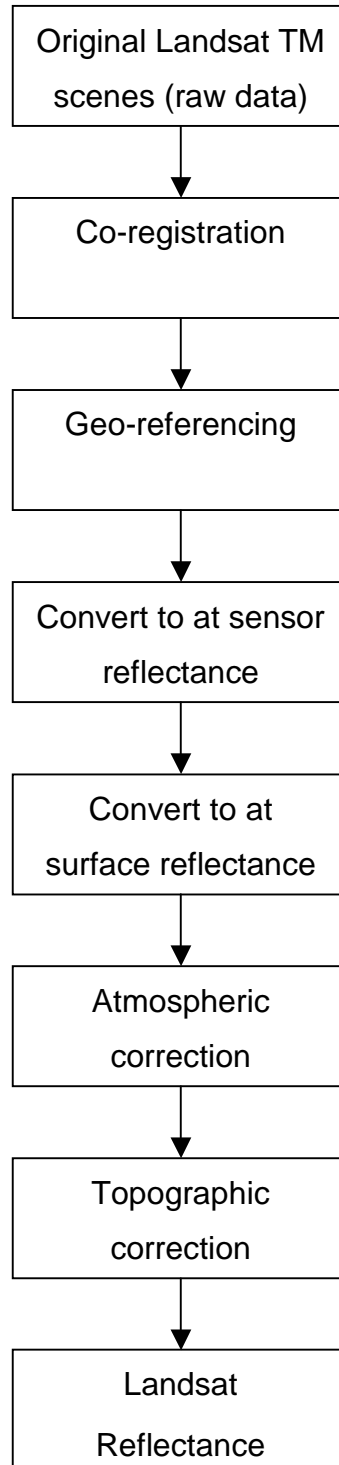
Figure 3.10. Scheme describing steps carried out in pre-processing of Landsat data for all sites.

All Landsat TM scenes used at the four sites in this study are listed in Table 3.4. The selection of scenes was based on the following criteria:

1) The acquisition time: scenes should be close to the date, when ground-truth measurements were made (the same day is of course ideal). In the case that

measurements were carried out over the growing season, a series of scenes that monitor the change of vegetation functions are required.

2) The quality: scenes should be cloud-free.

All Landsat data were subjected to the same pre-processing, which includes spatial co-registration, geo-referencing, atmospheric correction, and topographic correction as illustrated in Fig. 3.10. This is to ensure consistency of all Landsat images. At the end of this process, reflectance data were obtained, ready for use in land cover classification and LAI mapping. Details of the pre-processing description are given in Appendix A.

The land cover map was derived from Landsat reflectance images by two methods (see more detailed description in 3.2.2):

1) The traditional method is a pixel-wise classification, based on supervised classification and maximum likelihood classifier.

2) The new method is a patch-based classification.

As the results of study in Berchtesgaden will show, the classification of data which have gone through atmospheric correction and topographic correction, gave the best agreement to the ground truth, and the patch-based classification gave better results as compared to the pixel-based method. The patch-based classification has been applied for all four studied sites.

c. Forest inventory data and its derivation: LAI map

A forest inventory database was created within the framework of the projects "Mapping Site Characteristics in the National Park Berchtesgaden" (Konnert, 2001). The forest-inventory data were initially gathered in 1983/84. The updated measurements were made during the period 1995/97 (April to October each year) in order to obtain information on the development of the forests within the National Park. The inventory was carried out using the angle-counting method (as in the first inventory), as well as by using a method of concentric circles. Over the territory of the National Park Berchtesgaden a raster grid with 200 x 200 m^2 cells was created (Fig. 3.11). Nearly 4200 inventory points were monitored. The distance between the inventory points is 141 m. In the first forest inventory, 39952 trees were examined. During the second inventory 90.3 % of these trees were measured, 9.7 % disappeared, 11.2 % had newly established.

For each of the forest stands (at grid cell) a number of stand parameters was measured: stand age, tree height, stand density, DBH (diameter at breast height) etc. The ground plots in which stand parameters are measured are generally 50, 150 and 500 m^2 in size, depending on the DBH of trees to be measured (Table 3.5). Then all the data sampled in an individual circle are recalculated for 1 ha (Konnert, 2000).

The diameter at breast height was measured for all the trees falling into the ground plot (concentric circle) at 1.3 m above ground level. Trees were separated into different classes based on DBH. Stand age was measured with the counting of year rings on cores taken from the trees. Very old trees predominate clearly in all measured stands. According to age, all trees were grouped into age classes of every 20 years. Tree height was measured in every ground plot with Suunto altimeter (SUUNTO, CA, USA). Canopy density was estimated in every 500 m^2 circle to one tenth of ground cover
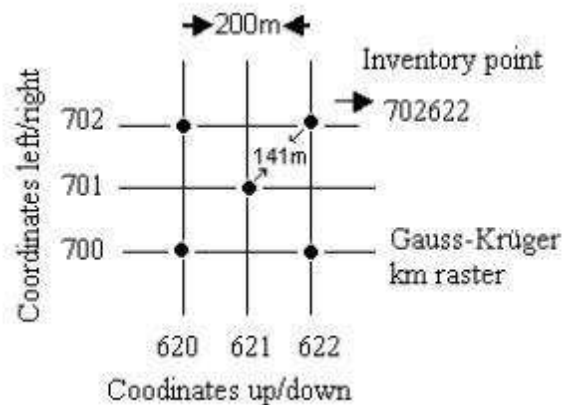
Figure 3.11. Forest inventory grid in Berchtesgaden National Park as used by Konnert et al. (2001).

Table 3.4. List of Landsat TM scenes in Berchtesgaden and other sites

Site	Date
National Park Berchtesgaden	
	September 14, 1999
Stubai Valley	
	September 13, 1999
	May 16, 2002
	June 17, 2002
	June 26, 2002
	July 19, 2002
	July 28, 2002
	September 14, 2002
Hesse Forest	
	March 31, 2001
	May 10, 2001
	July 5, 2001
	August 22, 2001
	November 10, 2001
	July 08, 2002
Tharandt Forest	
	February 15, 2001
	May 13, 2001
	June 14, 2001
	August 26, 2001
	October 20, 2001
	July 28, 2002

Table 3.5. Plot sizes according to DBH

DBH (cm)	Plot size (m^2)
0 - 5	25
6 - 11	50
12 - 19	150
≥ 20	500

3.2.1.2. Stubai Valley

a. Land cover map of Stubai Valley

The land cover map of Stubai Valley was created for investigating land-use changes in European terrestrial mountain ecosystems (as a part of ECOMONT project). The map was created by visual interpreting airborne CIR images and was used for validation of the land cover map derived from Landsat images. The map originally in ArcInfo shape file was converted into grid coordinates and resized to 30 m-resolution to make it comparable to the Landsat TM derived land cover map. The classes in the land cover map of Stubai Valley were combined and reclassified into a 6 distinct classes identical to the satellite based land cover classes: deciduous forest, coniferous forest, mixed forest, grassland, water, and non-vegetation surface (rocks, bare soil, and urban areas) (Fig. 3.8).

b. Landsat TM images and its derivations: reflectance and land cover

Six Landsat TM scenes in 2002 were collected to capture the development of grassland in the year 2002 (Table 3.4). The cloud-free scenes were used for assessment of the MODIS reflectance products. The best scene in the season was used for deriving a land cover map, which is subsequently used for validating the MODIS land cover product.

c. Forest inventory data and its derivation: LAI map

Within framework of ECOMONT and INTERREG II projects, a LAI map was also developed using inventory data for Neustift (a small part of Stubai Valley). The method used for developing of LAI map is the same as used in Berchtesgaden National Park, e.g. using allometric relationships to infer LAI from DBH. In this study, the ground truth LAI map was used to validate the LAI map derived from Landsat TM images in Stubai Valley, using the LAI-VIs model acquired from Berchtesgaden.

d. LAI measurements at grassland sites

Destructive harvesting was used to determine LAI in grassland sites over the course of the growing season in 2003, monitoring the development of four grasslands as well as changes at the time of cutting. Relating LAI measurements to vegetation indices derived from Landsat TM data helped to extrapolate LAI to

grasslands in the region, as well as to Berchtesgaden National Park. Details of the methods are given in section 3.2.2.3.

3.2.1.3. *Tharandt forest*

a. Land cover map of Tharandt

The land cover map of Tharandt forest was created in 1993 by using Landsat TM data. The map was created by supervised classification of Landsat images. The land cover map of Tharandt forest is composed of 7 distinct classes: deciduous forest, coniferous forest, mixed forest, grassland, agriculture land, water, and non-vegetation surface (bare soil, and urban areas) (Fig. 3.5).

b. Reflectance measurements of grassland and coniferous forest canopies

Field measurements of reflectance were taken in Tharandt forest sites at the time close to the time of acquisition of Landsat TM data using an Analytical Spectral Device (ASD) spectrometer (details are described in Chapter 4). Comparison of measured reflectance and Landsat reflectance was made to confirm the validity of the Landsat reflectance, which was then used for MODIS product assessments.

c. Landsat images and its derivations: reflectance and land cover

Five Landsat TM scenes in 2001 were collected to capture the vegetation development of the year 2001. An additional scene acquired on July 2002 was used for comparison to ground measurement of reflectance (Table 3.4). The cloud-free scenes were used for assessment of the MODIS reflectance products.

Due to land-use changes within the last 10 years, a new land cover map is needed. The best scene in the season 2001 was used for deriving a land cover map via the patched-based classification method.

c. Forest inventory data and its derivation: LAI map

Forest inventory was made in the plots within the 0.5 km circle surrounding the tower site (Fig. 3.6). More background information on the Tharandt site is also presented in Table 3.1. The dominant species is Norway spruce (*Picea abies*), which was planted as early as 1887. Other tree species include *Pinus sylvestris*, *Larix decidua*, *and Betula spp.,* but these only occupy a small area. At each plot, a number of stand parameters were measured: stand age, tree height, stand density, and DBH (diameter at breast height) distribution. LAI was obtained by summing the leaf area of each tree within the plot and then dividing by the plot area.

The existing allometric equation for spruce is for projected leaf area. Chen and Black (1992) demonstrated that in order to use 0.5 as the projection coefficient when the leaf angle distribution is spherical (random), LAI must be defined on the basis of half the total leaf area. To obtain half the total surface area, the projected area was corrected by the factor of 1.35 (Niinemets and Kull, 1995).

d. LAI measurements at grassland site

LAI measurements were carried out at the grassland site using destructive methods over the course of the growing season. Relating LAI measurements and vegetation indices derived from Landsat TM data helped to confirm validity of the model, which was developed for Stubai Valley. This model was used to extrapolate LAI to grasslands in the region as well as to other study sites. Details of the methods are given in part 3.2.2.3.

3.2.1.4. Hesse forest

a. Reflectance measurements of the deciduous forest canopy

Field measurements of reflectance were taken from above canopy in Hesse forest sites at the time close to acquisition of Landsat TM data using an ASD spectrometer (details provided in Chapter 4). Comparison of the measured reflectance and Landsat reflectance was made to confirm the validity of the Landsat reflectance, which then used for MODIS product assessments.

b. Landsat images and its derivations: reflectance and land cover

Five Landsat TM scenes in 2001 were obtained to capture development of the deciduous forest in the year 2001. An additional scene acquired on July 2002 was used for comparison to ground measurements of reflectance (Table 3.4).

c. Land cover map

The land cover map of Hesse forest was created in 1997 by supervised classification of a SPOT image. The land cover map of Hesse forest is composed of 7 distinct classes: young deciduous forest, mature deciduous forest, coniferous forest, grassland and agricultural land, bare soil, soil covered by sparse vegetation, and urban areas (Fig. 3.3). This land cover map was used as ground truth data for validating the new version of land cover map, which was created using Landsat data. The new land cover map covered a larger area as needed for assessment of MODIS data.

d. LAI measurements at deciduous forest site

In deciduous forest stands, LAI determination by collecting leaves in traps distributed below the canopy during leaf fall is a widely used non-destructive method. Litter has to be collected in a number of traps with a known collecting area over short intervals to avoid losses and decomposition (detail in part 3.2.2.3). This practice has been carried out over the long term in the context of monitoring studies at the site.

3.2.2. Strategy for evaluation

Within the framework of this study, measurements, mapping, and modeling activities were carried out at the four above-mentioned sites, each equipped with a meteorological flux tower that makes continuous measurements of energy, water, and carbon fluxes for a roughly 1-km^2 area. Procedures encompass the following:

1) Detailed ground level measurements for evaluation were conducted within the 1-km^2 surrounding the eddy flux tower.

2) The measurements were then used for evaluation of the products, which were derived from high-resolution remote sensing data (Landsat). Extrapolations of field measurements to high-resolution grids (reflectance, land cover, and LAI) were made using Landsat imagery and statistical models. Errors in these grids were estimated using independent field observations.

3) After processing and upscaling the Landsat product to MODIS scale, a direct comparison of MODIS and field-verified high-resolution Landsat-derived products were made to quantify errors and uncertainties that exist in MODIS products.

3.2.2.1. Evaluation of MODIS reflectance

a. Measurement of reflectance at three biomes: Coniferous forest, deciduous forest, and grassland.

Field measurements of reflectance were taken in Hesse forest, Tharandt forest, and Tharandt grassland sites at the time close to the passing time of the satellite. The spectra were averaged and integrated over the ETM+ spectral band to validate the ETM+ atmospherically corrected reflectance. Measurements were collected from the eddy covariance tower above the canopy in three different unshaded directions. The error bars on the ASD measurements represent the standard deviation

computed from the spectra collected at the location (30 measurements). The reflectance of the leaves was measured using an ASD spectrometer at 325 – 1075 nm in 2 nm steps, but only data in the range 400 to 1000 nm were used, to avoid the lower signal to noise at the extreme ends of the spectra. The measurements were performed with the same illumination conditions as measurements of canopy reflectance. The instrument was held at the normal from the leaf position, focusing on the leaf. The white reference reflectance was achieved using a reference plate (spectralon), having nearly lambertian properties.

Comparison of measured reflectance and Landsat-derived reflectance was made to confirm validity of the Landsat reflectance products.

b. Upscaling of Landsat reflectance to MODIS scale using a statistical model.

From numerical experiments using a three-dimensional (3D) atmospheric transfer model, Liang et al. (2001) found that upscaling of reflectance from 30 m to 1 km over vegetated surface is quite linear. It implies that one can linearly average the high resolution ETM+ reflectance up to the coarse resolution of MODIS. The average of 16 x 16 blocks of ETM+ pixels was calculated to generate a product at 460 m, which is the same as MODIS reflectance products.

c. Comparison of MODIS reflectance and Landsat reflectance.

Multidate Landsat TM scenes, which cover four study sites and relatively cloud-free, were used in comparison. Pixel by pixel comparison is possible due to the accuracy of geo-referencing of both MODIS and Landsat TM data.

3.2.2.2. *Evaluation of MODIS Land cover*

Land cover maps at four sites were collected from former studies. They are either derived from airborne photo image (National Park Berchtesgaden and Stubai Valley) or high-resolution satellite images (Hesse forest and Tharandt forest). The land cover change in recent years will, however, affect the accuracy of these maps. There is a necessity to develop a new set of land cover maps, which is compatible with the derivation of MODIS land cover products (LAI). This was carried out based on Landsat TM scenes and compared with the previous mapping work.

3.2.2.2.1. Image classification: concepts and methods

Box 3.1. Background on image classification

According to Schowengerdt (1997), image classification is the process used to produce thematic maps, which shows the spatial distribution of identifiable earth surface features and provides an informative description of a given area. As a result, the image is partitioned into some non-intersecting regions, such that each region is homogeneous and the union of two adjacent regions is heterogeneous. The classification process can use more parameters to classify than brightness, e.g., texture, shape, and directional reflectance of objects (Blaschke and Strobl, 2001). In general, the classification process involves the following steps.

Feature extraction: to transform the multispectral image to a subset of bands, indices or principal components in order to reduce the data dimensionality while increasing information richness. This step is optional. The multispectral image data can be used directly in a classification, but it contains various external influences, such as atmospheric scattering and topographic effects. Also, the data are often highly correlated between spectral bands, resulting in inefficient analysis. Furthermore, image-derived features, such as indices and measures of spatial structure, may extract the greatest amount of information from the original images for classification. In general, it is wise to use those features to better distinguish spectral classes.

Training: to extract the pixel to be used for training the classifier in order to recognize the spectral signature of the classes. The classification algorithm needs to be trained to distinguish those classes of interest from an image (and its deviation). Selections of the training area are used for this purpose. If training data from one image are used to classify another image, then all of the images should be corrected for atmospheric effects. If the atmospheric effects vary significantly across the scene, then spatially-dependent correction of atmospheric effects is needed (Richter, 1996). The training of classification algorithm can be supervised or unsupervised. In supervised classification, the training areas chosen are based on an existing ground truth map or visual photointerpretation, in order to find the most representative area of each class. It is important that the training area be homogeneous and at the same time reflects the range of variability for the class. Thus, more than one training area per class are often selected (Maxwell, 1976). In unsupervised classification, the training area is not labeled, but computer algorithms have to distinguish intrinsic spectral data. Results of this process are clusters, which are assumed to represent classes in the image and are used to calculate signature. However, these clusters often do not correspond to classes of interest. Supervised and unsupervised classifications are often used together to complement each other in hybrid classification. First the unsupervised classification is used to identify different clusters, which is a group of pixels in a distinguished region of

---

a multidimensional data space. Then the analyst chooses the training area within each cluster and assigns it to a certain class of interest.

Labeling: to apply the spectral signature to the entire feature image and label all pixels. If the training was supervised, the labels are associated with the spectral signature; if it was unsupervised, the analyst must supervise the labeling. The final result is to convert the numerical image into descriptive labels that classify different surface materials. It is clear that the spectral signature of a surface material is not characterized by a single spectral vector, but rather a distribution of a vector. The classification accuracy of a multispectral image is determined by the extent of overlap between class signatures.

The extraction of classes can be approached using a classical approach or fuzzy mathematical methodologies. The first group of techniques is based on histogram thresholding, edge detection, relaxation, and semantic and syntactic approaches. For example, the maximum likelihood classifier minimizes the total error in the classification, if estimation of the probability distributions is correct and achieves an optimum result. The resulting thematic map assumes that every pixel on the image can be labeled as belonging to one, and only one, class. This discrete categorization is convenient because of its simplicity, but is not particularly an accurate portrait of a real landscape as a mixture of several classes. This hard classification is produced by selecting the class label with the greatest likelihood of being correct. The feature space decision boundaries for a hard classification are well defined. The fuzzy mathematical approach accepts the fact that class signatures overlap and expresses that as a likelihood of membership in each class (Baatz and Schäpe, 2000). This method allows for multiple labels at each pixel, a soft classification is obtained. The feature space decision boundaries for a soft classification are ill-defined.

Pixel-oriented approach versus object-oriented approach

The availability and employment of high spatial resolution and hyperspectral sensors has led to much more precise land-cover classifications and a new range of applications (Franklin, 2001). On the other hand, new sensors have created new technical problems associated with the pixel-based approach (Schiewe et al., 2001). The internal variability and the noise within land-use or land-cover classes due to the high spatial resolution of the images increase with higher spatial resolution. If a traditional algorithm, such as Maximum Likelihood, is applied, the method produces too many or ill-defined classes (Schiewe et al., 2001). Recently, a new method of classification has been developed, in which the algorithm uses not only spectral signatures of the objects, but also texture characteristics and sharpness of object images (Baatz and Schäpe, 2000; Blaschke and Strobl, 2001).

There are several advantages in the application of a classification based on an object-oriented approach instead of a pixel-oriented approach. Image objects, besides

the spectral information, contain additional attributes (e.g. shape, texture, relational and contextual information) that can be used for classification purposes (Baatz and Schäpe, 2000). Moreover, segmentation produces homogeneous image objects, avoiding the induced salt-and-pepper effect.

The application of an object classification approach has already been applied in many studies. Shimabukuro et al. (1998). The studies demonstrate that by means of a region growing segmentation (based on the shade fraction of a Landsat TM image) combined with an unsupervised classification (based on a clustering algorithm), effective measurements of the areal extent of the Brazilian Amazonian deforestation are possible. Using a Landsat TM image, Hill et al. (1999) applied a combination of edge detection and region growing segmentation methods to classify tropical forest in southeast Peru. After the segmentation, a pixel-per-pixel classification (maximum likelihood classifier) was applied with acceptable results.

Baatz and Schäpe (2000), developed an algorithm based on fuzzy mathematics. The mathematical approach of fuzzy logic is to replace the strict logical statement 0 and 1 (i.e. no or yes) by a continuous range of [0…1], where 0 means "exactly no" and 1 means, "exactly yes" (Baatz et al., 2001). The classification algorithm, based on multi-resolution segmentation of the input image(s) described in the previous section, has shown promising results in application involving high-resolution images. The commercial software eCognition® (Baatz and Schäpe, 2000), implements the multi-resolution method and the classification algorithm based on fuzzy logic mentioned above. The algorithm uses the multi-resolution segmentation method, a classification procedure based on fuzzy rules, which are based either on one-dimensional membership functions or on a nearest neighbor classifier. Both approaches are supervised methods. Once the classification is obtained, the results can be refined by means of semantic context information mostly by describing neighborhood relationships or the composition of sub-objects (Baatz and Schäpe, 2000).

a. Derivation of land cover maps

Object-oriented classification was chosen due to its accuracy and its advantages (see Box 3.1). Results of the classification are presented in Chapter 5.

b. Upscaling of Landsat land cover to MODIS scale using a statistical model

Box 3.2. Background related to aggregation:

Aggregating based on dominant values also produces a sub-data set. A dominant value, such as dominant land cover type within an area, is used to present the area and form new data set with coarser resolution. This method tends to reduce the total variance, because low frequency distribution data may be excluded during aggregation. The frequency distribution of the aggregated data is dictated primarily by the spatial arrangement of the original data (Turner et al., 1989). A large cluster of the same land cover type (similar reflectance values) will be more likely retained when upscaling, while small cluster will disappear as result of upscaling. The dominant value procedure retains the values of the original data but may alter the spatial pattern at coarser resolution. It should be note that, this method may introduce bias as some class proportions will diminish and others will increase with scale depending on the spatial and probability distributions of the land cover types (Moody and Woodcock, 1994). A typical example is the Anderson land cover classification system for remote sensed data (Anderson et al., 1976). The system is a multilevel hierarchy, where adjacent small land cover area at a low level (finer resolution) can be aggregated to form larger area at a higher classification level (coarser resolution). For example, adjacent deciduous forest and mixed forest can merge into deciduous forest or mixed forest (depending on percentage of each land cover type).

According to the definition of MODIS land cover, a pixel is defined as belonging to a certain class of vegetation if there is at least 60 % of area within that pixel composed of the vegetation.

An algorithm was developed to count the number of pixels of each land cover class (derived from Landsat data) found within a corresponding MODIS pixel. The following rules were applied according to their priority.

- If a pixel has more than 60 % of coniferous forest, it is defined as a coniferous forest pixel. The same was applied to each of the other classes.
- If a pixel has more than 60 % of coniferous and deciduous forest combined, it is defined as a mixed forest pixel.
- If a pixel has more than 60 % of grassland and agricultural land, it is defined as grassland or agriculture land, depending on the majority representation.
- Any remaining pixels are kept undefined.

c. Assessment of MODIS land cover product

Assessment was made by comparison of MODIS land cover and Landsat land cover in 9 x 9 pixels surrounding the eddy covariance tower pixel at experimental

sites. Direct pixel by pixel comparison was made of the MODIS land cover product and defined Landsat up-scaled land cover in order to assess the accuracy of the MODIS land cover product.

3.2.2.3.   Evaluation of MODIS LAI

a. Ground measurements of LAI.

Validation of MODIS LAI was based on ground sampling of LAI. Spatial and temporal sampling of ground-based LAI was conducted at three sites: coniferous forest, deciduous forest, and grassland within the 1-km^2 surroundings of individual eddy covariance measurement towers as described for the individual experimental sites.

In this study, a number of direct and indirect methods have been used to estimate LAI at ground level. Direct measurement approaches include area harvest, application of allometric equations based on stand diameter data, and leaf litter collection. Numerous commercially available instruments, such as Decagon ceptometer, Li-Cor LAI-2000, DEMON and TRAC, are used to indirectly estimate LAI (Fassnacht et al., 1994; Chen et al., 1997); all of the instruments measure light transmittance and assume foliage is randomly distributed in the canopy.

Area harvest in Stubai Valley and Tharandt grassland

In general, the area harvest approach is more appropriate for short-stature ecosystems (e.g., grasslands, agriculture crops, tundra) than for forests because this approach is very laborious when done for an area of sufficient size to adequately characterize spatial heterogeneity.

The area harvest involves the periodic destructive sampling of vegetation in plots during the growing season. The plots should be located randomly in a representative area. The harvested foliage tissue is subsampled for specific leaf area measurement (SLA, the ratio of fresh leaf area to dry foliage mass, cm^2 g^{-1}. The remaining foliage mass is dried to a constant mass. Plant tissue samples should be dried at 60 – 70℃; higher temperatures should be avoided because volatilized compounds may be lost. If more than one species is present, separate estimates of leaf biomass and SLA should be obtained for each species because they differ among species (Landsberg and Gower, 1997). When sampling the foliage in the canopy, vertical stratification is required to account for the decrease of foliage:

branch mass and SLA deeper in the canopy. Also some attempt should be made to characterize the SLA by age of foliage because SLA can differ by twofold from new to old foliage (Landsberg and Gower, 1997).

Canopy structure was assessed in a destructive fashion by stratified clipping (Monsi and Saeki, 1953) of square plots of 0.25 m^2 during the respective peak season. Thickness of the harvested layers ranged between 0.05 and 0.1 m, depending on plant area density. The harvested plant material was separated according to combined functional and taxonomical criteria: Leaves were separated into those species that had the largest fractional contribution to the total plant area index (PAI m² plant area per m² ground area). The remaining leaves, as well as all stems, were pooled to two functional groups, namely remaining forbs and graminoids. The remaining plant components, i.e. reproductive organs, attached dead plant matter and cryptogams, were pooled over all species. Silhouette plant areas were determined by the means of an area meter (LI-3100, Li-Cor, USA). Silhouette areas of non-flat phytoelements were converted to hemi-surface area by multiplying with $\pi/2$, assuming them to be represented by cylinders (Campbell and Norman, 1998). Dry weight of plant samples was determined after oven drying at 70℃ for at least 72 h and weighting (AE-260, Mettl er Instrumente AG, Greifensee-Zürich, CH).

Measurement of LAI by litter collection in Hesse

In deciduous forest stands, collecting leaves in traps distributed below the canopy during leaf fall is a widely used non-destructive method. Litter has to be collected in a number of traps with a known collecting area in short interval to avoid losses and decomposition. Collected litter is dried (at 70℃ for 48 -72 h) and weighed to calculate the dry mass of litter as g m^{-2}. Leaf dry mass is then converted into leaf area by multiplying the collected biomass by the specific leaf area (SLA, m^2 g^{-1}). Finally, the LAI is the accumulated leaf area over period of leaf fall. As SLA varies with species, site fertility, and duration of collecting, the estimation of SLA is very critical (Burton et al., 1991; Niinemets and Kull, 1994).

Litter was collected during fall using 42 litter traps, each covering 0.25 m^2. Dry mass of litter was measured weekly during the leaf-fall period (from the beginning of October to the end of December), while a sub-sample of leaves was taken every two

weeks for measuring the leaf specific area (Delta-T area meter, Cambridge, UK, in order to convert dry mass into leaf area.

Measurement of LAI based on allometric relationships in National Park Berchtesgaden and Neustift area of Stubai Valley

---

BOX 3.3. Background on allometric methods for LAI determination:

Leaf area of forest stands can be estimated from allometric relationships applied to each tree surveyed in randomly located plots in the community of interest. Allometry is the relationship between the leaf mass or leaf area of a part (or all of a tree) and an independent variable. The dependent variable is indirectly estimated because it is difficult, and often laborious, to measure. The independent variables commonly used to estimate leaf mass (or area) is diameter at breast height (DBH), stem diameter, and sapwood cross sectional area. Direct measurement of biomass and area of plant parts using allometry involves harvesting plants that encompass the size range encountered in the survey plots, measuring the fresh mass of each component and subsampling each tissue for water content. The dry mass is calculated from the total wet mass and water content. Gower et al. (1992; 1997) gave a mathematical relationship, which is fit to the data:

$$M_D \text{ or } A = aD^b \qquad (3.1)$$

where M_D or A is dry mass or area, respectively, of a plant part, D is stem diameter, usually at breast height (i.e., DBH), and a and b are regression coefficients. The relationship depicted in Eq. (3.1) follows a power or exponential form and assumes a uniform variance of the dependent variable over the range of the independent variable. Often researchers describe the allometric relationship using Eq. (3.2)

$$\log M_D \text{ or } \log A = a + b \, (\log D) \qquad (3.2)$$

where log is the natural or base 10 logarithmic transformation. This equation is preferred over the Eq. (3.1) for two reasons. First, the assumption of uniform variance is often violated: the variance of the dependent variable often increases as D increases. The double logarithmic transformation model in Eq. (3.2) consistently corrects for this problem compared to other models. A second advantage of using Eq. (3.2) is that it facilitates the statistical comparison of two or more allometric equations because the comparison of two or more allometric equations is more difficult for curvilinear than linear relations. The predicted value derived from Eq. (3.2) has a small downward bias because of the logarithmic transformation.

Allometric equations correlating foliage mass to stem diameter (D) or sapwood cross sectional area at breast height (1.37 m) can be used to directly estimate LAI if specific leaf area (SLA) is known. Specific leaf area is an important physiological characteristic because it is positively correlated to maximum photosynthetic rate and percent leaf nitrogen concentration - key determinants of productivity (Reich et al., 1995). Specific leaf area is also an important parameter in ecosystem process models because it

provides the coefficient to convert foliage mass to leaf area (Landsberg and Gower, 1997).

Developing site-specific allometric equations is laborious; therefore scientists commonly use existing allometric equations. Numerous publications present allometric relationships between leaf area and stem diameter (Gholz et al., 1979; Gower et al., 1997). Using general allometric equations to estimate LAI for a specific stand can result in moderate to large errors because numerous abiotic and biotic factors influence the allometry coefficients. An understanding of the factors that influence leaf mass or area allometric equations can be used to help select an appropriate allometric equation, when more than one equation exists.

The factor that strongly influences the allometric coefficients is tree size. Estimating the leaf area of trees that have diameters that exceed the diameter range for the trees for which the equation were developed results in moderate to large over-estimates of leaf area (Grier and Milne, 1981; Marshall and Waring, 1986). Nutrient availability also influences the allometric coefficients. For example, boreal jack pine (*Pinus banksiana*) trees growing with a nitrogen-fixing green alder (*Alnus creneta*) understory support a greater leaf area than trees without the N-fixing alder. Fertilization also influenced the allometry of new foliage mass or area (Gholz et al., 1991; Gower et al., 1992). The influence of nutrient availability on leaf area allometry is suppressed if water availability is more limiting (Gower et al., 1993a). Leaf area allometric equations differ among plant species as well. For a similar diameter, tree with a greater longevity will have greater leaf area (Gower et al., 1993b). Also, shade-tolerant species support a greater leaf area than shade intolerant species (Grier and Logan, 1977; Chapman and Gower, 1991).

Attention should be made in selecting the allometric equation used to estimate LAI, if site-specific allometric equations cannot be developed. The two most important criteria to consider when selecting allometric equations are correctly matching the plant species and size. A slight variation of the allometric equation is the pipe model, which correlates the cross-sectional area of a stem or branch that is responsible for water transport (i.e., sapwood) to foliage mass (Shinozaki et al., 1964a, b). More recently, leaf area is used instead of foliage mass because transpiration is correlated to foliage surface area, not foliage mass. The form of the pipe model is usually linear. The physiological basis of the relationship between leaf area and cross-sectional sapwood area implies that the pipe model may alleviate the need for site-specific allometric equations. Waring et al. (1982) reported that the ratio of projected leaf area: sapwood cross-sectional area differs very little (0.15 – 0.18) for lodgepole pine (*Pinus contorta*) in three contrasting environments. However, in other case, the pipe model is influenced by the same environmental and ecological factors that affect the allometric coefficient (Gower et al., 1993b; Mencuccini and Grace, 1995).

Based on the forest inventory database of the National Park Berchtesgaden and similar databases for forested areas near Neustift, Stubai Valley, unique detailed LAI maps were created at landscape scale. By using the forest type map, leaf area index was derived using allometric relationships (relating BDH and LAI). LAI was calculated separately for coniferous forest (treated as spruce, *Picea abies*), and deciduous forest (treated as beech, *Fagus sylvatica*)

$$LAI=0.118*BDH^{1.565} \qquad (3.3)$$

$$LAI=0.1*BDH^{1.72} \qquad (3.4)$$

For the mixed forest, the mean value from both datasets was used (Bobeva, 2003).

In Tharandt tower footprint, LAI was calculated for each tree based on the site-specific allometric equation from Küssner (Küssner, 1999):

$$\log LeafArea = 3.329 + 2.216\log(BHD) \qquad (3.5)$$

LAI was obtained by multiplying to tree density within the plot and then dividing by the plot area.

b. Building models relating measured LAI and Vegetation indices derived from Landsat data.

Box 3.4. Background on vegetation indices (VIs):

Since the 1960s, scientists have extracted and modeled various vegetation biophysical variables using remotely sensed data. Much of the effort has gone into the development of vegetation indices. Vegetation indices are radiometric measures that function as indicators of relative abundance and activity of green vegetation. These often include leaf area index (LAI), percentage green cover, chlorophyll content, green biomass, and absorbed photosynthetically active radiation (APAR).

The designation of vegetation indices should:

-   Maximize sensitivity to plant biophysical parameters, preferably with a linear response in order that sensitivity is available for a wide range of vegetation condition, and to facilitate validation and calibration of the indices;

-   Normalize or model external effects such as sun angle, viewing angle, and the atmosphere for consistent spatial and temporal comparisons. Remember that atmospheric effects such as scattering act to increase the reflectance values in band TM3 but decrease the reflectance in band TM4 and, hence, reduce the vegetation indices.

-   Normalize internal effects such as canopy background variations, including topography (slope and aspect), soil variations, and differences in senesced or

---

woody vegetation (non-photosynthetic canopy components);

- Be coupled to some specific measurable biophysical parameter such biomass, LAI, and APAR.

There are more than 20 vegetation indices in use. Some of them are functionally equivalent in information content, while some provide unique biophysical information.

Numerous ratio-based VIs have been proposed, with the most common being the simple ratio (SR) and the normalized difference vegetation index (NDVI) (Baret and Guyot, 1991; Goward et al., 1991). Both of these are based on ratios of red (R) to near-infrared (NIR) reflectance.

Birth and McVey (1968) introduced the first true vegetation index as the SR, which is the NIR to red reflectance ratio.

$$SR = \frac{\rho_{NIR}}{\rho_{red}} \qquad (3.6)$$

where ρ_{NIR} and ρ_{red} are the surface bi-directional reflectance for their respective bands.

Rouse et al. (1974) developed the NDVI:

$$NDVI = \left(\frac{\rho_{NIR} - \rho_{red}}{\rho_{NIR} - \rho_{red}} \right) \qquad (3.7)$$

The NDVI index was widely used and applied to the original Landsat remote sensor data. The advantage of R and NIR ratio-based indices is the contrasting response of R and NIR to increases in vegetation cover from an unvegetated condition, and the compensating effect on variations in reflectance caused by differences in Sun-surface-sensor geometry (Chen, 1996).

These two indices respond to changes in amount of green biomass and chlorophyll content. The utility of the NDVI and related indices for satellite and airborne assessment of the vegetation cover has been demonstrated for almost thirty years. In a number of studies, it has been shown that the LAI correlates well with the NDVI (Knyazikhin et al., 1998a; b) or with a simple ratio (Chen et al., 2000). The time series analysis of seasonal NDVI data have provided a method for estimating net primary production of many biome type, monitoring phenological patterns of the vegetation, and estimating LAI, land cover percentage as well as the length of the growing season ((Huete and Liu, 1994; Ramsey et al., 1995).

Global vegetation studies were initially based on linearly regressing NDVI values (derived from AVHRR, Landsat MSS, Landsat TM, and SPOT data with in situ measurements of LAI, APAR, percent cover, and biomass. This empirical approach revolutionized global land cover biophysical analysis in one decade (Running, 1994). Many studies has shown that the empirically derived NDVI products can be site specific dependent, which depend on species, varies with soil color and moisture condition, bidirectional reflectance distribution function (BRDF) effects, atmospheric conditions,

presence of undercanopy vegetation, and percentage of dead material in the canopy itself (Qi et al., 1995). Although the NDVI has been shown to be useful in estimating vegetation properties, many important external and internal influences restrict its global utility.

Efforts has been made to the development of improved vegetation indices that will take advantage of calibrated hyperspectral sensor system such as the Moderate Resolution Imaging Spectrometer (MODIS) (Running et al., 1994). The improved indices normalize atmospheric effects and take into account a soil adjustment factor.

In this study, vegetation indices are derived after atmospheric and topographic correction of the data was made, reducing the atmospheric effects and helping to improve quality of the vegetation indices. On the other hand, LAI values at these study sites are relatively high, resulting in a low effect of the background reflectance on the canopy reflectance (Huemmrich and Goward, 1997). Therefore, SR and NDVI are used in this study to derive LAI from Landsat data, offering the opportunity for "scaling up" from the plot level to larger areas. By correlating the vegetation indices and LAI measurements spatially and temporally, one can build the models to indirectly calculate LAI as a function of vegetation indices. The best model correlating LAI and vegetation indices was chosen for each specific site.

c. Mapping LAI at four study sites

LAI maps based on satellite images of four sites were derived based on above-mentioned LAI = f (VIs) models. If there were no ground measurements of LAI at the site, the model from the site, which has similar conditions, is applied in extrapolations. Results of LAI mapping are presented in Chapter 6.

d. Upscaling of Landsat LAI to MODIS scale using statistical model.

From the definition of LAI, it is clear that LAI values over large areas are an integrated value of LAI values of all small areas within. The average method is used here as in case of reflectance to upscale the high resolution LAI maps to coarse resolution, which is comparable to MODIS. The average of 32 x 32 blocks of 30 m x 30 m pixels was calculated to generate a product at 960 m, which is the same as MODIS LAI products.

e. Comparison of MODIS LAI and Landsat LAI at 9x9 pixels surrounding tower pixel.

Pixel by pixel comparison of MODIS LAI and Landsat LAI were made at four study sites. Temporal variations of LAI were also examined depending on the data availability. The effects of land-cover misclassification on MODIS LAI estimates were isolated.

CHAPTER 4.   EVALUATION OF MODIS REFLECTANCE

4.1. Results and Discussion

The Moderate Resolution Imaging Spectroradiometer (MODIS) onboard EOS Terra satellite provides major advances in moderate resolution earth observation. An improvement of spatial resolution (at 250 and 500 m at finest), temporal resolution (daily), and spectral resolution (36 bands) provide new opportunities for global change research. Surface reflectance is one of the key products from MODIS and is crucial for generating several higher-order land products such as LAI and Fraction of Photosynthetically Active Radiation (FPAR). The surface reflectance has gone through an atmospheric correction process, in which the removal of water vapor and aerosol effects is undertaken.

Standard MODIS pixels of about 1 km on a side are identified over heterogeneous landscapes. Therefore, ground measurements are not feasible for direct comparisons to MODIS data. In this study, ground measurements at Hesse forest and Tharandt forest were used to calibrate land surface reflectance derived from Landsat ETM+ imagery at 30 m, which were then aggregated to the MODIS resolution for determining the accuracy of the MODIS reflectance. The validation results from ground measurements and ETM+ images acquired in 2001 and 2002 showed that these products are reasonably accurate, with typically less than 10 % absolute error. However the relationship is affected by clouds and haze.

4.1.1. Georeferencing

All ETM+ images were acquired at level 1G processing, with a cell size of 30 m, and UTM (WGS84) projection. Each TM scene was geo-referenced to the projection of ancillary datasets of the sites (e.g. Austria Zone 1 projection in Stubai Valley). The aerial photo images (in Hesse and Stubai Valley) were also registered into the projection of the remote sensing images to help identify the experimental sites with confidence. Fig. 4.1 shows an aerial photo of Stubai Valley and Landsat TM image for the same area, which visually indicates an error of less than one pixel. The white polygons are locations that were made by on-screen digitizing of the aerial photo. Table 4.1 indicates that for all study sites, the registration accuracy of images did not deviate by more than half of one pixel, and that the root mean square of error (RMSE) was less than 0.3 pixel when utilizing at least 40 ground control points and

nearest-neighbor resampling technique. The accuracy of georeferencing is sufficient for further processing and analysis of the images.

Table 4.1. Georeferencing accuracy of Landsat TM images

Site	Number of GCPs	RMSE
Hesse	40	0.10
Tharandt	45	0.12
Stubai Valley	55	0.15
Berchtesgaden	62	0.23

a)   b)
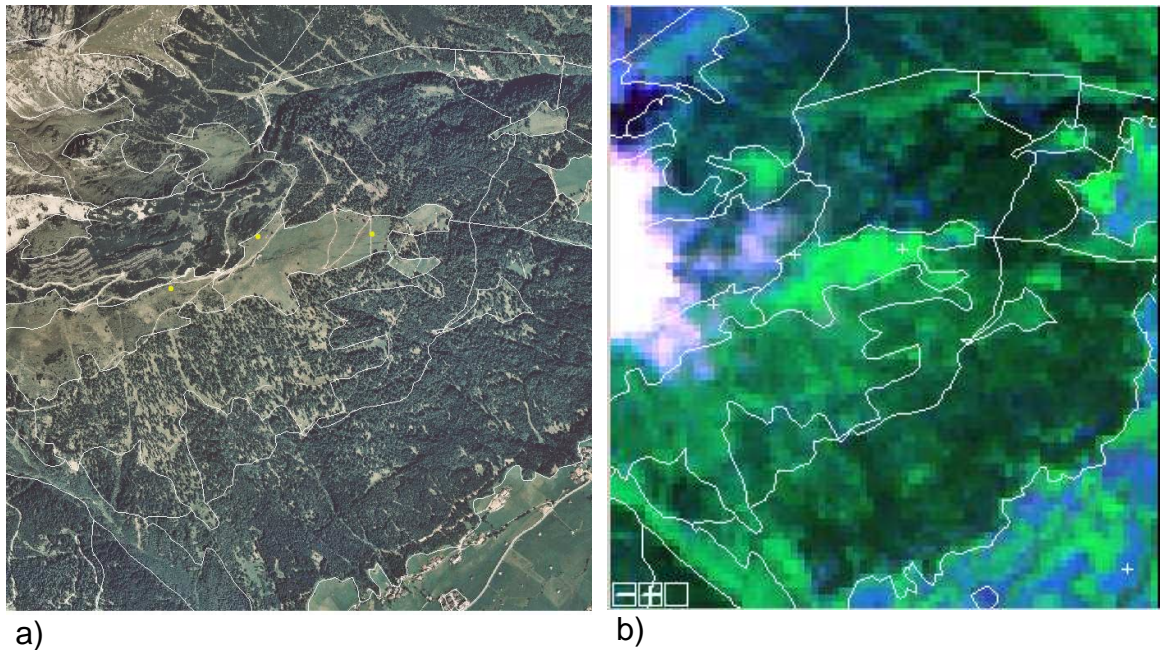
Figure 4.1. a) Aerial photo of Stubai Valley; b) Landsat TM composite band 1, 4, 7 in the same area. The white polygons are locations that are determined by on-screen digitizing of the aerial photo. Visual analysis showed an error of less than one pixel.

In order to compare with MODIS data, the Landsat images and aerial photos were further reprojected into ISIN projection and WGS84 datum in accordance to MODIS data. Results shown in Fig. 4.2 indicate that MODIS products are provided with sub-pixel accuracy, approaching the operational MODIS geolocation goal of 50 m at nadir (Wolfe et al., 2002). The accuracy provided by the MODIS geolocation product is sufficient to allow us to create and analyze the scenes further without any loss of information associated with improving the geolocation accuracy of MODIS

products. The grid in Fig. 4.2a and b is 1x1 km, and this applied for all subsequent figures.

a)   b)
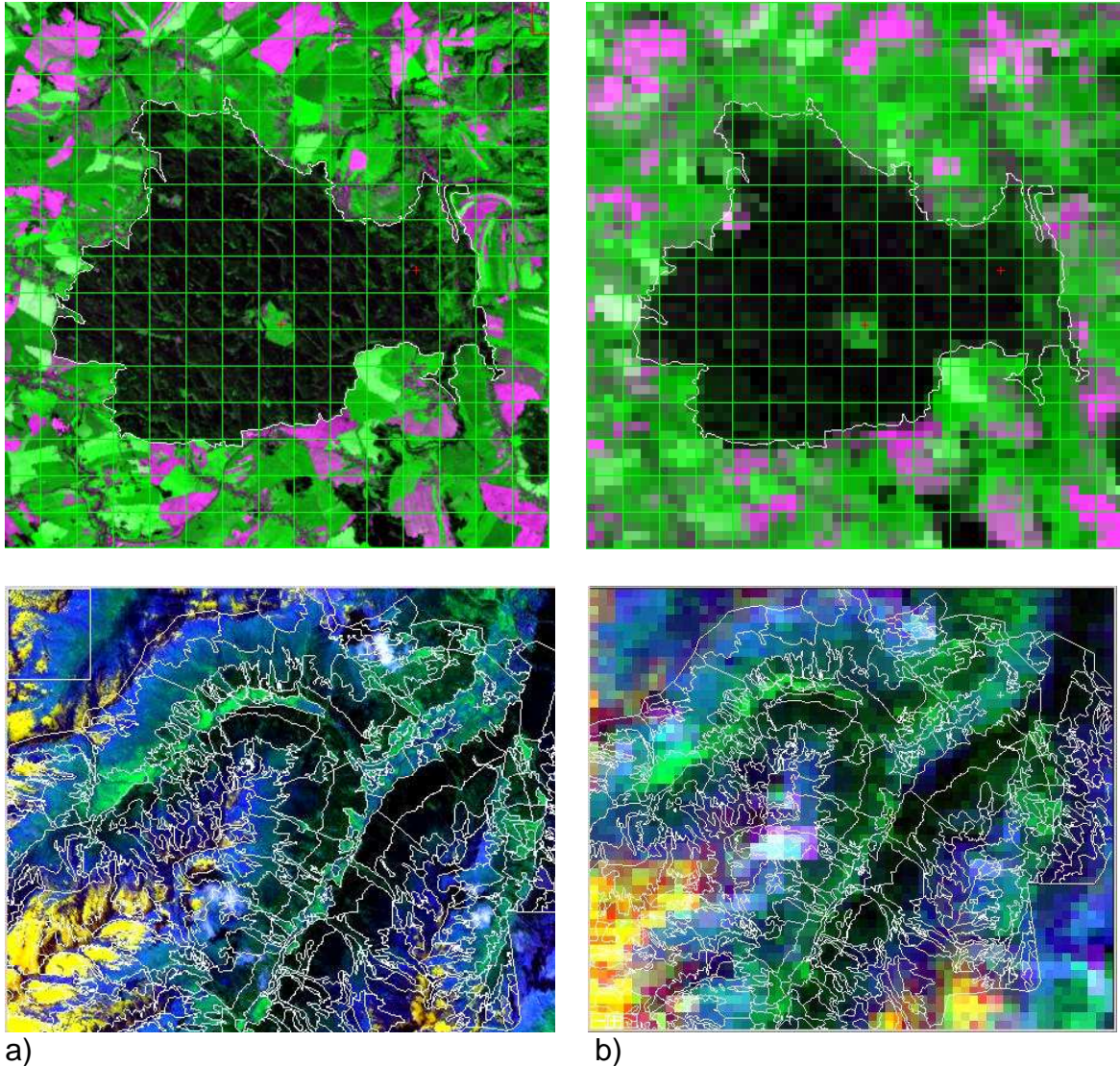
Figure 4.2. a) Landsat TM composite (bands 1, 4, 7); b) MODIS 250 m (bands 3, 2, 7) showing sub-pixel accuracy of registration of MODIS product (< 50 m) in Tharandt (upper) and Stubai Valley (lower) sites.

4.1.2. *Measurement of reflectance at two forest sites*

Field measurements of reflectance were taken in Hesse and Tharandt forest sites at the time close to the passing time of the satellite. The spectra were averaged and integrated over the ETM+ spectral band to validate the ETM+ atmospherically corrected reflectance and therefore indirectly evaluate the MODIS surface reflectance. Measurements were collected at the flux measurement towers above the canopy in three different unshaded directions. The error bars on the ASD

measurements represent the standard deviation computed from the spectra collected at each location (30 measurements). The reflectance of the leaves was measured using an ASD spectrometer at 325 – 1075 nm in 2 nm steps, but only data in the range 400 to 1000 nm were used to avoid the lower signal to noise at the extremes. The measurements were performed under the same illumination conditions as measurements of canopy reflectance. The instrument was held at the normal from the leaf position, focusing on the leaf. The white reference reflectance was achieved using a reference plate (spectralon), having nearly lambertian properties.

Fig 4.3a shows the reflectance of leaf, bark, and litter at Hesse forest. It can be seen that the field-measured spectra of leaves are characteristic of photosynthetically active vegetation. The leaf reflectance was approaching 5.5 % in the red spectral and 65 % in near-infrared spectral regions. This result differed from that reported by Huemmrich and Goward (1997), 0.06 and 0.48 in red and infrared, respectively. However, the results are in agreement with the measurements reported by Aster spectral library (*http://speclib.jpl.nasa.gov/*). In comparison to leaf reflectance, the reflectance of the bark is higher in red region (25 compared to 5 %) and lower in near infrared (55 compared to 65 %), which leads to a lower NDVI. It is important to note that the difference in NIR and red reflectance of the bark is significantly higher than that of the litter; this might lead to high values of NDVI during leaf-off seasons (range from 30 to 40 %). Thus, the stem material played a small but significant role in determining canopy reflectance in woody plant canopies, especially those with low LAI. Asner (1998) found that LAI and leaf angle distribution strongly controlled canopy reflectance, because LAI defines the area that interacts with solar radiation and provides much of the reflected radiation which is captured by sensors. On the other hand, leaf optical properties (and thus foliar chemistry) are affected most directly at the canopy level in the NIR. At low LAI, leaf optical variability played a relatively small role in driving canopy reflectance. At high LAI, the effects of leaf optical properties were more pronounced in the NIR.

Fig 4.3.b shows the reflectance of leaf and bark in Tharandt. The leaf reflectance approaches 2.7 % in the red and 36 % in the near-infrared spectral regions. This result is similar to that reported by the Aster library

(*http://speclib.jpl.nasa.gov/*). The litter reflectance was lower than litter in Hesse forest, 0.15 in red and 0.23 in NIR spectral regions.
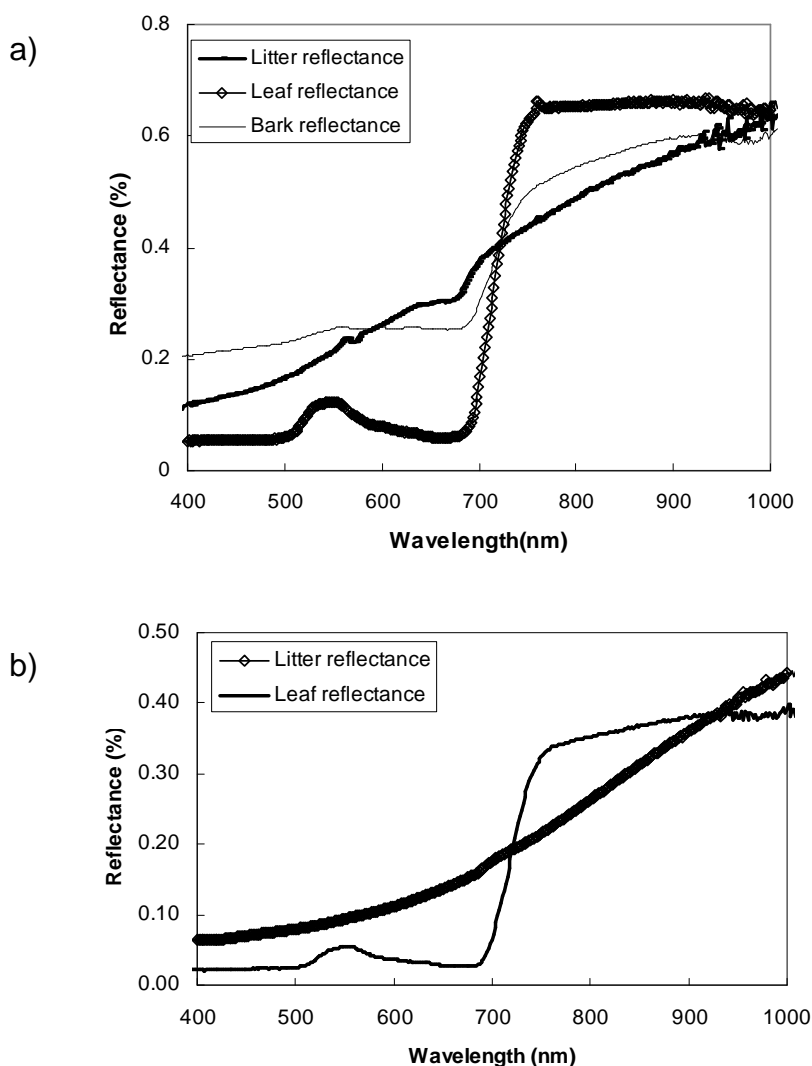
Figure 4.3. a) Reflectance measurements of leaf, bark, and litter in Hesse forest during July 2002; b) Reflectance measurements of leaf and bark in Tharandt forest during July 2002.

Fig. 4.4 shows the reflectance measurements of the canopy at Hesse forest, Tharandt forest, and Tharandt grassland, respectively. At Hesse, the canopy reflectances were lower as compared to leaf reflectance in both the red and infrared regions. In the red region, canopy reflectance was 2 % compared to 5.5 % of leaf reflectance, while in the infrared region, canopy reflectance was 45 % compared to 65 % of leaf reflectance. It can be seen that there is little variation in the visible chlorophyll absorption region, while there is a considerable variation in the NIR.

The same trend was observed at Tharandt forest, where canopy reflectance was lower than leaf reflectance both in the red and NIR (2 % in red and 18 % in NIR). This can be explained by the nature of canopy structure. When the light rays reach the top canopy, most of the light passed through the top leaf layer, while some was reflected, absorbed and transmitted through the leaves. The multiple reflections between adjacent leaves and between leave and stems lead to trapping of radiation within canopy. This effect is particularly pronounced for dense forests, such as at Hesse and Tharandt, where LAI and leaf angle distribution are dominant controls on canopy reflectance (Asner, 1998). The variation of reflectance within the canopy was much higher in Tharandt coniferous forest as compared to Hesse deciduous forest and the Tharandt grassland. This can be explained by differences in canopy structure. Coniferous trees have a conical shape and leaves are clumped with different leaf angle distribution, causing higher bidirectional reflectance effects. The leaves in deciduous forest and grassland are randomly distributed which leads to lower bidirectional reflectance effects as compared to that of coniferous forest. BRDF effects are particularly strong in errectophile canopies if soil background influences are negligible, and are reduced in planophile canopies. This led to higher variation of reflectance within canopy in coniferous forest and lower variation in deciduous forest and grassland (Fig. 4.4).
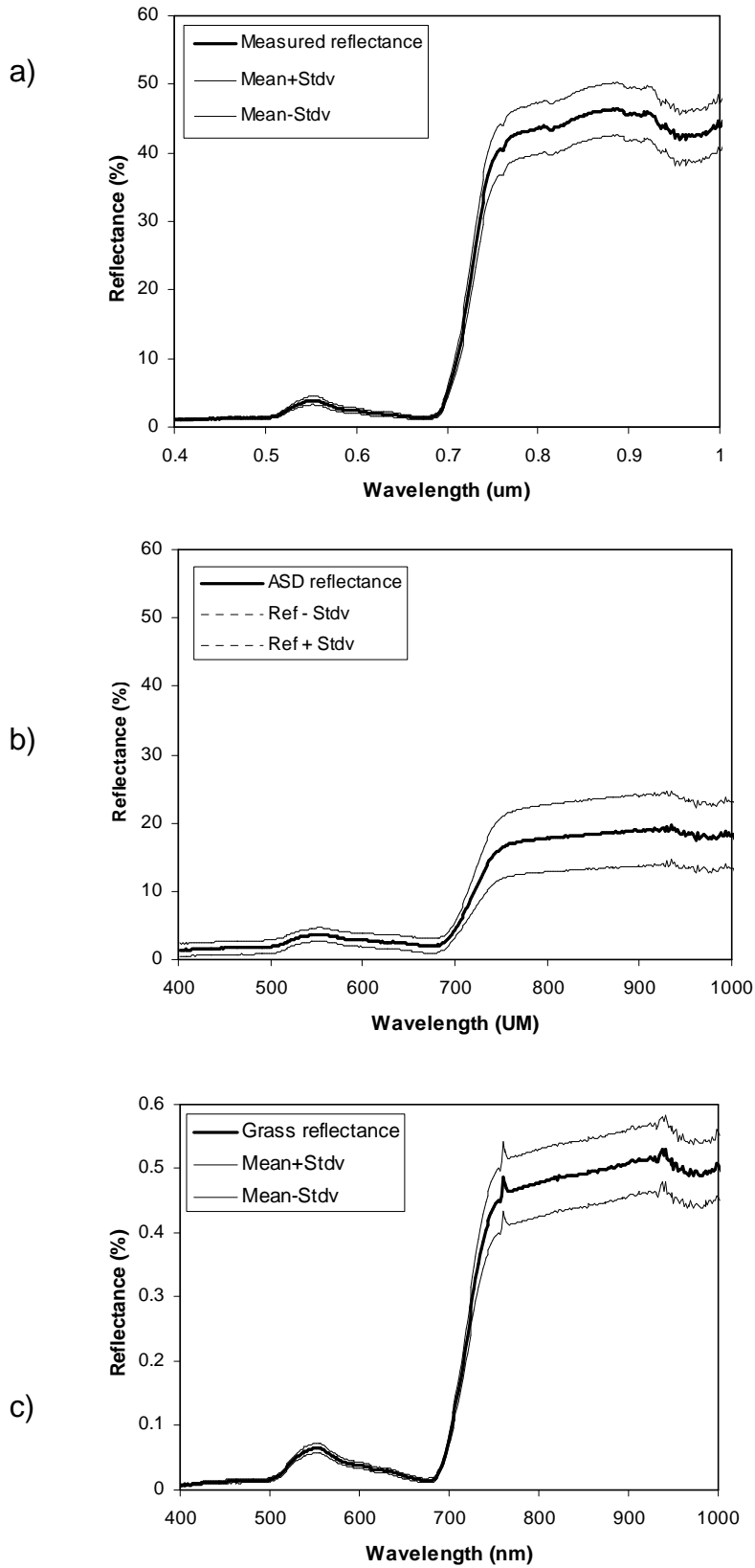
Figure 4.4. Reflectance measurements of the vegetation canopy at a) Hesse; b) Tharandt forest; and c) Tharandt grassland.

It should be noted that the reflectance in the red spectral region of three different functional vegetation types (broadleaf forest, coniferous forest, and grassland) is almost the same, about 2 %. On the other hand, reflectance in the NIR spectral region is much different. Coniferous forest in Tharandt has highest LAI (8.2) and lowest NIR reflectance of 18 %, while grassland in Tharandt has lowest LAI (4.7) and highest NIR reflectance of 48 %, and deciduous forest in Hesse has LAI of 7.3 and NIR reflectance of 45 %. This demonstrates that the relationship between LAI and reflectance (hence vegetation indices) is vegetation type dependent, and is influenced strongly by canopy structure and foliar chemistry.

4.1.3. Measurements of foliar chemistry
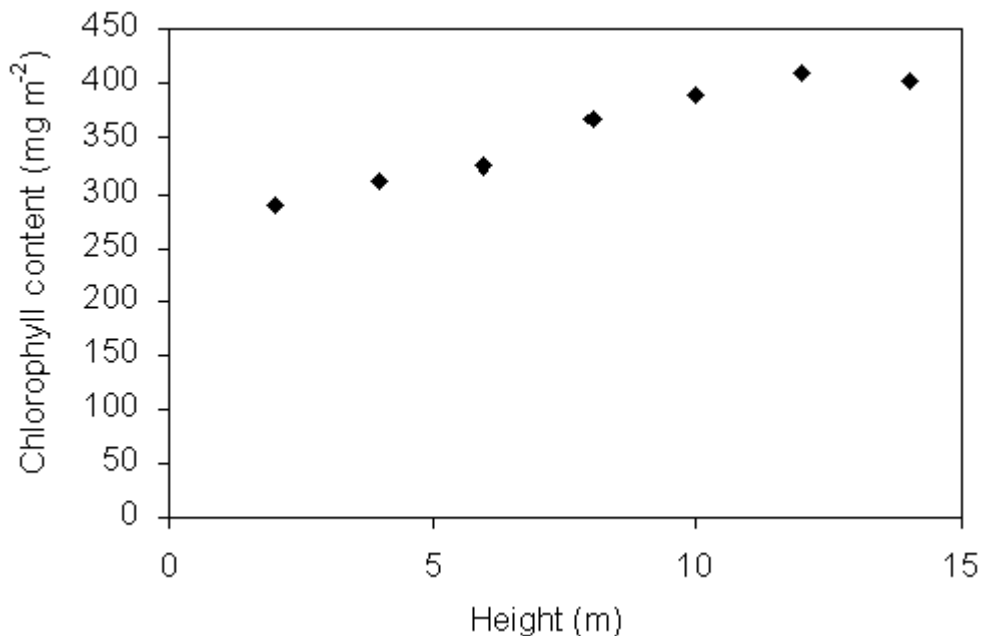
Figure 4.5. Chlorophyll content as a function of height in Hesse forest.

Table 4.1, Table 4.2 and Fig. 4.5 show the measurements of chlorophyll content, leaf nitrogen, and specific leaf weight in Hesse forest vertically and spatially. Vertically, e.g. with increasing height, the chlorophyll content of canopy increases. The top layer of the canopy has the highest chlorophyll content, reaching 400 mg m$^-$^{2}, while the lower layer has lower chlorophyll content of 290 mg m^{-2} (note that data set is independent of tree height). Spatially, the chlorophyll content seems to be consistent within the forest stand, with the mean value of 340 mg m^{-2} and coefficient of variance less than 10 %. This is also true with leaf nitrogen and Specific leaf weight (SLW). The leaf nitrogen ranged from 22.4 g m^2 in plot 24 to 26.7 g m^{-2} in plot

97 with an average value of 24.3 g m^{-2} and coefficient of variance less than 5 %. SLW varied from 81.1 g m^{-2} in plot 75 to 92.0 g m^{-2} in plot 73 with average value of 86.4 g m^{-2} and coefficient of variance less than 5 %. The foliar chemistry variables are used in the radioactive transfer model to predict LAI from canopy reflectance as discussed in Chapter 6.

Table 4.2. Chlorophyll data as a function of height in Hesse forest

Height (m)	2	4	6	8	10	12	14
Number of measurements	28	30	30	55	55	42	68
Mean (mg m^2)	290.2	312.0	325.5	366.5	389.6	409.7	402.4
Median	286.8	303.0	327.0	369.1	387.8	406.7	408.3
SD	27.5	34.2	26.2	33.1	30.6	26.4	62.5

Table 4.3. Spatial measurements of leaf nitrogen, specific leaf weight (SLW), and chlorophyll content in Hesse forest

Plot	Leaf N	SLW	LAI	Chlorophyll content
-	g/kg	g/m^2	m^2 m^2	(mg m^2)
24	22.4	87.7	7.89	352.4
35	24.2	83.6	6.73	369.6
53	24.3	85.1	7.52	346.7
73	22.8	92.0	4.72	313.9
75	25.0	81.1	4.67	349.8
91	26.7	90.8	4.74	380.8
128	25.6	81.2	6.91	346.0
1000	22.8	90.2	7.30	294.0
106	25.2	86.2	5.89	329.6
Average	24.3	86.4	6.30	342.5
SD	1.5	4.1	1.30	26.7

4.1.4. Cloud screening

a)

b)
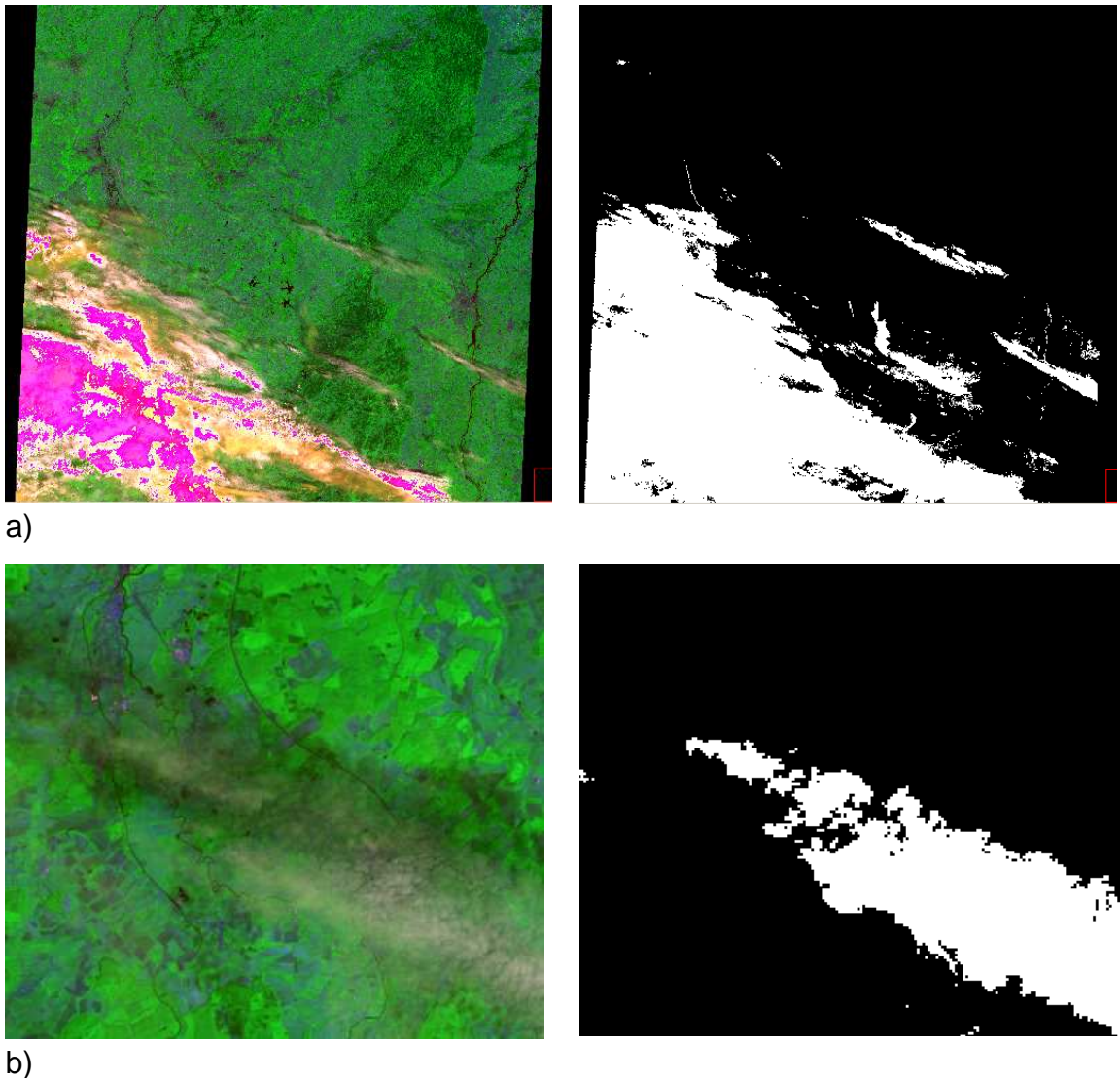
Figure 4.6. a) Landsat ETM (band 1, 4, 7) acquired on 5 July 2001 and cloud mask; b) Illustration of how the algorithm works with thin cloud and haze.

Rigorous cloud screening was performed for the Landsat TM data sets. Fig. 4.6a shows the Landsat TM scene acquired on 5 July 2001 at Hesse and a cloud mask, which passes the cloud-screening algorithm. The cloud pixels represent 30.6 % of the scene. There are numerous clouds covering the southwest part of the scene. The haze, which is observed in the middle of the ETM+ image, is not so evident in the MODIS image due to the late time overpass, or due to spectral differences. The improved algorithm utilizes two additional bands, takes advantage of the enhanced TM6 (thermal band), and ancillary data of surface temperature at the time of acquisition. The algorithm works well for most areas in the world (Irish, 2000). The

Fig. 4.6b shows how well the algorithm works with thin cloud and haze, the most problematic for the cloud screening algorithm. The measurements of temperature at the site helped to define the T° threshold for sepa rating clouds from urban areas, which normally have as high a reflectance as clouds. This helps to separate clouds from the scene and make a comparison between the ETM+ and MODIS possible.
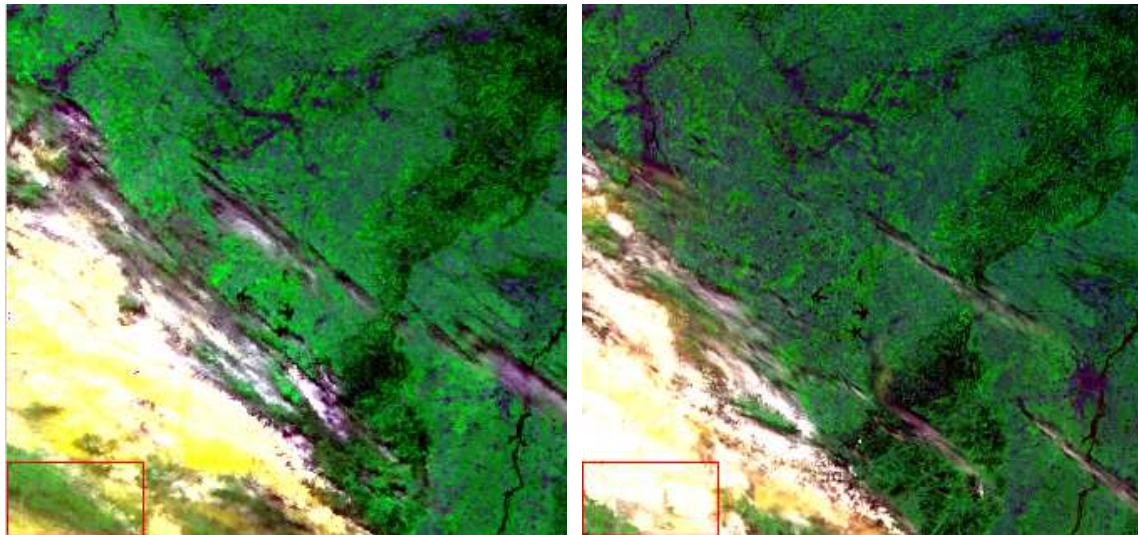
a)   b)
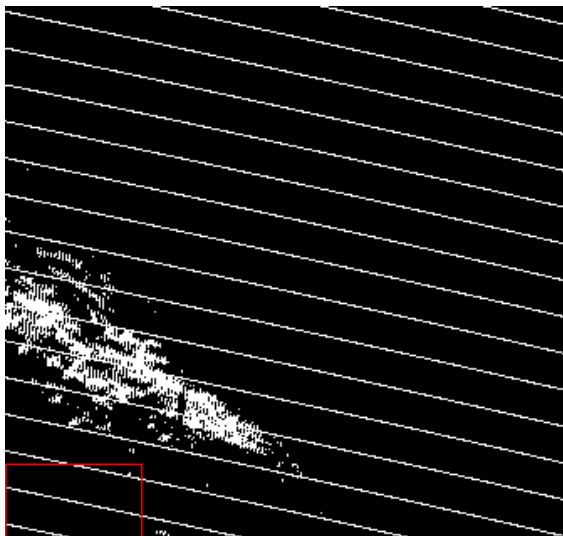
c)

Figure 4.7. a) MODIS (band 3, 2, 7) 500 m resolution acquired on 5 July 2001; b) Landsat ETM (band 1, 4, 7) acquired on 5 July 2001 aggregated into 500 m resolution; c) MODIS cloud mask detected by MODIS reflectance algorithm. Strips are bad data pixels.

Fig. 4.7 shows the difference in patterns of cloud in the TM scene and MODIS data acquired on 5 July 2001 in Hesse. The difference between MODIS and ETM+ cloud could be attributed not only to the MODIS cloud detection algorithm but also the difference in time of acquisition. As MODIS and TM acquire 40 min from each other (MODIS acquires later than Landsat), the cloud pattern is shifted an appreciable distance, which depends on the wind velocity. It is clear that only thick cloud was screened out of the MODIS reflectance product, but the thin cloud and haze remains.

4.1.5. Atmospheric correction

4.1.5.1. Atmospheric correction using ATCORR method

The reflectance obtained from ETM+ by correcting the atmospheric effects was compared to field measurements collected at three different sites (deciduous, coniferous forest, and grassland).

Fig 4.8 shows the comparison between the surface measurements and the ETM+ surface reflectance as a function of the central wavelength of each ETM+ band (0.47, 0.55, 0.67, 0.87 μm). The error bars on the ETM+ reflectance represent the standard deviation computed from 3 x 3 pixels surrounding the pixel where the reflectance measurements take place. This was done to avoid the effects of not correctly georeferenced. The standard deviation of ASD measurements was computed from spectra collected at the sites (about 30 measurements).

At stand level (or level of ETM+ scale), the variation of reflectance is greatest in deciduous forest at Hesse, while it is quite small in the case of coniferous forest and grassland at Tharandt. This implies that at stand scale, the coniferous forest and grassland in Tharandt are more homogeneous than deciduous forest at Hesse. The coniferous forest site gives the best results, especially in the case of TM3 and TM4 (for simplicity, any reference to a specific spectral band will be numerically noted after the TM acronym, e.g. TM4), probably because this is the largest uniform area of the three locations. Even ASD measurements show relative heterogeneity (high standard deviation) at canopy scale. The grassland site shows high uniformity with both ASD measurements and at ETM+ pixel level (low standard deviation). In general, the ETM+ reflectance fell within one standard deviation of the mean measured reflectance, except for TM3. The deciduous forest shows homogeneity at

canopy level and heterogeneity at ETM+ pixel level, but the ETM+ reflectances are still within one standard deviation of the mean ASD reflectance.

We can see that after atmospheric correction was applied, the surface reflectance in visible spectral regions decreases as compared to reflectance measured by the satellite sensor (top of atmosphere reflectance - TOA). In contrast, in NIR spectra, surface reflectance increases as compared to TOA reflectance. The reason is that the atmospheric influence is wavelength dependent. That means that it will alter the brightness of each spectral band in a different way. The atmospheric particles, namely aerosols, scatter the light in visible wavelengths. The shorter the wavelength, the more the effect from scattering is. On the other hand, water vapor absorbs light of NIR wavelengths causing less brightness of objects, as it would be seen from a satellite without atmospheric effects. At the grassland site, the TM3 reflectance is slightly higher than that measured by ASD, while the TM4 is slightly lower than measured by ASD. This might be due to the chosen visibility (optical depth equivalence) which is a bit lower than it should be, so that the atmospheric correction algorithm cannot compensate for the effects. Alternatively, the ASD measurements accidentally fall into low biomass areas.

Based on this limited dataset, we can say that the ETM+ corrected reflectances are in agreement with the ground measurements and contain no bias due to atmospheric correction. Therefore, they can be used to indirectly estimate the accuracy of the MODIS reflectance product via the process of aggregation.

a)

b)

c)
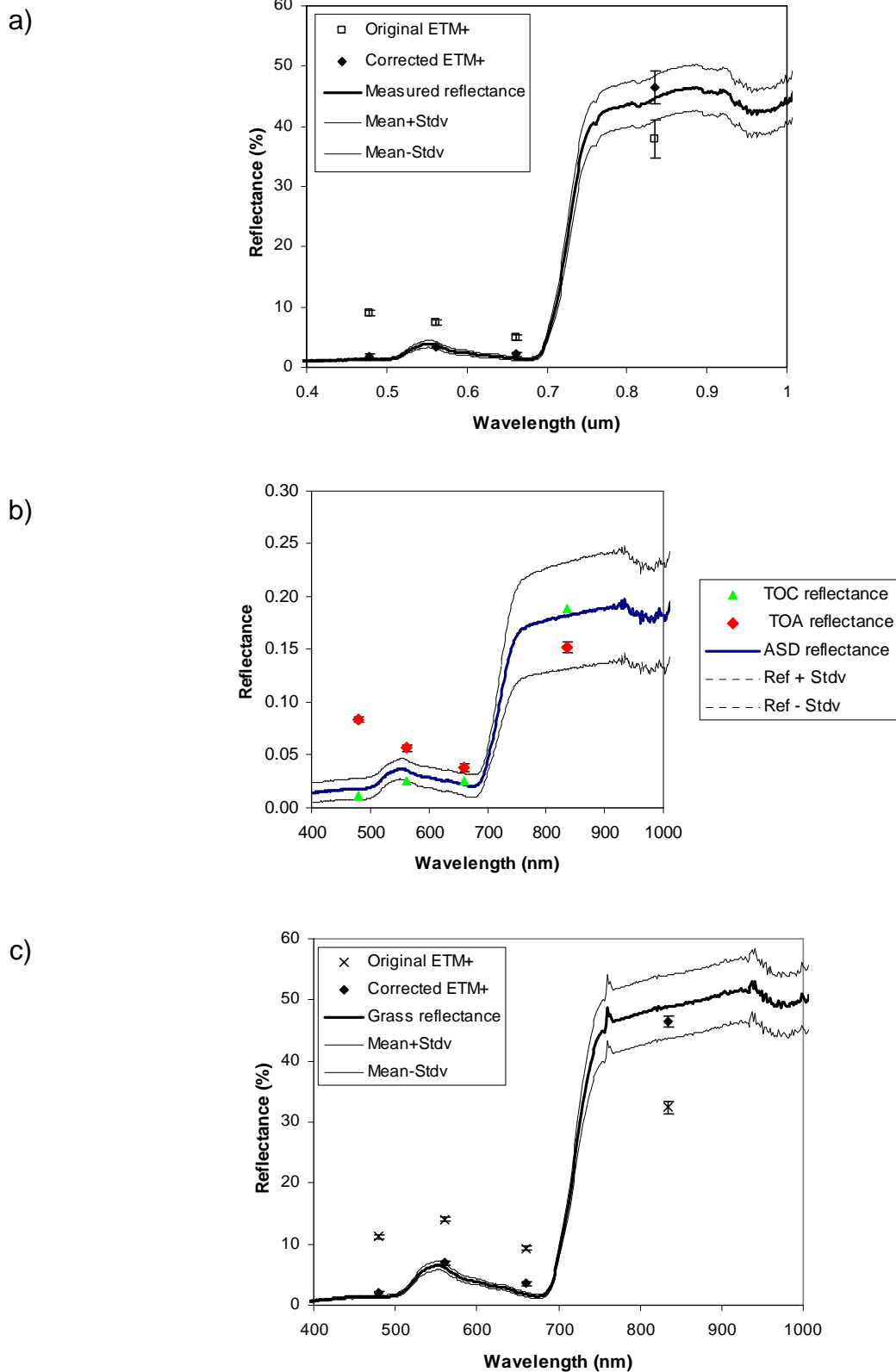
Figure 4.8. Validating retrieved surface reflectance of atmospherically corrected ETM+ by ground measurements (ASD) for a) the deciduous forest; b) the coniferous forest; c) the grassland plot.

4.1.5.2. ATCOR method versus 6S method

Fig. 4.9 shows the comparison of atmospherically corrected ETM+ reflectance, which was corrected by 6S and Atcor methods in Tharandt (March, 2001). In this small area, the visibility (or optical depth) is defined and assumed to be constant. For both methods, the same set of required parameters for atmosphere type/concentration profiles of gases (winter middle latitude), aerosol type and concentration (rural area), flight and ground elevation, illumination and view angles, and visibility/optical depth has been chosen.

There is a high correlation between the two methods of atmospheric corrections for each band as one can expect. The correlation can be explained by the fact that both methods used the same underlying physically-based models to compute the atmospheric scattering and absorption and for the same input of atmospheric conditions input. In all bands, the correlation coefficients (r^2) are close to 1 and intercepts are close to zero, while the slopes are 0.98, 0.99, 1.01, 1.00, 1.01, and 1.01 in ETM+ bands 1, 2, 3, 4, 5, and 7, respectively. TM1 produces the largest difference of 2 % (Table 4.3). Here, the radiometric resolution of output data of the two methods may play a role. The output image of 6S method is stored in 8 bits data format, which re-scale reflectance with a factor of 2.55. That means that each brightness level is about 0.4 %. While ATCOR re-scale reflectance with a factor of 4, each brightness level is about 0.25 %. In the range of high reflectance, the influence of radiometric resolution is not so important because the relative difference is very low. In the low range of reflectance (e.g. TM1, TM2, TM3), the relative difference can be as high as 20 % due to radiometric resolution alone (Fig. 4.9). The results show small differences between the two methods of atmospheric correction, but this difference is still smaller than error bar, which is described in Vermote et al (2002). So, the Atcor method is comparable to 6S method and will be used for atmospheric correction of Landsat ETM+ images in this study.
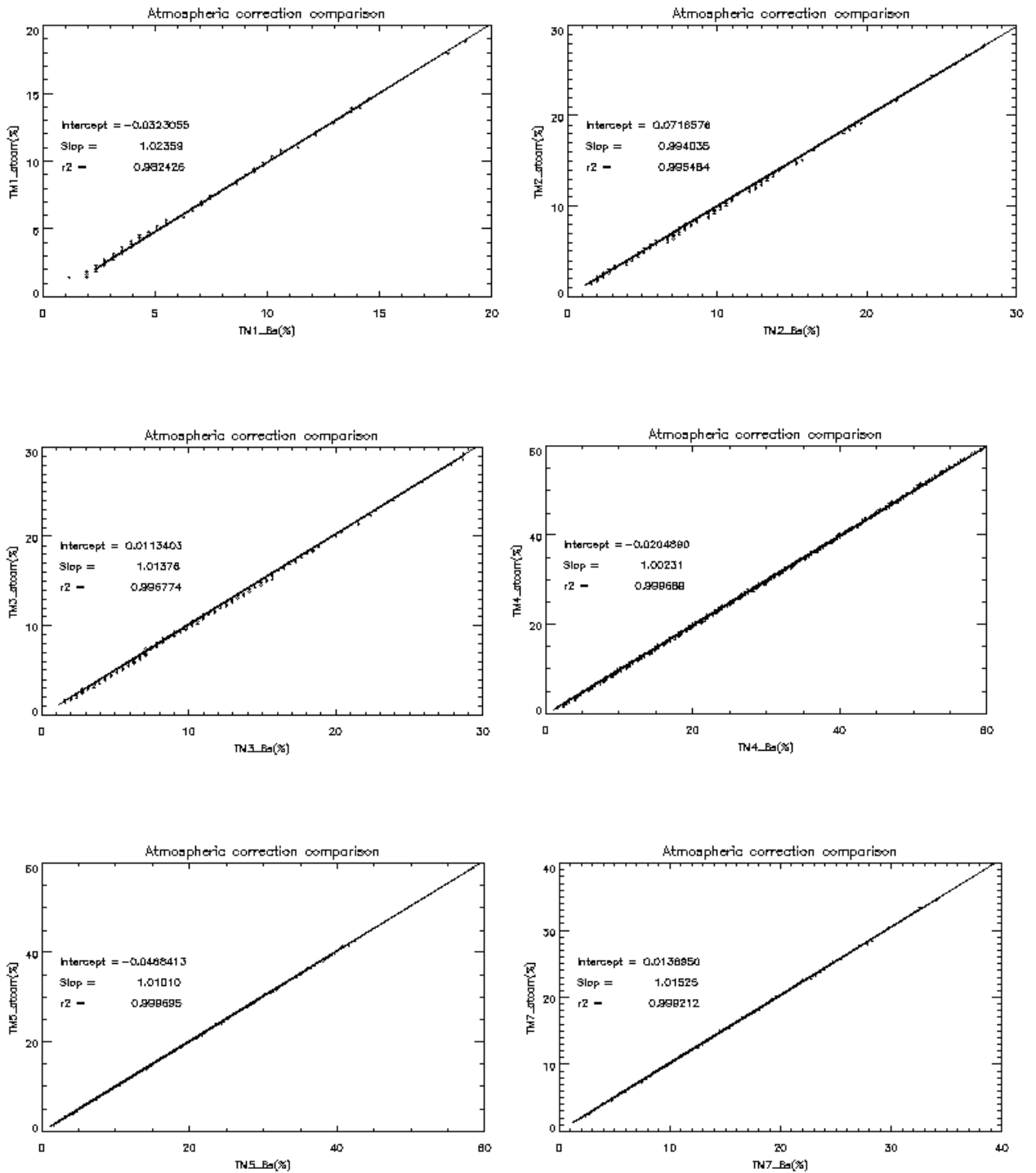
Figure 4.9. Comparison of two atmospheric correction methods: ATCOR (x-axis) and 6S (y-axis) applied for Landsat ETM+ imagery in Tharandt (March, 2001).

4.1.6. Topographic correction

Fig. 4.10 shows Landsat ETM+ composite imagery (bands 1, 4, 7) acquired over the Stubai Valley site on 16 May 2002. At the time of the satellite overpass, the

sun position in relation to the test site center on 47° 07' N, 11° 17' E is at a solar zenith angle of 32.7° and 128.3° azimuth. A digital elevation model (DEM) with a resolution of 30 m in x- and y-axis and 1 m for elevation was available. Data sets for slope and aspect factors were derived from this DEM (Fig. 4.10a-c). In Fig. 4.10d-f, the original image and the resulting images of the atmospheric correction, and topographical correction steps are shown. To enable a comparison, the images are not processed by image enhancement techniques except for a linear histogram stretching, applied to all three images.

The difference between the original image (Fig. 4.10d) and atmospherically corrected image (Fig. 4.10e-f) is apparent. The uncorrected image (Fig. 4.10d) appears blurred and demonstrates the hazy atmospheric conditions at the time of satellite overpass. Details in the valley bottom cannot be distinguished and the topographically induced illumination variations are emphasized, resulting in dark color in the northwest-facing slope. With the atmospheric correction (Fig. 4.10e) the TM bands are corrected solely by using the atmospheric correction component. Thus, the only factor corrected is the altitude dependent effect of the atmosphere. As no illumination correction was applied, the topographically induced illumination variations are still emphasized. Moreover, the spatial resolution seems improved by a reduction of the atmospheric hazing. Details in the valley bottom as well as in the alpine agricultural regions are enhanced as a result of the correction. Green color is more saturated in comparison with the raw image, e.g. the green of the meadows, and the red color is less saturated resulting in more yellow color of the rocky areas. The reason are that the red gun (corresponding to TM1) of original data is higher than that of the atmospheric corrected data, leading to apparent red appearance; while the green gun (corresponding to TM4) is increased in the corrected image. The image appears more homogeneous over the various altitudes. No artifacts brought in by the atmospheric correction can be detected.

An impressive improvement of the satellite data from a visual point of view could be obtained. The correction of the illumination effects is proved to be successful. In the medium and highly illuminated areas, the illumination effect is corrected properly. The relief impression is lost and these parts of the image appear flat (best seen in the small valley). The faintly illuminated surfaces, however, are overcorrected in some shadowed areas and expose artifacts, e.g. along the ridges

and in the V-shape valley. The artifacts are most probably due to an insufficient spatial resolution of the DEM used in the study. The impact of the DEM inaccuracies is emphasized by a mixed signature problem. Surfaces along ridges are often bare limestone with high reflectance properties. A pixel of the region just behind the ridge consists of dark shadowed areas and highly reflective limestone. The mixed signature of such a ridge pixel is influenced by the brightening effect; with regard to the proportion of dark and bright parts within the pixel, the surface appears to be bright, and as a consequence it is overcorrected.

Fig. 4.11 shows histograms of TM5 raw data corrected for atmospheric and topographical effects (Figs. 4.11d) in the Stubai Valley. The site was chosen because it contains areas dominated by forest and alpine grassland under various illumination conditions between 880 and 3460m. In the spectral range of TM5 the correction of illumination effects should result in a bimodal histogram, the peaks representing forest and alpine grassland areas. In contrast to this, the histograms of the radiometric raw and the atmospheric corrected image should appear non-bimodal, since they are influenced by the impact of topographically induced illumination effects.

Indeed the non-bimodality can be seen in the original band 5 (Fig. 4.11d), although the blurring influence of the atmosphere reduces the impact of illumination on the histogram shapes. The atmospheric correction reveals a contrast enhancement by reducing the scattering effect of the atmosphere. Thus illumination effects are emphasized and cause a strong heterogeneous appearance of the objects in the satellite imagery. In spite of the predominant presence of two discriminant object classes, the histogram of the atmospheric corrected image appears non-bimodal. By the combination of illumination and atmospheric correction (Fig.4.11d), however, the impact of illumination on the appearance of the histogram can be eliminated successfully. The bimodality of the histogram clearly shows the frequency distribution of the two dominant object classes of forest and grassland.
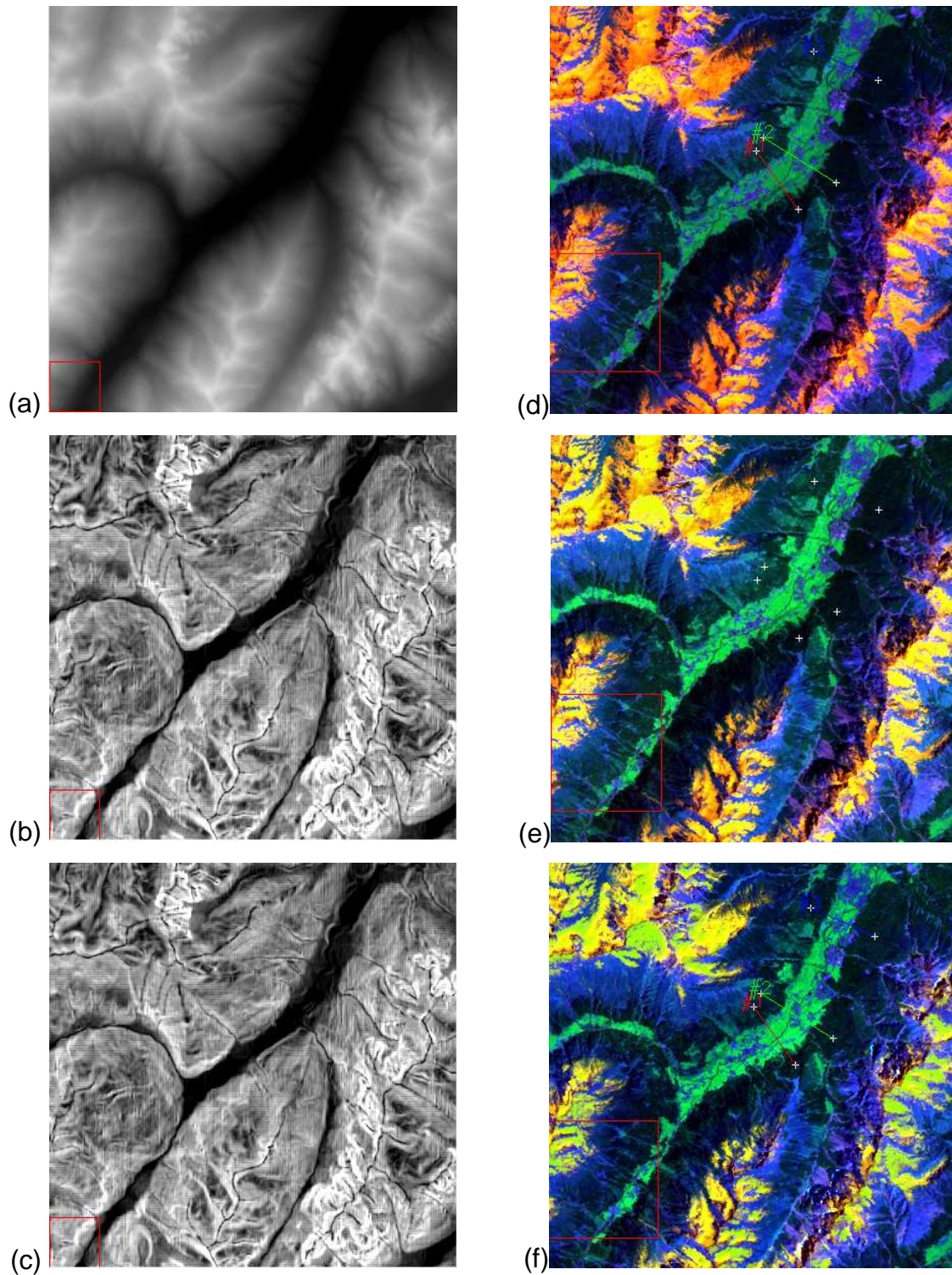
Figure 4.10. a) DEM; b) Aspect; and c) Slope images used for topographic correction. Landsat TM composite imagery (bands 1, 4, 7) d) Original image; e) image applied atmospheric correction; and f) image applied atmospheric correction and topographic correction.

The correction of atmospheric and illumination effects lead to an improved separability of the classes in the raw data: meadows, grassland and farm pasture located on a mean altitude of 900 – 1200 m are more strongly affected by atmospheric effects than the alpine agricultural areas which are found on a mean altitude of 1500 m. Thus the removal of the atmospheric impact on the spectral appearance improves the classification. Also site-specific influences of illumination effects can bias the classification results; an object predominantly lying in shadowed areas is probably easier to classify since shadows are reduced. This is discussed further in the next Chapter.

Fig. 4.11(a-c) shows the horizontal profile no.1 across Stubai Valley from left to right, as the slope changed from very steep (> 40°) on the southeast facing slope to flat at the bottom of the Stubai valley, and again to steep on the northwest facing slope (30 – 40°). With this configuration of sun-su rface-sensor, the BRDF of the surface causes additive reflectance in the southeast facing slope and reductive reflectance in the northwest facing slope.

The atmospheric corrections of the TM3 and TM4 (Fig. 4.11a and b) are shown. The only factor corrected is the altitude dependent effect of the atmosphere, no illumination correction was applied. The figure illustrates that the atmospheric correction algorithm reduces TM3, while increasing TM4 from the original images. The degree of alteration changes along the profile, depending on optical thickness and altitude. At low altitude, the reduction of TM3 is small as compared to higher altitude. The increase of TM4 appears to be reversed, higher at low altitude and lower at higher latitude due to the lower humidity. After atmospheric corrections, the topographic effects are still pronounced in both TM3 and TM4, leading to higher reflectance on the southeast facing slope. The Fig. 4.11a and b also showed results of topographic correction. The atmospheric correction takes place only on non-flat surfaces, and has almost no correction on flat areas. The results show that, both reflectance TM3 and TM4 increase on the northwest facing slope and decrease on the southeast facing slope. These makes coniferous forests on both slopes, which are the same in LAI, have the same range of reflectance (as it should be without topographic effects).

It is demonstrated that atmosphere and topography have a crucial impact on the spectral appearance of objects in a satellite image. Using ATCOR and the

topographic correction algorithm leads to the elimination of the adverse effect of the atmosphere and topographically induced illumination variations.

a)

b)

c)
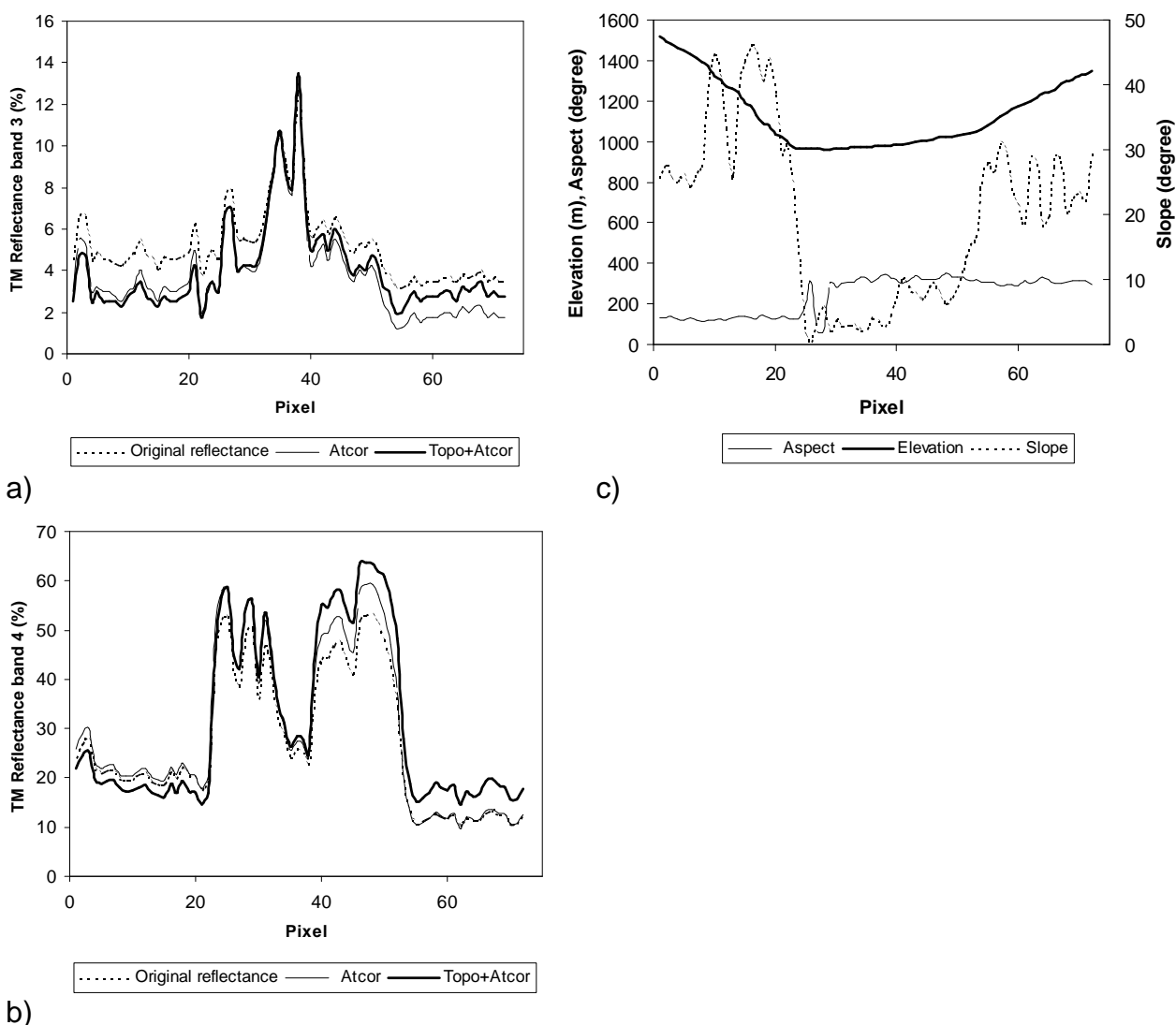
Figure 4.11. Profile no.1 across Stubai Valley showing the changes in reflectance of original data, atmospherically corrected data, and image applied atmospheric correction and topographic correction in a) Landsat TM band 3; b) Landsat TM band 4; in accordance with c) Change in elevation, slope, and aspect along the profile.

4.1.7. Evaluation of MODIS reflectance

4.1.7.1. Upscaling from ETM scale to MODIS scale

From numerical experiments using a three-dimensional (3D) atmospheric transfer model, Liang et al. (2001) found that upscaling of reflectance from 30 m to 1 km over vegetated surface is quite linear. It implies that one can linearly average

the high resolution ETM+ reflectance up to the coarse resolution of MODIS. The average of 16 x 16 blocks of ETM+ pixels was calculated to generate a product at 460 m, which is the same as MODIS reflectance products.

Fig. 4.12a shows a detailed description of the surface at 30 m resolution of Landsat ETM+ data surrounding Hesse forest. It should be noted that the higher resolution of ETM+ shows many features that are not apparent in MODIS data. Fig. 4.12a details the river, roads, and grassland features in the Hesse area, while corresponding MODIS suggests that only a few different surface regimes exist. This example illustrates the effects of spatial resolution on feature recognition. The difference in possible interpretation is probably not important for regional and global climate studies because satellite derived parameters must be aggregated to the scale appropriate for climate modeling which is on the order of 10 km (Price, 1982). The issue is whether the results of aggregation of ETM+ data are similar to MODIS data.

The aggregated image at 500 m resolution (Fig. 4.12b) loses detail in information but still shows large objects, e.g. the forest. Within the forest, the variation of reflectance is low (Fig. 4.12c), indicating the relative homogeneity of the forest. The areas mixed with several land cover types have higher standard deviation of reflectance. Visual comparison of Landsat ETM+ and MODIS data reveals the same reflectance pattern, but further statistical analysis is needed for a quantitative conclusion.
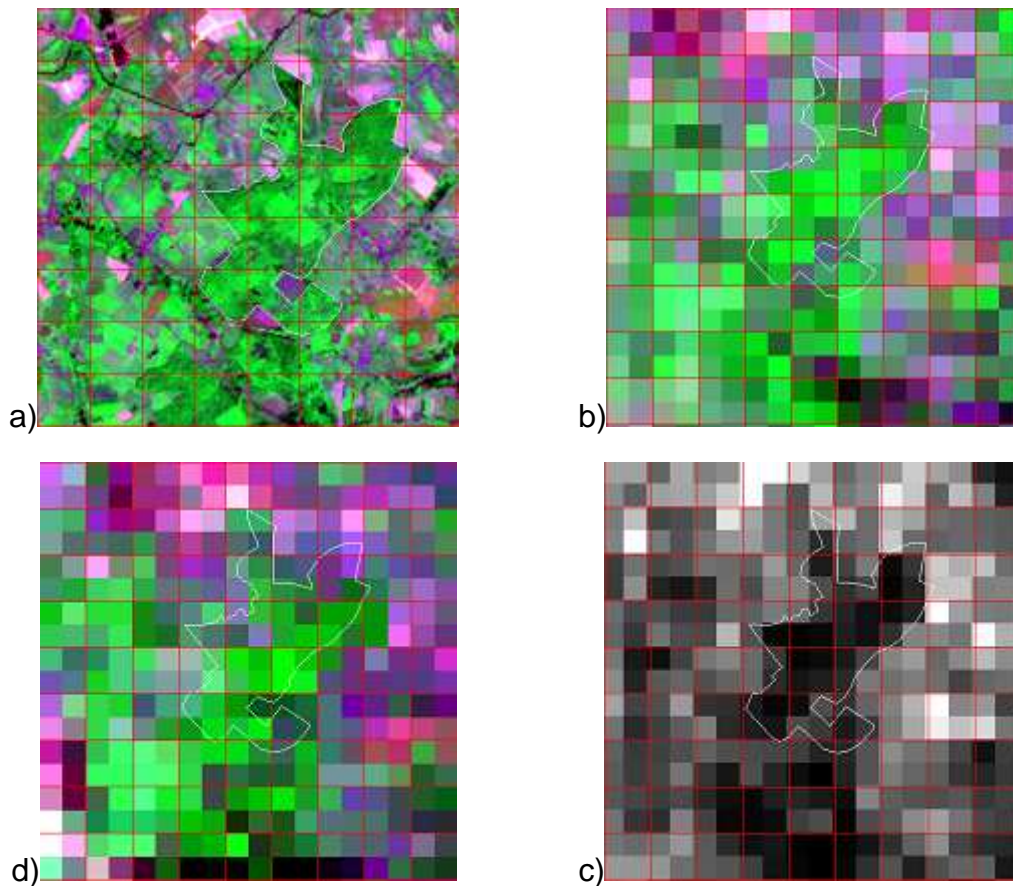
Figure 4.12. a) Landsat ETM bands 3, 4, 7 composite; b) aggregated Landsat ETM 500 m resolution; with c) standard deviation of reflectance within aggregated pixel; compare to d) MODIS band 1, 4, 7 composite in Hesse site on August, 2001.

4.1.7.2.   Comparison between ETM reflectance and MODIS reflectance

Since Landsat ETM+ and MODIS bands have the same spectral response functions (Vermote et al., 2002), it is possible to make a direct comparison of MODIS data to aggregated ETM+. Both Landsat ETM+ and MODIS have a narrow width in the red and near-IR part of the spectrum, eliminating the effect of the water absorption NIR region and also making the red band more sensitive to chlorophyll absorption (Van Leeuwen et al., 1999). Slope and R-squared are used to characterize the fitting.

As the initial part of the evaluation process, a comparison was made in the small regions, 13 x 13 pixels and 21 x 21 pixels surrounding the flux tower pixel. Fig. 4.13 shows the high correlation of Landsat ETM+ band 3 and MODIS reflectance band 1. MODIS band 1 reflectance is slightly higher than TM 3 : 4 % and

2 %, respectively. As we go to larger area, the coefficient of correlation (r^2) seems to decrease. This may be explained by the fact that the portion of pixels with higher reflectance variation increases (Fig 4.12b and c). Another reason is that the dynamic range of land reflectance is not very well represented in the selected area.

In heterogeneous areas (higher reflectance variation), the accuracy of image georeferencing plays an important role. If the error of georeferencing is 90m, the area with incorrect registration would be 10 – 15 % and would cause considerable change in reflectance due to change in distribution of land cover types in the pixel of interest. Disney et al. (2004) showed that not only the physiological parameter (e.g. LAI) of the surface but also the spatial distribution of land cover types determine the spectral characteristics of the surface. For example, from space, the equally distributed mixed forest would look greener than clustered mixed forest having the same green biomass.
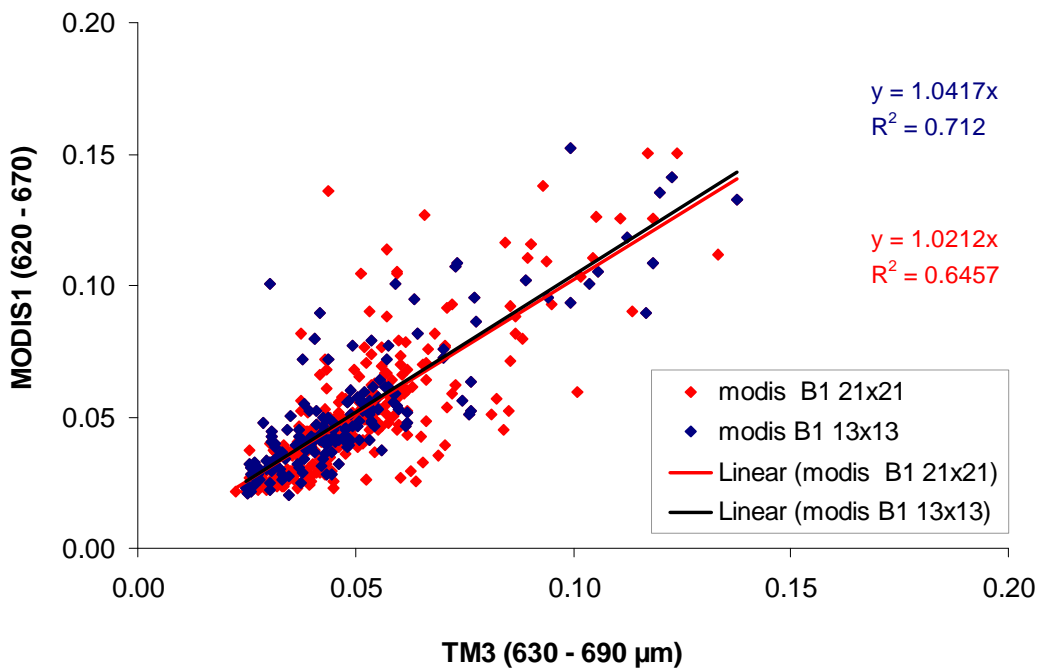
Figure 4.13. Comparison of MODIS band 1 and Landsat ETM+ reflectance in Hesse forest (22/08/2001).
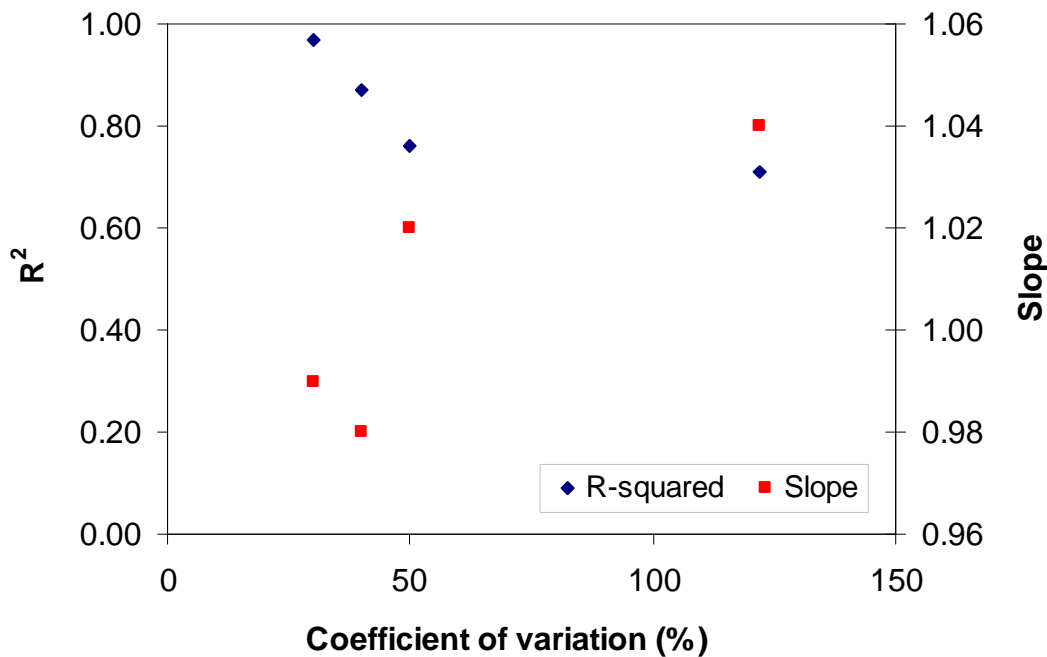
Figure 4.14. Dependency of the slope and r^2 on the way of choosing pixels for comparison based on variation of reflectance (in Hesse forest).

Fig. 4.14 shows the dependency of the slope and r^2 as influenced by the means of choosing pixels for comparison (based on variation of reflectance within pixels of consideration). As the variation of TM pixels within the aggregated pixel decrease (from less homogeneous to more homogeneous landscape), the coefficient of correlation increases to 1 and slope moves closer to 1 with a coefficient of variation is 30 %. This implies that only in homogeneous areas (e.g. large forests), is the accuracy of image georeferencing negligible, because the nearby area has a similar reflectance to the area of mis-registration.

The MODIS instrument scans a broader swath than the 180-km of ETM+, so each ETM+ data set is fully within MODIS data coverage (Fig. 4.7). Fig. 4.15 and Table 4.4 show comparisons between MODIS reflectance and ETM+ reflectance at corresponding wavelength for entire ETM+ scenes. Only pixels, which have a coefficient of variation smaller or equal to 20 %, are taken into consideration. The selections of these pixels make it possible to compare with the results from a previous study (Vermote et al., 2002). Note that the MODIS and ETM+ were acquired at a similar viewing geometry and overpass time.

The quantitative comparisons of the aggregated ETM+ reflectance and MODIS reflectance product are shown in Fig. 4.15 and Table 4.6. Two parameters used for

assessment of correlation are slope and coefficient of correlation (r^2). At first glance, we can say that MODIS and ETM+ reflectances are in very good agreement, taking into account that we forced the fitting line through the origin. Comparisons from all bands and all dates show the difference between MODIS reflectance and ETM+ reflectance varies from -5 to +7 %. The difference in the green band (TM2) are the largest as compared to other bands. This may be explained by the difference in spectral response of MODIS and ETM+ sensors which is largest at green wavelengths (Table 4.5). Vermote et al. (2002) found that there is a difference in spectral response between MODIS and ETM+ bands. The largest difference occurs in MODIS band 3 (0.47 μm), where MODIS surface reflectance is about 4 % lower than the corresponding TM2 (Table 4.5).

The degree of correlation between the ETM+ surface reflectance and MODIS reflectance varies greatly from scene to scene. For example in the scenes which cover Hesse forest, the r^2 between ETM+ reflectance TM2 and MODIS band 4 reflectance is 0.69, 0.79, and 0,91 for 31 March 2001, 5 July 2001, and 22 August 2001, respectively. Temporal variation of reflectance at the Hesse tower site for 2001 is shown in Table 4.6. The MODIS reflectances are well within the standard deviation of ETM+ reflectances, except for the blue band (TM1).

Fig. 4.15 shows the comparisons of the MODIS reflectance product with aggregated ETM+ product acquired on August 22, 2001. In this partly cloudy scene, the mean differences of the two reflectances are small with slopes ranging from 0.96 to 1.01. Although there is a large scatter in these plots, they contain around 10000 pixels and the density in the middle of the scattered data are very high. Thus, the coefficients of correlation of the two products is also very high, ranging from 0.86 in TM4 to 0.93 in TM3 and TM5. The correlation between MODIS and ETM+ reflectances is high because most of the uncertainty in the MODIS sub-pixels scale is eliminated by filtering out all the pixels, which have high coefficient of deviation. On the other hand, the dynamic range of land reflectance (from very low to very high) is very well represented in the scene.

In Fig. 4.15b and c there are pixels where MODIS band 1 and 2 values are much larger than TM3 and TM4, which somehow impair the correlation of MODIS and ETM+ reflectances. The reason is that the MODIS reflectance product could not mask out all of the cloudy pixels, so the MODIS reflectances remain very high at

those pixels whereas ETM+ reflectances are low (at the time of ETM+ acquisition those pixels are not covered by clouds).

Another error in the MODIS reflectance product may come from inaccurate atmospheric input parameters, mainly aerosol optical depths and water vapour content (Liang et al., 2002). Aerosol optical depth represents the most critical issue in the atmospheric correction process since it has a large effect on the visible and near IR bands. Remember that, ETM+ data is atmospherically corrected by the ATCOR method, in which the image based derivation of aerosol optical depth is inferred from band TM2, TM3 and TM7 (0.47 µm, 0.67 µm, and 2.13 µm) as it is done in MODIS reflectance (Richter, 2001; Vermote et al., 2002). So this possible error may be compensated.

One important source of error comes from differences in the radiometric resolution of MODIS and ETM+ data (Table 4.8). The ETM+ is stored in 8 bits data format, which re-scale reflectance with a factor of 4. This means that each brightness level is about 0.25 %. MODIS is stored in 12 bits format, which re-scales reflectance with factor of 100, each brightness level is about 0.01 %. This may lead to relatively large differences at lower reflectance and a large scatter in the plots. Fortunately, the upscaling process of ETM+ data may reduce the discrepancies, since within small area reflectances follow a normal distribution in most cases, especially in homogeneous areas. This error compensation explains why the scatter is small at low reflectance.

The finding from this study is generally in accordance to the study of Vermote et al. (2002) as seen in Table 4.6. However, the coefficient of correlation is significantly lower than that reported by Vermote due to the fact that they made a comparison of surface reflectance for a smaller area (21 x 18 km) as compared to full ETM+ scenes included in this study.
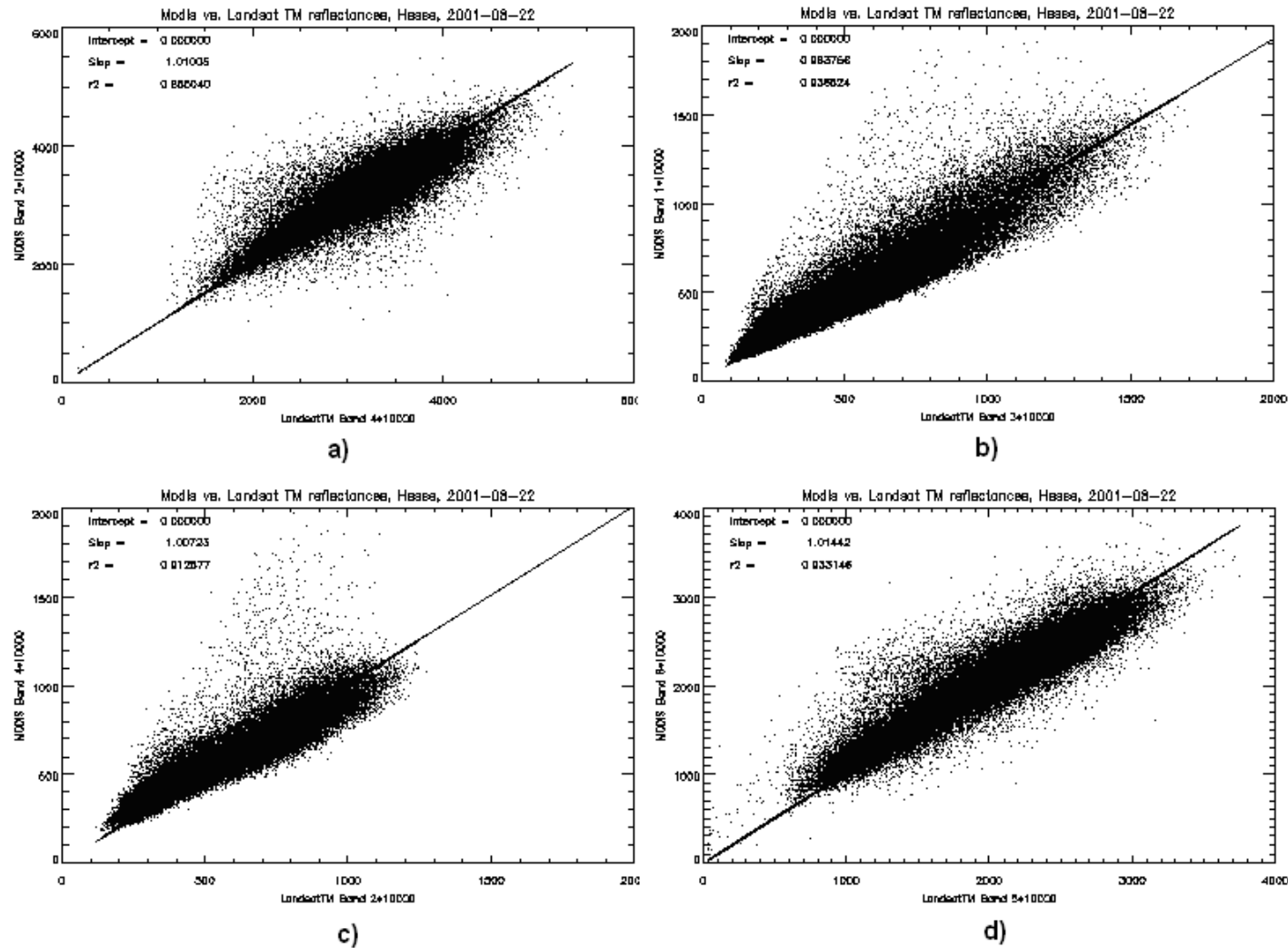
Figure 4.15. Comparison of the surface reflectance derived from ETM+ (x-axis) with the MODIS reflectance product (y-axis): a) Landsat B4 – MODIS B2; b) Landsat B3 – MODIS B1; c) Landsat B2 – MODIS B4; d) Landsat B5 – MODIS B6.

Table 4.4. Correlation of Landsat TM reflectance which is atmospherically corrected by ATCOR and 6S methods

TM1			TM2			TM3			TM4			TM5			TM7		
A	b	r^2	A	b	r^2	a	b	r^2	a	b	r^2	a	b	r^2	a	b	R^2
-0.03	1.02	0.98	0.07	0.99	0.99	0.01	1.01	0.99	-0.02	1.00	0.99	-0.04	1.01	0.99	0.01	1.01	0.99

a: intercept, b: slope, r^2: coefficient of correlation

Table 4.5. Comparison of spectral response from ASD measurements integrated over ETM+ and MODIS bands. MODIS(i)=a*TM(i) (where i = 1 to 7)

	A
MODIS band 3	0.93
MODIS band 4	0.97
MODIS band 1	0.97
MODIS band 2	1.03
MODIS band 6	1.02
MODIS band 7	1.03

Table 4.6. Comparisons of the aggregated ETM+ reflectance and MODIS reflectance.

Bands ETM (MODIS)	B2 (B4)		B3 (B1)		B4 (B2)		B5 (B6)	
Date	Slope	r^2	Slope	r^2	Slope	r^2	Slope	r^2
17/06/2002	0.98	0.92	1.03	0.87	1.02	0.91	1.01	0.84
31/03/2001	1.05	0.69	1.02	0.86	0.98	0.69	0.99	0.69
05/07/2001	1.01	0.79	0.97	0.85	1.01	0.68	1.01	0.85
22/08/2001	1.01	0.91	0.96	0.93	1.01	0.86	1.01	0.93
10/11/2001	0.97	0.69	0.98	0.69	0.99	0.91	0.99	0.84
14/06/2001	1.00	0.68	0.95	0.69	0.99	0.78	1.03	0.78
26/08/2001	1.05	0.69	1.02	0.68	1.03	0.71	1.01	0.80
20/10/2001	0.95	0.92	0.96	0.91	1.02	0.76	1.07	0.60
Vermote (2002)	1.05	0.96	0.97	0.96	1.00	0.92	1.02	0.93

Table 4.7. Comparison of MODIS and Landsat ETM+ reflectances in Hesse for 2001

TM B1		TM B2		TM B3		TM B4		TM B5		TM B7	
Slope	r^2	Slope	r^2	Slope	r^2	Slope	r^2	Slope	r^2	Slope	r^2
0.80	0.58	0.95	0.97	0.96	0.85	1.02	0.98	1.00	0.84	1.04	0.85

Table 4.8. Bandwidths (nm) and radiometric resolution of MODIS and ETM+ reflectances

Sensor	TM B2– MODIS B3	TM B3 – MODIS B1	TM B4 – MODIS B2	TM B5– MODIS B6	TM B7– MODIS B7	Radiometric resolution
ETM+	450 - 515	630 - 690	750 - 900	1550 -1750	2090-2350	0 - 255
MODIS	457 - 479	620 - 670	841 - 876	1628 - 1652	2105-2155	0 - 10000

4.2. Conclusions with Respect to MODIS Reflectance

An evaluation of MODIS reflectance products has to rely on ground measurements. However, the direct comparison of ground point measurements with MODIS products is not feasible. The key step in the MODIS evaluation is the upscaling process from ground point measurements to MODIS resolutions using high-resolution images (ETM+). The evaluation approaches presented in this work are quite general and straightforward, and they have been applied successfully in other studies of the land surface products from MODIS (Liang et al., 2002; Vermote et al., 2002; Disney et al., 2004; Fang et al., 2004).

Field measurements were conducted in Hesse forest, Tharandt forest, and Tharandt grassland sites. Ground measurements were used to "calibrate" high-resolution products from ETM+ imagery. The limited dataset of ground measurements of reflectance are successfully used to calibrate high-resolution Landsat ETM+ products. Therefore, ground measurements are indirectly used for evaluating the MODIS products.

Since high-resolution images measure the top of atmosphere radiance, they should undergo a process of atmospheric correction to convert them into the at canopy reflectance products which are comparable to MODIS reflectance. Subsequently, Landsat ETM+ imagery can be upscaled to the MODIS resolutions for evaluating the MODIS reflectance products.

The initial evaluation results show that the MODIS reflectance product is reasonably accurate (less than 10 % absolute error). The MODIS team is still developing the algorithms to improve the quality of reflectance product. The final conclusion about the uncertainties of these products must be made after MODIS data reprocessing. Note that the evaluation results were based on ETM+ scene from 8 days in 2001 and 2002 and across typical landscapes in Europe. It is quite important that such tests be made, in order to understand potential influences of landscape structure in the areas of interest.

In the current atmospheric correction procedure, the surface has been assumed to be a Lambertian. This assumption was used in atmospheric correction because we have not been able to determine surface BRDF properties at the ETM+ resolution. It is probably not a serious issue at this point since the MODIS atmospheric correction algorithm currently is also making such an assumption Vermote et al. (2002), but it is certainly an important area to be improved in the future.

CHAPTER 5. EVALUATION OF MODIS LAND COVER

5.1. Results and Discussion

5.1.1. Land cover classification at Berchtesgaden National Park

5.1.1.1. Habitat mapping by aerial photography in Berchtesgaden National Park

Aerial color infrared (CIR) photos taken in 1997 were used to map habitats in the Berchtesgaden National Park within the framework of the Project "Alpine Habitat Diversity–HABITALP–INTERREG IIIB Alpine Space Program" by the administration of the National Park Berchtesgaden (Franz, 2000). In general, aerial CIR photography is considered to provide the best method for accurate classification of land cover over large areas due to the high resolution of the image. One drawback is that the interpretation is visually carried out, so that it is very laborious and time consuming. A set of criteria was developed to define 153 biotope types in the National Park Berchtesgaden. To differentiate biotope types, the brightness, texture and surface, shadows, and stereoscopic effect of the image was used (Kias et al., 1999). Homogeneous areas satisfying specific criteria were identified and assigned into one of 153 biotypes (Franz, 2000). The alpine habitat map is used in this study as the ground truth map to validate the land cover map derived via remote sensing imagery.

The initial map was reduced and reclassified into six classes based on functional type of the vegetation and to reflect the dominant plant growth forms at the study sites as shown in Fig. 5.1a. The six classes are: deciduous forest, coniferous forest, mixed forest, grassland, water, and rocks. In the National Park Berchtesgaden, the deciduous forest refers to broadleaf forest which defoliates during winter and it is dominated by *Fagus sylvatica* and *Alnus viridis.* The coniferous forest includes forest types with needle-like leaves which include stands dominated by *Picea abies* and *Pinus mugo* in Berchtesgaden. The mixed forest is defined as a mixture of deciduous broadleaf and needleleaf species where each occupies at least 25 % of the area (Küchler, 1988).

5.1.1.2. Supervised classification results with Landsat images of National Park Berchtesgaden.

Supervised classification was performed using Landsat ETM+ images in Berchtesgaden and Stubai Valley. In supervised classification, the basic steps are: (1) select training samples which are representative and typical for that information class, spectral characteristics of each class is defined; (2) perform classification with the training samples set and specific classification algorithms; (3) assess the accuracy of the classified image through analysis of a confusion matrix which is generated by comparing to reference data.

According to the fieldwork survey of the study area and ancillary data, there are seven classes that need to be identified by image classification in Berchtesgaden: deciduous, needleleaf, mixed forest, grassland, water, shrubland, and rock (bare soil). Training samples were selected according to the ground truth from the fieldwork and using aerial photography. These homogeneous areas are identified in the image to form the training samples for all of the classes. What is important to be mentioned here is that the ground truth used for training samples for classification are independent from the ground truth used for accuracy assessment in order to objectively evaluate the quality of the classification result. The number of pixels in a training area for a given class was based on the proportional representation of the class. Care was also taken to adhere to the rule of 3n pixels per training class where n represents the number of bands (Mather, 1987). Once the training sites for each land cover type are chosen, the spectral signatures from the specified regions of interest are derived. For every object class a spectral signature (spectral response) in bands 1 to 7 (except 6) Landsat TM was derived.

The maximum likelihood classifier is selected for performing the supervised classification due to its advantage compared to other algorithms such as minimum distance. The assumptions, calculation characteristics, and advantage and disadvantage of this classification algorithm have been described in detail in Chapter 2. Supervised classification of Landsat image of Berchtesgaden (with 6 bands) resulted in Fig. 5.1b.

a)

Unclassified
Coniferous forest
Mixed forest
Deciduous forest
Grassland and Cropland
Water
Rocks

b)

Unclassified
Coniferous forest
Mixed forest
Deciduous forest
Grassland and Cropland
Water
Rocks
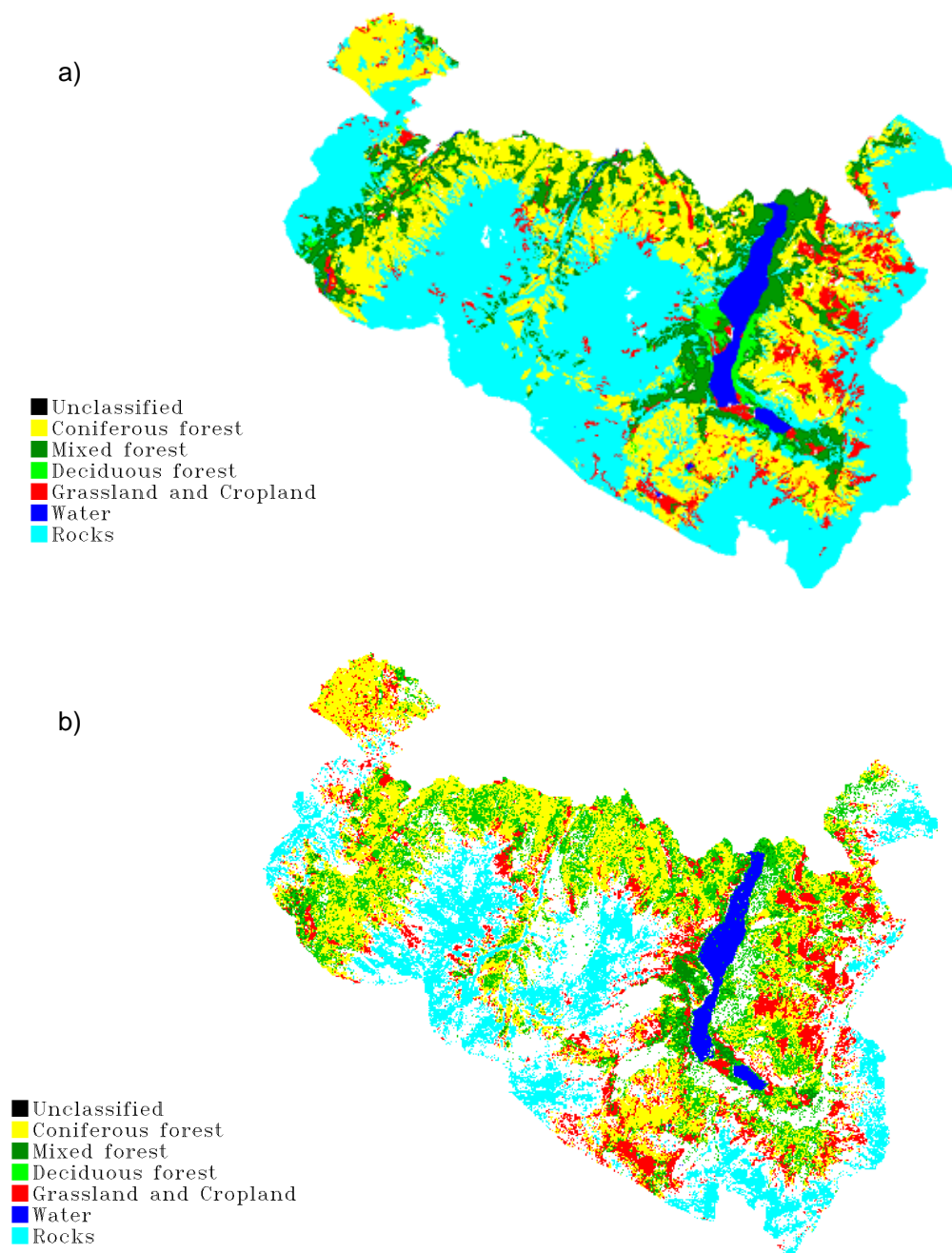
Figure 5.1. a) The land cover map of National Park Berchtesgaden (ground truth map); b) The land cover map of National Park Berchtesgaden derived from Landsat TM by using Maximum Likelihood classifier.

a)   b)
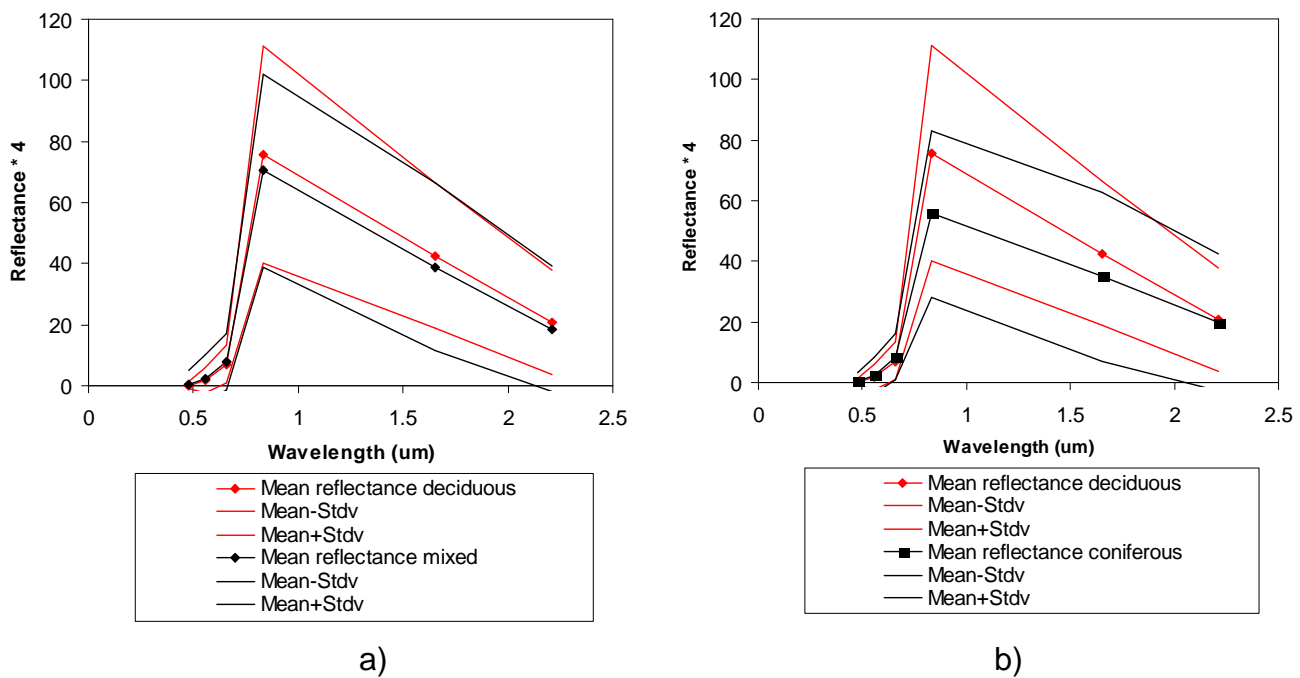
Figure 5.2. a) Comparison between spectral signature of deciduous forest and mixed forest; b) Comparison between spectral signature of deciduous forest and mixed forest.

Accuracy assessment for supervised classification of Landsat data can be evaluated from the error matrix in Table 5.1 that is generated using the ground truth map. From Table 5.1, it can be seen that the classification has an overall accuracy of 55.2 %. The producer's accuracy of the coniferous forest is quite good (55 %). This means 55 % coniferous area has been correctly identified. The user's accuracy of this class is 56.6 %; this means 56.6 % of the areas identified as coniferous forest within the classification is truly of that category. Other vegetated classes are deciduous forest, mixed forest and grassland. From Table 5.1, it can be seen that those classes have relatively low producer's and poor user's accuracy.

The spectral signatures of water and rock are extremely different from other vegetated classes due to the spectral characteristics of the Landsat. This explains why the producer's accuracies of those classes are 96.1 % and 96.9 %, respectively. The overall accuracy of 55.2 % is confused (Campbell, 2002) but reasonable, considering the complexity of the region, and improved in comparison to a previous study in this region (Bobeva, 2003). The greatest difficulty limiting positive results is the occurrence of shadows, which cannot be removed by topographic correction of the remote sensing data. Another reason comes most probably from the basic differences between the ground truth map and remote sensing based classification

map. The former is polygon based, while the land cover map, deriving by maximum likelihood classifier of remote sensing data is pixel based. The ground truth map was made in 1994 while the satellite image was acquired in 1999.

Table 5.1. Error matrix according to the ground truth map for supervised Landsat classification in Berchtesgaden

Class	Reference data						Total
	Water	Rock	Mixed forest	Deciduous forest	Grassland	Coniferous forest	
Water	96.06	0.00	2.28	0.95	0.39	0.34	4.00
Rock	0.80	96.87	11.92	13.00	35.30	19.90	36.88
Mixed forest	2.11	1.09	32.01	41.54	11.19	18.50	16.44
Deciduous	0.42	0.01	3.44	22.22	1.88	0.85	1.97
Grassland	0.42	1.01	5.29	3.78	25.27	5.43	7.35
Coniferous	0.19	1.01	45.05	18.50	25.97	54.98	33.36
Total	100.00	100.00	100.00	100.00	100.00	100.00	100.00

Class	Producer' accuracy		User's accuracy	
	(Percent)		(Percent)	
Water	96.06	5016/5222	82.72	5016/6064
Rock	96.87	32566/33617	58.32	32566/55842
Mixed forest	32.01	10326/32263	41.47	10326/24899
Deciduous	22.22	957/4307	32.05	957/2986
Grassland	25.27	6070/24020	54.56	6070/11125
Coniferous	54.98	28590/51997	56.60	28590/50510

Overall Accuracy = (83525/151426) 55.2 %

Kappa coefficient = 0.41

A more careful inspection of the error matrix shows that there is significant confusion between the mixed forest and deciduous forest. This occurs because these two land cover types have close spectral values within the image data of Landsat. This may be due to the fact that the Landsat image was taken in September, when the canopy of deciduous forest was fully developed. The mixed forest as defined above (Küchler, 1988) tended to have the spectral signal of closed deciduous forest. Fig. 5.2a indicates similarity in the spectral signature of deciduous

forest and mixed forest. This similarity leads to difficulty in distinguishing the two forest types. Thus, these two forest types have subsequently been merged into one class, namely deciduous forest. The only reliable vegetated class associated with this overall classification from both a producer's and a user's perspective is the coniferous forest, since the spectral signature of coniferous forest is significantly different from other forested classes (Fig. 5.2b).

5.1.1.3. *Object-based classification of National Park Berchtesgaden*

As indicated in Chapter 3, eCognition classifies an image based on an object-based approach. The classification process is divided into three steps: image segmentation, classification and accuracy assessment. In contrast to traditional image processing methods, in which the basic units are single pixels, the basic units of object-based image analysis are image objects or segments. An advantage of the object-based approach is the fact that the expected result of image classification is the extraction of real world objects, e.g. the forest patches. This expectation cannot be achieved with common, pixel-based approaches.

5.1.1.3.a. Image segmentation

One of the main features which made eCognition different from other image processing package is object-oriented processing of the image. The first step in eCognition is to extract image objects by grouping pixels, which have the same spectral characteristics and exist adjacent to each other. The image objects will become basic building blocks for subsequent classification, and each object will be treated as a whole in the classification. The segmentation rule is to create image objects as large as possible and at the same time as small as necessary. After segmentation, a great variety of information can be derived from each object for classifying the image since an image object offers substantially more information in comparison to a single pixel.

eCognition uses a newly developed multi-resolution/multi-spectral segmentation procedure, which is based on the possibility to generate image object primitives in any chosen scale, using data with different resolution and different spectra. The segmented image then can be used in image analysis to extract the objects of interest such as land cover/land use units. The segmentation procedure follows a relatively general assumption of homogeneity within basic objects. Thus in

most cases, objects of interest cannot be directly extracted, but require grouping of some adjacent basic objects. For the object oriented approach to image analysis in eCognition, image objects resulting from a segmentation procedure are, therefore, intended to be image object primitives, serving as information carriers and building blocks for further classification. In this sense, the best segmentation result is one that provides optimal information for further processing.

In order to receive optimal raw material for object oriented image analysis, the development of multi-resolution/spectral segmentation aims to:

1. Produce highly homogeneous segments for the optimal separation and representation of image objects/regions.

2. Produce highly homogeneous segments where the average size of image objects must be adaptable to the scale of interest.

Multi-resolution/spectral segmentation is a basic procedure in eCognition for object oriented image analysis. It is used here to produce image object primitives as a first step for a further classification and other processing procedures.

Multi-resolution/spectra is a bottom up region-merging technique starting with one-pixel objects. In numerous subsequent steps, smaller image objects are merged into bigger ones. Throughout this pair-wise clustering process, the underlying optimization procedure minimizes the weighted heterogeneity of resulting image objects. In each step, that pair of adjacent image objects is merged, which results in the smallest growth of the defined heterogeneity. If the smallest growth exceeds the threshold defined by the scale parameter, the process stops.

Throughout the segmentation procedure, the whole image is segmented and image objects are generated based upon several adjustable criteria of homogeneity in color and shape. Adjusting the so-called scale parameter indirectly influences the average object size: a larger value leads to bigger objects and vice versa. Additionally the influence of shape as well as the image's channels on the object's homogeneity can be adjusted.

a)

b)

c)

d)
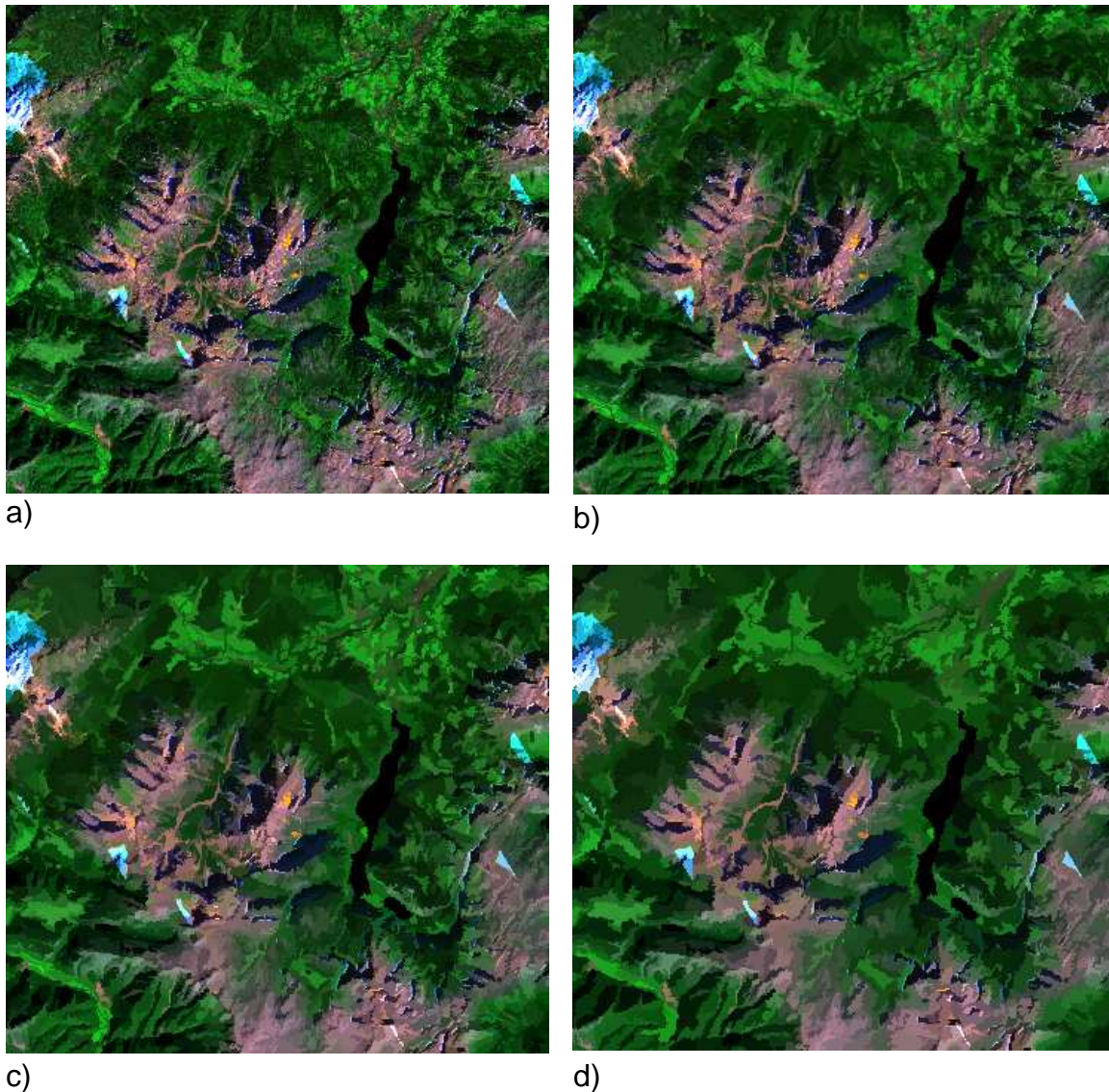
Figure 5.3. a) Original image (without segmentation); b) Segmentation result 1 with parameters of Scale 10, color 0.8, and shape 0.2, smoothness 0.9, compactness 0.1; c) Segmentation result 2 with parameters of Scale 20, color 0.8, and shape 0.2, smoothness 0.9, compactness 0.1; d) Segmentation result 3 with parameters of Scale 30, color 0.8, and shape 0.2, smoothness 0.9, compactness 0.1.

In performing the segmentation of the Landsat ETM, visible and NIR spectral region (bands 1, 2, 3, 4, 5, and 7) with 30 m spatial resolution were included into the segmentation process with equal full weighting (set weight 1.0). The segmentation process based on a high spatial resolution promotes use of the detailed information actually derived from the earth surface.

The scale parameter of the procedure was set to 10. The composition of homogeneity criteria was the following: color 0.8, shape 0.2. For the shape criterion,

smoothness was 0.9 and compactness was 0.1. Subsequently the parameters were varied as discussed below to optimize performance in relation to the ground truth map.

5.1.1.3.b. Comparison of segmentation results with different scale parameters

Figs. 5.3a-d show the effect of segmentation results using different segmentation parameters. Except for differences in scale, other parameters that influence the segmentation result (color, shape, smoothness and compactness) were kept constant. Fig. 5.3a is the original image Landsat ETM bands 3, 4, and 7 before segmentation. Fig. 5.3b is the segmentation result with a scale parameter 10. Comparing this segmentation result with the original image, it is found that neighbor pixels are grouped into pixel clusters-objects, but because of the low value of the scale parameter, relatively small objects were created. Fig. 5.3c&d are the segmentation results with scale parameter 20 and 30, respectively. Comparing these with Fig. 5.3b, it is clear that higher scale parameter values generate larger objects.

By comparison of the patterning in the segmentation in relation to ground truth maps, a scale parameter of 10 was selected as appropriate because the segmentation result provides the best fit to the information class extraction, especially considering fragmentation of the area (Fig. 5.4). The extracted image in the left panel of Fig. 5.4a is composed of homogeneous forest and more heterogeneous areas of grassland. The outcome of the segmentation in the image in the right panel with a higher scale parameter value shows larger unrealistic objects for the forest and smaller unrealistic objects for the grassland area. Thus, by choosing the scale parameter of 10, the fragmentation of grassland in this region is well described.

Thus, the multi-resolution segmentation extracts regions of local contrast. If areas of interest are small, multi-resolution segmentation should be applied with a smaller scale parameter value extracting principal image objects of smaller average size. The typical result of a segmentation run with a smaller scale parameter is: larger homogeneous image objects, smaller heterogeneous image objects and smaller homogeneous image objects embedded in a high contrast region as seen in Fig. 5.4.

a)   b)
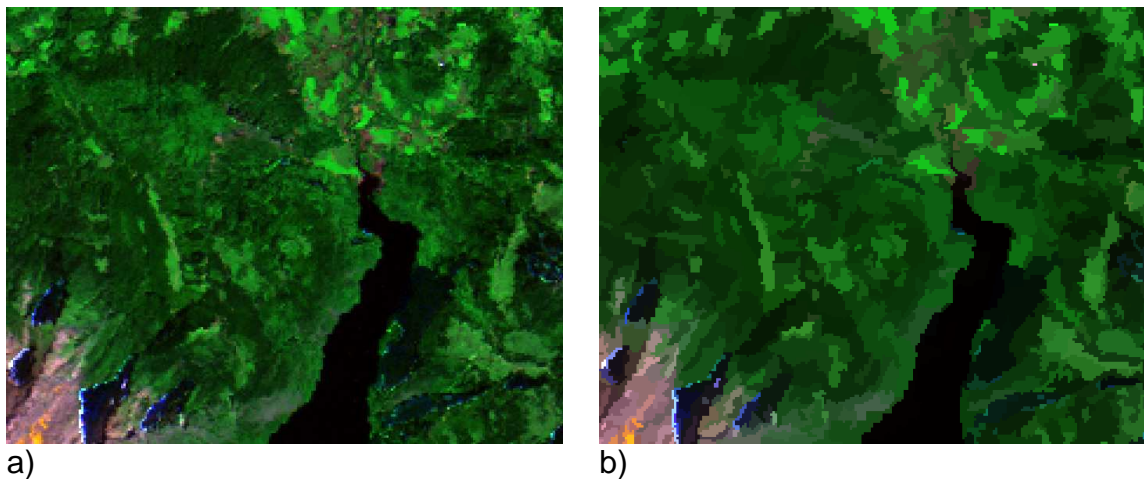
Figure 5.4. Image segmentation result produced for the area at the north end of Königsee in the Berchtesgaden National Park with a) scale parameter = 10; and b) with scale parameter = 20 or larger.

Object-based classification of Landsat image in Berchtesgaden (with 6 bands) results in Fig. 5.5. Accuracy assessment for object-based classification of Landsat data can be evaluated from the error matrix in Table 5.2 that is generated using the same ground truth map as discussed above. From Table 5.2, it can be seen that there is a significant improvement of the classification, which has an overall accuracy of 75.8 %, and Kappa coefficient of 0.63. The producer's accuracy of all classes increase, only producer's accuracy of rock class remains very high at 96 % (Table 5.3). The producer's accuracy of deciduous forest and grassland are nearly double that obtained with supervised classification at 57 and 49 %, respectively, while producer's accuracy of coniferous forest increase significantly from 54 to 76 %. The improvement of object-based classification is even more profound when looking into user's accuracy (Table 5.4). The user's accuracies of all classes increase, except producer's accuracy of grassland decreases from 54 to 48 % (Table 5.3). This is due to the occurrence of many small areas of grasslands which are situated within the forest. Those small areas are not detected by the segmentation process, are included into forest areas, and lead to an underestimated area of the grassland class.

On other hand, there is also a large increase in user's accuracies of deciduous forest (55 %) and rocks (90 %), while the user's accuracy of the coniferous forest is slightly improved (63 %) compared to supervised classification (56 %). It is clear that

object-based classification avoids the so-called "salt and pepper pattern", which occurs when using pixel-based classification in the forests and rock areas. Especially in steep mountain regions, topographic effects cause shadows which make the salt and pepper pattern even worse.

Table 5.2. Error matrix by ground truth map for object-based classification of Landsat image in Berchtesgaden

Class	Reference data					
	Coniferous	Deciduous	Grassland	Water	Rock	Total
Coniferous	76.79	35.62	32.36	1.26	1.64	40.70
Deciduous	12.93	57.09	15.98	1.58	1.08	16.22
Grassland	1.96	1.88	49.10	0.50	1.04	3.61
Water	0.01	0.31	0.55	96.40	0.06	2.85
Rocks	8.31	5.10	2.01	0.26	96.18	36.62
Total	100	100	100	100	100	100

Class	Producer' accuracy		User's accuracy	
	(Percent)		(Percent)	
Coniferous	76.79	52821/68782	62.98	52821/83867
Deciduous	57.09	18366/32171	54.94	18366/33427
Grassland	49.10	3592/7315	48.29	3592/7438
Water	96.40	5667/6200	96.53	5667/5871
Rocks	96.18	67952/71604	90.04	67952/75469

Overall Accuracy = (99915/131667) 75.9 %
Kappa coefficient = 0.63.

a)

b)
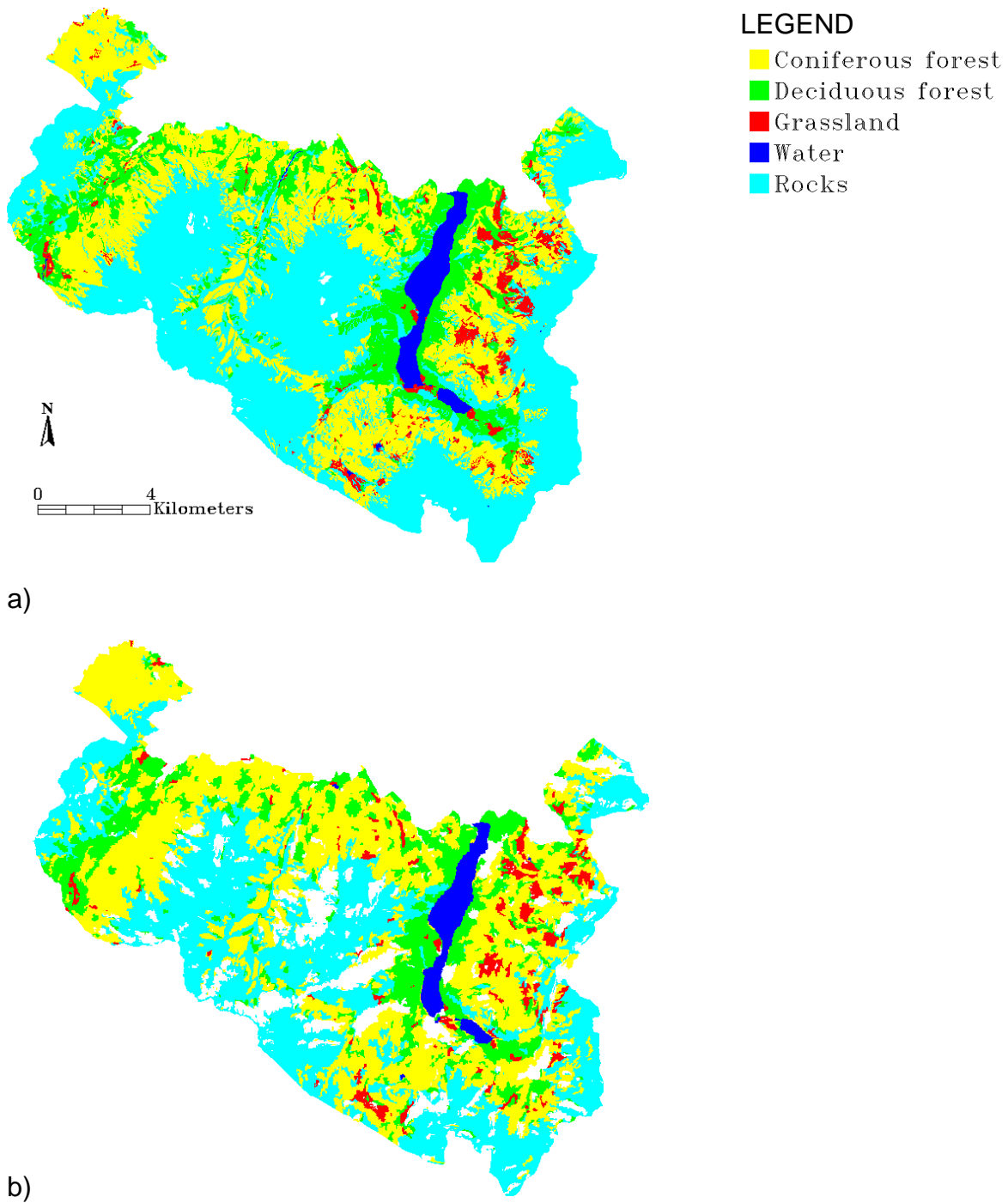
Figure 5.5. Result of object-based classification in Berchtesgaden a) Ground truth map; and b) Object-based land cover map.

Table 5.3. Comparison of producer's accuracy of pixel-based and object-based classifications of Landsat image in Berchtesgaden

	Water	Rock	Deciduous	Grassland	Coniferous
Pixel-based classification	96.06	96.87	22.22	25.27	54.98
Object-based classification	96.40	96.18	57.09	49.10	76.79

Table 5.4. Comparison of user's accuracy of pixel-based and object-based classifications of Landsat image in Berchtesgaden

	Water	Rock	Deciduous	Grassland	Coniferous
Pixel-based classification	82.72	58.32	32.05	54.56	56.60
Object-based classification	96.53	90.04	54.94	48.29	62.98

5.1.2. *Land cover classification in Stubai Valley and at Tharandt and Hesse Forests*

The same trend toward higher accuracy was obtained with object-based classification of Landsat images in Stubai Valley, as seen in Fig. 5.6 and summarized in Tables 5.5 to Table 5.8.

In Stubai Valley, with pixel-based classification one can achieve relatively high overall accuracy 72.1 % (Kappa coefficient = 0.58). This result is higher than obtained in Berchtesgaden, since the topographic effects in Stubai Valley are not as profound as in Berchtesgaden. The result is also better than previously obtained for this mountain region of the Alps using maximum likelihood classification (Bobeva, 2003). But overall accuracy is lower than another study in the Alps using a rule-based fuzzy logic classifier, and combining the spectral information with ancillary data layers and a knowledge base (Stolz et al., 2005). By taking into account the probability of occurrence of a land use class dependent on environmental and physical factors such as slope, altitude, soil and climate, Stolz et al. (2005) achieved an accuracy of 88 %.

In the case of Stubai Valley, it is worth to mention that the study extends over a large watershed, where rough terrain is about one third of the total area. The overall accuracy of 72 % is a satisfying result (Campbell, 2002). But a closer evaluation of the classified categories reveals some problems. Although the image acquisition date allows a high number of grasslands to be differentiated, the confusion of high elevation grassland with meadows and several other classes is evident. The poor separability between grassland and meadows is a result of the similar spectral signatures of these two classes and may not be avoidable. The misclassification of meadows and rocks is mainly due to limitations in the ground truth map, which was produced almost 15 years ago. At the current time, meadows appear to have expanded above treeline due to global warming effects, and this change is seems to be captured well by the remote sensing data. There is significant confusion between the deciduous forest and coniferous forest classes, where 31.7 % of deciduous forest is misclassified as coniferous. Fortunately, this has little effect on overall accuracy because deciduous forest covers less than 1 % of the Stubai Valley. The two classes, coniferous forest and rocks, covering 70 % of the area have been well classified with accuracies of 73 and 78 % respectively.

The object-based classification of Landsat data in Stubai Valley achieve even higher overall accuracy of 80.8 % (Kappa coefficient = 0.7) (Table 5.7). The producer's accuracy of all classes increases. The producer's accuracy of deciduous forest, urban and meadow classes are approximately double that obtained with supervised classification at 63, 76 and 56 %, respectively, while producer's accuracy of grassland increases significantly from 48 to 64 %. The two main classes, coniferous forest and rocks, obtain only little improvement. The improvements obtained with object-based classification are also evidenced when looking into user's accuracy (Table 5.8), where object-based classification achieves higher accuracies in all classes. Using the combination of texture and shape with spatial information on an object, object-based classification leads to much higher accuracy. The consistency of high accuracy with object-based classification of Landsat TM images over two mountainous areas supported the idea to apply this method for land cover classification in Hesse and Tharandt forest, and this was subsequently carried out.

Going beyond the methodological limits of pixel-based approaches, multi-scale image segmentation and object-based approaches were used for land cover

classification in Hesse and Tharandt forest. The results are shown in Table 5.9. In comparison to the ground truth data, which are derived from different sources of ancillary data: inventory data, SPOT image, etc. (see Chapter 3), very high accuracies of 82.8 % in Hesse (Kappa coefficient = 0.78) and 91.3 % in Tharandt (Kappa coefficient = 0.88) were achieved. The higher accuracy in Tharandt seems due to lower complexity of the landscape at the Tharandt forest site, where the coniferous forest covers most of area, surrounded by agriculture fields. The deciduous forest at Hesse covers a smaller portion of the scene and is surrounded by meadows and agricultural areas.

Table 5.5. Error matrix by ground truth map for pixel-based classification of Landsat image in Stubai Valley

Class	Coniferous	Grassland	Urban	Rocks	Meadow	Deciduous	Total
Coniferous	73.48	9.29	2.30	3.99	13.01	31.77	24.40
Grassland	13.18	62.20	37.29	1.10	8.44	16.68	10.45
Urban	0.45	2.89	52.65	0.14	0.23	0.00	0.75
Rocks	3.55	6.18	7.75	78.31	27.70	0.00	45.63
Meadows	8.16	17.16	0.00	16.38	50.38	15.75	17.99
Deciduous	1.19	2.28	0.00	0.07	0.25	35.79	0.78
Total	100	100	100	100	100	100	100

Overall Accuracy = (187405/259812) 72.1 %
Kappa coefficient = 0.58.

Table 5.6. Error matrix by ground truth map for object-based classification of Landsat image in Stubai Valley

Class	Coniferous	Grass	Urban	Rocks	Meadow	Deciduous	Total
Coniferous	84.75	12.08	1.89	3.79	11.29	23.07	27.32
Grassland	4.61	64.73	21.72	0.94	4.23	9.62	7.64
Urban	0.20	3.14	76.19	0.12	0.00	0.00	0.79
Rocks	3.79	7.67	0.00	86.85	28.23	0.00	50.32
Meadows	5.92	10.37	0.21	8.27	55.91	3.76	13.15
Deciduous	0.72	2.01	0.00	0.02	0.34	63.55	0.78
Total	100	100	100	100	100	100	100

Overall Accuracy = (209984/259945) 80.8 %
Kappa coefficient = 0.7.

Table 5.7. Comparison of producer's accuracy of pixel-based and object-based classifications of Landsat image in Stubai Valley

	Coniferous	Grassland	Urban	Rocks	Meadows	Deciduous
Pixel-based classification	81.48	48.24	38.89	89.8	31.85	26.76
Object-based classification	84.75	64.73	76.19	89.85	55.91	63.55

Table 5.8. Comparison of user's accuracy of pixel-based and object-based classifications of Landsat image in Stubai Valley

	Coniferous	Grassland	Urban	Rocks	Meadows	Deciduous
Pixel-based classification	73.48	62.2	52.65	78.31	50.38	35.79
Object-based classification	83.93	68.63	52.81	90.35	58.34	47.7

Table 5.9. Overall accuracy and Kappa coefficient of Landsat land cover products compared to the "ground truth" land cover map

	Berchtesgaden	Stubai	Hesse	Tharandt
Overall auracy	(99915/131667) 75.9 %	209984/259945 80.7 %	(15685/19128) 82.8 %	(15685/19128) 91.3 %
Kappa cefficient	0.63	0.70	0.78	0.88

a)   b)
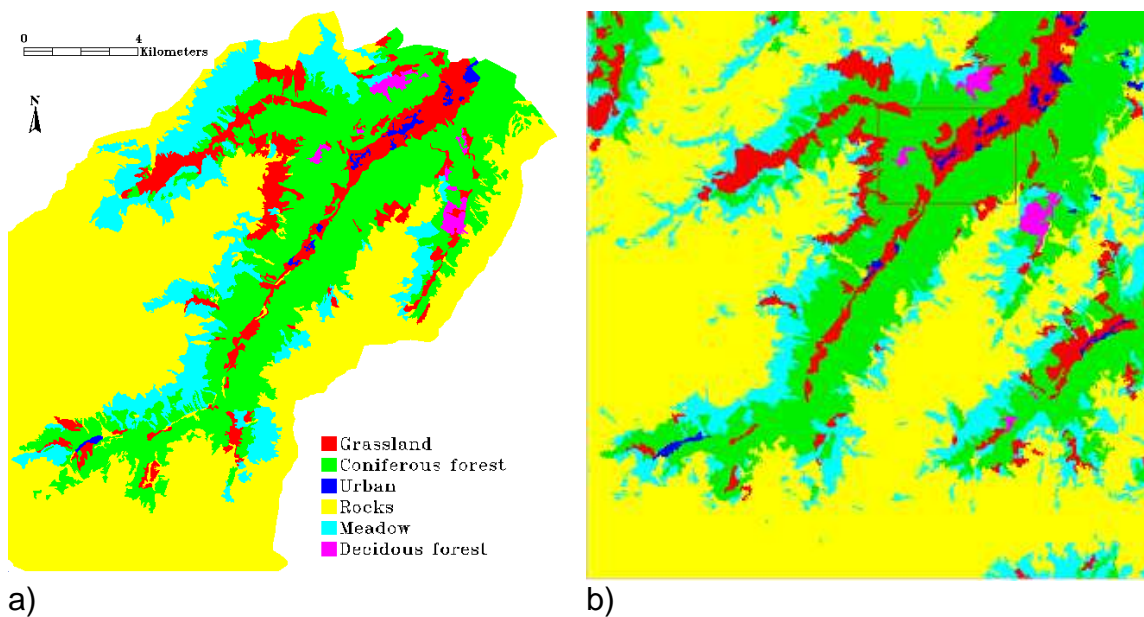
Figure 5.6. Land cover map resulting from object-based classification in Stubai Valley a) Ground truth map; b) Object-based land cover map.

5.1.3. Scaling up of land cover to evaluate the MODIS product

5.1.3.1. MODIS land cover products

In order to compare the land cover maps developed for specific sites in this thesis to MODIS land cover, and to assess or validate MODIS land cover descriptions, the 6 site-specific classes must be assigned to suggested equivalent MODIS land cover classes. This practice of translation equating local land cover with analyses developed for global scale applications has been viewed as a means for evaluating errors associated with MODIS land cover products (Turner et al., 1996).

MODIS land cover descriptions are produced on a 32-day basis using decision tree and trained artificial neural network classifiers (Strahler et al., 1999). There are several different descriptions for land cover that are included in the MODIS12Q1 product catalog (Morisette et al., 2002). In this study, land cover type 1 and type 3 are of interest. The land cover type 1 is in accordance with a scheme that has been accepted by the International Geosphere-Biosphere Programme (IGBP) for regional to global scale land cover classification, identifying 17 classes (Table 5.10) (Loveland et al., 2000). The land cover type 3, which is subsequently used to produce the MODIS LAI/FPAR product, identifies 6 biomes based on biophysical and physiological characteristics of the biomes and 3 additional land covers (Table 5.11) (Myneni et al., 1997a). The six-biome scheme is promoted to enable researchers to identify characteristics via relatively coarse resolution satellite data, which are important to ecosystem bio-geochemistry.

Table 5.10. MODIS land cover type 1 (IGBP Land cover Units)

1	Evergreen Needleleaf Forests	Lands dominated by woody needleleaf vegetation with a percent cover > 60 % and height exceeding 2 meters. Almost all trees remain green all year. Canopy is never without green foliage.
2	Evergreen Broadleaf Forests	Lands dominated by woody broadleaf vegetation with a percent cover > 60 % and height exceeding 2 meters. Almost all trees and shrubs remain green year round. Canopy is never without green foliage.
3	Deciduous Needleleaf Forests	Lands dominated by woody needleleaf vegetation with a percent cover > 60 % and height exceeding 2 meters. Consists of seasonal needleleaf tree communities with an annual cycle of leaf-on and leaf-off periods.
4	Deciduous Broadleaf Forests	Lands dominated by woody broadleaf vegetation with a percent cover > 60 % and height exceeding 2 meters. Consists of broadleaf tree communities with an annual cycle of leaf-on and leaf-off periods.
5	Mixed Forests	Lands dominated by trees with a percent cover > 60 % and height exceeding 2 meters. Consists of tree communities with interspersed mixtures or mosaics of the other four forest types. None of the forest types exceeds 60 % of landscape.
6	Closed Shrublands	Lands with woody vegetation less than 2 meters tall and with shrub canopy cover > 60 %. The shrub foliage can be either evergreen or deciduous.
7	Open Shrublands	Lands with woody vegetation less than 2 meters tall and with shrub canopy cover between 10 – 60 %. The shrub foliage can be either evergreen or deciduous.
8	Woody	Lands with herbaceous and other understory systems, and with forest

	Savannas	canopy cover between 30 – 60 %. The forest cover height exceeds 2 meters.
9	Savannas	Lands with herbaceous and other understory systems, and with forest canopy cover between 10 – 30 %. The forest cover height exceeds 2 meters.
10	Grasslands	Lands with herbaceous types of cover. Tree and shrub cover is less than 10 %.
11	Permanent Wetlands	Lands with a permanent mixture of water and herbaceous or woody vegetation. The vegetation can be present in either salt, brackish, or fresh water.
12	Croplands	Lands covered with temporary crops followed by harvest and a bare soil period (*e.g.*, single and multiple cropping systems). Note that perennial woody crops will be classified as the appropriate forest or shrub land cover type.
13	Urban	Land covered by buildings and other man-made structures.
14	Cropland Vegetation Mosaics	Lands with a mosaic of croplands, forests, shrubland, and grasslands in which no one component comprises more than 60 % of the landscape.
15	Snow and Ice	Lands under snow/ice cover throughout the year.
16	Barren	Lands with exposed soil, sand, rocks, or snow and never has more than 10 %.
17	Water Bodies	Oceans, seas, lakes, reservoirs, and rivers. Can be fresh or saltwater bodies.

Table 5.11. MODIS land cover type 3 (LAI/FPAR)

1	Grasses/cereal crops
2	Shrubs
3	Broadleaf crops
4	Savanna
5	Broadleaf forest
6	Needleleaf forest
7	Unvegetated area
8	Urban area
9	Water

Table 5.12. Equivalence utilized in comparing site-specific land cover classes to MODIS type 1 and MODIS type 3 classes

a) Berchtesgaden National Park

Site-specific class	MODIS type 1 (IGBP Class)	MODIS type 3 (For LAI/PAR)
Coniferous forest	Evergreen and deciduous needleleaf forest	Needleleaf forest
Mixed forest	Mixed forest	Needleleaf forest or Broadleaf forest based on majority
Deciduous forest	Deciduous broadleaf forest	Broadleaf forest
Grassland and Cropland	Grassland	Grasses/cereal crops
Water	Water	Water
Rocks	Barren	Barren

b) Stubai Valley

Site-specific class	MODIS type 1 (IGBP Class)	MODIS type 3 (For LAI/PAR)
Coniferous forest	Evergreen and deciduous needleleaf forest	Needleleaf forest
Deciduous forest	Deciduous broadleaf forest	Broadleaf forest
Meadows	Grassland	Grasses/cereal crops
Grassland	Grassland	Grasses/cereal crops
Urban	Urban/Built-up	Barren
Rocks	Barren	Barren

c) Hesse forest

Site-specific class	MODIS type 1 (IGBP Class)	MODIS type 3 (For LAI/PAR)
Coniferous forest	Evergreen and deciduous needleleaf forest	Needleleaf forest
Matured deciduous forest	Deciduous broadleaf forest	Broadleaf forest
Young deciduous forest	Deciduous broadleaf forest	Broadleaf forest
Grassland	Grassland	Grasses/cereal crops
Cropland	Cropland	Grasses/cereal crops
Rocks and bare soil	Barren	Barren

d) Tharandt forest

Site-specific class	MODIS type 1 (IGBP Class)	MODIS type 3 (For LAI/PAR)
Coniferous forest	Evergreen and deciduous needleleaf forest	Needleleaf forest
Mixed forest	Mixed forest	Needleleaf forest or Broadleaf forest based on majority
Deciduous forest	Deciduous broadleaf forest	Broadleaf forest
Grassland	Grassland	Grasses/cereal crops
Cropland	Cropland	Grasses/cereal crops
Rocks and bare soil	Barren	Barren

5.1.3.2.   Site-specific equivalence or translation of classes

Table 5.10 and 5.11 list the 6 site-specific classes used for land cover at all four study-sites and indicate how they are equated with MODIS type 1 and MODIS type 3 land cover maps. There is no ambiguity in translation to MODIS type 1 land cover, since similarly defined classes occur. At the Hesse site, two classes of mature and young deciduous forest are included into a single deciduous broadleaf forest

class with reduction in number of objects. The same reduction in numbers of classes occurs in Stubai Valley, where grassland and cropland are defined as grassland. MODIS type 3 land cover has no mixed forest (Table 5.11). Thus, mixed forest was translated into deciduous forest or needleleaf forest depending on which class represented the major portion of the MODIS scale pixel.

5.1.3.3. *Scaling up of the land cover map*

Since almost all pixels at the 1 km scale of the MODIS image are a mixture of several land cover types, a definition of a "pure pixel" is required in the upscaling process. Here a pure pixel was defined when the representation of an individual land cover type exceeds 60 %. If this criterion was not met, the pixel remained unclassified and was eliminated from the evaluation. The upscaling results of Landsat land cover map to MODIS scale are shown in Fig. 5.7, 5.8, 5.9 and 5.10. Landscape complexity, either as a disturbance of the image via shading or extreme fragmentation, directly influences the upscaling results. In Berchtesgaden, the most complex landscape, only 45 % of area could be successfully translated into a MODIS 1 km scale land cover map. The rest remains unclassified (Fig. 5.7). As landscape goes from more to less complex, the classified area increases from 77 % to 85 and 88 % in Stubai Valley, Hesse forest and Tharandt forest respectively (Fig. 5.8, 5.9 and 5.10).

a)

b)

c)

LEGEND

- ■ Unclassified
- ■ Coniferous forest
- ■ Deciduous forest
- ■ Mixed forest
- ■ Grassland
- ■ Grass/Crop mosaic
- ■ Rock/Bare soil
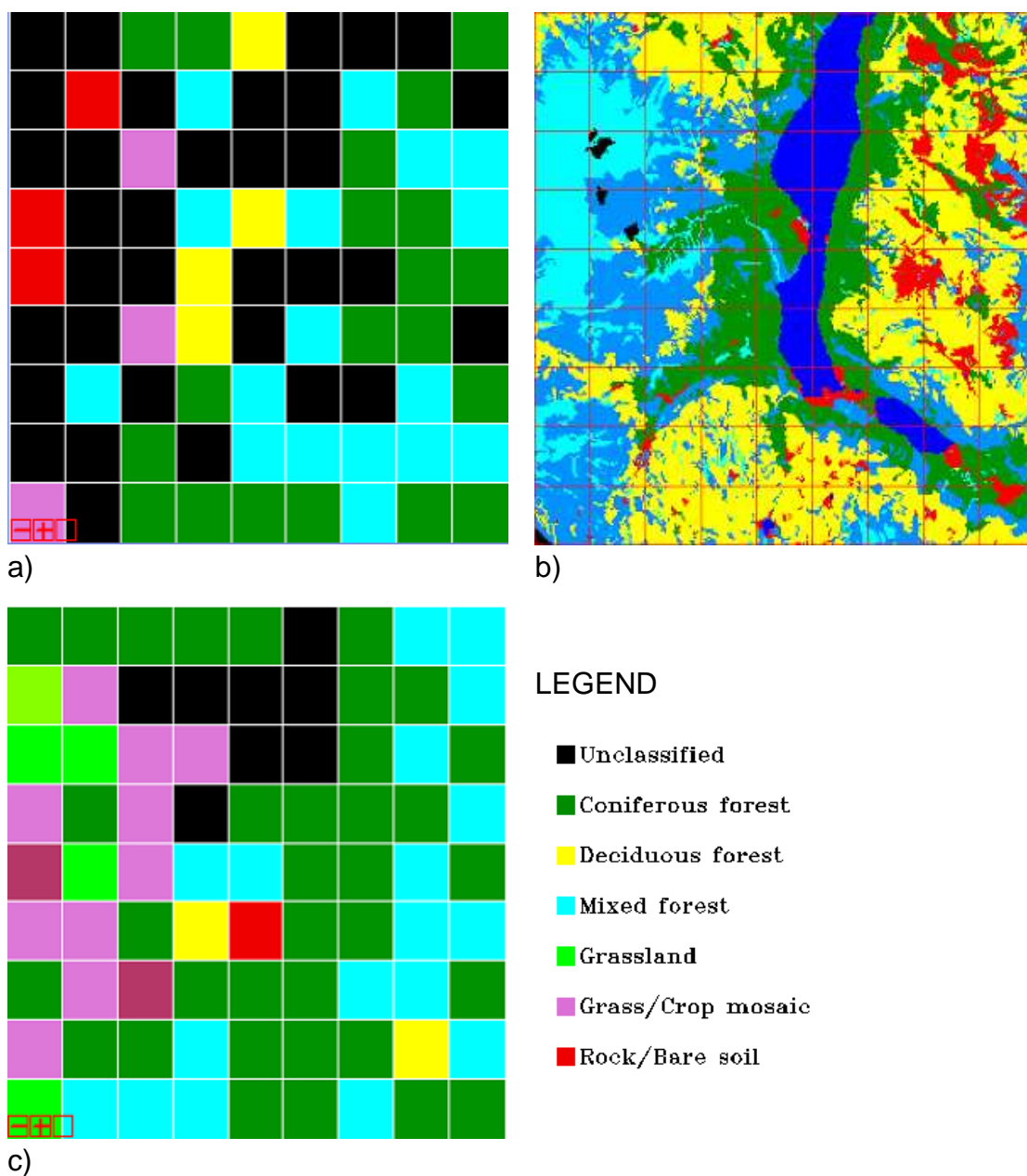
Figure 5.7. Land cover map of Berchtesgaden: a) Upscaling to MODIS resolution at threshold of 0.6; b) Derived from Landsat TM; and c) Derived from MODIS data.

a)

b)

c)

LEGEND
- ■ Unclassified
- ■ Coniferous forest
- ■ Evergreen Broadleaf forest
- ■ Deciduous forest
- ■ Mixed forest
- ■ Shrublands
- ■ Grasslands
- ■ Croplands
- ■ Rocks
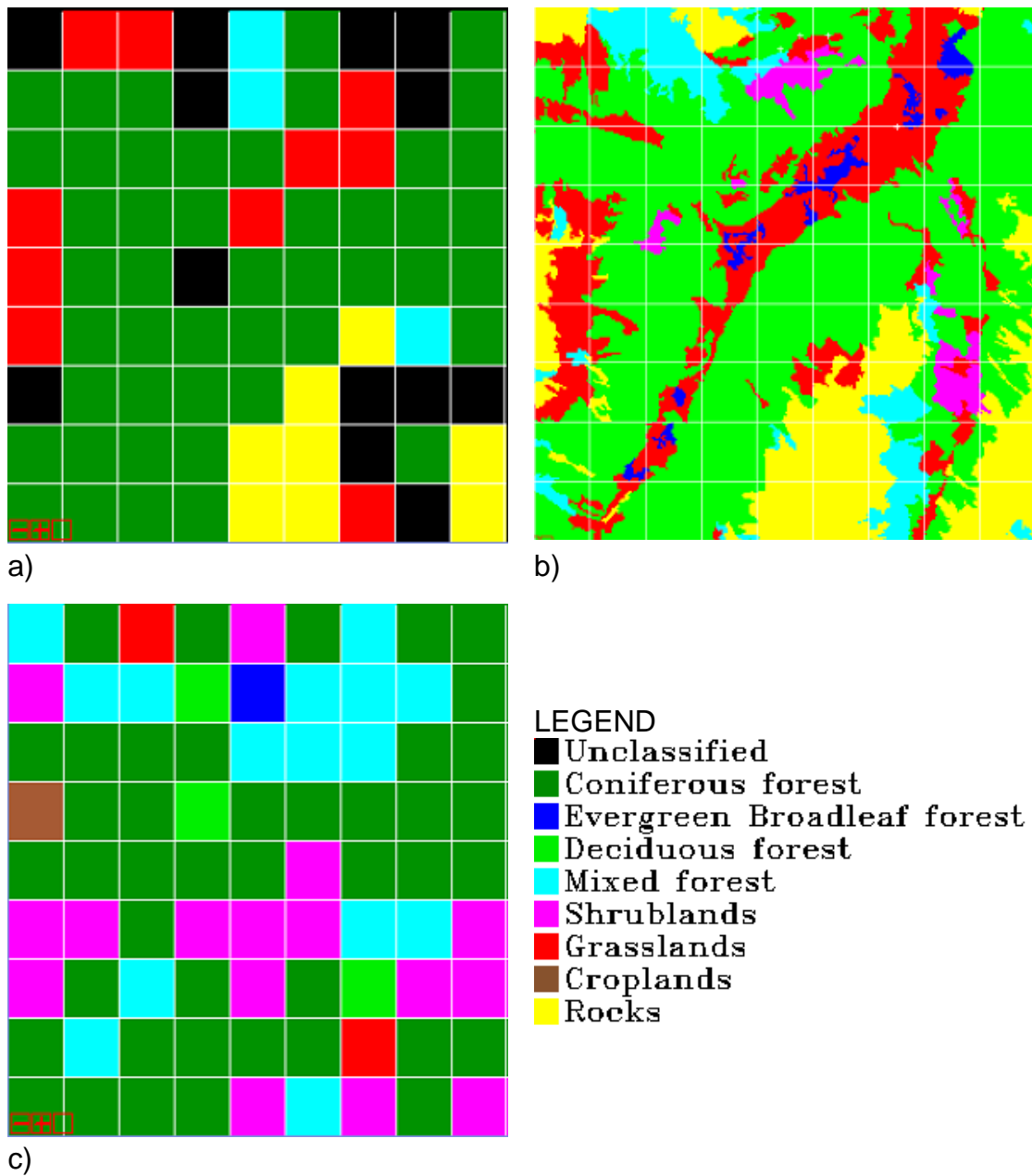
Figure 5.8. Land cover map of Stubai Valley: a) Upscaling to MODIS resolution at threshold of 0.6; b) Derived from Landsat TM; and c) Derived from MODIS data.
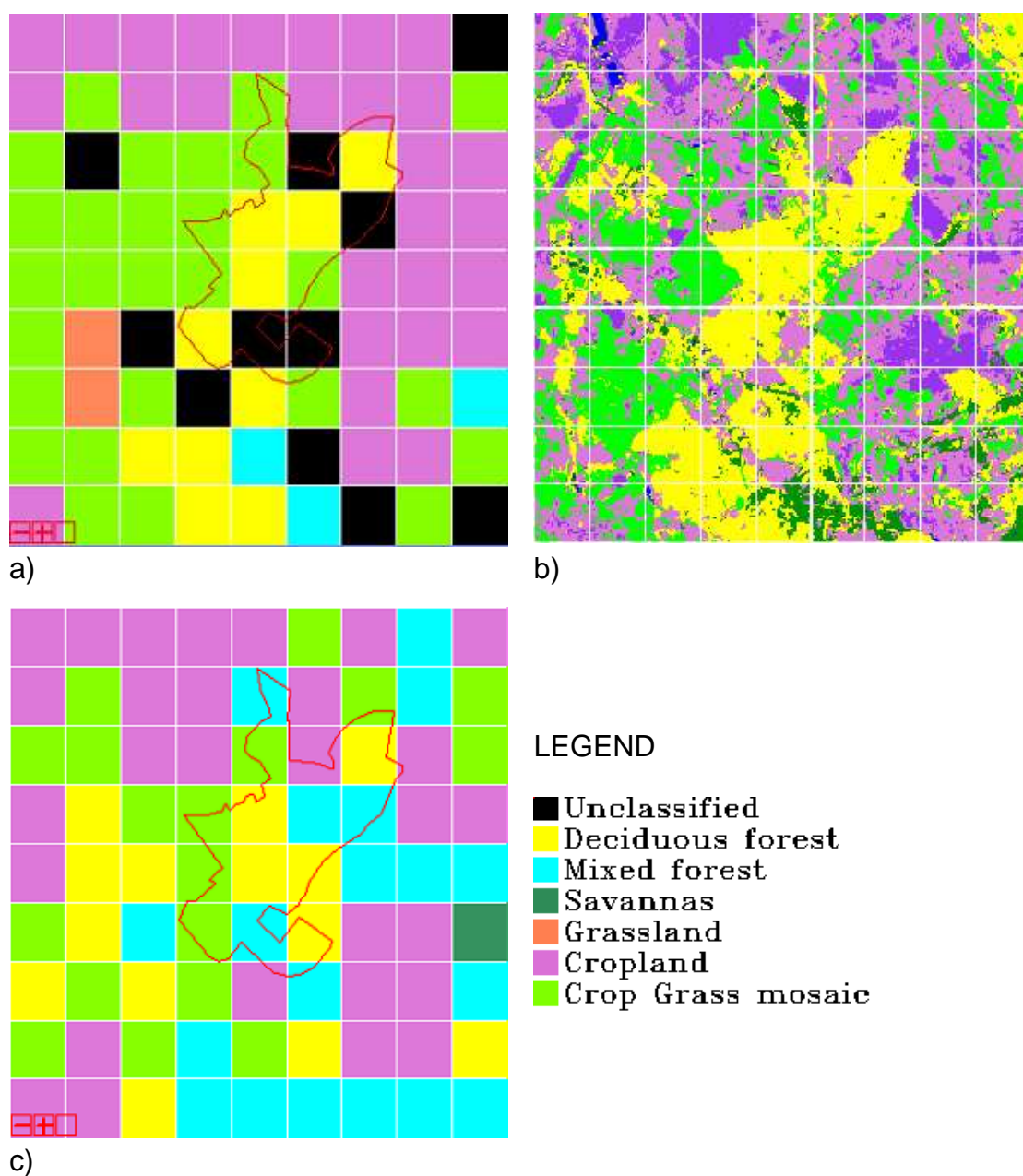
Figure 5.9. Land cover map of Hesse forest: a) Derived from Landsat TM; b) Upscaling to MODIS resolution at threshold of 0.6; and c) Derived from MODIS data.
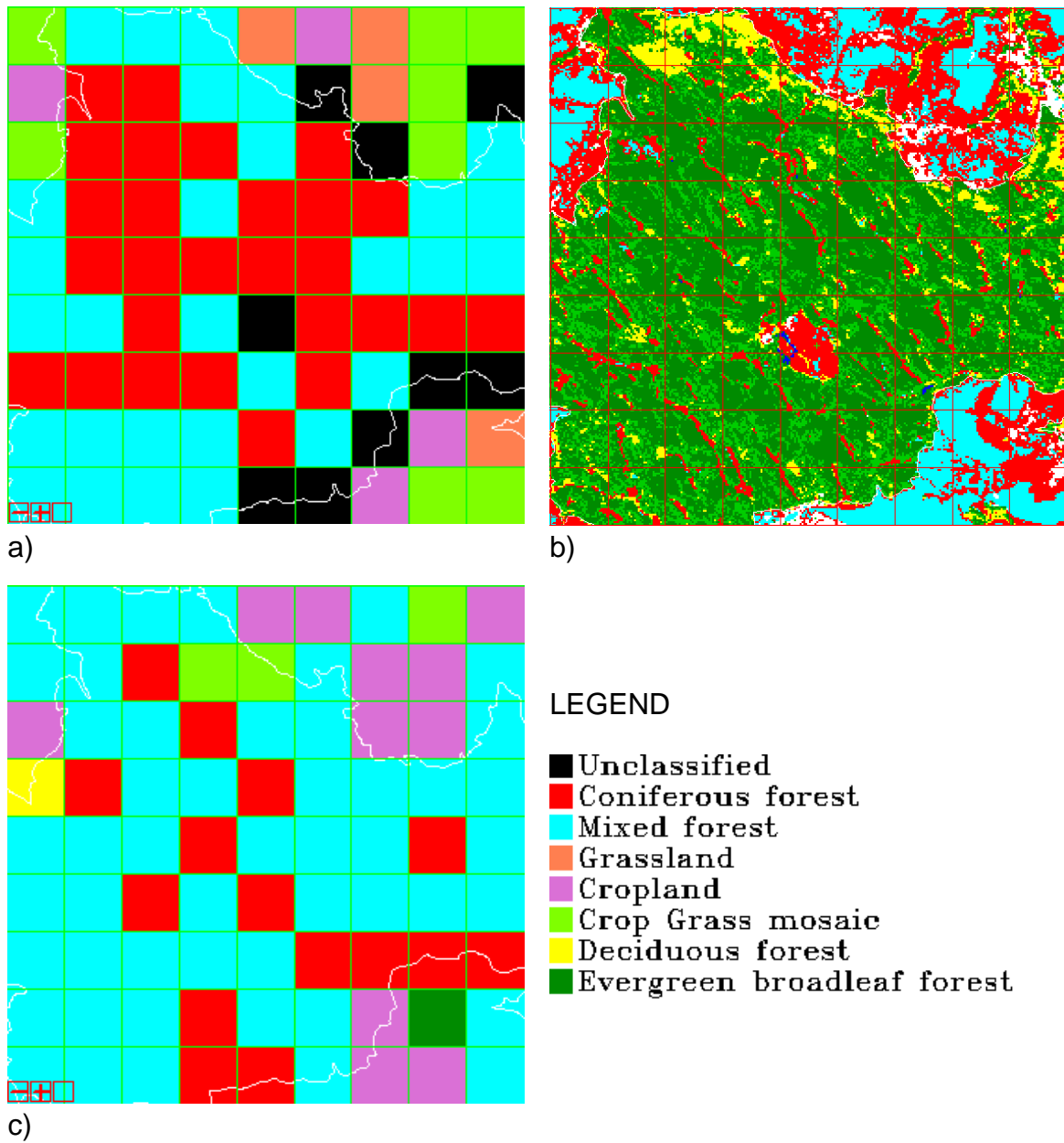
Figure 5.10. Land cover map of Tharandt forest: a) Upscaling to MODIS resolution at threshold of 0.6; b) Derived from Landsat TM; and c) Derived from MODIS data.

5.1.4. Comparison of the MODIS land cover map and ground truth maps

5.1.4.1. Areal comparison

a) <u>MODIS land cover type 1 and Landsat land cover</u>

Fig. 5.11 shows the total areas (in percentage) of the 4 main land cover classes in Berchtesgaden, which results from Landsat data (30 m resolution) and MODIS data (1km resolution). The total areas of 4 main land cover classes are quite similar except for mixed forest. The large percent difference for mixed forest obtained in this study is similar to earlier findings reported by Bobeva (2003). In this specific case, discrepancies can be explained by the difference in the definitions of "mixed forest" in the MODIS classification scheme and Landsat classification scheme. In the MODIS classification scheme, mixed forests are defined as lands dominated by trees with a percent cover of 60 % and higher and height exceeding 2 m, none of the forest types exceeds 60 % of landscape. In Landsat TM classification scheme, the threshold for mixed forest is 70 % tree cover and tree height greater than 3 m. The difference of scale also contributes to the discrepancies. The mixed forest, which covered 40 % of total area in Berchtesgaden in the Landsat land cover map at 30 m resolution, is not equally distributed over the area. The MODIS land cover map can depict 22 % of the area as mixed forest at 1km resolution, the rest of the area is made up of other land cover classes. Deciduous forest represents approximately 4 % of total area of Berchtesgaden, thus making it difficult to delineate the boundaries with coarse resolution MODIS data, where only 2.5 % of the area is defined as deciduous forest. There are better agreements in areal statistics of coniferous forest and grasslands/croplands, which compose of 36 % and 17 % of cover at Landsat resolution and 43 % and 17.3 % at MODIS resolution respectively. The area of coniferous forest is higher in the MODIS land cover than in Landsat land cover. In contrast, the area of deciduous forest is higher in Landsat land cover than in MODIS land cover. This result may due to the misclassification with the MODIS land cover algorithm.

The results of areal statistical analysis of Stubai Valley, Hesse forest, and Tharandt forest are shown in Table 5.13a, b, c.

Areal statistics of LANDSAT and MODIS
Landcover (type1)
(Berchtesgaden)
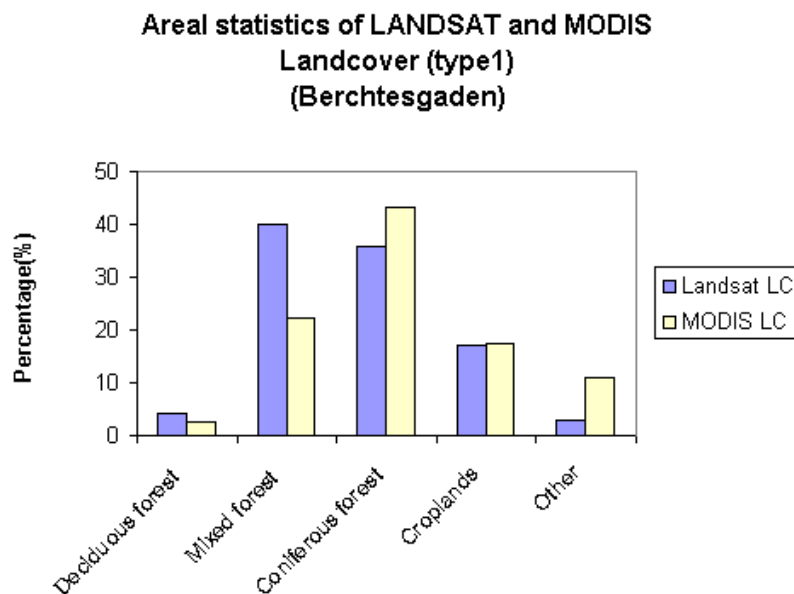
Figure 5.11. Areal statistics of the land cover map in Berchtesgaden, as mapped by MODIS land cover map (type 1) and Landsat TM land cover.

In Stubai Valley, the MODIS land cover map underestimates the area of bare soil/rock and croplands/grassland. It can depict only 1.2 % of area as bare soil/rock, while this class composes 21 % of area in the Landsat land cover map. Similarly, only 4.9 % of croplands/grassland land cover occurs in the MODIS land cover map, while it is 20.4 % in the Landsat land cover map. On the other hand, the MODIS land cover map shows considerably large area of mixed forest (18.5 %) and woody savanna (17.2 %) which are not classified in the Landsat land cover map. Here the differences in classification scheme and resolution certainly play a role, because in the Landsat scheme, there are no mixed forest and woody savanna classes. The area of mixed forest in the MODIS land cover map may be a mixture of forest, grassland and bare soil/rock. Deciduous forest represents approximately 1.9 % of total area of Stubai Valley, thus making it difficult to delineate the boundaries with coarse resolution MODIS data. There is highest agreement in areal statistics of coniferous forest, which compose of 53.5 and 53.0 % at Landsat resolution and MODIS resolution, respectively.

In Hesse forest, the classification eliminates mixed forest and woody savanna from consideration in the Landsat land cover map, while they are 23.5 and 1.2 % in the MODIS land cover map respectively. In contrast, the MODIS land cover could not depict the existence of coniferous forest and bare soil/rock, which are visible at

Landsat resolution. The bare soil surrounding Hesse forest exists only seasonally due to harvesting and ploughing. This area could be classified as cropland in the MODIS scheme because they use multiple scenes for classification during the growing seasons. The croplands/grassland areas in both products are in good agreement with 60 % in Landsat and 58 % in the MODIS land cover map. The deciduous forest is also in fair agreement with 25 % in Landsat and 17 % in the MODIS land cover map.

Table 5.13. Areal statistical analysis of Landsat and MODIS land cover maps in a) Stubai Valley, b) Hesse forest, and c) Tharandt forest

a) Stubai Valley

	Deciduous forest	Mixed forest	Coniferous forest	Croplands/ Grassland	Woody Savanna	Bare soil/ Rock	Urban
Landsat LC	1.90	0.0	53.5	20.44	0.0	21.1	3.0
MODIS LC	4.93	18.5	53.1	4.93	17.3	1.2	0.0

b) Hesse forest

	Deciduous forest	Mixed forest	Coniferous forest	Croplands/ Grassland	Woody Savanna	Bare soil/ Rock
Landsat LC	25.1	0.0	4.9	60.24	0.00	9.5
MODIS LC	17.3	23.5	0.0	58.02	1.23	0.0

c) Tharandt forest

	Deciduous forest	Mixed forest	Coniferous forest	Croplands	Grassland	Bare soil/ Rock
Landsat LC	5.90	19.2	43.70	11.0	17.9	2.0
MODIS LC	1.23	61.7	19.75	13.6	3.7	0.0

In Tharandt forest, small areas of bare soil exist in the Landsat land cover map, but do not exist in the MODIS land cover map. Other land cover classes show significant discrepancies in certain areas. Mixed forest occupies 19 % in Landsat land cover map, while it occupies 61 % in the MODIS land cover map. In contrast, coniferous forest covers 44 % in Landsat land cover map, much higher than that of

20 % found with MODIS. The discrepancies here are mainly due to scale differences. At larger scale, the MODIS land cover map can depict the mixture of coniferous and deciduous forest as mixed forest. As a result the sum of forest areas in both Landsat and MODIS land cover maps are quite similar, 70 % in Landsat and 82 % in the MODIS land cover maps.

In the previous studies, Giri (2005) showed a much better agreement between MODIS land cover maps and GLC-2000 at global scale. The percent agreement of global area totals of forest, grasslands, croplands, urban lands, barren lands, and mosaic of croplands/natural vegetation are 91, 82, 87, 93, 97 and 75 %, respectively. The percent agreement for shrublands/ savannas and wetlands are 58 and 37 %. This agreement can be explained by the fact that, the GLC-2000 was based primarily on SPOT VEGETATION, where daily 1-km data were acquired in 1999/2000 (Fritz et al., 2002). Thus the time difference of approximately 10 months between GLC-2000 and the MODIS land cover map is negligible; and the effect of resolution differences can be ignored.

Table 5.14. Confusion metric of Land cover classification in Hesse forest

Class	Ground truth														
	Coniferous forest		Deciduous forest		Mixed forest		Grassland		Cropland		Crop Grass Mosaic		Bare soil		Total	
	pixels	%	pixels	%	pixels	%	pixels	%	pixels	%	pixels	%	pixels	%	pixels	%
Coniferous forest	0	0	0	0	0	0.0	0	0	0	0.0	0	0.0	0	0	0	0.0
Deciduous forest	0	0	3	30	0	0.0	1	50	0	0.0	8	29.6	0	0	12	17.4
Mixed forest	0	0	4	40	2	66.7	0	0	5	18.5	3	11.1	0	0	14	20.3
Grassland	0	0	0	0	0	0.0	0	0	0	0.0	0	0.0	0	0	0	0.00
Cropland	0	0	1	10	0	0.0	0	0	19	70.4	7	25.9	0	0	27	39.1
Crop Grass Mosaic	0	0	2	20	1	33.3	1	50	3	11.1	9	33.3	0	0	16	23.2
Bare soil	0	0	0	0	0	0.00	0	0	0	0.0	0	0.0	0	0	0	0.0
Total	0	0	10	100	3	100	2	100	27	100	27	100	0	0	69	100

Table 5.15. Confusion metric of Land cover classification in Tharandt forest

Class	Ground truth											
	Coniferous forest		Mixed forest		Grassland		Cropland		Crop Grass Mosaic		Total	
	pixels	%	pixels	%	pixels	%	pixels	%	pixels	%	pixels	%
Coniferous forest	7	25.9	4	14.3	0	0	0	0.0	0	0.0	11	15.7
Mixed forest	20	74.1	22	78.6	2	50	1	33.3	2	25.0	47	67.1
Grassland	0	0.0	0	0.0	0	0	0	0.0	0	0.0	0	0.00
Cropland	0	0.0	0	0.0	2	50	2	66.7	5	62.5	9	12.9
Crop Grass Mosaic	0	0.0	2	7.1	0	0	0	0.0	1	12.5	3	4.3
Total	27	100	28	100	4	100	3	100	8	100	70	100

Table 5.16. Confusion metric of Land cover classification in Stubai Valley

Class	Ground truth											
	Coniferous forest		Deciduous forest		Mixed forest		Grassland		Opened Shrubland		Total	
	pixels	%	pixels	%	pixels	%	pixels	%	pixels	%	pixels	%
Coniferous forest	22	55.0	1	100	1	100	6	54.5	2	33.33	32	54.24
Deciduous forest	1	2.5	0	0	0	0	0	0.0	0	0.00	1	1.69
Mixed forest	8	20.0	0	0	0	0	2	18.2	2	33.33	12	20.34
Grassland	2	5.0	0	0	0	0	0	0.0	0	0.00	2	3.39
Opened Shrubland	7	17.5	0	0	0	0	3	27.3	2	33.33	12	20.34
Total	40	100	1	100	1	100	11	100	6	100	59	100

Table 5.17. Confusion metric of Land cover classification in Berchtesgarden

Class	Ground truth											
	Coniferous forest		Deciduous forest		Mixed forest		Bare soil		Crop Grass Mosaic		Total	
	pixels	%	pixels	%	pixels	%	pixels	%	pixels	%	pixels	%
Coniferous forest	15	75	2	50	8	53.3	0	0	1	50	26	60.5
Deciduous forest	0	0	1	25	1	6.7	0	0	0	0	2	4.65
Mixed forest	5	25	1	25	5	33.3	0	0	0	0	11	25.6
Bare soil	0	0	0	0	0	0.00	0	0	0	0	0	0.0
Crop Grass Mosaic	0	0	0	0	1	6.7	2	100	1	50	4	9.3
Total	20	100	4	100	15	100	2	100	2	100	43	100

5.1.4.2. Spatial (per-pixel) comparison

a. Comparison of MODIS land cover type 1 and Landsat land cover:

The per-pixel agreement between MODIS land cover and Landsat land cover type 1 is presented in Table 5.10. In general, the per-pixel agreement between upscaled Landsat land cover and MODIS Land Cover is lower than the area comparison.

In Hesse forest, the overall accuracy is 47.8 % with a Kappa coefficient of 0.28. Cropland and mixed forest agree best with the ground truth data, having accuracies of 70.4 and 66.7, respectively (Table 5.14). Only 30 % of deciduous forest and 33.3 % of the crop-grass mosaic are correctly classified. It is easy to understand because 40 % of deciduous forests are misclassified as mixed forest due to the similarity in these reflectance signals. On the other hand, the definitions of MODIS deciduous forest and mixed forest make it even more ambiguous, since more than 60 % of deciduous forest is required to decide on deciduous forest, and below 60 %, deciduous forest would often be classified as mixed forest. The crop-grass mosaic is mainly misclassified as cropland (26 %) due to similarity between the two classes, while 11 % of the area of cropland is classified as crop-grass mosaic.

In Tharandt forest, the overall accuracy is 45.7 % with a Kappa coefficient of 0.18. Mixed forest and crops land have the best agreement to the ground truth data, with accuracies of 78.6 % and 66.7 %, respectively (Table 5.15). While only 25.9% of coniferous forest and 12.5% crop-grass mosaic are correctly classified. Grassland is either classified as cropland (50 %) or mixed forest (50 %). The rest of coniferous forest (74.1 %) is classified as mixed forest due to the similarity of reflectance signals and the ambiguous definition of MODIS classes. The crop-grass mosaic is mainly misclassified as cropland (62.5 %) due to similarity between the two classes. While 33.3 % cropland and 25.0 % crop-grassland mosaic are misclassified as mixed forest.

In Stubai Valley, the overall agreement is 50.8 % with a Kappa coefficient of 0.19. Coniferous forest is most in agreement with the ground truth data, with accuracy of 55 % (Table 5.16), while the other land cover classes are mostly misclassified. Grassland is either classified as coniferous forest (54.5 %) or mixed forest (18.2 %) or open shrubland (27.3 %). Only 33 % of open shrubland are in agreement with ground truth data, while 33 % of the area is misclassified as mixed

forest, and the rest are misclassified as coniferous forest. In addition to the highly fragmented nature of the landscape in Stubai Valley, the roughness of the Alpine mountains contributes to the difficulties of the classifications.

In Berchtesgaden, after aggregation into 6 land cover classes, the overall per-pixel agreement is 51.2 % with a Kappa coefficient of 0.22 (Table 5.17). The highest agreement was found in coniferous forest, where 75 % of the areas are correctly classified; while 25 % of the coniferous forest areas were classified as mixed forest. The other land cover classes are mostly misclassified. While 50 % of the areas of crop-grassland mosaic are in agreement with ground truth data, 50 % of the areas were classified as coniferous forest. Only 33 % of mixed forest areas are in agreement with ground truth data, while 53.3 % of the areas were misclassified as coniferous forest and the rest are misclassified as deciduous forest (6.6 %). Only 25 % of deciduous forests were correctly classified. Most of the deciduous forests were classified as either coniferous forest (50 %) or mixed forest (25 %). All of the bare soil areas were misclassified as crop-grassland mosaic.

The detailed comparison between MODIS land cover type 1 and upscaled Landsat land cover maps reveals some important characteristics of the MODIS land cover products. In the mountainous areas, namely Stubai Valley and Berchtesgarten, where the coniferous forest is dominant, the MODIS land cover algorithm works quite well with the coniferous class, having accuracies of 55 % and 75 %, respectively. However, many of the coniferous areas were misclassified as mixed forest due to the similarity of the spectral signals of the two land cover types as well as the ambiguous definition of the MODIS land cover product. In the relatively low and flat areas of Tharandt and Hesse forest, which are composed mainly of mixed forest, the MODIS land cover algorithm works well, with accuracies of 78.6 % and 66.7 % respectively. Again, most of the misclassification occurs between mixed forest and coniferous forest. The largest problem with the MODIS land cover algorithm is in dealing with grassland, cropland, and crop-grassland mosaic classes. In addition to the similarity of the spectral signal of these three classes, the fragmentation of the landscape plays an important role here. In Hesse, the cropland areas, which make up of nearly half of area, are relatively homogeneous and result in high accuracies of the MODIS land cover product. In contrast, in the other regions, grassland, cropland, and crop-grassland mosaic are

very fragmented. This makes it more difficult to differentiate between the three above-mentioned land cover types at the 1 km^2 scale.

The differences among the classifications are also due to the distributed pattern of forest and surrounding grassland patches. The low resolution of MODIS classifications is unable to reproduce the level of detail found in Landsat data. It is surprising that there is no significant difference in accuracies of MODIS land cover type 1 with respect to the complexity of the terrain. In the Berchtesgaden site, where terrain is the most complex, the MODIS land cover agrees well with Landsat classifications with an overall accuracy of 51.2 %. While the terrain in Tharandt forest is least complex, the overall accuracy is 45.7 %. With the same range of overall accuracy, one cannot identify the effect of terrain roughness with respect to results from the classification algorithm.

b. Comparison of MODIS land cover type 3 and Landsat land cover:

Table 5.18 and 5.19 show the overall accuracy and Kappa coefficient of MODIS land cover type 1 and type 3. The overall accuracy of MODIS land cover type 3 is significantly higher than that of land cover type 1 due to the aggregation of similar land cover classes. The grassland, cropland, and crop-grassland mosaic were aggregated into grasses/cereal crops; mixed forest can be either coniferous forest or deciduous forest based on their majority. The accuracies of MODIS land cover type 3 are much improved in all four study sites because there is no confusion between mixed forest and other forest classes; or in grassland and cropland, or crop-grassland mosaics.

The complexity of the terrain similarly showed no effect on the accuracies of MODIS land cover type 3 classification. At the Berchtesgaden site, the MODIS land cover agrees well with Landsat classifications with an overall accuracy of 94.4 %. The homogeneity of the land cover may play a crucial role because the land cover is much more homogeneous in Berchtesgaden compared to other sites.

Table 5.18. Overall accuracy and Kappa coefficient of MODIS land cover products (type 1) compare to "ground truth" land cover map, which is upscaled from Landsat TM land cover map

	Berchtesgaden	Stubai	Hesse	Tharandt
Overall Accuracy	51.2%	50.8%	47.8%	45.7%
Kappa Coefficient	0.20	0.19	0.28	0.17

Table 5.19. Overall accuracy and Kappa coefficient of MODIS land cover products (type 3) compare to "ground truth" land cover map, which is upscaled from Landsat TM land cover map

	Berchtesgaden	Stubai	Hesse	Tharandt
Overall Accuracy	94.4%	63.1%	70.1%	84.7%
Kappa Coefficient	0.88	0.18	0.32	0.68

5.2. Conclusion with respect to MODIS land cover products

Previous results from the MODIS validation team have suggested that the MODIS land cover product is realistic, and that the algorithm performs well at the global scale. At site scale, this study comes to the following conclusions:

1) The areal statistical analysis shows that MODIS classification results obtained at lower spatial resolution are generally comparable to those from Landsat TM. The discrepancies here are mainly due to resolution differences of the two land cover maps. Land cover classes with small area cannot be depicted by the MODIS land cover map, but still appeared in the Landsat land cover map. The discrepancies occur mostly in some regions with mixed land surface cover, where brightness variations of mixed surface types can produce a mathematical ambiguity that cannot be resolved without additional information.

2) Spatial analysis has proven that MODIS land cover maps type 3 with the six biomes better agree with the Landsat reference maps than the MODIS land

cover type 1 with 17 classes (IGBP). Fragmentation in European landscapes is a fundamental problem encountered in the use of MODIS products. A true representation of the land surface cannot be obtained from the current MODIS land cover classifications at 1 km scale. The IGBP classification scheme is not compatible with the structural classification schemes commonly used in the study area, e.g. woody savanna class in MODIS IGBP cannot fit to any land cover type of the region. The lack of local training data and the coarse spatial resolution are also sources of inconsistencies.

The problem with misclassification of cropland and grassland was evident in the MODIS land cover type 1 product, but the combination of cropland and grassland in MODIS land cover type 3 results in similar estimates to the Landsat land cover. In the same manner, the misclassification of needleleaf or broadleaf forest as mixed forest was profound in MODIS land cover type 1. The separation of needleleaf forest and broadleaf forest in MODIS land cover type 3 helps to improve the ambiguity of mixed forest in comparison to the other forest types.

3. The complexity of the terrain showed no or small effect on the accuracies of the MODIS land cover classification. While the homogeneity of the land cover shows a significant effect on the quality of MODIS land cover product. The homogeneous land cover in National Park Berchtesgaden contributes to higher accuracies of MODIS land cover products as compared to other sites.

4. Despite the limitation of the MODIS land cover products, the results are encouraging and conclusively demonstrate the quality of MODIS data for land cover mapping applications, especially the MODIS land cover type 3. MODIS data clearly provides a significant improvement in terms of quality relative to the heritage AVHRR data. The major advantage of MODIS land cover data is that a consistent methodology is applied across the globe and is repeatable. The quality of the results might support large-scale land cover mapping. The major weakness of this approach is the lack of local/regional validation. The use of these descriptors in models describing land surface properties may potentially lead to large errors at local/regional scale. Thus, exchange between the land surface and the atmosphere of water and CO_2 as estimated

by models using MODIS inputs will have a high level of uncertainty, and the results must be considered with caution.

5. The study shows the limitation of pixel-based classification compared to object-based classification, because object-based classification can incorporate more contextual information into classification algorithm. The MODIS land cover algorithm is based on supervised classification methodology, which uses a decision tree classification approach and exploits a global database of training sites. Therefore, classification results produced from MODIS data are heavily dependent on the integrity and representation of global land cover in the site data.

6. MODIS land cover also has a limitation of pixel-based classification. Object-based classification which incorporates more contextual information into the classification algorithm might improve the accuracies of the MODIS land cover product, especially at landscape and regional scales. For regional or landscape scale studies, MODIS at 250-m resolution would produce more detailed results for land cover, while still taking advantage of frequent temporal coverage by MODIS.

CHAPTER 6.   EVALUATION OF MODIS LAI PRODUCTS

6.1. Derivation of LAI-Vegetation Index (LAI-VI) models for coniferous forest in mountainous Alpine areas (Berchtesgaden National Park and Stubai Valley)

6.1.1. LAI measurement in Berchtesgaden

The LAI map of Berchtesgaden, which was derived from forest inventory data, is shown in detail in figure 6.1a, b, c. It should be recognized that the forest inventory database of the National Park Berchtesgaden is a unique dataset in the context of long-term ecological monitoring and the degree of detail of the measurements (see Konnert et al., 2001 – reference on the inventory here).
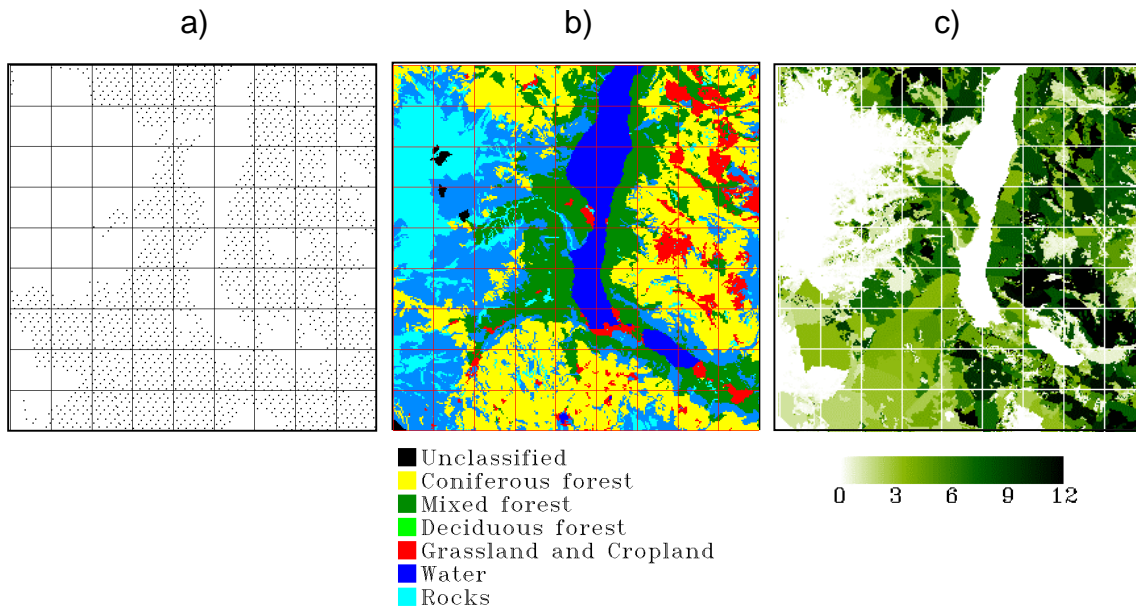
Figure 6.1. a) Forest inventory points; b) Land cover map; and c) derived LAI map of Berchtesgaden National Park.

Utilizing the inventory data, forest type map, and allometric relationships relating BDH and LAI, a detailed LAI map was created at landscape scale. LAI was calculated at each plot separately for coniferous forest (assumed to be Norway spruce, *Picea abies*), and deciduous forest (treated as beech, *Fagus sylvatica*) (see details in chapter 3.2.2.3, eq. 3.3 and 3.4.)

Once the LAI at each plot was calculated, plots were grouped into patches according to the tree types, tree age, and tree density. Thereafter, the LAI of each patch was

calculated by averaging all plot LAI values. In Berchtesgaden forest, LAI varied greatly, from 2 to 12, with an average value of 6.5. The coniferous forest has a substantially higher LAI as compared to deciduous forest, mostly due to the higher density and age of coniferous forest in comparison to that of deciduous forest and higher leaf mass per tree. The LAI on the west-facing slopes is also higher than on the east-facing slopes, apparently due to the fact that east-facing steep slopes prevent establishment of deeper soil, increase soil erosion, and reduce the stability of forest trees.

a)   b)
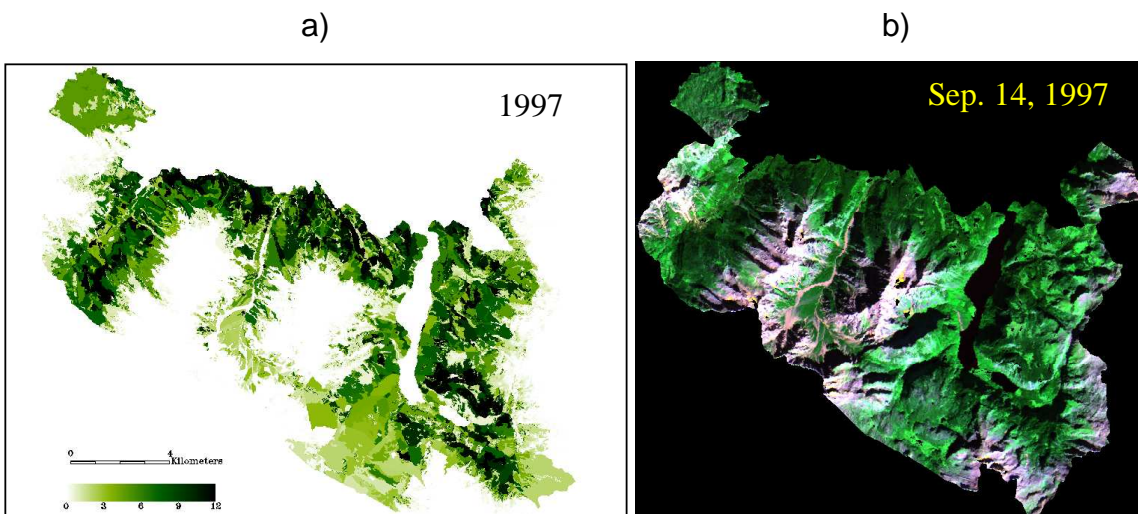
Figure 6.2. a) LAI map of Berchtesgaden National Park. b) Landsat true color image composite (Bands 3, 4, 7.) for the park.

Fig. 6.2a provides a broader view of the LAI map of Berchtesgaden National Park (as of 1997) in accordance to the Landsat true color composite image acquired on Sep. 14, 1997 (Fig. 6.2b. Apparently, we can observe the correlation of denser forest with the dark green color signature in the Landsat image, indicating higher LAI areas in the LAI map, while the thinner forest (light green color) is in correlation with lower LAI areas.

6.1.2. *Selecting LAI-VI models and derivation of LAI map from Landsat data in Berchtesgaden*

An attempt was made to relate LAI and vegetation indices (VIs) derived from Landsat images and based on pixel-by-pixel comparison of the two images in Fig. 6.2. This resulted in a poor correlation with a low r^2 of 0.18. This is largely due to the error in the co-registration process. Although a rigorous effort was made to

obtain high precision in the image to image registration between the LAI map and Landsat image, an error of half pixel makes it impossible to guarantee that the LAI measured plot on the ground corresponds exactly to specified satellite pixel. In addition, the LAI point grid data were obtained via allometric equations and averaging within the 200 x 200 m inventory grid, which does not correspond to the Landsat grid (30 m x 30 m).

In the patch-based LAI map, each LAI values represent leaf area index for larger forest stands, not for a single inventory point determination. The variation of LAI within a patch also contributes to the above-mentioned low correlation of LAI and VIs. This result is in accordance with the previous conclusion, that the internal variance of the objects affects the correlation of LAI and VIs (Tian et al., 2002a, b; Wang et al., 2003). Therefore, pixel-by-pixel comparison of the Landsat image and LAI map should only be considered in the ideal situation, where the homogeneous objects are observed on the ground (Tian et al., 2002a, b; Wang et al., 2003).
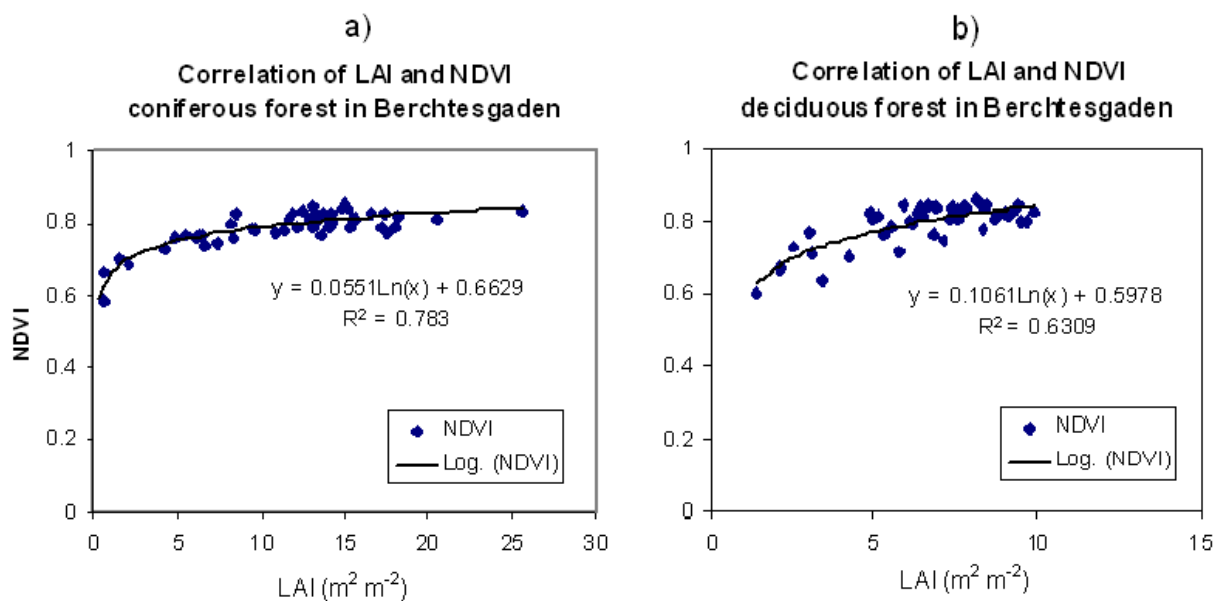
Figure 6.3. Patch-based comparison between LAI and NDVI of a) coniferous forest in Berchtesgaden. b) deciduous forest in Berchtesgaden.

To avoid these problems, a patch-based comparison of VIs derived from Landsat data and LAI was analyzed. The patches in consideration are regarded as homogeneous forest polygons which have an average LAI value. Each patch may consist of several measured plots. By averaging VIs of the pixels within an LAI patch, one obtains a VI representative for the patch.

Fig. 6.3 illustrates the relatively tight correlation between LAI and NDVI of both coniferous and deciduous forests in Berchtesgaden, with r^2 of 0.78 and 0.63, respectively. Previous studies also reported higher correlation coefficients of patch-based analyses as compared to pixel-per-pixel correlation of LAI and VIs (Tian et al., 2002b; Wang et al., 2004). The two models relating NDVI and LAI were obtained for coniferous (6.1) and deciduous (6.2) forest as follows:

$$NDVI = 0.0551 * Ln(LAI) + 0.6629 \qquad (6.1)$$

$$NDVI = 0.1061 * Ln(LAI) + 0.5978 \qquad (6.2)$$

The coniferous model ($r^2 = 0.78$) far outperformed the deciduous model ($r^2 = 0.63$). These results are in agreement with a previous study by Fassnacht et al. (1997). However, in comparison of the performance of the two models, it must be noted that there is greater variability in the coniferous LAI data than in the deciduous data, and this distribution of LAI data might explain the differences in predictive performance.

Other studies have reported that the reflectance received by the satellite sensor, hence NDVI saturates at LAI between 4 and 8 (Peterson et al., 1987; Spanner et al., 1994). In this study, deciduous LAIs range from 2 to 10, whereas most of the deciduous plots had LAI greater than 4; this suggests that the majority of data may have fallen within the region of saturation. The coniferous plots, in contrast, had LAIs ranging from 1 to 15, whereas data in the range from 1 to 5 (where the satellite signal was more sensitive to changes in LAIs) contribute strongly to derivation of the coniferous model.

As has been suggested previously (Spanner et al., 1994), the LAI-VIs models can be sufficient for prediction of LAI from satellite data when $r^2 > 0.5$. Thus, the two above-mentioned models can be used with confidence to derive LAI maps from Landsat (Landsat LAI) images at 30 x 30 m resolution in Berchtesgaden. The patch-based Landsat LAI map was then created by averaging all pixels of Landsat LAI, which fall within a corresponding patch in the measured LAI.

a)

b)
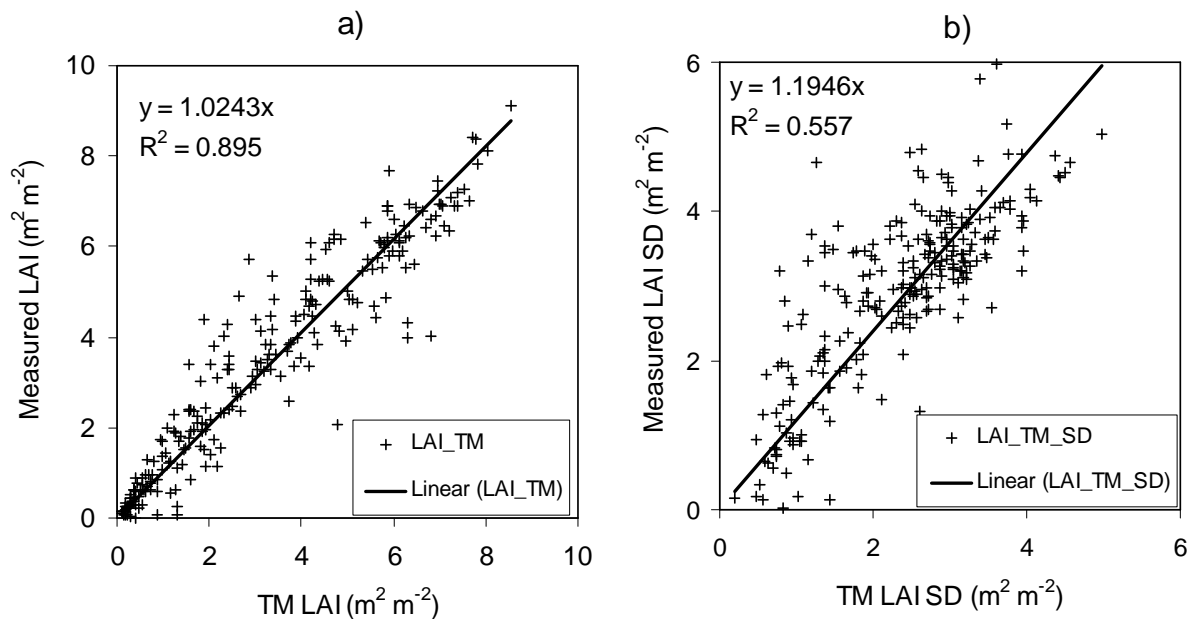
Figure 6.4. a) Correlation between patch-based measured LAI and Landsat estimated LAI and b) Correlation between standard deviation (SD) of measured LAI and Landsat TM estimated LAI in Berchtesgaden.

The slope of the correlation between patch-based measured LAI and Landsat estimated LAI and is very close to 1. Of course the LAI-NDVI models are derived from the measured LAI itself. It is nevertheless important to recognize that a high value is obtained for the correlation coefficient (r^2 = 0.9) and RMSE (= 0.24). The tight correlation between measured LAI and Landsat LAI confirms the usefulness of these two LAI-NDVI models, which were used to derive a fine resolution LAI map at 30 x 30 m scale for the Berchtesgaden National Park (Fig 6.14). The RMSE value indicates that there is considerable uncertainty in the LAI which was derived from Landsat data. In other words, it sets a limit on the accuracy of LAI maps derived from Landsat images.

The relatively high correlation coefficient (r^2 = 0.56) between standard deviation (SD) within patches of measured LAI and Landsat TM LAI in Berchtesgaden (Fig. 6.4b) is explained by the fact that both measured and remote sensing methods capture the inner variation of LAI within the patches. On other hand, the SD of measured LAI within the patches is significantly higher that that of Landsat LAI (20 %). The main factor, which contributes to this difference, is the sampling distance (space). In the former method, the sampling distance is 141 m and the sampling area is 500 m^2; each measurement is isolated and regarded as an

independent measurement. In the case of Landsat LAI, the data is continuously sampled and the sampling distance is only 30 m. This makes the measurement highly auto-correlated, causing a lower standard deviation from the Landsat LAI.

6.1.3. *Validation of Landsat-derived LAI maps in Berchtesgaden*

The empirical forest LAI models were extrapolated to and tested in Stubai Valley, which has a similar landscape as well as climate conditions. An LAI map was derived using inventory data for forest parcels near Neustift, a small section of the Stubai Valley. The method used for LAI map development was the same as used in Berchtesgaden National Park. The measured LAI map was used as "ground truth" LAI map to test a Landsat LAI map based on equations 6.1 and 6.2 applied in Stubai Valley.
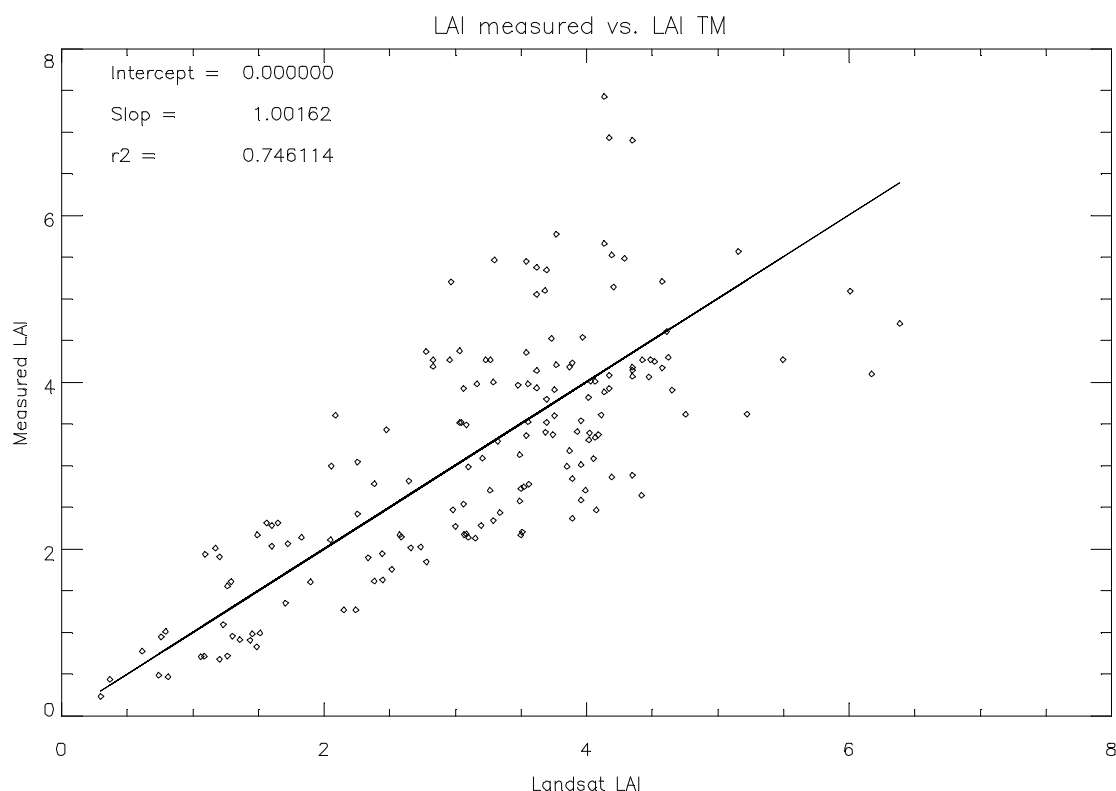
Figure 6.5. Correlation between patch-based measured LAI and Landsat LAI in Stubai Valley.

Fig 6.5 shows the correlation between the two LAI maps at Neustift, where the regression is forced through origin. The high correlation coefficient ($r^2 = 0.76$) demonstrates that the LAI-NDVI models acquired in Berchtesgaden are effective in Stubai Valley, and may be confidently used in other similar Alpine regions. This is

also expressed by the slope of the trend line (~1). The similarity of the two LAI relationships results due to application off the same methods, using inventory data to develop the "ground truth" LAI map at the two sites. On the other hand, Landsat images obtained under similar conditions, e.g., September 13, 1999 and September 14, 1999, were used to develop Landsat LAI maps in Stubai Valley and Berchtesgaden, respectively.

Going from low to high LAI, the difference between measured and Landsat LAI increases, reflecting the nature of the allometric methods for LAI determination. The exponential relationship between LAI – DBH leads to potentially large errors when estimating with large DBH. Even so, the RMSE of 0.30 is comparable to other studies (Bobeva, 2003; Wang et al., 2004). The biggest challenge for validation of the moderate (> 1 km) resolution MODIS LAI product is the scarcity of ground-truth measurements. Considering the small scale of *in situ* measurements and the large amount of work associated with field measurements, it is unrealistic to expect sufficient data for a pixel-by-pixel comparison for all sites. An alternative is to use the LAI-VI models acquired in Berchtesgaden for coniferous and deciduous forests as well as grassland (acquired in Stubai Valley, see next section) for examination of the two Alpine mountainous sites studied here, and to derive in turn fine resolution "ground truth" LAI maps which are then used for evaluating MODIS LAI.

6.2. Derivation of a high resolution LAI map in Stubai Valley from Landsat data

6.2.1. *Grassland LAI measurements in Stubai Valley*

LAI in Stubai Valley was sampled at two grassland sites, corresponding to different management practices: the grassland site at the bottom of Stubai Valley was cut three times during the year (site 1), while the meadow site on a south-facing slope was abandoned and exhibited natural changes in LAI without management (site 2).

The Landsat images were chosen from 6 days, corresponding with vegetative or critical growing conditions at the grassland sites. Different LAI-VIs models were tested which led to the result that the simple ratio (SR) is the most suitable vegetation index for use in correlation with the measured LAI.
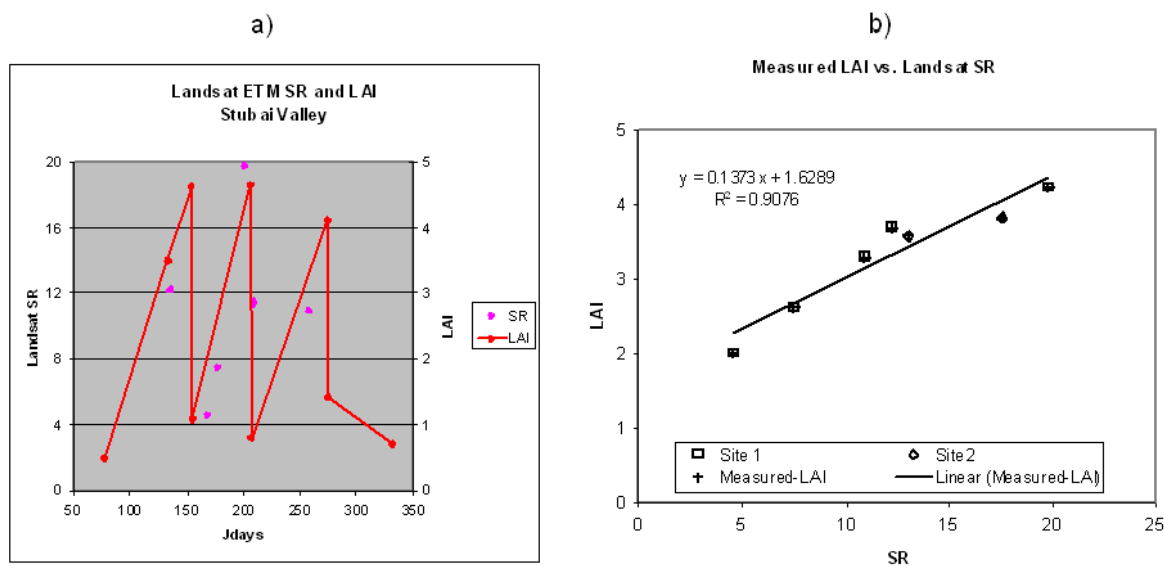
Figure 6.6. a) The Landsat SR time series compared to measured LAI; b) Correlation between measured LAI (from 2 local sites) and Landsat SR in Stubai Valley.

Fig 6.6a shows 9 LAI measurements (in red diamonds), and the assumed course for seasonal change in LAI at the valley bottom site (red line), which was linearly interpolated between measurements. The SR index (in pink diamonds) corresponds well to the changes in LAI over the course of growth. The two first cuts are clearly identified. Only in the case 2 days after the 2nd cut (day 208) is the SR still relatively high compared to measurements, due to the effect of dead green materials left over on the field after the cut. These still can absorb and reflect the incoming light. This case was excluded from further analysis because of its abnormality. The SR ranges from 5 to 20, while LAI ranges from 2.0 to 4.2 suggesting that the majority of data fall within a range, where the satellite signal sensitively to changes in LAI is high. A tight correlation between Landsat SR and LAI was observed ($r^2 = 0.90$). LAI alone can explain 90 % the variation in SR.

To examine the influence of the satellite data resolution on the LAI-VI relationship, correlations between LAI and MODIS VIs (NDVI and SR) at different resolutions (250, 500, and 1000 m) were examined. Statistical analysis indicated that the MODIS SR is better correlated with LAI. as already found in case of Landsat SR. Furthermore, MODIS SR 250 m resolution was more strongly correlated with the three cuts at days 154, 206, and 274 than the coarser resolutions. Thus, the effects of mixed pixels, which include another land cover type in the case of more coarse

resolution, clearly influence the results. Therefore, only MODIS SR 250 m resolution was used for further study.
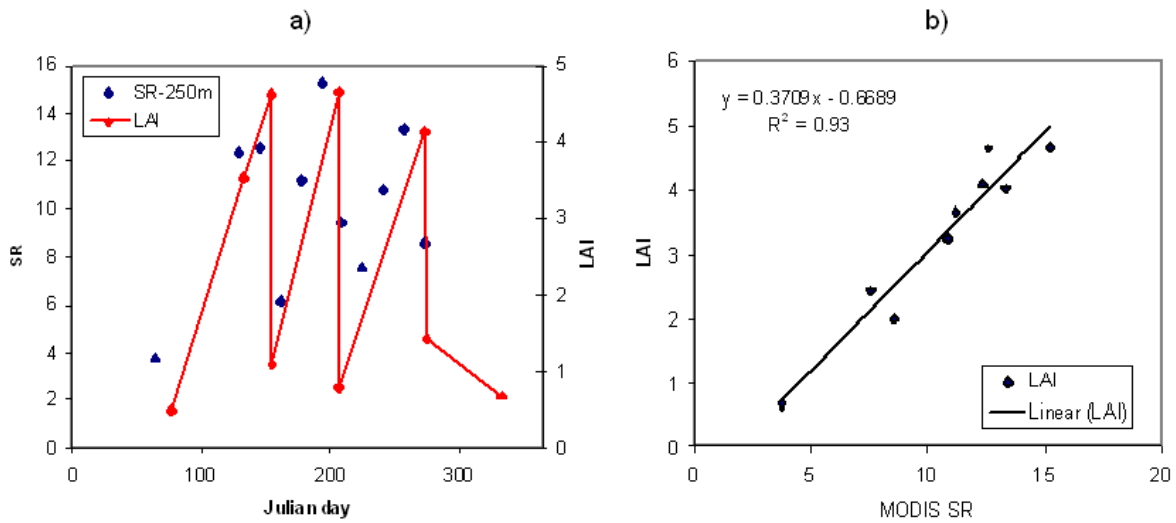
Figure 6.7. a) The MODIS SR time series in accordance to measured LAI at the valley bottom site; b) Correlation between measured LAI and MODIS SR in Stubai Valley at the valley bottom site.

The comparison between measured LAI and MODIS SR at 250 m resolution is shown in Fig 6.7a and b. Even at the finest resolution of MODIS products, the size of the measured plots is still relatively small compared to the pixel size. Nevertheless, the MODIS SR index was well correlated with the changes in LAI. The three cuts of grassland during the year 2002 could be clearly identified (Fig. 6.7a). After removing abnormal data obtained immediately after the 2nd and 3rd cuts, an r^2 = 0.93 was obtained. It is important to note that, when LAIs vary from 1 to 4.5, the MODIS SR changes from 6 to 15, while Landsat SR changed from 4 to 20.

6.2.2. *Selecting LAI-VI models and derivation of LAI map from Landsat data in Stubai Valley*

The model relating SR and LAI from Landsat for grassland and meadow is as follows:

$$LAI = 0.1373 * SR + 1.63 \qquad (6.3)$$

With three models (6.1), (6.2), and (6.3) for coniferous forest, deciduous forest and grassland, respectively, the fine resolution LAI maps were derived for Berchtesgaden and Stubai Valley.

6.3. Derivation of LAI map in Tharandt forest from Landsat data

6.3.1. Grassland LAI measurements in Tharandt

LAI measurements in Tharandt forest were carried out at the grassland site using destructive and non-destructive methods over the course of the growing season in 2004.
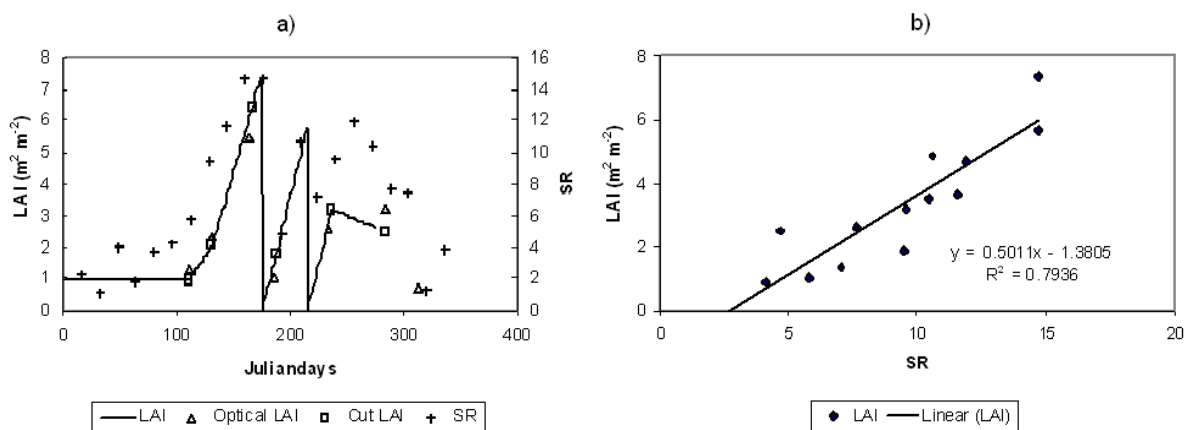
Figure 6.8. a) The MODIS SR time series in accordance to measured LAI (2004); b) Correlation between measured LAI (from 2 local sites) and MODIS SR in Grassland Tharandt (2004).

Fig 6.8a presents the LAI measurements in Tharandt obtained by different methods: optical method (in open triangle), destructive method (open square) and measured LAI course of growth (as a continuous line and linearly interpolated between measurements. Because of the lack of cloud free Landsat data in 2004, the MODIS reflectance data at 250 m resolution had to be used for analysis. The MODIS SR index (in plus sign) corresponds well to the change of LAI. The SR ranges from 4 to 15, while LAI ranges from 1 to 7. The majority of data are in the range of LAIs where the satellite signal is sensitive to changes in LAI. Only within the range from 6 to 7 is it possible that a saturation occurs in the reflectance signal. However, a relatively strong linear LAI – SR relationship ($r^2 = 0.79$) was also observed at this site (Fig. 6.8b).
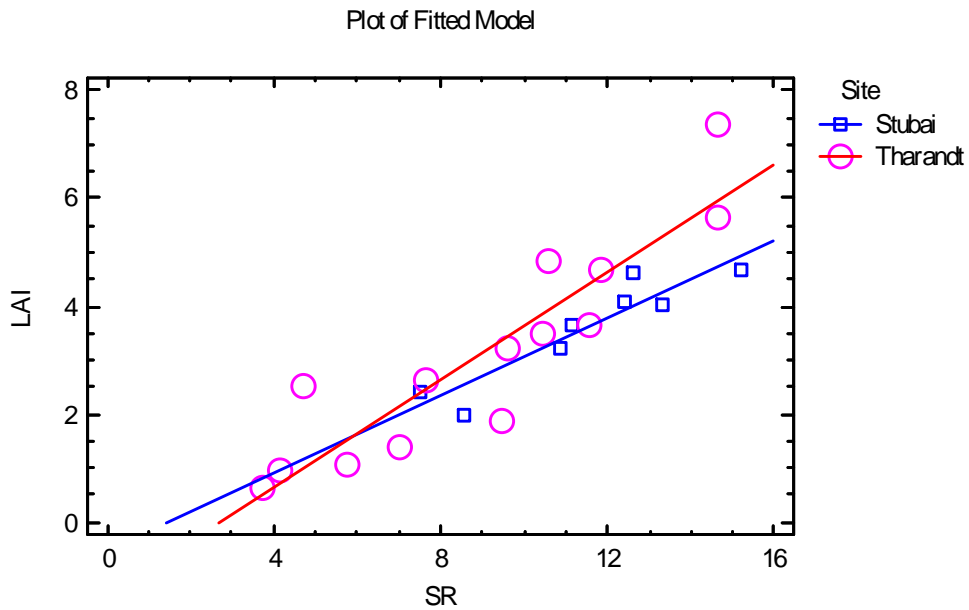
Figure 6.9. Comparison between 2 models correlating measured grass LAI and MODIS SR in Stubai Valley and Tharandt.

Fig. 6.9 shows the statistical analysis of the data which compares results of the relationships obtained at the grassland sites in Stubai Valley and Tharandt.. The results indicate that there was no statistically significant difference in the slopes for two models, but a small different in the intercepts of the LAI-SR equations (Fig. 6.9) in Stubai Valley and Tharandt. Because of the inaccuracy in low LAI determinations (at values below 1.0), this difference was ignored In general, deviations in the equations may occur due to differences in the harvesting methods applied by the two different research groups.

6.3.2. *Selecting LAI-VI models and derivation of LAI map from Landsat data in Tharandt forest*

The models (6.1) and (6.3) were used for coniferous forest and grassland, respectively to establish a fine resolution LAI map for Tharandt. For deciduous forest stands, the model obtained from Hesse forest (shown in the next section) was used (eq. 6.4).

6.3.3. Comparison of the Landsat-derived LAI map for coniferous forest in Tharandt to older estimates
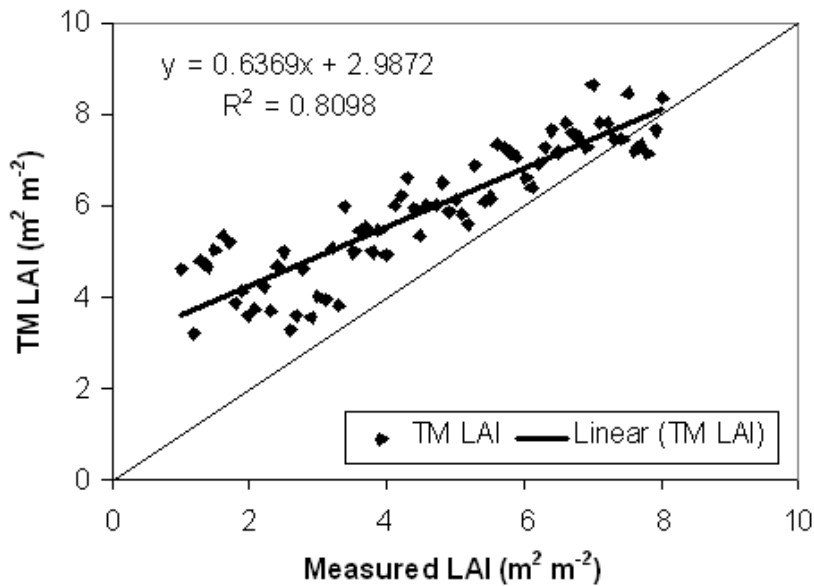
Figure 6.10. Comparison between measured LAI as determined in 1993 and Landsat LAI estimated in 2001 for coniferous forest in Tharandt.

In Tharandt, there were measurements of LAI in spatially distributed coniferous forest stands carried out in 1993 according to the allometric method. We should expect a close correspondence in those studies with the relationships from Berchtesgaden and Stubai Valley. The environmental conditions in Tharandt Forest do not differ strongly and methods were in principle the same. However, during 8 years, the natural growth of forest as well as the management activities would have influenced LAI. Comparison with the August 2001 Landsat estimates can shed light on this change.

Fig. 6.10 illustrates a strong linear relationship ($r^2 = 0.81$) between measured LAI in 1993 and Landsat estimated LAI in 2001 for coniferous forest in Tharandt despite branch cutting and removal of fallen materials. The major of data and, therefore, the trend line lies well above the 1 : 1 line, which confirms growth of the forest with increasing LAI. However, Landsat LAI (2001) is significantly higher than measured LAI (1993) only in the low range of LAIs, whereas small difference is found at high LAI. This probably demonstrates differences in the growth characteristics in stands of different ages and/or density. At the higher LAI (old forest and/or dense forest), the forest is probably already at the maximum capacity for

supporting needle materials, while at the lower LAI, this biomass pool has potential to increase.

6.4. Derivation of LAI map for Hesse forest from Landsat data

6.4.1. LAI measurements in Hesse forest

a)   b)
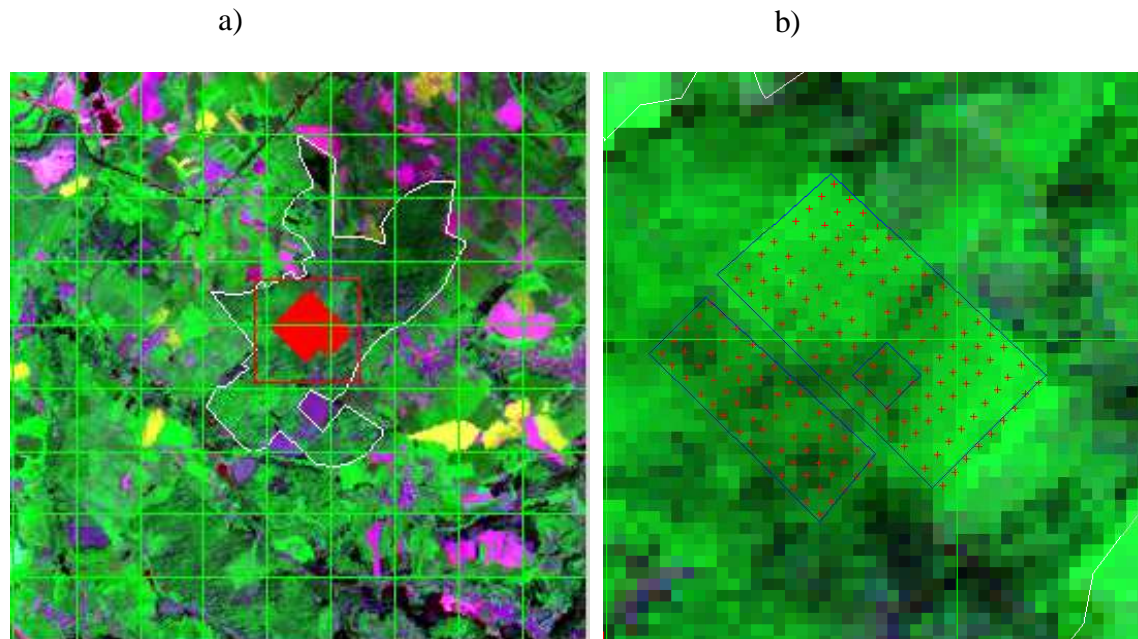
Figure 6.11. a) Landsat TM true color composite of Hesse forest, the measurement area is in red; b) Spatial grid for measurement of LAI in two forest stands, young stand is in the larger light green rectangle (with tower at the center of the small square), and an old stand is in the smaller rectangle.

In Hesse deciduous forest, LAI was temporally measured by collecting leaves in traps and spatially by applying optical methods and using a DEMON leaf area analyzer (detail in section 3.2.2.3). Results are shown in Fig. 6.11.

The spatial measurements were carried out in 2001 and 2002 at two forest stands (Fig. 6.11a and b). The data was rasterized to correspond to a 30 x 30 m resolution image using Arview software. The young forest stand has an average LAI of 8.1, while the old forest stand has an average LAI of 5.8. The data also showed that LAI in 2002 was greater than in 2001.
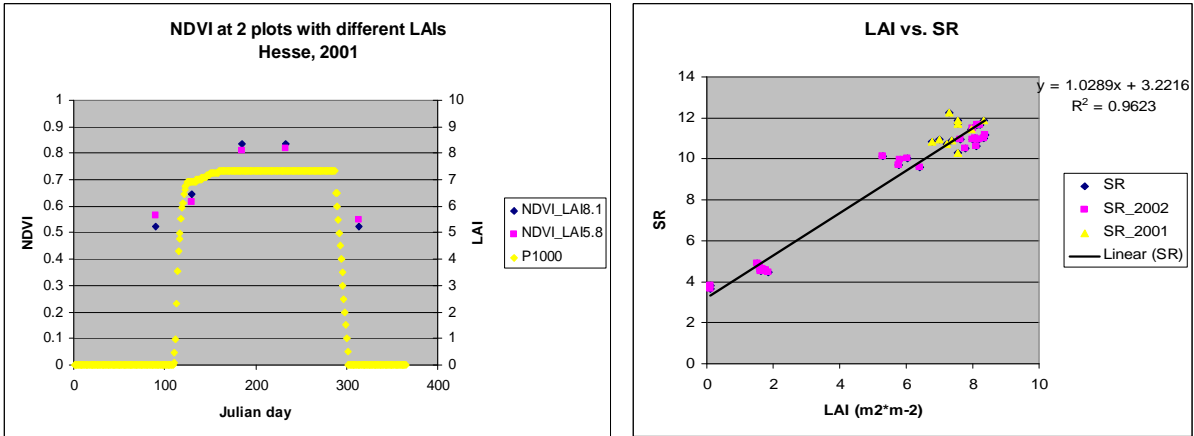
Figure 6.12. a) Temporal measurements of LAI at the Hesse tower site in 2001 illustrated as the linear interpolation between the measurements (yellow diamonds) and NDVI determined at different times from Landsat; b) Correlation between measured LAI and Landsat SR in 2001 (yellow triangle) and 2002 (purple square) in Hesse forest.

Fig. 6.12a shows temporal measurements of LAI in 2001 at the tower site in comparison to average NDVI of the old forest stand (purple squares) and young forest stand (blue diamonds). The LAI at the tower is 7.3, somewhat lower than the average LAI of young forest stand. The NDVI of the young forest is higher than the old forest during full canopy development because of higher LAI, but lower during the leaf-off season. That may be explained by the fact that the understory of old forest is more developed than young forest, due to higher light availability during the growing season.

Fig. 6.12b shows the patch-based relationship between measured LAI in 2001 and 2002 in Hesse forest and SR which is derived from Landsat data acquired at full canopy development in the corresponding years (August 22, 2001 and July 08, 2002). The linear model is:

$$LAI=1.03*SR + 3.22 \hspace{2cm} (6.4)$$

The high observed-correlation ($r^2 = 0.96$) is due not only to the sensitivity of the satellite signal to the change of LAI, but also the effect of LAI observations, since there is no data in the middle range of LAI (from 2 to 5). Therefore, care must be taken when interpreting this result.

6.4.2. Selecting LAI-VI models and derivation of the LAI map from Landsat data for Hesse forest

The models (6.1), (6.3), and (6.4) were used for coniferous forest, grassland, and deciduous forest respectively to establish the fine resolution LAI maps in Hesse.

6.4.3. Validation and/or consistency of the Landsat-derived LAI map for Hesse forest

Since we do not have an independent dataset for validation of the Landsat LAI map for beech forest, the quality and consistency of LAI maps at the same stage of development was examined. The LAI maps derived from 2 Landsat scenes acquired on July 5, 2001 and August 22, 2001 were chosen. Both maps were upscaled to 1000 m resolution in order to take advantage of patch-based comparison and to avoid the errors associated with incorrect image registration. A very strong relationship ($r^2 = 0.92$) between the two LAI maps (Fig. 6.13) was observed as expected. The LAI in August was estimated about 6 % higher than LAI in July which may be ascribed to the canopy development. From visual examination of the two LAI maps, some changes of LAI in grassland and cropland were observed due to management activities. This change is seen in the scatter diagram of Fig. 6.13, where LAI ranges from 3 to 4. The LAI-VI models were judged to be reliable for validation of MODIS LAI in the next steps for the Hesse site, although future work should include comparisons across sites with independent deciduous forest LAI determinations.
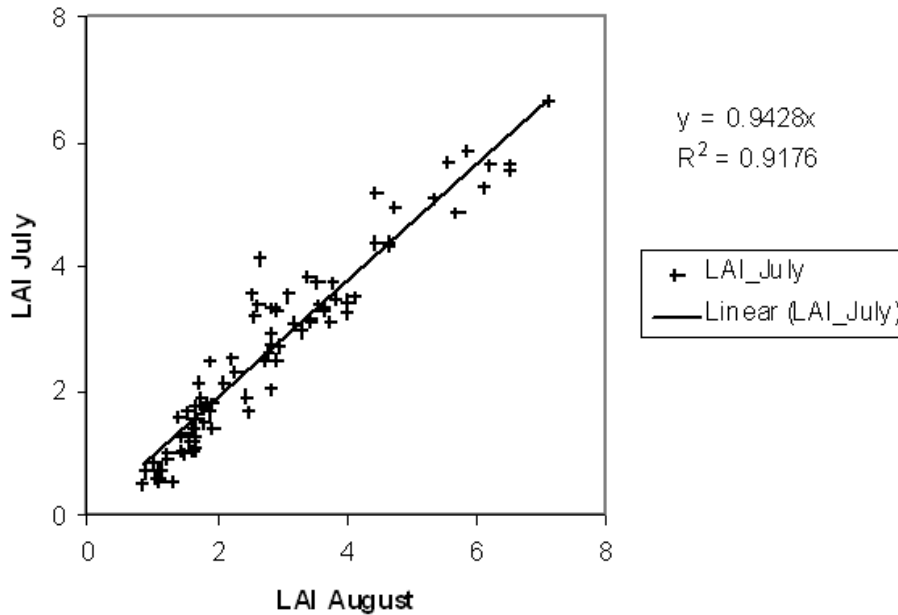
Figure 6.13. Comparison of LAI maps on July 5, 2001 and August 22, 2001 in Hesse forest (scale 1 km).

6.5. Upscaling Landsat LAI to 1 km resolution

With respect to upscaling, LAI values over larger areas should be the integrated LAI value of included small areas. The high resolution Landsat LAI maps were upscaled to coarse resolution comparable to MODIS LAI as illustrated in Fig 6.14. As we can see in this figure, most of the 1 x 1 km pixels are composed of different land cover types and variation LAI within 1 x 1 km pixel is apparent.

While every effort has been made to accurately georeference the maps, this still does not guarantee that the Landsat maps exactly overlay the MODIS maps. The error of geo-referencing likely changes the composition of land cover within individual 1 x 1 km pixels, which in turn causes a change in the average upscaled Landsat LAI of the pixel. An analysis of the effects of incorrect geo-referencing on the LAI upscaling process was made (Fig. 6.15). In the georeferencing process, MODIS and Landsat data are subject to an error of 50 m and 30 m, respectively (see Chapter 3). Therefore, in the worst case, MODIS and Landsat data in this study might have an error as large as 80 m when overlaid on each other. Fig. 6.15 shows the correlation of upscaled LAI to that of the cases, where the error of MODIS-Landsat georeferencing are 90 m to the north, south, east, and west. In all cases, the correlations in LAI are very tight ($r^2 \approx 1$) and relations are 1 : 1, suggesting that

the effect of incorrect geo-referencing on upscaled Landsat LAI is very small and can be ignored.

| TM LAI 20/06/2000 (jday 171) | Upscaled TM LAI | MODIS LAI (jday 169-177) |

0   3   6   9   12

| TM LAI 17/06/2002 (jday 168) | Upscaled TM LAI (jday 168) | MODIS LAI (jday 160-168) |

0   3   6   9   12
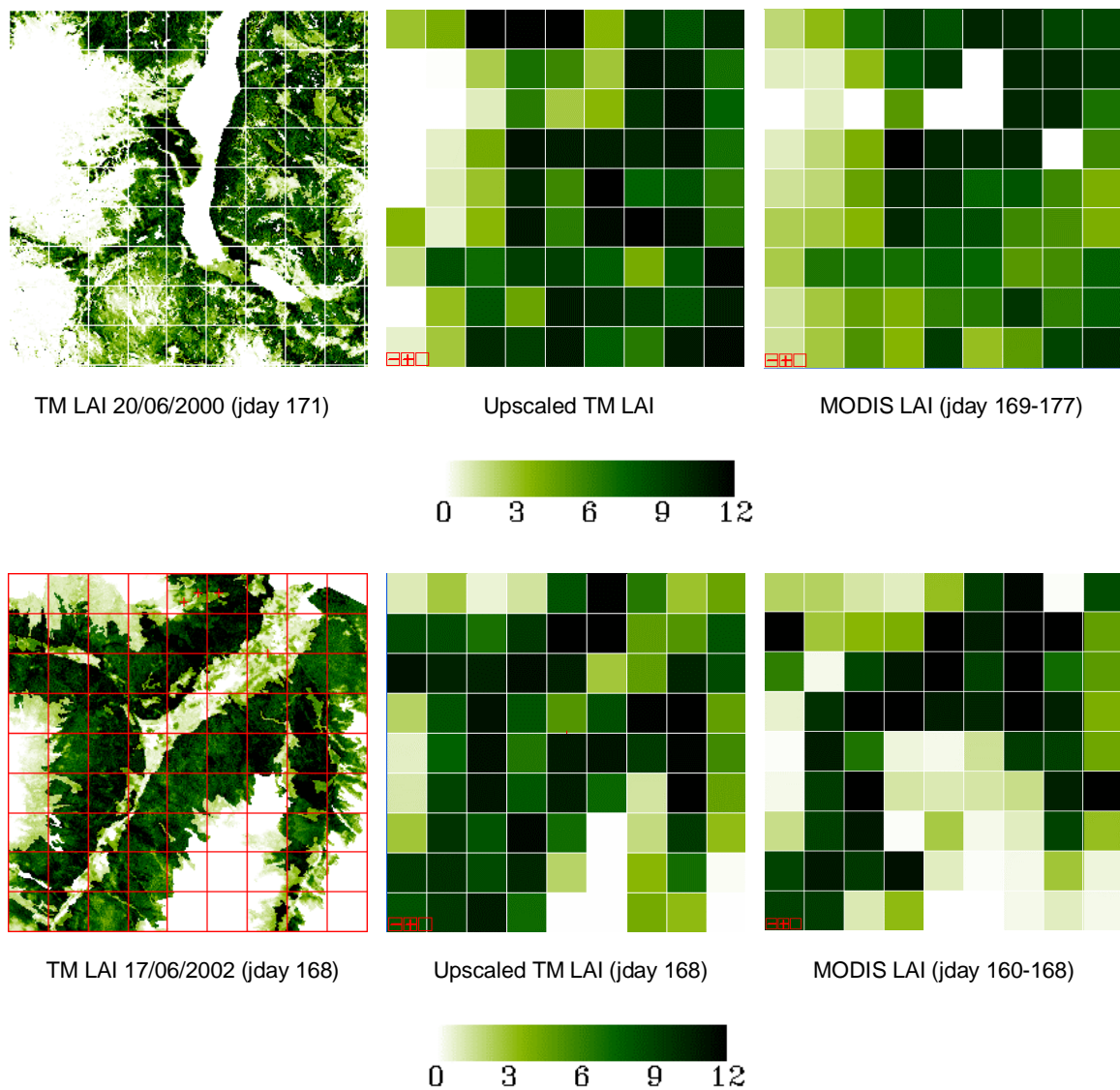
Figure 6.14. Upscaling of Landsat LAI to MODIS LAI resolution in Berchtesgaden and Stubai Valley during early summer.
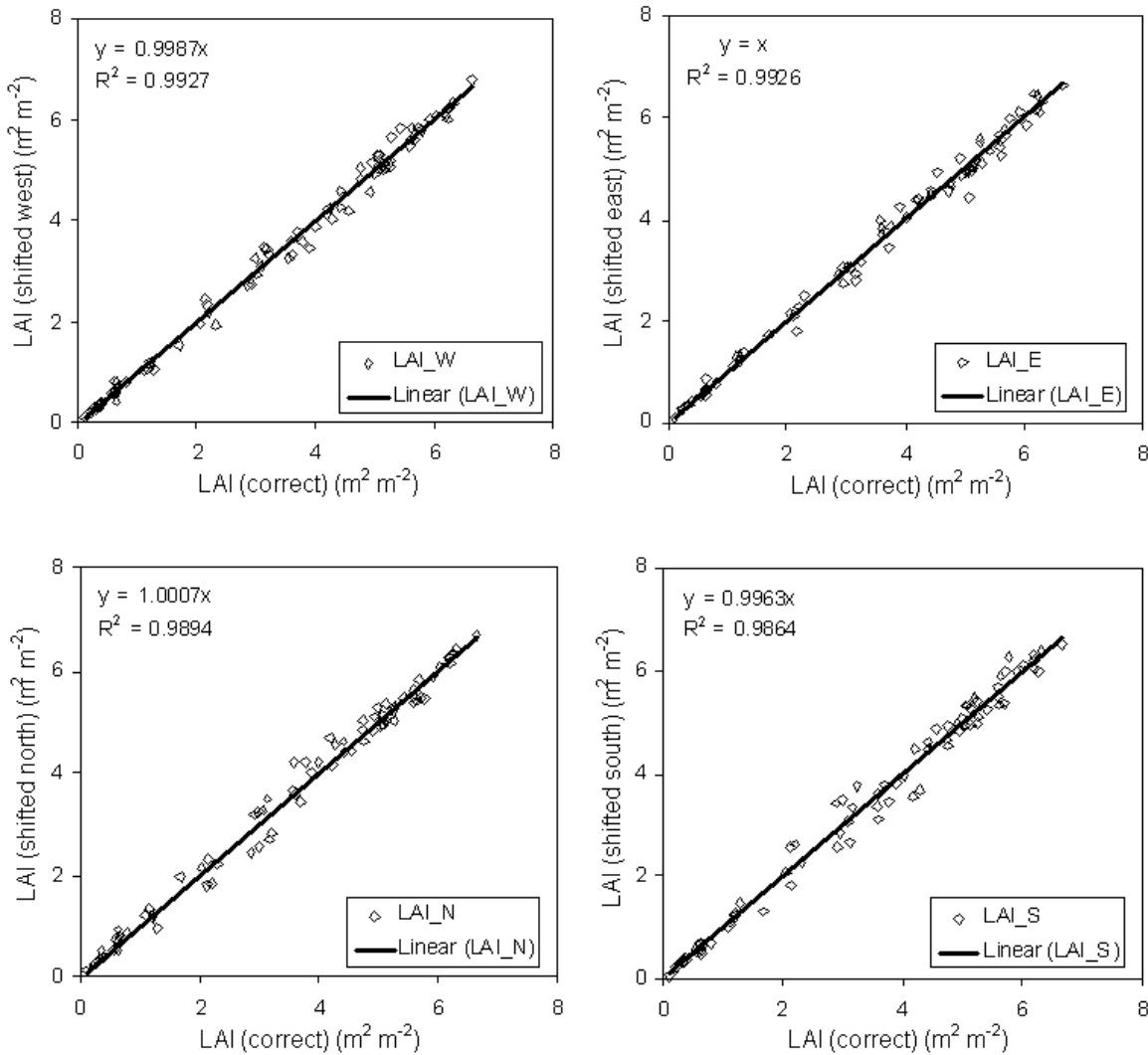
Figure 6.15. Effect of incorrect geo-referencing on scaled Landsat LAI in Berchtesgaden.

6.6. Evaluation of MODIS LAI products

Validation is defined as the process of assessing the quality of the MODIS LAI products by independent means (Landsat LAI). The validation procedure requires aggregation of the fine resolution Landsat LAI map to moderate resolution through an averaging procedure. The comparison between these two LAI maps provides a quantitatively accurate assessment of the MODIS LAI products. The public MODIS LAI product (MOD15A2) is composited over an 8-day-period based on the maximum LAI value retrieved. Its accuracy is expected to be 0.5 LAI. The MODIS LAI data also include quality assessment (QA) data. The QA dataset include information about the overall condition of input data and the algorithm to retrieve LAI.

The MODIS LAI algorithm uses a biome classification map and atmospherically corrected MODIS spectral reflectances at 1 km resolution to retrieve LAI. It compares measured reflectances with those determined from a suite of canopy models, which depend on biome type, canopy structure, and soil/understory reflectances. The canopy/soil/understory models are used to derive the distribution of all possible solutions of LAI. The mean values of these distribution functions are achieved. The overall uncertainty (Wang et al., 2001) in model and observations are set to 20 %. When the main algorithm fails, a backup algorithm is triggered to estimate LAI using vegetation indices. In the case of a dense canopy, its reflectance can be insensitive to LAI. When this happens, the canopy reflectance is said to belong to the saturation domain, and LAI is retrieved using a backup model with saturation (Knyazikhin et al., 1998b).
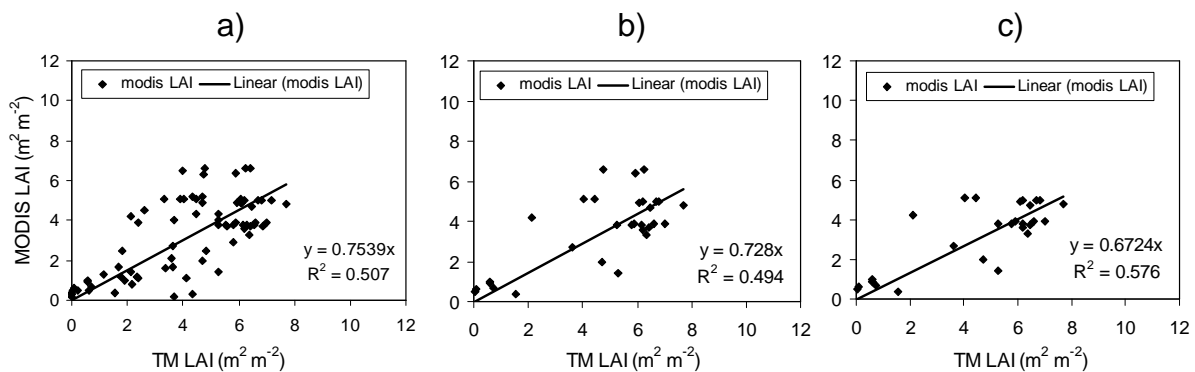
Figure 6.16. Comparison of MODIS LAI and Landsat LAI in Berchtesgaden in different cases: a) All 9 x 9 pixels; b) Only pixels that are correctly classified by MODIS Land cover algorithm; and c) Only via the radiative transfer model.

The Landsat LAI maps were compared to MODIS LAI maps, which were obtained on the same days. Three cases were examined to determine the effect of land cover classification on the retrieval of MODIS LAI and the difference between MODIS LAI algorithms: radiative transfer model (RT) and back up model.

Case 1: Using all data available

Case 2: Using data with correct land cover identification

Case 3: Using data with correct land cover identification and the RT model

When all pixels are included into the analysis, the correlation between MODIS LAI and Landsat LAI is relatively high ($r^2 = 0.50$; Fig. 6.16a) and the MODIS LAI is

an underestimate by about 25 %. When only pixels, which are correctly classified by MODIS land cover maps are taken into comparison, the correlation is similar (r^2 = 0.49; Fig. 6.16b) and the underestimation is in the same range (27 %). This result contradictory to the results found at other study sites (see next section).

MODIS LAI derived by the RT model showed much higher correlation with the Landsat TM (r^2 = 0.58; Fig. 6.16c) compared to MODIS LAI derived by both RT and backup models. This means that the RT model works better than the backup model (Fig. 6.16b). The result is in agreement with previous studies (Tian et al., 2002b; Yang et al., 2006). Nevertheless, the RT model more substantially underestimated LAI (33 %) as compared to backup + RT models (27 %). This is due to the fact that the backup model works mainly in the saturation domain, estimating a very high value of LAI (approx. 6.0), whereas the RT model works best in the range of lower LAI (0 – 5).

The analysis also showed that MODIS LAI is better correlated with the Landsat LAI than measured LAI in Berchtesgaden in all three cases 1, 2, and 3. This was true both in terms of slope and the coefficient of correlation (r^2) as shown in Table 6.1, and even though Landsat LAI and measured LAI are highly correlated (Fig. 6.4). This result can be explained by the fact that, both MODIS LAI and Landsat LAI are derived from reflectance with the same underlying physics, and these reflectances in different resolutions are highly correlated (Chapter 4). This means that Landsat LAI is a more suitable measure for validation of the MODIS LAI product because measurement designs probably do not capture the variation of LAI within 1 km^2 areas, while the Landsat data does capture that variation better.

Table 6.1. Correlation of MODIS LAI – measured LAI and MODIS LAI – Landsat LAI at 1 x 1 km resolution in Berchtesgaden

Correlation at 1 x 1 km resolution	Case 1		Case 2		Case 3	
	Slope	r^2	Slope	r^2	Slope	r^2
MODIS LAI - Measured LAI	0.68	0.45	0.65	0.44	0.60	0.58
MODIS LAI - Landsat LAI	0.75	0.50	0.73	0.49	0.67	0.58

Table 6.2. Correlation of MODIS LAI - Landsat LAI at 1x1km resolution in 4 study sites

Site	Date	Case 1		Case 2		Case 3		Note
		Slope	r^2	Slope	r^2	Slope	r^2	
Berchtesgaden	20.06.2000	0.75	0.50	0.73	0.49	0.67	0.58	
Tharandt	13.05.2001	0.68	0.42	0.79	0.57	0.67	0.70	best
	14.02.2001	0.70	0.03	0.80	0.17	0.49	0.15	worst
Hesse	05.07.2001	0.77	0.41	0.83	0.57	0.59	0.57	best
	10.11.2001	1.24	0.09	1.33	0.14	1.19	0.19	worst
Stubai Valley	17.06.2002	0.78	0.42	0.85	0.61	0.75	0.65	best
	16.05.2002	1.06	0.03	1.15	0.12	0.53	0.77	worst

Table 6.2 shows the evaluation results of MODIS LAI in all 4 study sites using Landsat TM LAI maps. Except in Berchtesgaden, where there is only one dataset, the days with best and worst results are shown.

Where all data are taken into consideration at the peak of vegetation development, the MODIS LAI shows a better agreement with the reference Landsat LAI maps (r^2 = 0.41 – 0.50); but substantially underestimated from 25 % to 32 %. In the winter season, MODIS LAI shows different behavior at different sites. While MODIS LAIs were overestimated 24 % in Hesse, where deciduous forest dominates, it underestimated 30 % in Tharandt, where coniferous forest dominates. The worst agreements with the reference Landsat LAI were also found during the winter season. There might be several reasons that account for the lower correlation of the two LAI maps during winter: i) the RT model of MODIS LAI is less sensitive in the

low range of reflectance in the winter time compared to the LAI-SR model as in the case of Landsat LAI. This causes overestimation of LAI at the Hesse site in the winter time, when the forest is leafless. ii) the low sun angle in the winter leads to a low reflectance value and causes underestimation of MODIS LAI in the Tharandt site, where LAI is relatively constant during the year.

When only correctly classified pixels are taken into consideration, the slope and coefficient of correlation at all sites increases, which indicates a better correlation of the MODIS LAI and reference Landsat LAI. The underestimations of MODIS LAI in the best correlations are from 15 % (Stubai Valley) to 27 % (Berchtesgaden). In the worst correlation situation, the MODIS LAI overestimates in Hesse by 33 % and in Stubai Valley by 15 %, while it underestimates in Tharandt by 20 %. This result demonstrates the crucial importance of the MODIS land cover map as input data into the MODIS LAI algorithm, since the MODIS LAI algorithm works better in the areas, which are correctly classified.

Where only pixels evaluated via the RT model are taken into consideration, the coefficients of correlation increase significantly at all 4 sites. In the best correlation cases, the coefficients of correlation are high (from $r^2 = 0.58 – 0.70$). On the other hand, the slopes of the correlations decrease dramatically. In the best correlations, the underestimates are 25 % in Stubai Valley to 40 % at Hesse. In the worst cases, the overestimates of MODIS LAI are 19 % in Hesse, and 50 % in Tharandt and Stubai Valley. The results confirm that the MODIS LAI RT model works better than the backup model (Table 6.) and agree with previous studies (Tian et al., 2002b; Yang et al., 2006). On other hand, the RT model underestimates LAI even more than the case of using both backup + RT models.

6.7. Conclusion with respect to MODIS LAI

The usefulness of MODIS LAI within the continent of Europe depends on its success to reproduce average LAI over 1 km^2 areas that are likely to include different land cover types. The analysis and attempted validation effort carried out here depends upon the application of consist methods to derive spatially distribute LAI maps of high resolution. This chapter summarizes the investigation of attempted validation of MODIS LAI products at four European study sites. The validation of MODIS LAI products includes three steps: i) sampling of LAI in field campaigns and

collection of ancillary data; ii) derivation of a fine resolution reference LAI map based on field data and satellite images; and iii) comparison of MODIS LAI product with the aggregated reference LAI map. The following conclusions appear justified:

1. While the field measurements of LAI via both direct and indirect optical methods are laborious, they are necessary for validation or rejection of MODIS LAI. The unique measurement datasets used in this study are well suited to the aim of MODIS LAI validation spatially and temporally. The accuracies of the indirect methods depend upon the allometric equations applied, the accuracy of optical devices and the variation of the LAI at the field sites along with ability to sample it. A direct comparison between sparsely sampled point field measurements and corresponding MODIS LAI products (1 km) can be a challenging task, and is perhaps impossible because ground-based measurements are spatially limited, and scale-mismatch, georeferencing errors, and land surface heterogeneity cannot be fully included into the analysis.

2. The accuracy of the LAI-VI models is a function of (i) the degree of non-linearity of the models and (ii) the intra-patch spatial heterogeneity. The choice of an LAI-VI model is site dependent and may need to be considered before upscaling. Because empirical functions are used in such extrapolations, atmospheric corrections are mandatory. The LAI-SR relationship showed better correlation at the grassland sites (Tharandt, Stubai Valley) and deciduous forest in Hesse with ground-based data. The LAI-NDVI relationship provided a better correlation in Berchtesgaden for both deciduous and coniferous forest. The LAI-VI models could be successfully applied at other sites (cf. Berchtesgaden vs. Stubai Valley comparison).

3. The accuracy of the MODIS LAI algorithm depends on the accuracy of reflectance and land cover products. While the MODIS reflectance product is well within the error limit, the MODIS land cover product showed much less accuracy than expected. Therefore, the MODIS LAI algorithm showed better correlation to the reference LAI in those areas which are correctly classified by MODIS land cover mapping. Improvement in accuracy of the MODIS biome map used as input into the LAI algorithm is critical to the improvement of MODIS LAI products.

4. The MODIS LAI algorithm works better in the low range of LAI, where the RT model is used. At the higher range of LAI, the use of the backup model results in weak correlation of the MODIS LAI maps and reference LAI maps. Seasonality in evergreen needleleaf forests appears exaggerated in the MODIS LAI product, and there are significant inaccuracies in LAI during the winter season. In general, the MODIS LAI algorithm works better during the growing season. Previous studies show that complex terrain makes difficulties for both fine- and coarse-resolution reflectance estimation, which again limits the applicability of the MODIS LAI algorithm. In contrast, this study found no difference in usefulness of the MODIS LAI algorithm in complex or non-complex terrain. The MODIS LAI substantially underestimated deciduous and needleleaf LAI at all 4 sites (except deciduous LAI in the leaf-off season). This result is in contrast with other studies where MODIS LAI overestimated broadleaf and mixed-woodland LAI (Fernandes et al, 2003).

5. Surface reflectances are highly contaminated by clouds and snow, especially during the wintertime, which significantly limits the retrieval rate of the main RT algorithm and causes anomalous seasonality over needleleaf forests, as well as abnormality in estimation of the growing season. For example, in needleleaf forest there were large fluctuations in LAI values, even between consecutive periods within the same season. Because these large fluctuations are unlikely, the observed decreases in LAI values were attributed to changes in atmospheric conditions. A gap-filled MODIS LAI product is proposed, in which the bad quality data are replaced by interpolated data from good data acquired from period before and after. The first result is promising as slope and coefficient of correlation of all 3 cases in Berchtesgaden increase; there is less underestimation and a stronger correlation of MODIS LAI in comparison to reference LAI.

CHAPTER 7.   GENERAL CONCEPT AND OVERALL RESULTS

7.1. Goals of the Current Thesis

Questions currently investigated in ecological research are dominated by the phenomenon of global change. In particular, questions related to carbon dioxide exchange between the biosphere, the atmosphere and the oceans are important to understand, since changing climate depends on atmospheric CO_2 concentration, and the impact on mankind of climate change is a growing concern worldwide. In order to understand carbon dioxide exchange between the land surface and the atmosphere in general, large networks have been set up to monitor CO_2 and water fluxes in different types of vegetation. One of the first networks was developed in Europe with the designation EUROFLUX, which was then succeeded by the network project CarboEurope (*www.carboeurope.org*). Observations from sites across Europe have been included into a large database available for modelling. Internationally, there are similar projects in North America (AmeriFlux), in Asia (AsiaFlux), and on other continents. Even though there are now several hundred monitoring sites, a problem that remains is to generalize these observations at local, national, continental and global scales; and to extrapolate them to large areas that provide global estimates of CO_2 exchange at hourly, daily, monthly and annual temporal scales.

In order to extrapolate in time and space, the carbon flux community depends on information from remote sensing, and in theory especially from the MODIS platforms which were specifically built for the purpose of gathering information for global change studies. Via spectral reflectance signals that are received daily and averaged over 8 day periods, the MODIS effort provides to the research community a variety of products at ca. 1 km^2 resolution such as NDVI, maps of land cover, and estimates of LAI. These variables are key components of land surface models applied at different spatial and temporal scales. The purpose of the research reported here is to determine the reliability of the MODIS spectral reflectance, land cover and LAI products for European landscapes which are highly fragmented and not necessarily homogeneous at 1 km scale. A stepwise analysis has been carried out for reflectance, land cover and LAI products, comparing results from ground truth data and from high resolution remote sensing images (Landsat) to the coarser scale

MODIS information. In this way, the influence of landscape fragmentation on the MODIS products should be clear and advice can be given about how they should be used in land surface modelling efforts.

Four European locations were chosen for study; landscapes dominated by deciduous forest at Hesse, France; by coniferous forest at Tharandt, Germany, and by forest and grassland in mountainous terrain in the Berchtesgaden National Park, Germany and in Stubai Valley, Austria. All of these landscapes, however, have a mixture of land use. Large homogeneous landscapes simply do not exist in Central Europe. The inhomogeneities influence the reflectance signals received by the MODIS satellite. On the other hand, the selected sites are favourable for these remote sensing investigations because many additional ecological studies have been carried out at these locations. In all situations, unique databases on LAI and/or forest structure have been assembled based on ground level investigations. Furthermore, land use maps exist at high resolution that allow direct comparisons with remote sensing data. The observations of LAI allow for direct testing of the MODIS LAI product.

Finally, the sites represent two types of terrain that are totally different, relatively flat terrain at Hesse and Tharandt, and steep mountain terrain in Berchtesgaden and Stubai Valley. The results can also be examined in this context, i.e., whether the MODIS products provide information that is more useful in flat terrain and is progressively less reliable in complex mountainous terrain. These questions are quite important, since approximately 20 % of the terrestrial land surface is covered by mountains. Surface exchange in mountain regions influences water balances of those regions which deliver fresh water to flatland areas with large populations.

At the selected sites, the following hypotheses were tested with respect to MODIS satellite data:

(1) The MODIS reflectance product characterizes the landscape in the same way as fine resolution Landsat TM does.

(2) The complexity of European landscape does not affect the performance of MODIS reflectance algorithm.

(3) The MODIS landcover product permits adequate differentiation of European landcover types.

(4) The fragmentation and roughness of European landscapes confines the robustness of MODIS landcover algorithm and limits its usefulness.

(5) Despite coarse resolution, MODIS LAI product characterizes well the leaf area index (biomass) of vegetation in European landscapes.

(6) Fragmentation and roughness of the landscape decreases the accuracy of the MODIS LAI algorithm.

7.2. Data Organization Tasks

In order to evaluate the hypotheses, considerable effort was required to organize a supporting database that provided similar information for all four study sites (Chapter 3). Land cover maps were obtained as recent products from the individual research groups at the sites. In some cases, it was necessary to derive an update of these directly from Landsat scenes acquired during the years 1999, 2001 and 2002 (Table 3.4). A single Landsat scene was analyzed for reflectance information for the Berchtesgaden National Park, obtained as close as possible to the time during which forest inventory data were collected. At Hesse, Tharandt and Stubai Valley, chronosequences of scenes during 2001 and 2002 were analyzed for reflectance in order to have information related to seasonal leaf area development. Forest inventory provided maps of LAI for the Berchtesgaden National Park, in Stubai Valley and in Tharandt Forest, while harvest data were obtained at the meadows in Tharandt Forest and Stubai Valley. LAI changes in the Hesse Forest were obtained as time sequence data on litter collection. Details of the methods applied and the projection of ground measurements to create LAI maps were discussed in detail in Chapter 3.

7.3. Comparison of Reflectance from Ground Truth Plots to the MODIS Scale

In order to compare measurements at intensive study plots with MODIS (1 km resolution), it was necessary to build a bridge via remote sensing data derived with Landsat TM (30 m resolution). It was demonstrated that for all study sites, the registration accuracy of Landsat TM images did not deviate by more than half of one pixel, and that the root mean square of error (RMSE) was less than 0.3 pixel when utilizing at least 40 ground control points and nearest-neighbor resampling technique. Comparing Landsat images with aerial photography clearly demonstrated

that specific study sites on the ground could be identified and that the measured characteristics could be associated with Landsat pixel properties. In the case of MODIS images, the accuracy was within the 50 m planned by the operations team. Thus, here again specific features of vegetation cover and ground truth sites were recognizable in both Landsat TM and MODIS 250 m NDVI images, i.e., overlap occurred and it was possible to relate ground-based observations with remotely-sensed signals. Thus, the path was clear to accomplish generalizations across the scene, and upscaling of information to MODIS scale was accomplished. There is no doubt that the accuracy of georeferencing was sufficient for further processing in order to test the proposed hypotheses.

7.4. Evaluation of MODIS Reflectance Products

The upscaling process for reflectance from ground point measurements to MODIS resolution using high-resolution images (ETM+) was conducted for the Hesse Forest, the Tharandt Forest, and Tharandt grassland sites. The evaluation results showed that the MODIS reflectance product is reasonably accurate (less than 10 % absolute error). Certainly it is appropriate to utilize reflectance data from the two types of satellite images and to use these information in comparative examinations of land cover mapping and leaf area index estimation. The Landsat images do provide useful and appropriate information for upscaling from ground truth sites and for testing MODIS products. Thus, hypotheses (1) and (2) may be accepted as true within reasonable bounds, at least they are true enough to permit evaluation of the following hypotheses via a Landsat and MODIS comparison.

7.5. Evaluation of MODIS Landcover Products

The digital data with 30 m resolution of Landsat images provide a means for testing the accuracy of MODIS landcover products. As a first step, it is necessary to relate the Landsat images to ground truth determinations of land cover. This was carried out via two methodologies, namely supervised classification and object-based classification. It was demonstrated that object-based classification provided maps with a much better correspondence to ground truth than supervised classification. Especially with the object-based methodology, one has the possibility to characterize land cover change in the highly fragmented landscapes of Central

Europe (Table 5.9). The methods were tested especially in complex terrain of the Berchtesgaden National Park and in Stubai Valley, since shadowing in the remote sensing images adds to the problems encountered with land use fragmentation. Even in these landscapes, an accuracy of ca. 75 to 80 % was achieved in overall classification, when attempting to distinguish 6 land cover categories. The land cover maps that are obtained from Landsat images allow us to manipulate effectively the spatial land cover data and to compare a high resolution approximation of land cover to the coarse scale land cover achieved via MODIS. The two approaches are compatible, since reflectance data for the two satellites are comparable as has been discussed above.

The comparison demonstrates that both the scale applied in classifications and the number and type of land use categories that are permitted lead to important shifts in the characterization of landcover. In area comparison, MODIS landcover products were found to underestimate bare rock/soil complexes in alpine regions, ascribing vegetation characteristics to these areas instead, apparently as a result of scattered vegetation. The dense Norway spruce forests were described relatively well. Deciduous forest and croplands were distinguished well at Hesse, but important problems were revealed that are related to seasonally bare soil (similarly in Tharandt). It was averaged into cropland due to multiple scenes employed in the MODIS classification method. Forest types were not well distinguished in Tharandt due to patterns of mixing of stands and the scales of observation by MODIS.

The pixel-by-pixel agreement between upscaled Landsat landcover and MODIS Land Cover was less satisfying than the areal comparison. Cropland and mixed forest were identified best at Hesse, but deciduous forest and crop-grassland mosaic was poorly classified. At Tharandt it was similar, but coniferous forest and crop-grassland was poorly identified. In alpine regions, 50 % overall agreement was found on a pixel-by-pixel comparison. The Norway spruce coniferous forest was identified best, apparently dominating large contiguous areas. Other landcover was poorly classified. MODIS landcover type 3 performed better than landcover type 1. It seems probable that Hypothesis (3) must be rejected in general, although for certain applications it might be possible to justify use of MODIS landcover. Individual investigators must confront this problem and take responsibility for MODIS landcover

use in European studies. In this sense Hypothesis (4) correctly summarizes the situation.

The problems in classification that are encountered lead to further difficulties in land surface characterization, since the retrieval of LAI uses landcover as an input variable (see 7.5). Thus, fragmentation in European landscapes is a fundamental problem encountered in the use of MODIS products. A true representation of the land surface cannot be obtained from the current MODIS classifications. The use of these descriptors in models describing land surface properties may potentially lead to large errors. Thus, exchange between the land surface and the atmosphere of water and CO_2 as estimated by models using MODIS inputs will have a high level of uncertainty, and the results must be considered with caution.

7.6. Evaluation of MODIS LAI Products

The validation of MODIS LAI products was carried out via three consecutive steps: i) sampling of LAI in field campaigns and collection of ancillary data; ii) derivation of a fine resolution reference LAI map based on field data and Landsat satellite images; and iii) comparison of MODIS LAI product with the aggregated reference LAI map from Landsat data. LAI data based on forest inventory and allometric equations was available from two Norway spruce sites in the Berchtesgaden National Park and in Stubai Valley near Neustift. LAI was estimated for forest patches and compared to Landsat NDVI to derive equations that allowed continuous mapping of coniferous forest over the study site landscapes. The same equations were applied at Tharandt. Harvesting of biomass at grassland sites in Stubai Valley and Tharandt allowed predictive equations to be derived that estimate grassland LAI in dependency on the simple ratio vegetation index (SR). Spatial studies of LAI in the Hesse Forest in France provided a similar equation for deciduous forest in dependence on SR. The four equations were applied to Landsat images to obtain high resolution (30 m) maps of leaf area index at the four sites.

These "ground truth" maps were then used to evaluate MODIS LAI products by aggregating high resolution data to 1 km resolution and comparing to MODIS LAI estimates. Due to difficulties that occur in mapping land cover with MODIS at 1 km resolution (see 7.4 – high fragmentation of European landscapes means that most 1 km pixels are in fact mixed), a single selected algorithm to estimate MODIS LAI

does not provide the same information as would be derived at higher resolution (even with MODIS 250 m data). The correlation of MODIS values to the Landsat based values is best when landcover is correctly classified (dominant landcover is clearly a single type). Also better predictions occur when LAI is in general low. At the peak of vegetation development, MODIS LAI appears to strongly underestimate values of the Landsat based maps. During winter, the comparison is even worse, but is not consistent from grassland to deciduous forest and coniferous forest. Possible reasons have been discussed. In general, Hypothesis (5) must be rejected, while Hypothesis (6) is supported.

The results cast doubt on the usefulness of MODIS LAI products as input to continental scale simulation models for carbon and water balances, at least in Europe where landcover is highly modified and fragmented due to centuries of human use and management. Use of the MODIS products in Europe requires that new techniques be considered to search for compatability in averaging and aggregating information on land cover and reflectance that is used to estimate LAI for large areas (1 km^2 or more). It may be possible to treat 1 km^2 pixels of MODIS in some way that the mixed composition can be determined and used to differentiate LAI for the component vegetation or biomes.

CHAPTER 8.   REFERENCES

Anderson, J.R., Hardy, E.E., Roach, J.T., Witmer, R.E., 1976. A land use and land cover classification system for use with remote sensor data. Geol. Survey Prof. Paper 964(8).

Asner, G.P., 1998. Biophysical and Biochemical Sources of Variability in Canopy Reflectance-the SAIL model. Rem. Sen. Environ. 64(3): 234-253.

Asner, G.P., Wessman, C.A., Schimel, D.S., Archer, S., 1998. Variability in leaf and litter optical properties- Implications for BRDF model inversions using AVHRR, MODIS, and MISR. Rem. Sens. Environ. 63(3): 243-257.

Asrar, G., Fuchs, M., Kanemasu, E.T., Hatfield, J.L., 1984. Estimating Absorbed Photosynthetic Radiation and Leaf Area Index from Spectral Reflectance in Wheat. Agronomy J. 76(2): 300.

Asrar, G., Myneni, R.B., Choudhury, B.J., 1992. Spatial heterogeneity in vegetation canopies and remote sensing of absorbed photosynthetically active radiation. A modeling study. Rem. Sens. Environ. 41(2): 85-103.

Baatz, M., Heynen, M., Hofmann, P., Lingenfelder, I., Mimier, M., Schape, A., Weber, M., Willhauck, G., 2001. eCognition User Guide 2.0: Object Oriented Image Analysis. Definiens Imaging GmbH, Trappentreustrasse 1, 80339 München, Germany.

Baatz, M., Schäpe, A., 2000. Multi-resolution Segmentation: an optimization approach for high quality multi-scale image segmentation. In: Strobl, J., Blaschke, T., Griesebner, G. (Ed.). Proceedings of the Angewandte Geographische Informationsverarbeitung XII Beiträge Zum AGIT-Symposium Salzburg, pp. 12–23.

Baldocchi, D., Valentini, R., Running, S., Oechel, W., Dahlman, R., 1996. Strategies for measuring and modelling carbon dioxide and water vapour fluxes over terrestrial ecosystems. Glob. Change Biol. 2(3): 159-168.

Ballantine, J.A.C., Okin, G.S., Prentiss, D.E., Roberts, D.A., 2005. Mapping North African landforms using continental scale unmixing of MODIS imagery. Rem. Sen. Environ. 97(4): 470-483.

Baret, F., Guyot, G., 1991. Potentials and limits of vegetation indices for LAI and APAR assessment. Rem. Sen. Environ. 35(2-3): 161-173.

Birth, G.S., McVey, G.R., 1968. Measuring the Color of Growing Turf with a Reflectance Spectrophotometer. Agronomy J. 60(6): 640.

Bitter, A., Eilermann, F., Küßner, R., Röhle, H., Wickel, A., Wienhaus, O., Zimmermann, F., 1998. Waldentwicklung und Schadgeschehen. In: Nebe W., R.A., and Vogel M. (Ed.). Forstwissenschaftliche Beiträge Tharandt. Technische Universität Dresden, pp. 50-57.

Bitterlich, W., Pöttinger, C., Kaserer, M., Hofer, H., Aichner, M., Tappeiner, U., Cernusca, A., 1999. Effects of land-use changes on soils along the Eastern alpine transect. In: Cernusca, A., Tappeiner, U. and Bayfield, N. (Ed.). Land-use Changes in European Mountain Ecosystems. Blackwell Science Ltd, Berlin, Wien, pp. 233–243.

Blaschke, T., Strobl, J., 2001. What's wrong with pixels? Some recent developments interfacing remote sensing and GIS. GIS. GeoBIT/GIS: J. Spatial inform. Decision Making, No. 6/2001, pp. 12-17.

Bobeva, A. 2003. *Quantifying the distribution of forest functional types and forest Leaf Area Index in the Alps.* PhD thesis. University of Bayreuth, Bayreuth

Bonan, G.B., 1995. Land-atmosphere interactions for climate system models: Coupling biophysical, biogeochemical, and ecosystem dynamical processes. Rem. Sen. Environ. 51(1): 57-73.

Bonan, G.B., 1996. A land surface model (LSM version 1.0) for ecological, hydrological, and atmospheric studies: technical description and user's guide. PB--97-131494/XAB, National Center for Atmospheric Research, Boulder, CO (United States). Climate and Global Dynamics Div.

Burton, A.J., Pregitzer, K.S., Reed, D.D., 1991. Leaf area and foliar biomass relationships in northern hardwood forests located along an 800 km acid deposition gradient. Forest Sci. 37(4): 1041-1059.

Campbell, G.S., Norman, J.M., 1998. An Introduction to Environmental Biophysics. Springer.

Campbell, J.B., 1996. Introduction to Remote Sensing. Taylor and Francis.

Campbell, J.B., 2002. Introduction to Remote Sensing. Taylor & Francis.

Cernusca, A., Tappeiner, U., Bayfield, N., 1999. Land-use changes in European mountain ecosystems: ECOMONT: concept and results. Berlin, Germany: Blackwell Wissenschafts; Malden, Mass.: Blackwell Science.

Chapman, J.W., Gower, S.T., 1991. Aboveground production and canopy dynamics in sugar maple and red oak trees in southwestern Wisconsin. Can. J. Forest Res. 21(10): 1533-1543.

Chen, J.M., 1996. Optically-based methods for measuring seasonal variation of leaf area index in boreal conifer stands. Agri. Forest Meteorol. 80(2-4): 135-163.

Chen, J.M., Black, T.A., 1992. Defining leaf area index for non-flat leaves. Plant Cell Environ. 15(4): 421-429.

Chen, J.M., Cihlar, J., 1996. Retrieving Leaf Area Index of Boreal Conifer Forests Using Landsat TM Images. Rem. Sen. Environ. 55(2): 153-162.

Chen, J.M., Leblanc, S., 1997. A 4-scale bidirectional reflection model based on canopy architecture. IEEE Trans. Geosci. Remote Sens. 35: 1316–1337.

Chen, J.M., Plummer, P.S., Rich, M., Gower, S.T., Norman, J.M., 1997. Leaf area index measurements. J. Geophys. Res. 102(D24): 29,429-429,443.

Chen, X., Tan, Z., Schwartz, M.D., Xu, C., 2000. Determining the growing season of land vegetation on the basis of plant phenology and satellite data in Northern China. Int. J. Biometeorol. 44(2): 97-101.

Colwell, R.N., 1997. History and place of photographic interpretation. In: Philipson, W.R. (Ed.). Manual of photographic interpretation (2nd ed.), p. 3-47. American Society for Photogrammetry and Remote Sensing, Bethesda, Maryland., pp. 3–47.

de Jong, S.M., Bagre, A., van Teeffelen, P.B.M., van Deursen, W.P.A., 2000. Monitoring Trends in Urban Growth and Surveying City Quarters in Ouagadougou, Burkina Faso Using SPOT-XS. Geocarto Int. 15(2): 63-70.

Deering, D.W., 1989. Field measurements of bidirectional reflectance. In: Asrar, G. (Ed.). Theory and Applications of Optical Remote Sensing. Wiley-Interscience, pp. 14–65.

Dickinson, R.E., 1984. Infrared radiative cooling in the mesosphere and lower thermosphere. J. Atmospheric Terres. Phys. 46: 995-1008.

Disney, M., Lewis, P., Thackrah, G., Quaife, T., Barnsley, M., 2004. Comparison of MODIS broadband albedo over an agricultural site with ground measurements and values derived from Earth observation data at a range of spatial scales. Int. J. Rem. Sens. 25(23): 5297-5317.

Eklundh, L., Harrie, L., Kuusk, A., 2001. Investigating relationships between Landsat ETM+ sensor data and leaf area index in a boreal conifer forest. Rem. Sen. Environ. 78(3): 239-251.

Epron, D., Farque, L., Lucot, E., Badot, P.M., 1999. Soil CO_2 efflux in a beech forest: the contribution of root respiration. Ann. For. Sci. 56(4): 289–295.

Fang, H., Liang, S., Chen, M., Walthall, C., Daughtry, C., 2004. Intercomparison of MISR land surface reflectance and albedo products with ETM+ and MODIS products. int. J. Rem. Sens. 25: 409-422.

Fang, H., Liang, S., Kuusk, A., 2003. Retrieving leaf area index using a genetic algorithm with a canopy radiative transfer model. Rem. Sen. Environ. 85(3): 257-270.

Fassnacht, K.S., Gower, S.T., Norman, J.M., McMurtrie, R.E., 1994. A comparison of optical and direct methods for estimating foliage surface area index in forests. Agri. Forest Meteorol. 71(1-2): 183-207.

Floyd, F.S., 1987. Remote Sensing: Principles and Interpretation, 2nd edn. WH Freeman and Co, New York.

Franklin, S.E., 2001. Remote Sensing for Sustainable Forest Management. Lewis Publishers. Boca Raton.

Franz, H., 2000. Landscape monitoring using infrared aerial photos, EUROPARC Expertise Exchange, Topical Workshop: Organisation of Monitoring in Protected Areas, April 12 - 16.

Friedl, M., 1995. Scaling and uncertainty in the relationship between the NDVI and land surface biophysical variables- An analysis using a scene simulation model and data from FIFE. Rem. Sens. Environ. 54(3): 233-246.

Friedl, M., 2002. Global land cover mapping from MODIS algorithms and early results. Rem. Sen. Environ. 83(1): 287-302.

Friedl, M.A., 1996. Relationships among Remotely Sensed Data, Surface Energy Balance, and Area-Averaged Fluxes over Partially Vegetated Land Surfaces. J. Appl. Meteorol. 35(11): 2091-2103.

Fritz, S., Bartholome, E., Belward, A., Hartley, A., Stibig, H.J., Eva, H., Mayaux, P., Bartalev, S., Latifovic, R., Kolmert, S., 2002. Harmonisation, mosaicing and production of the Global Land Cover 2000 database. Joint Research Center (JRC), Ispra, Italy (2003).

Gao, B.C., Goetz, A.F.H., 1995. Retrieval of equivalent water thickness and information related to biochemical components of vegetation canopies from AVIRIS data. Rem. Sen. Environ. 52(3): 155-162.

Gholz, H.L., Grier, C.C., Campbell, A.G., Brown, A.T., 1979. Equations for estimating biomass and leaf area of plants in the Pacific Northwest. Research Paper 41. Forest Research Laboratory, Oregon State University, p. 37.

Gholz, H.L., Vogel, S.A., Cropper Jr, W.P., McKelvey, K., Ewel, K.C., Teskey, R.O., Curran, P.J., 1991. Dynamics of Canopy Structure and Light Interception in Pinus Elliottii Stands, North Florida. Ecol. Monogr. 61(1): 33-51.

Giri, C., Zhu, Z., Reed, B., 2005. A comparative analysis of the Global Land Cover 2000 and MODIS land cover data sets. Rem. Sen. Environ. 94(1): 123-132.

Gobron, N., Pinty, B., Verstraete, M.M., 1997. Theoretical limits to the estimation of the leaf area index on thebasis of visible and near-infrared remote sensing data. IEEE Transactions on Geosci. Rem. Sens. 35(6): 1438-1445.

Goel, N.S., Kuusk, A., 1992. Evaluation Of One Dimensional Analytical Models For Vegetation Canopies. Geoscience and Remote Sensing Symposium. IGARSS '92. International, pp. 505-507.

Gopal, S., Woodcock, C.E., Strahler, A.H., 1999. Fuzzy Neural Network Classification of Global Land Cover from a 1o AVHRR Data Set-The generation of global fields of terrestial biophysocal parameters from satellite data. Rem. Sen. Environ. 67(2): 230-243.

Govaerts, Y.M., Verstraete, M.M., Eumetsat, D., 1998. Raytran: a Monte Carlo ray-tracing model to compute lightscattering in three-dimensional heterogeneous media. IEEE Transactions on Geosci. Rem. Sens. 36(2): 493-505.

Goward, S.N., Markham, B., Dye, D.G., Dulaney, W., Yang, J., 1991. Normalized difference vegetation index measurements from the Advanced Very High Resolution Radiometer. Rem. Sens. Environ. 35(2): 257-277.

Gower, S.T., Haynes, B.E., Fassnacht, K.S., Running, S.W., Hunt Jr, E.R., 1993a. Influence of fertilization on the allometric relations for two pines in contrasting environments. Can. J. Forest Res. 23(8): 1704-1711.

Gower, S.T., Kucharik, C.J., Norman, J.M., 1999. Direct and indirect estimation of leaf area index, f (APAR), and net primary production of terrestrial ecosystems. Rem. Sen. Environ. 70(1): 29-51.

Gower, S.T., Reich, P.B., Son, Y., 1993b. Canopy dynamics and aboveground production of five tree species with different leaf longevities. Tree Physiol. 12(4): 327-345.

Gower, S.T., Vogel, J.G., Norman, J.M., Kucharik, C.J., Steele, S.J., Stow, T.K., 1997. Carbon distribution and aboveground net primary production in aspen, jack pine, and black spruce stands in Saskatchewan and Manitoba, Canada. J. Geophys. Res. 102(D24): 29-029.

Gower, S.T., Vogt, K.A., Grier, C.C., 1992. Carbon Dynamics of Rocky Mountain Douglas-Fir: Influence of Water and Nutrient Availability. Ecol. Monogr. 62(1): 43-65.

Granier, A., Ceschia, E., Damesin, C., DufrÊNe, E., Epron, D., Gross, P., Lebaube, S., Le Dantec, V., Le Goff, N., Lemoine, D., 2000. The carbon balance of a young Beech forest. Funct. Ecol. 14: 312-325.

Grier, C.C., Logan, R.S., 1977. Old-Growth Pseudotsuga menziesii Communities of a Western Oregon Watershed: Biomass Distribution and Production Budgets. Ecol. Monographs 47(4): 373-400.

Grier, C.C., Milne, W.A., 1981. Regression equations for calculating component biomass of young Abiesamabilis (Dougl.) Forbes. Can. J. Forest Res. 11(1): 184-187.

Gutman, G.G., 1991. Vegetation indices from AVHRR- An update and future prospects. Rem. Sen. Environ. 35: 121-136.

Hall, F.G., Townshend, J.R., Engman, E.T., 1995. Status of remote sensing algorithms for estimation of land surface state parameters. Rem. Sens. Environ. 51(1): 138-156.

Hill, M.J., Vickery, P.J., Furnival, E.P., Donald, G.E., 1999. Pasture Land Cover in Eastern Australia from NOAA-AVHRR NDVI and Classified Landsat TM-geographical relationships. Rem. Sen. Environ. 67(1): 32-50.

Hofman, P., 2001. Detecting buildings and roads from IKONOS data using additional information. GeoBIT/GIS: J. Spatial Infor. Decision Making 6: 28-33.

Hu, B., Qian, S.E., Haboudane, D., Miller, J.R., Hollinger, A.B., Tremblay, N., Pattey, E., 2004. Retrieval of crop chlorophyll content and leaf area index from decompressed hyperspectral data: the effects of data compression. Rem. Sen. Environ. 92(2): 139-152.

Huemmrich, K.F., Goward, S.N., 1997. Vegetation Canopy PAR Absorptance and NDVI: An Assessment for Ten Tree Species with the SAIL Model. Rem. Sen. Environ. 61(2): 254-269.

Huete, A.R., Liu, H.Q., 1994. An error and sensitivity analysis of the atmospheric-andsoil-correcting variants of the NDVI for the MODIS-EOS. Geosci. Remote Sen. 32(4): 897-905.

Irish, V.F., 2000. Variations on a theme: flower development and evolution. Genome Biol. 1(2): 1015.

Jacquemoud, S., Baret, F., Andrieu, B., Danson, F.M., Jaggard, K., 1995. Extraction of Vegetation Biophysical Parameters by Inversion of the PROSPECT+ SAIL Models on Sugar Beet Canopy Reflectance Data. Application to TM and AVIRIS Sensors. Rem. Sen. Environ. 52(3): 163-172.

Janssen, L.L.F. 1993. *Methodology for updating terrain object data from remote sensing data.* Landbouw Universiteit Wageningen, Wageningen, The Netherlands

Jones, A.S., Guch, I.C., Vonder Haar, T.H., 1998. Data Assimilation of Satellite-Derived Heating Rates as Proxy Surface Wetness Data into a Regional Atmospheric Mesoscale Model. Part II: A Case Study. Mon. Weath. Rev. 126(3): 646-667.

Kang, S., Running, S.W., Lim, J.H., Zhao, M., Park, C.R., Loehman, R., 2003. A regional phenology model for detecting onset of greenness in temperate mixed forests, Korea: an application of MODIS leaf area index. Rem. Sen. Environ. 86(2): 232-242.

Kaufman, Y.J., 1989. The atmospheric effect on remote sensing and its correction. In: Asrar, G. (Ed.). Theory and Applications of Optical Remote Sensing. Wiley-Interscience, pp. 336-428.

Kerr, J.T., Ostrovsky, M., 2003. From space to species: ecological applications for remote sensing. Trends Ecol. Evol. 18(6): 299-305.

Kias, U., Demel, W., Funck, W., Schäfer, D., Rausch, E., 1999. Erstellung eines Orthophotokataloges und Nachführung der Biotop- und Nutzungstypen für das Biosphärenreservat Berchtesgaden. Ein Forschungsvorhaben am Landschaftsinformatikzentrum der Fachhochschule Weihenstephan im Auftrag der Nationalparkverwaltung Berchtesgaden.

Kimball, J.W., 2005. Kimball's Biology Pages: The leaf.

Kimes, D., Gastellu-Etchegorry, J., Esteve, P., 2002. Recovery of forest canopy characteristics through inversion of a complex 3D model. Rem. Sens. Environ. 79(2): 320-328.

Kimes, S., 1995. Optical Remote Sensing of Vegetation: Modeling, Caveats, and Algorithms. Rem. Sens. Environ. 51: 169-188.

Knyazikhin, Y., Martonchik, J.V., Diner, D.J., Myneni, R.B., Verstraete, M., Pinty, B., Gobron, N., 1998a. Estimation of vegetation canopy leaf area index and fraction of absorbed photosynthetically active radiation from atmosphere-corrected MISR data. J. Geophys. Res. 103(D24): 32239-32256.

Knyazikhin, Y., Martonchik, J.V., Myneni, R.B., Diner, D.J., Running, S.W., 1998b. Synergistic algorithm for estimating vegetation canopy leaf area index and fraction of absorbed photosynthetically active radiation from MODIS and MISR data. J. Geophys. Res. 103(D24): 32257-32276.

Konnert, V., 2000. Gemeinsame Auswertung der ersten und zweiten permanenten Stichproben-Inventur. Forschungsbericht Nationalpark Berchtesgaden 43: 3-92.

Konnert, V., 2001. Mapping site characteristics in the National Park Berhtesgaden – Project in coorperation with Technical University of Munich, Dept. of Ecology, the Faculty of Forest Science and Resource Management, Dept. of Geobotany (Prof. Dr. Anton Fischer), and the Administration of the National Park Berchtesgaden.

Küchler, A.W., 1988. The classification of vegetation. Kluwer Academic Publishers, pp. 67-80.

Küssner, R., 1999. Ein auf Strahlungsmessungen basierendes Verfahren zur Bestimmung des Blattflächenindexes und zur Charakterisierung der Uberschirmung in Fichtenbeständen: methodische Untersuchungen und Anwendung in der wald- baulichen Praxis. (ed. Roloff A), In: Forstwissenschaftliche Beiträge Tharandt, Heft 5. Verlag Eugen Ulmer, Stuttgart.

Kuusk, A., 1985. The hot spot effect of a uniform vegetative cover. Soviet J. Remote Sensing 3(4): 645–658.

Landsberg, J.J., Gower, S.T., 1997. Applications of Physiological Ecology to Forest Management. J. appl. Ecol. 34(5): 1322-1323.

le Maire, G., François, C., Dufrêne, E., 2004. Towards universal broad leaf chlorophyll indices using PROSPECT simulated database and hyperspectral reflectance measurements. Rem. Sen. Environ. 89(1): 1-28.

Lewis, P., 1999. Three-dimensional plant modelling for remote sensing simulation studies using the Botanical Plant Modelling System; Utilisation du Botanical Plant Modelling System pour modeliser en 3D des plantes pour des etudes de simulation par teledetection. Agronomie 19(3-4): 185-210.

Li, X., Strahler, A.H., 1986. Geometrical-optical bi-directional modeling of a conferous forest canopy. Geosci. Remote Sensing: 906-919.

Li, X., Strahler, A.H., 1992. Geometric-optical bidirectional reflectance modeling of thediscrete crown vegetation canopy: effect of crown shape and mutualshadowing. Geosci. Remote Sensing 30(2): 276-292.

Li, X., Strahler, A.H., Woodcock, C.E., 1995. A hybrid geometric optical-radiative transfer approach for modelingalbedo and directional reflectance of discontinuous canopies. IEEE Transactions on Geosci. Rem. Sens. 33(2): 466-480.

Liang, S., Fang, H., Chen, M., 2001. Atmospheric correction of Landsat ETM+ land surface imagery. I. Methods. IEEE Transactions on Geosci. Rem. Sens. 39(11): 2490-2498.

Liang, S., Fang, H., Chen, M., Shuey, C.J., Walthall, C., Daughtry, C., Morisette, J., Schaaf, C., Strahler, A., 2002. Validating MODIS land surface reflectance and albedo products- methods and preliminary results. Rem. Sens. Environ. 83(1): 149-162.

Lillesand, T.M., Kiefer, R.W., Chipman, J.W., 2004. Remote sensing and image interpretation. John Wiley & Sons Ltd Chichester, UK.

Limp, W.F., 2002. Quick-Take Review of eCognition. Geoworld 0204: 53–54.

Loveland, T.R., Reed, B.C., Brown, J.F., Ohlen, D.O., Zhu, Z., Yang, L., Merchant, J.W., 2000. Development of a global land cover characteristics database and IGBP DISCover from 1 km AVHRR data. Int. J. Rem. Sens. 21(6): 1303-1330.

Loveland, T.R., Zhu, Z., Ohlen, D.O., Brown, J.F., Reed, B.C., Yang, L., 1999. An analysis of the IGBP global land-cover characterization process. Photogr. Engin. Rem. Sens. 65(9): 1021-1032.

Marshall, J.D., Waring, R.H., 1986. Comparison of Methods of Estimating Leaf-Area Index In Old-Growth Douglas-Fir. Ecol. 67(4): 975-979.

Maxwell, E.L., 1976. Multivariate system analysis of multispectral imagery. Photogr. Engin. Rem. Sens. 42: 1173-1186.

McVicar, T.R., Jupp, D.L.B., 1998. The current and potential operational uses of remote sensing to aid decisions on drought exceptional circumstances in Australia: a review. Agric. Systems 57(3): 399-468.

Mencuccini, M., Grace, J., 1995. Climate influences the leaf area/sapwood area ratio in Scots pine. Tree Physiol. 15(1): 1-10.

Mirzaei, H. 2008. *Assessment of grassland ecosystem functioning: Carbon dioxide exchange and the dynamics of carbon and nutrient pools in temperate and Mediterranean grasslands.* PhD thesis. University of Bayreuth, Bayreuth

Monsi, M., Saeki, T., 1953. Ueber den Lichtfactor in den Pflanzengesellschaften und seine Bedeutung fuer die Stoffproduktion. Jpn. J. Bot. 14: 22-52.

Moody, A., Woodcock, C.E., 1994. Scale-dependent errors in the estimation of land-cover proportions: implications for global land-cover datasets. Photogr. Engin. Rem. Sens. 60(5): 585-594.

Morisette, J.T., Privette, J.L., Justice, C.O., 2002. A framework for the validation of MODIS Land products. Rem. Sens. Environ. 83(1): 77-96.

Myneni, R.B., 1991a. Modeling radiative transfer and photosynthesis in three-dimensional vegetation canopies. Agri. Forest Meteorol. 55(3-4): 323-344.

Myneni, R.B., 1991b. A Three-Dimensional Radiative Transfer Method for Optical Remote Sensing of Vegetated Land Surfaces. Geoscience and Remote Sensing Symposium, 1991. IGARSS '91. Remote Sensing: Global Monitoring for Earth Management., International, pp. 1541-1542.

Myneni, R.B., Hoffman, S., Knyazikhin, Y., Privette, J.L., Glassy, J., Tian, Y., Wang, Y., Song, X., Zhang, Y., Smith, G.R., 2002. Global products of vegetation leaf area and fraction absorbed PAR from year one of MODIS data. Rem. Sen. Environ. 83(1): 214-231.

Myneni, R.B., Nemani, R.R., Running, S.W., 1997a. Algorithm for the estimation of global land cover, LAI and FPAR based on radiative transfer models. IEEE Trans. Geosci. Rem. Sens. 35: 1380–1393.

Myneni, R.B., Ramakrishna, R., Nemani, R., Running, S.W., 1997b. Estimation of global leaf area index and absorbed par usingradiative transfer models. IEEE Transactions on Geosci. Remote Sens. 35(6): 1380-1393.

Myneni, R.B., Williams, D.L., 1994a. On the relationship between FAPAR and NDVI. Rem. Sen. Environ. 49(3): 200-211.

Myneni, R.B., Williams, D.L., 1994b. On the relationship between FAPAR and NDVI. Rem. Sens. Environ. 49(3): 200-211.

Nebe, W., Fiedler, H.J., 1985. Das Ökologische Messfeld der Sektion Forstwirtschaft der TU Dresden II. Standortskundliche Charakterisierung. Wissenschaftliche Zeitschrift der Technischen Universität Dresden 34, Heft 1, 15-27, pp. 349-354.

Ni, W., Li, X., Woodcock, C.E., Caetano, M.R., Strahler, A.H., 1999. An analytical hybrid GORT model for bidirectional reflectance overdiscontinuous plant canopies. IEEE Transactions on Geosci. Rem. Sens. 37(2 Part 2): 987-999.

Niinemets, U., Kull, K., 1994. Leaf weight per area and leaf size of 85 Estonian woody species in relation to shade tolerance and light availability. Forest Ecol. Manag. 70(1): 1-10.

Niinemets, U., Kull, O., 1995. Effects of light availability and tree size on the architecture of assimilative surface in the canopy of Picea abies: variation in needle morphology. Tree Physiol. 15(5): 307-315.

North, P.R.J., 1996. Three-dimensional forest light interaction model using a MonteCarlo method. IEEE Transactions on Geosci. Rem. Sens. 34(4): 946-956.

Oberdorfer, E., 1993. Süddeutsche Pflanzengesellschaften. Fischer Verlag, Stuttgart.

Oker-Blom, P., Kaufmann, M.R., Ryan, M.G., 1991. Performance of a canopy light interception model for conifer shoots, trees and stands. Tree Physiol. 9(1): 227-243.

Peterson, D.L., Running, S.W., 1989. Applications in forest science and management. In: Asrar, G. (Ed.). Theory and Applications of Optical Remote Sensing. Wiley-Interscience, pp. 429–473.

Peterson, D.L., Spanner, M.A., Running, S.W., Teuber, K.B., 1987. Relationship of Thematic Mapper simulator data to leaf area index of temperate coniferous forests. Rem. Sen. Environ. 22(3): 323-342.

Price, J.C., 1982. On the Use of Satellite Data to Infer Surface Fluxes at Meteorological Scales. J. Appl. Meteorol. 21(8): 1111-1122.

Price, J.C., 1993. Estimating leaf area index from satellite data. IEEE Transactions on Geosci. Rem. Sens. 31(3): 727-734.

Privette, J.L., Myneni, R.B., Tucker, C.J., Emery, W.J., 1994. Invertibility of a 1-D discrete ordinates canopy reflectance model. Rem. Sens. Environ. 48(1): 89-105.

Qi, J., Moran, M.S., Cabot, F., Dedieu, G., 1995. Biophysical parameter estimations using multidirectional spectral measurements. Rem. Sens. Environ. 54(1): 71-83.

Ramsey, R.D., Falconer, A., Jensen, J.R., 1995. The Relationship between NOAA-AVHRR NDVI and Ecoregions in Utah. Rem. Sens. Environ. 53(3): 188-198.

Reich, P.B., Ellsworth, D.S., Uhl, C., 1995. Leaf carbon and nutrient assimilation and conservation in species of differing successional status in an oligotrophic Amazonian forest. Func. Ecol. 9(1): 65-76.

Richter, K., 1996. The EOQ repair and waste disposal model with variable setup numbers. Europ. J. Operat. Res. 95(2): 313-324.

Richter, R., 2001. Atmospheric Correction Methodology for Imaging Spectrometer Data. In: Wooding, M., Harris, R.A. (Eds.). The Digital Airborne Spectrometer

Experiment (DAISEX), Proceedings of the Workshop held July, 2001. European Space Agency, ESA SP-499, ESTEC, The Netherlands, p. p.97.

Rouse, J.W., Haas, R.H., Schell, J.A., 1974. Monitoring vegetation systems in the Great Plains with ERTS. Proc. 3rd ERTS-1 Symp. pp. 301-319. .

Running, S.W., 1994. Testing Forest-BGC Ecosystem Process Simulations Across a Climatic Gradient in Oregon. Ecol. Appl. 4(2): 238-247.

Running, S.W., Justice, C.O., Salomonson, V., Hall, D., Barker, J., Kaufmann, Y.J., Strahler, A.H., Huete, A.R., Muller, J.P., Vanderbilt, V., 1994. Terrestrial remote sensing science and algorithms planned for EOS/MODIS. Int. J. Rem. Sens. 15(17): 3587-3620.

Sandmeier, S., Deering, D.W., 1999. Structure Analysis and Classification of Boreal Forests Using Airborne Hyperspectral BRDF Data from ASAS-an overview. Rem. Sen. Environ. 69(3): 281-295.

Schiewe, J., Tufte, L., Ehlers, M., 2001. Potential and problems of multi-scale segmentation methods in remote sensing. GIS. Geo-Informations-Systeme 6: 34-39.

Schowengerdt, R.A., 1997. Remote Sensing Models and Methods for Image Processing Second Edit. ACADEMIC PRESS, Sandiego, pp243-245.

Sellers, P.J., Dickinson, R.E., Randall, D.A., Betts, A.K., Hall, F.G., Berry, J.A., Collatz, G.J., Denning, A.S., Mooney, H.A., Nobre, C.A., 1997. Modeling the Exchanges of Energy, Water, and Carbon Between Continents and the Atmosphere. Science 275(5299): 502-509.

Sellers, P.J., Meeson, B.W., Hall, F.G., Asrar, G., Murphy, R.E., Schiffer, R.A., Bretherton, F.P., Dickinson, R.E., Ellingson, R.G., Field, C.B., 1995. Remote sensing of the land surface for studies of global change: models-algorithms-experiments. Rem. Sens. Environ. 51(1): 3-26.

Sellers, P.J., Tucker, C.J., Collatz, G.J., Los, S.O., Justice, C.O., Dazlich, D.A., Randall, D.A., 1994. A global 1° by 1° NDVI data se t for climate studies. Part 2: The generation of global fields of terrestrial biophysical parameters from the NDVI. Int. J. Rem. Sens. 15(17): 3519-3545.

Shimabukuro, Y.E., Batista, G.T., Mello, E.M.K., Moreira, J.C., Duarte, V., 1998. Using shade fraction image segmentation to evaluate deforestation in Landsat Thematic Mapper images of the Amazon Region. Int. J. Rem. Sens. 19(3): 535-541.

Shinozaki, K., Yoda, K., Hozumi, K., Kira, T., 1964a. A quantitative analysis of plant form—the pipe model theory. I. Basic analyses. Jap. J. Ecol. 14(3): 97-105.

Shinozaki, K., Yoda, K., Hozumi, K., Kira, T., 1964b. A quantitative analysis of plant form: the pipe model theory: II. Further evidence of the theory and its application in forest ecology. Jap. J. Ecol. 14(4): 133-139.

Spanner, M., Johnson, L., Miller, J., McCreight, R., Freemantle, J., Runyon, J., Gong, P., 1994. Remote sensing of seasonal leaf area index across the Oregon transect. Ecol. Appl. 4(2): 258-271.

Stolz, R., Braun, M., Probeck, M., Weidinger, R., Mauser, W., 2005. Land use classification in complex terrain: the role of ancillary knowledge. EARSeL eProceedings pp. 94-105.

Strahler, A., Muchoney, D., Borak, J., Friedl, M., Gopal, S., Lambin, E., Moody, A., 1999. MODIS land cover product, algorithm theoretical basis document (ATBD), version 5.0. Center for Remote Sensing, Boston University, Boston, Massachusetts, 72p.

Tasser, E., Prock, S., Mulser, J., 1999. The impact of land-use on vegetation along the Eastern Alpine transect. In: Cernusca, A., Tappeiner, U., Bayfield, N. (Ed.). Land-Use Changes in European Mountain Ecosystems. ECOMONT—Concepts and Results. Blackwell Wissenschafts-Verlag, Berlin, pp. 235–246.

Tenhunen, J.D., Valentini, R., Koestner, B., Zimmermann, R., Granier, A., 1998. Variation in forest gas exchange at landscape to continental scales; Variations des echanges gazeux des forets de l'echelle locale a l'echelle continentale. Annales des Sciences Forestieres 55(1-2): 1-11.

Thomlinson, J.R., Bolstad, P.V., Cohen, W.B., 1999. Coordinating methodologies for scaling landcover classifications from site-specific to global: Steps toward validating global map products. Rem. Sen. Environ. 70(1): 16-28.

Tian, Y., Woodcock, C.E., Wang, Y., Privette, J.L., Shabanov, N.V., Zhou, L., Zhang, Y., Buermann, W., Dong, J., Veikkanen, B., 2002a. Multiscale analysis and validation of the MODIS LAI product. I. Uncertainty assessment. Rem. Sens. Environ. 83(3): 414-430.

Tian, Y., Woodcock, C.E., Wang, Y., Privette, J.L., Shabanov, N.V., Zhou, L., Zhang, Y., Buermann, W., Dong, J., Veikkanen, B., 2002b. Multiscale analysis and validation of the MODIS LAI product. II Sampling strategy. Rem. Sens. Environ. 83(3): 431-441.

Turner, D.P., Dodson, R., Marks, D., 1996. Comparison of alternative spatial resolutions in the application of a spatially distributed biogeochemical model over complex terrain. Ecol. Modellin 90(1): 53-67.

Turner, M.G., O'Neill, R.V., Gardner, R.H., Milne, B.T., 1989. Effects of changing spatial scale on the analysis of landscape pattern. Lands. Ecol. 3(3): 153-162.

Valentini, R., Matteucci, G., Dolman, A.J., Schulze, E.D., Rebmann, C., Moors, E.J., Granier, A., Gross, P., Jensen, N.O., Pilegaard, K., 2000. Respiration as the main determinant of carbon balance in European forests. Nature 404(6780): 819-820.

Van Leeuwen, W.J.D., Huete, A.R., Laing, T.W., 1999. MODIS vegetation index compositing approach: A prototype with AVHRR data. Rem. Sens. Environ. 69(3): 264-280.

Verma, S.B., Sellers, P.J., Walthall, C.L., Hall, F.G., Kim, J., Goetz, S.J., 1993. Photosynthesis and stomatal conductance related to reflectance on the canopy scale. Rem. Sen. Environ. 44(1): 103-116.

Vermote, E.F., El Saleous, N.Z., Justice, C.O., 2002. Atmospheric correction of MODIS data in the visible to middle infrared- First results. Rem. Sen. Environ. 83(1): 97-111.

Verstraete, M.M., Pinty, B., Myneni, R.B., 1996. Potential and Limitations of Information Extraction on the Terrestrial Biosphere from Satellite Remote Sensing. Rem. Sens. Environ. 58(2): 201-214.

Wang, Q., Tenhunen, J., Granier, A., Reichstein, M., Bouriaud, O., Nguyen, D., Breda, N., 2004. Long-term variations in leaf area index and light extinction in a Fagus sylvatica stand as estimated from global radiation profiles. Theor. Appl. Climatol. 79(3): 225-238.

Wang, Y., Buermann, W., Stenberg, P., Smolander, H., Häme, T., Tian, Y., Hu, J., Knyazikhin, Y., Myneni, R.B., 2003. Hyperspectral remote sensing of vegetation canopy: Leaf area index and foliage optical properties. Rem. Sens. Environ. 85: 304–315.

Wang, Y., Tian, Y., Zhang, Y., El-Saleous, N., Knyazikhin, Y., Vermote, E., Myneni, R.B., 2001. Investigation of product accuracy as a function of input and model uncertainties- Case study with SeaWiFS and MODIS LAI/FPAR algorithm. Rem. Sens. Environ. 78(3): 299-313.

Waring, R.H., Schroeder, P.E., Oren, R., 1982. Application of the pipe model theory to predict canopy leaf area. Can. J. Forest Res. 12(3): 556-560.

Wohlfahrt, G., 2004. Modelling Fluxes and Concentrations of CO_2, H_2O and Sensible Heat Within and Above a Mountain Meadow Canopy: A Comparison of Three Lagrangian Models and Three Parameterisation Options for the Lagrangian Time Scale. Boundary-Layer Meteorol. 113(1): 43-80.

Wolfe, R.E., Nishihama, M., Fleig, A.J., Kuyper, J., 2002. Achieving sub-pixel geolocation accuracy in support of MODIS land science. Rem. Sen. Environ. 83(1): 31-49.

Yang, W., Tan, B., Huang, D., Rautiainen, M., Shabanov, N.V., Wang, Y., Privette, J.L., Huemmrich, K.F., Fensholt, R., Sandholt, I., 2006. MODIS Leaf Area Index Products: From Validation to Algorithm Improvement. IEEE Trans. Geosci. Rem. Sens. 44(7): 1885.

Yoshioka, H., Miura, T., Huete, A.R., Ganapol, B.D., 2000. Analysis of Vegetation Isolines in Red-NIR Reflectance Space. Rem. Sens. Environ. 74(2): 313-326.

Zaitsev, A.S., Chauvat, M., Pflug, A., Wolters, V., 2002. Oribatid mite diversity and community dynamics in a spruce chronosequence. Soil Biol. Biochem. 34(12): 1919-1927.

Zarco-Tejada, P.J., Rueda, C.A., Ustin, S.L., 2003. Water content estimation in vegetation with MODIS reflectance data and model inversion methods. Rem. Sen. Environ. 85(1): 109-124.

Zeller, V., Bahn, M., Aichner, M., Tappeiner, U., 2000. Impact of land-use change on nitrogen mineralization in subalpine grasslands in the Southern Alps. Biol. Fertil. Soils 31(5): 441-448.

Zeller, V., Bardgett, R.D., Tappeiner, U., 2001. Site and management effects on soil microbial properties of subalpine meadows: a study of land abandonment along a north–south gradient in the European Alps. Soil Biol. Biochem. 33(4-5): 639-649.

Zhang, X., Friedl, M.A., Schaaf, C.B., Strahler, A.H., Hodges, J.C.F., Gao, F., Reed, B.C., Huete, A., 2003. Monitoring vegetation phenology using MODIS. Rem. Sen. Environ. 84(3): 471-475.

Zhou, Q., Robson, M., 2001. Automated rangeland vegetation cover and density estimation using ground digital images and a spectral-contextual classifier. Int. J. Rem. Sens. 22(17): 3457-3470.

DECLARATION

I hereby declare that this submission is my own account of my own research and that, to the best of my knowledge and belief, it contains neither material previously published or written by another person nor material which to a substantial extent has been accepted for the award of any other degree or diploma of the university or other institute of higher learning, except where due acknowledgment has been made in the text.

ERKLÄRUNG

Hiermit erkläre ich, dass ich die Arbeit selbstständig verfasst und keine anderen als die angegebenen Hilfsmittel verwendet habe.

Weiterhin erkläre ich, dass ich nicht anderweitig mit oder ohne Erfolg versucht habe, eine Dissertation einzureichen oder mich einer Doktorprüfung zu unterziehen.

Bayreuth, den 27 Mai 2009   _____

                                                      Nguyen Quoc Dinh